NUREG/CR-6918, Rev. 3

U.S.NRC
United States Nuclear Regulatory Commission
Protecting People and the Environment

VARSKIN 6

A Computer Code for Skin Contamination Dosimetry

Office of Nuclear Regulatory Research

AVAILABILITY OF REFERENCE MATERIALS IN NRC PUBLICATIONS

NRC Reference Material

As of November 1999, you may electronically access NUREG-series publications and other NRC records at NRC's Library at www.nrc.gov/reading-rm.html. Publicly released records include, to name a few, NUREG-series publications; *Federal Register* notices; applicant, licensee, and vendor documents and correspondence; NRC correspondence and internal memoranda; bulletins and information notices; inspection and investigative reports; licensee event reports; and Commission papers and their attachments.

NRC publications in the NUREG series, NRC regulations, and Title 10, "Energy," in the *Code of Federal Regulations* may also be purchased from one of these two sources.

1. **The Superintendent of Documents**
   U.S. Government Publishing Office
   Washington, DC 20402-0001
   Internet: bookstore.gpo.gov
   Telephone: (202) 512-1800
   Fax: (202) 512-2104

2. **The National Technical Information Service**
   5301 Shawnee Road
   Alexandria, VA 22312-0002
   www.ntis.gov
   1-800-553-6847 or, locally, (703) 605-6000

A single copy of each NRC draft report for comment is available free, to the extent of supply, upon written request as follows:

Address: **U.S. Nuclear Regulatory Commission**
Office of Administration
Multimedia, Graphics, and Storage & Distribution Branch
Washington, DC 20555-0001
E-mail: distribution.resource@nrc.gov
Facsimile: (301) 415-2289

Some publications in the NUREG series that are posted at NRC's Web site address www.nrc.gov/reading-rm/doc-collections/nuregs are updated periodically and may differ from the last printed version. Although references to material found on a Web site bear the date the material was accessed, the material available on the date cited may subsequently be removed from the site.

Non-NRC Reference Material

Documents available from public and special technical libraries include all open literature items, such as books, journal articles, transactions, *Federal Register* notices, Federal and State legislation, and congressional reports. Such documents as theses, dissertations, foreign reports and translations, and non-NRC conference proceedings may be purchased from their sponsoring organization.

Copies of industry codes and standards used in a substantive manner in the NRC regulatory process are maintained at—

The NRC Technical Library
Two White Flint North
11545 Rockville Pike
Rockville, MD 20852-2738

These standards are available in the library for reference use by the public. Codes and standards are usually copyrighted and may be purchased from the originating organization or, if they are American National Standards, from—

American National Standards Institute
11 West 42nd Street
New York, NY 10036-8002
www.ansi.org
(212) 642-4900

Legally binding regulatory requirements are stated only in laws; NRC regulations; licenses, including technical specifications; or orders, not in NUREG-series publications. The views expressed in contractorprepared publications in this series are not necessarily those of the NRC.

The NUREG series comprises (1) technical and administrative reports and books prepared by the staff (NUREG–XXXX) or agency contractors (NUREG/CR–XXXX), (2) proceedings of conferences (NUREG/CP–XXXX), (3) reports resulting from international agreements (NUREG/IA–XXXX), (4) brochures (NUREG/BR–XXXX), and (5) compilations of legal decisions and orders of the Commission and Atomic and Safety Licensing Boards and of Directors' decisions under Section 2.206 of NRC's regulations (NUREG–0750).

NUREG/CR-6918, Rev. 3

U.S.NRC
United States Nuclear Regulatory Commission
Protecting People and the Environment

VARSKIN 6

A Computer Code for Skin Contamination Dosimetry

Manuscript Completed: December 2017
Date Published: October 2018

Prepared by:
D. M. Hamby
C. D. Mangini

School of Nuclear Science and Engineering
Oregon State University
Corvallis, OR 97331-5902

V. Shaffer, NRC Project Manager

Office of Nuclear Regulatory Research

ABSTRACT

The original VARSKIN computer code, an algorithm to calculate skin dose from radioactive skin contamination, has been modified on several occasions. VARSKIN is a U.S. NRC computer code used by staff members and NRC licensees to calculate occupational dose to the skin resulting from exposure to radiation emitted from hot particles or other contamination on or near the skin. These assessments are required by 10 CFR 20.1201(c) in which the assigned shallow dose equivalent is to the part of the body receiving the highest exposure over a contiguous 10 cm^2 of skin at a tissue depth of 0.007 centimeters (7 mg/cm^2).

As with previous versions, five different predefined source configurations are available in VARSKIN to allow simulations of point, disk, cylinder, sphere, and slab sources. Improvements to the earlier VARSKIN versions included enhanced photon and electron dosimetry models, as well as models to account for air gap and cover materials for photon dosimetry. With a simple check box activated by the user, VARSKIN 6 gives the user the option to have the code automatically include all decay products in dosimetry calculations or to allow the user to manually add progeny. Additionally, the option to calculate skin dose using ICRP 107 nuclide decay data (ICRP 2008) has been added. Both ICPR 38 (1983) and ICRP 107 (2008) nuclide libraries are available at the user's option and contain data on gamma rays, X rays, beta particles, internal conversion electrons, and Auger electrons. Although the user can choose any dose-averaging area, the default area for skin dose calculations is 10 square centimeters, to conform to regulatory requirements pursuant to Title 10 of the *Code of Federal Regulations*, Section 20.1201(c). Data entry is condensed to a single screen, a variety of unit options are provided (including both British and International System (SI) units), and the source strength can be entered in units of total activity or distributed in units of activity per unit area or activity per unit volume. The output page and the user's ability to add radionuclides to the library are greatly simplified. VARSKIN allows the user to eliminate radionuclides that are not of interest and thus build a customized library.

The enhanced photon model, introduced in VARSKIN 4, accounts for photon attenuation, charged particle buildup, and electron scatter at all depths in skin. The model allows for volumetric sources and clothing/air gaps between source and skin. The electron dosimetry model was upgraded in VARSKIN 5 to better account for beta energy loss and particle scatter. Dose point kernels are now Monte-Carlo based and results agree very well with EGS and MCNP probabilistic simulations.

This document describes the VARSKIN 6 dosimetry code, provides basic operating instructions, presents detailed descriptions of dosimetry models, and suggests methods for avoiding misuse of those models.

TABLE OF CONTENTS

LIST OF FIGURES

LIST OF TABLES

ACKNOWLEDGMENTS

This report was prepared to document work performed by Oregon State University (OSU) for the U.S Nuclear Regulatory Commission (NRC) under Contract Nos. **NRC-HQ-60-15-C-0011, NRC-HQ-11-C-04-0011** and **NRC-04-08-137**. Staff at the Pacific Northwest National Laboratory wrote initial versions of VARSKIN (Traub et al. 1987), with later versions amended at Colorado State University and then the Center for Nuclear Waste Regulatory Analyses (Durham 1992; Durham 2006). The activities reported here, and in previous versions (Hamby et al. 2011; Hamby et al. 2014), were performed by the team at OSU on behalf of the NRC Office of Nuclear Regulatory Research, Division of System Analysis. This report is a product of OSU and does not necessarily reflect the views or regulatory position of the NRC.

The team at OSU is very appreciative of the technical assistance received from D. Neville, L. Anspach, N. McDaniel, J. Caffrey, M. Tang, J. Parson, M. Ryan, and S. Marshall in the production of previous reports and their findings. We are also grateful to V. Shaffer, S. Bush-Goddard, M. Saba, and S. Sherbini for their support during development and maintenance of the enhanced photon and electron dosimetry models. Beta testers of this and earlier versions of VARSKIN include M. Jimenez, E. Dickson, P. Lee, S. Reese, J. Chase, J. Dubeau, K. Sejkora, M. Thornhill, R. Struckmeyer, and J. DeCicco.

Authors of earlier versions of the VARSKIN code were indebted to L. Howard for technical review and D. Turner for programmatic review of reports. These authors also thanked L. Selvey for document preparation; E. Hanson for editorial review; and H. Karagiannis, S. Sherbini, A. Roecklein, S. Bush-Goddard, and E. Dickson of the NRC for their support, suggestions, and patience during the development of VARSKIN 3. The following people helped develop models for VARSKIN 3: J. Chase, B. Plain, M. Wierzbicki, M. Lantz, and K. Krobl. The following people provided comments after testing VARSKIN 3: G. Chabot, J. Dwyer, J. Lebda, E. Mercer, R. Nimitz, A. Salame-Alfie, M. Stabin, G. Sturchio, B. Tharakan, T. Vandermey, and M. Charles.

ABBREVIATIONS AND ACRONYMS

2D	Two Dimensional
3D	Three Dimensional
BSCF	Backscatter Correction Factor
CFR	Code of Federal Regulations
CPE	Charged Particle Equilibrium
CPU	Central Processing Unit
CSDA	Continuous Slowing Down Approximation
DPK	Dose Point Kernel
DSP	Depth Scaling Parameter
EDK	Energy Deposition Kernel
EGS	Electron-Gamma Shower
ESP	Energy Scaling Parameter
GUI	Graphical User Interface
ICRP	Interactional Commission on Radiological Protection
ICRU	International Commission on Radiation Units and Measurements
ITS	Integrated TIGER Series
KERMA	Kinetic Energy Released in Matter
MCNP	Monte Carlo N-Particle
NCRP	National Council on Radiation Protection and Measurement
NIST	National Institute of Standards and Technology
NRC	National Research Council (Canada)
NRC	Nuclear Regulatory Commission
OSU	Oregon State University
RSICC	Radiation Safety Information Computational Center
RSO	Radiation Safety Officer
SADD	Scaled Absorbed Dose Distribution
SI	Systeme Internationale
STP	Standard Temperature and Pressure
TCPE	Transient Charged Particle Equilibrium
V&V	Verification and Validation

1 INTRODUCTION

The original VARSKIN computer code (Traub, et al., 1987) was intended as a tool for the calculation of tissue dose at various depths as the result of skin contamination. The contamination was assumed a point or an infinitely thin disk source located directly on the skin. Soon after the release of VARSKIN, the industry encountered a “new” type of skin contaminant. This contaminant consists of discrete microscopic radioactive particles, called “hot” particles. These particles differ radically from uniform skin contamination in that the particles have a thickness associated with them, and many of the skin exposures result from particles on the outside of protective clothing. These assessments are required by 10 CFR 20.1201(c) in which the assigned shallow dose equivalent is to the part of the body receiving the highest exposure over a contiguous 10 cm^2 of skin at a tissue depth of 0.007 centimeters (7 mg/cm^2).

VARSKIN MOD2 (Durham, 1992) contained all the features of the original VARSKIN, with many significant additions. Additional features in MOD2 included the modeling of three-dimensional sources (cylinders, spheres, and slabs) that accounted for self-shielding, modeling of materials placed between the source and skin (including air gaps) that would attenuate beta particles, and, in specific cases, modeling hot particle photon doses. VARSKIN MOD2 also used a correction for backscatter for one- and two-dimensional beta sources under limited conditions. Finally, the VARSKIN MOD2 package incorporated a user interface that greatly simplified data entry for calculating skin dose, in addition to providing guidance in the form of help screens.

MOD2 contained a volume-averaged dose model and an offset particle model that have been retained in subsequent VARSKIN coding. The volume-averaged model allows the user to calculate dose averaged over a volume of tissue defined by a cylinder with a diameter equal to that of the dose averaging area and bounded at the top and bottom by two selected skin depths (see Figure 1-1). This model is useful for calculations of dose that then can be compared to the dose measured by a finite-volume instrument (e.g., a thermoluminescent dosimeter). The offset particle model, which allows dose to be calculated for a particle that is not centered over the dose area of interest, is useful for calculating dose to a singular given skin area from multiple hot particles.

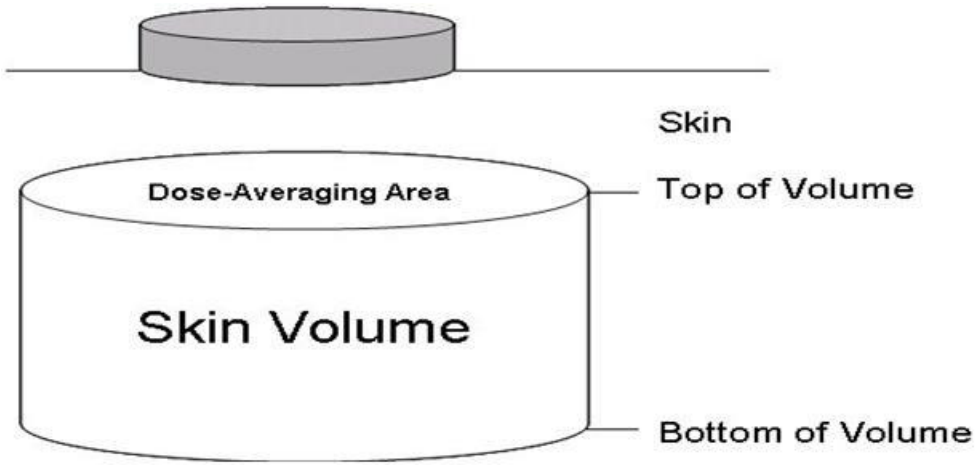

Figure 1-1 Depiction of Cylindrical Dose Averaging Volume

Finally, VARSKIN MOD2 gave the user the ability to select a composite source term, thus allowing the calculation of total dose from a mixture of radionuclides instead of requiring the

code to be executed separately for each constituent. This feature was altered in VARSKIN 3 (Durham 2006), allowing the user to select up to twenty radionuclides in a single calculation. One drawback of removing this feature in VARSKIN 3 is that the user must explicitly add radioactive progeny; we have corrected this shortcoming with the issuance of VARSKIN 6.

Enhancements that were incorporated into VARSKIN 4 (Hamby et al. 2011) focused on the photon dosimetry model. The photon model is fundamentally unchanged in VARSKIN 6 and includes charged-particle buildup and subsequent transient equilibrium, along with photon attenuation, air and cover attenuation, and the option to model volumetric sources. The VARSKIN 5 (Hamby et al. 2014) package provided an updated electron dosimetry model that better accounts for charged-particle energy loss as the particle moves through the source, cover material, air, and tissue. Likewise, the electron dosimetry model is fundamentally unchanged in VARSKIN 6.

Section 2 of this report describes the content of VARSKIN 6, primarily focused on instructions for code execution. Section 3 discusses the technical basis for VARSKIN 6 and describes the dosimetry models, while Section 4 contains the results of validation and verification testing. Section 5 describes new features of the code and its limitations. Section 6 explains the correct method for modeling “infinite” sources and how to hand-calculate the maximum dose to a single 10-square-centimeter (10 cm^2) area from multiple contamination sources. Additionally, Appendices A and B provide graphical results from photon and electron validation and verification (V&V), and Appendix C presents four detailed solutions to practical examples using VARSKIN 6.

2 VARSKIN 6 USER'S MANUAL

This section serves as a user's guide for VARSKIN 6. It includes operating instructions and a description of the features of VARSKIN 6.

2.1 Running VARSKIN

Users simply download the VARSKIN folder and double-click the VARSKIN executable icon to run the code. There is no need to uninstall previous versions of VARSKIN or install the new version. Subsequent versions of VARSKIN will be available on the NRC/RAMP website, as necessary. Obtaining new versions is as simple as downloading the new folder and beginning execution. Multiple folders, containing different versions of VARSKIN, can be opened and operated simultaneously, if the user so chooses.

2.1.1 Hardware and Software Requirements

A personal computer with a Pentium II processor or newer is required. The VARSKIN 6 folder requires approximately 25 megabytes of disk space. Over the years, VARSKIN has been tested under a variety of Windows® operating systems. An error may occur for international users of VARSKIN 6 or users who may have changed their computer settings. This error occurs when trying to add a nuclide in the user list from the nuclide library for use. The error relates to using comma rather than period as the decimal system; and likewise, the period rather than comma as the digit-grouping symbol. If this error occurs, the user should change their computer settings in "Change date, time or number formats".

Operations in VARSKIN 6 are designed to be intuitive. After double-clicking the VARSKIN executable icon, the user will see the Main Input window (Figure 2-1). If necessary, the "Help" dropdown list provides the user with an "About VARSKIN 6.0" window containing basic code information and contact numbers (Figure 2-2). The user defines the exposure scenario by selecting various boxes, buttons, and data entry fields provided in the input window.

2.1.2 Source Geometry

Although VARSKIN 6 allows the user to enter data in any order, the source geometry should be chosen first, because changing the geometry package will cause certain parameters to appear and others to be removed. Five geometry packages are available (upper left of window Figure 2-1): point source, disk source (infinitely thin), cylinder source (thick), spherical source, and slab source (rectangular). Source activity is assumed to be evenly distributed throughout the area or volume of all source geometries.

The point source geometry (Figure 2-3(A)) is very simple and should be used as an initial screening tool for contamination that is confined to an extremely small area of the skin, or for a quick calculation to determine whether a regulatory limit is being approached or exceeded. The point source geometry does not account for electron self-shielding, so a three-dimensional source geometry is best for particulate contamination. The point source model does not require any data describing the physical dimensions of the source and will generally yield the highest dose rate for a given activity of any of the available source geometries. For electron dosimetry, a point source is automatically (due to historical code constraints) modeled as a cylindrical source with a thickness of 1 micron, a radius of 1 micron, and a density of 0.001 grams per

cubic centimeter (g/cm^3). An offset particle model (discussed below) is available for photons in the point source geometry.

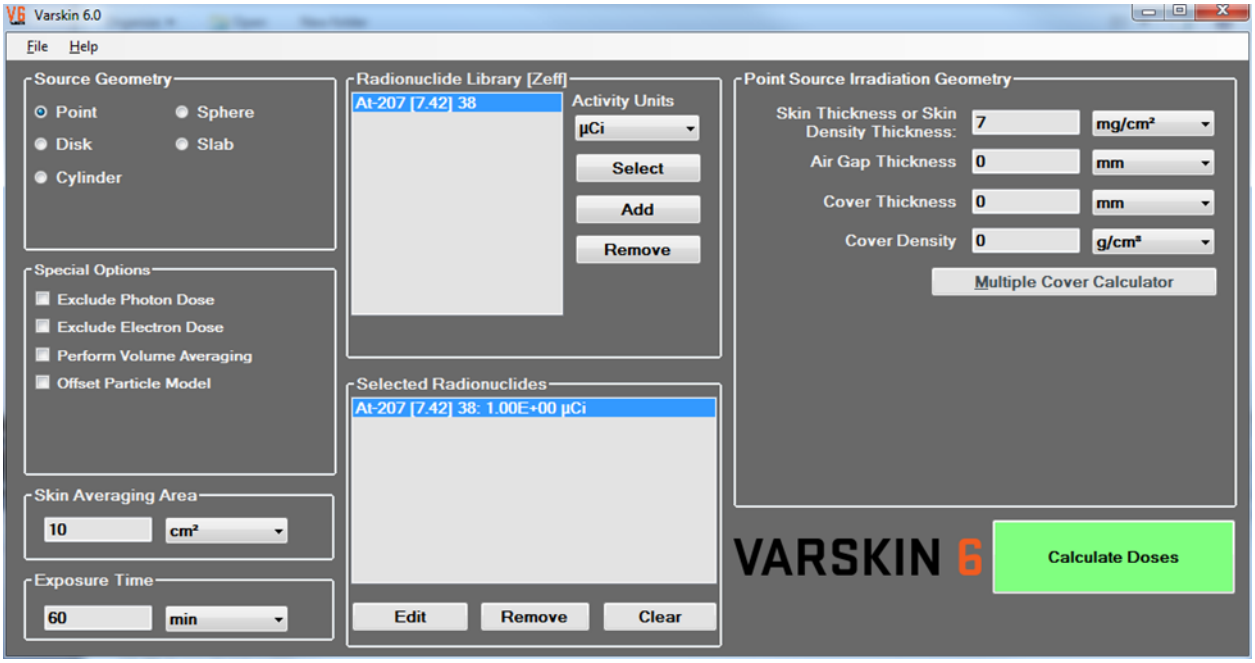

Figure 2-1 Initial View and Main Input Window (Source Geometry option box in upper left corner)

Figure 2-2 "About VARSKIN 6.0" Window

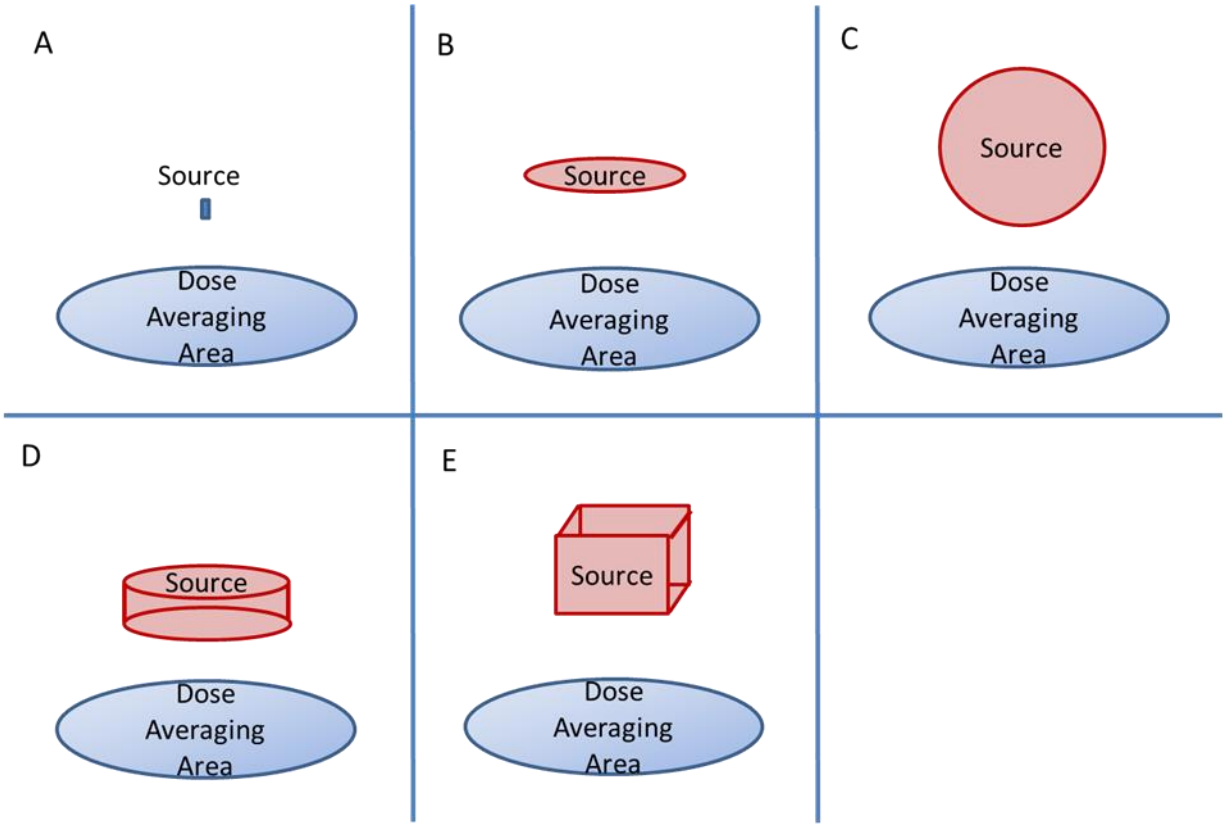

Figure 2-3 Schematic Representations of the Five Geometry Options

The infinitely thin disk source geometry model (Figure 2-3(B)) is simple and is recommended for modeling skin contamination events caused by liquid sources. The disk source geometry requires the user to enter either the source diameter or the source area at the bottom of the Disk Source Irradiation Geometry box. Entering the area of the contamination is useful for modeling sources when the area is known. Enter the area of the source in the text box labeled "Source Area." When the user enters the diameter of the source area, VARSKIN 6 calculates the area of the two-dimensional (2D) disk with that diameter. Similarly, when the user enters the area of the source, VARSKIN 6 calculates the diameter of the disk with the same area. If the area of contamination is not circular, entering the area of the actual contamination will generally result in a reasonable estimation of skin dose.

The spherical source geometry (Figure 2-3(C)) is perhaps the simplest three-dimensional (3D) geometry to use for dose calculations because it requires knowledge of source density and only one source dimension, its diameter. The spherical source geometry assumes that the source is surrounded by air and touches the skin or cover material only at the bottom point of the sphere. For photon dosimetry, it is assumed that the source material is equivalent to air for attenuation calculations. Choosing a spherical source will generally overestimate dose compared to a similarly sized cylindrical source (same radius and length) with the same total activity. The air surrounding the bottom hemisphere does not shield the source particles as efficiently as the source material (which would be encountered by the particle in the cylinder or slab models), and a larger area of skin will be exposed, resulting in consistently higher doses.

The cylindrical source model (Figure 2-3(D)) requires knowledge of density and two dimensions, the cylinder diameter and its height (thickness). The cylindrical source geometry assumes that

the source is surrounded by air and that the entire bottom of the cylinder is in contact with skin or cover material. Of the two dimensions describing a cylinder, the calculated dose is much more sensitive to changes in the cylinder height as opposed to the cylinder diameter.

The slab source geometry (Figure 2-3(E)) requires knowledge of density and three physical dimensions: the first side length, the second side length, and the slab's thickness. Generally, as with the cylindrical model, slab thickness will have more influence on tissue dose than will lateral dimensions.

The following general rules should govern the choice of geometry package, progressing from the most conservative to least conservative dose estimate:

- If nothing is known about the particle size and shape, use the point source geometry option. This option is also recommended for a quick comparison to regulatory limits since the point geometry typically overestimates actual skin dose.
- If the diameter is known, but the thickness cannot be estimated, or if a distributed source is being modeled (i.e., with a known source strength per unit area), use the two-dimensional disk source geometry option. If an infinite plane source is desired, a source area of at least 15 cm^2 is generally sufficient.
- If the particle is known to be spherical (few particles are truly spherical), use the spherical source geometry option.
- If the thickness and the diameter of the source can be estimated, but the shape is unknown, use the cylindrical source geometry option because this geometry requires only two dimensions (thickness and diameter) to describe the particle.
- If the particle is known to be rectangular, use the slab or cylinder source geometry options. The height of the particle should be preserved, and the area of the contact surface should be selected such that the source volume is preserved. Executing both slab and cylinder will aid in providing bounding doses.

It is not intended that VARSKIN models be used to simulate large volumetric sources and the user is cautioned against using dimensions greater than a few centimeters. For all source geometries, dose is averaged over an infinitely thin disk centered below the central axis of the source. When using the offset particle model (available only for photon point sources), dose is calculated to the disk with its center located at the user-supplied offset distance from the center of the source.

2.1.3 Adding Radionuclides to the Library

VARSKIN 6 employs two master decay libraries and a user library that contains only those radionuclides that have been selected and added by the user. Nuclide decay information is obtained from abridged datasets published by the International Commission on Radiological Protection (ICRP), namely the ICRP 38 (1983) or ICRP 107 (2008) databases; VARSKIN 6 defaults to the ICRP 38 database. In VARSKIN, the user selects the nuclear database from which to extract decay data when radionuclides are selected from the master library to be added to the user library. Additionally, the user will choose between the automatic inclusion of decay progeny (designated by "D"), or manual (or none) progeny selection. The user can reference the "DaughterList" files in the *dat* folder to obtain a listing of decay products and branching ratios being included by the VARSKIN 6 code when choosing the "D" option.

Radionuclides are added to the VARSKIN user library through the use of a FORTRAN executable file entitled *SadCalc.exe*. The purpose of the program, which is an adaptation of a

stand-alone program originally called SADDE Mod 2 (Reece, et al., 1989), and modified by Mangini (2012), is to produce data files that contain the information needed to calculate both electron and photon doses. In addition to selecting the master library (either ICRP 38 or ICRP 107, with or without progeny), and the nuclide from that library, the user must specify an effective atomic number (Z_{eff}) to characterize the source material in which the radioactivity is incorporated. The default value for Z_{eff} is 7.42 (the effective atomic number of water), meaning the radioactivity itself is assumed to be dissolved or suspended in water.

When choosing to include decay progeny ("D"), radioactive progeny follows the parent in secular equilibrium when selected from the master library. Selecting the non-progeny datasets will include parent nuclides only. The selection of decay progeny results in a single calculation of dose (one each for electrons and photons) for the parent and progeny incorporating the entire decay chain (with branching ratios greater than 1%). Individual doses for each member of the chain are not provided. If the user wishes to have this information, the user may select the dataset(s) without progeny inclusion and manually selecting each member of the decay series.

If evaluating dose from progeny alone, the user must note its half-life and include the correct dose calculation (decay corrected or not) in the dose estimate. For example, in the case of ^{137m}Ba as a stand-alone product of ^{137}Cs decay, the user should report the "Dose (No Decay)" result for ^{137m}Ba dose; this would force the assumption that ^{137m}Ba is continuously supplied by the decay of ^{137}Cs (in this example, the branching ratio from ^{137}Cs to ^{137m}Ba is 94.6%). However, if the "Decay-Corrected Dose" is used, the very short decay time of ^{137m}Ba will cause the dose to be significantly underestimated.

When VARSKIN is first executed, a few preselected radionuclides may appear in the user library. VARSKIN is designed to allow the user to customize the user library so that only the nuclides of interest can be maintained for ready use. To add a radionuclide to the user library, the user clicks the "Add" button (shown in the upper center of Figure 2-1), after which a new window appears to obtain the user's choice of nuclide decay database and whether decay products are to be included (Figure 2-4a). Once this selection is made, another window will appear (Figure 2-4b) that displays every radionuclide for which data are available (a total of 838 radionuclides in ICRP 38 and 1252 radionuclides in ICRP 107). In addition to selecting the decay database, the user must specify an effective atomic number (Z_{eff}) to characterize the source material in which the radioactivity is incorporated. As stated above, the default value for Z_{eff} is 7.42 (the effective atomic number of water). The user then highlights the radionuclide and clicks the "Add Radionuclide" button, or simply double-clicks the name of the radionuclide. A large number of radionuclides are available in the master library, each of which could be added to the VARSKIN user library, each from a different decay database, and each with its own effective atomic number (i.e., multiple selections of the same nuclide can be made, but with different values of Z_{eff}).

Once the "Add Radionuclide" button is selected (Figure 2-4), calculations are performed internally to populate the user library for the selected radionuclide; this can take up to a minute or so, depending on the processing power of your computer. In these calculations, data are extracted from the appropriate data files *.dat*, *.idx*, and *.bet* (all of which are located in the *dat* subdirectory of the application directory). If the radionuclide emits electrons, an electron energy spectrum is generated for all emissions with yield greater than 0.1%. Photons with energy greater than 2 keV and decay yield greater than 1% are also collected from these data files.

The data are processed by *SadCalc.exe*, and output files that contains the average emitted electron energy, electron yield, electron range, the scaled absorbed dose distribution, and the

photon energies and yields are generated for the selected nuclide with the extensions ".rad" and ".photon" (these can be seen in the *dat* folder).

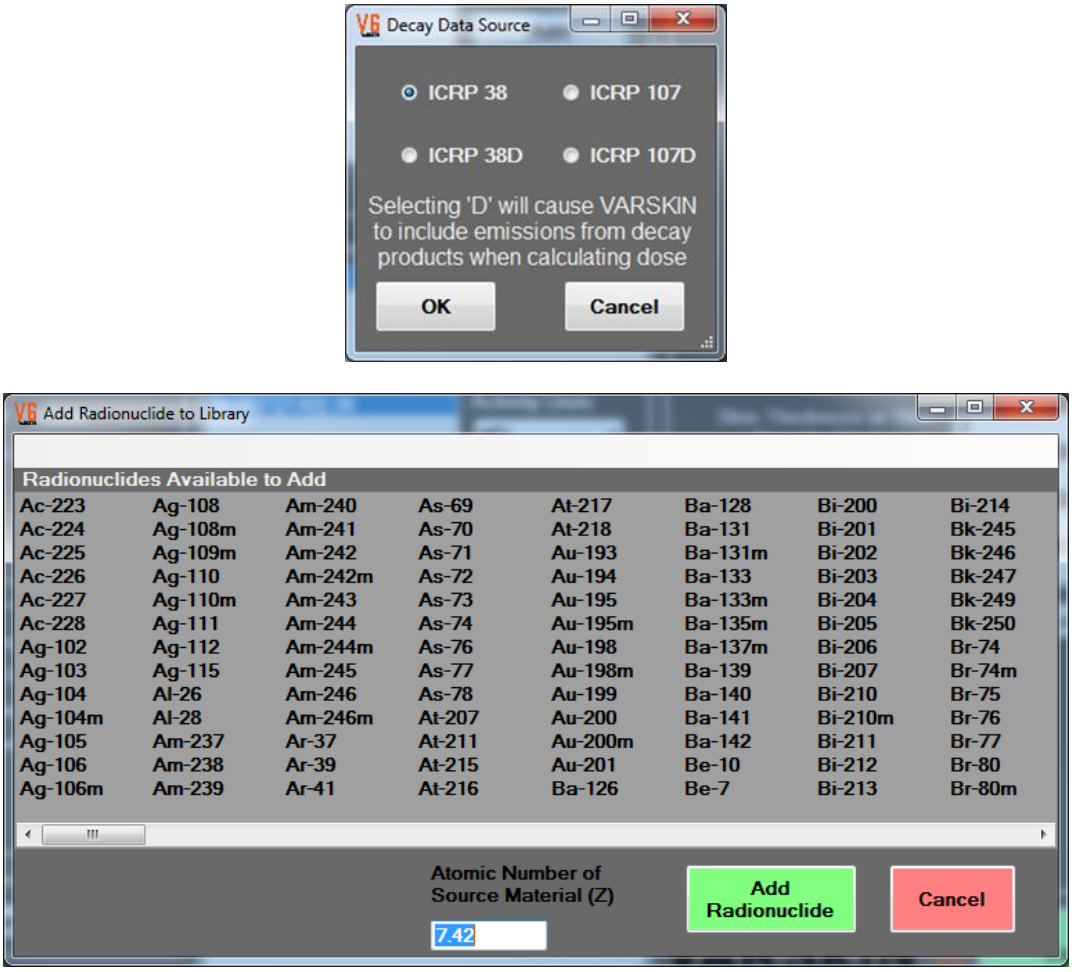

Figure 2-4 (a) Decay Data Source Window and (b) Add Radionuclide Window

When the process of adding the radionuclide is completed, the Main Input window will return, and the added radionuclide will be visible in the user list (upper middle) of available radionuclides. The nuclide name will indicate the database from which the data were drawn ("38" or "107"), the effective atomic number of the source material (e.g., "[7.42]"), and whether decay progeny are included ("D" or blank). Each nuclide could be added to the VARSKIN user library, and each with its own effective atomic number (i.e., multiple selections of the same nuclide can be made, but with different values of Z_{eff}).

Once a radionuclide is added to the library, it is available to be used in all subsequent calculations until the user purposefully removes the radionuclide from the library. Note that not all the radionuclides emit electrons or photons; some of the radionuclides emit only alpha particles, which do not contribute to skin dose. In that case, the user will be notified that the radionuclide does not emit these types of radiation, and no library file will be produced. The added radionuclide will remain in the user library for subsequent calculations unless the user purposefully removes it using the "Remove" button (Figure 2-1) on the Radionuclide Library frame; the nuclide data will always remain in the master library.

In VARSKIN 6, electron energy spectra for beta emitters are obtained from data files located in the *dat* subdirectory of the VARSKIN folder and contains the maximum energy and the yield information for each of a number of energy bins. Index files (*.idx*) are used to quickly locate nuclide information in the very large data files. In addition to beta-emission information, the files also contain data on internal conversion or Auger electrons emitted by the radionuclide. The graphical user interface (GUI) collects spectral data for a selected radionuclide and writes the file *sadinput.dat* which contains the radionuclide name, the yield, the half-life, the maximum beta energy, the beta spectrum, and the energy and yield of any electrons. *SadCalc.exe* reads this file; adds conversion and Auger electrons to the beta spectrum to form a new spectrum that includes all electrons; calculates various parameters and writes these data to the file *sadout.dat*. The GUI reads *sadout.dat* and writes library files with the extensions *.rad* and *.photon*. Note that *sadout.dat* and *sadinput.dat* are internal files and are not normally accessed by the user.

2.1.4 Selecting Radionuclides for the Dose Scenario

Radionuclides in the user library (upper-middle) are selected for a dose calculation by double-clicking the radionuclide name or by highlighting the desired radionuclide and clicking the "Select" button (Figure 2-1). If the nuclide name signifies the inclusion of decay products ("D"), doses calculated for that nuclide will include all energy emissions from all of its decay progeny (with >1% branching). The default unit of measure for activity is the microcurie (μCi). Users may change the activity unit by selecting a different unit from the Activity Units list box. The new unit must be chosen before selecting the radionuclide. When a radionuclide is selected, a message box will appear asking the user to enter the value of the activity in the chosen units. Once the activity is entered, the radionuclide and its activity will be added to the Selected Radionuclide list box (lower-middle). A user may select up to 20 radionuclides for a given scenario; nuclides with progeny are counted as only one (i.e., the parent) nuclide. If the "D" database is used for a given parent nuclide, all decay progeny, regardless of time, are assumed to be in equilibrium with the parent. If the user knows this not to be true, the progeny should be selected manually (non-starred decay database) so that independent dose values will be calculated for each decay product.

For geometry packages other than the point source, the "Use Distributed Source" checkbox will appear (see Figure 2-5). The distributed source option allows the user to enter the source strength in activity-per-unit-area for a 2D disk source or activity-per-unit-volume for a 3D volumetric source. The distributed source option applies only to radionuclides that are chosen after the checkbox has been selected. If the distributed source option is unchecked, subsequently selected radionuclides will have activities expressed as total inventory instead of distributed activity. The user is cautioned to be certain of the activity units in a given dosimetry calculation.

2.1.5 Geometry Parameters and Multiple Cover Calculator

The geometry parameter Source Irradiation Geometry box (Figure 2-5, shown on the right above the large VARSKIN 6 logo) changes contingent on the particular geometry chosen for the calculation (slab geometry in this example). The user can choose the units of each parameter from the dropdown lists provided to the right of each input field. The units can be mixed for the different parameters; VARSKIN 6 makes the necessary conversions internally. Table 2-1 shows the default values for the various parameters.

2.1.6 Default State

VARSKIN 6 allows the user to save one default state for easy retrieval at a later time. If the user wishes to change the default settings of Table 2-1, the following actions should be taken. From the File dropdown menu, if the user selects “Save Default State,” a file is written that contains all input parameters for the geometry described at that moment. At a later time, if that geometry is to be run again, the user can select “Load Default State,” and all parameter values will return to their values at the time the default state was last saved.

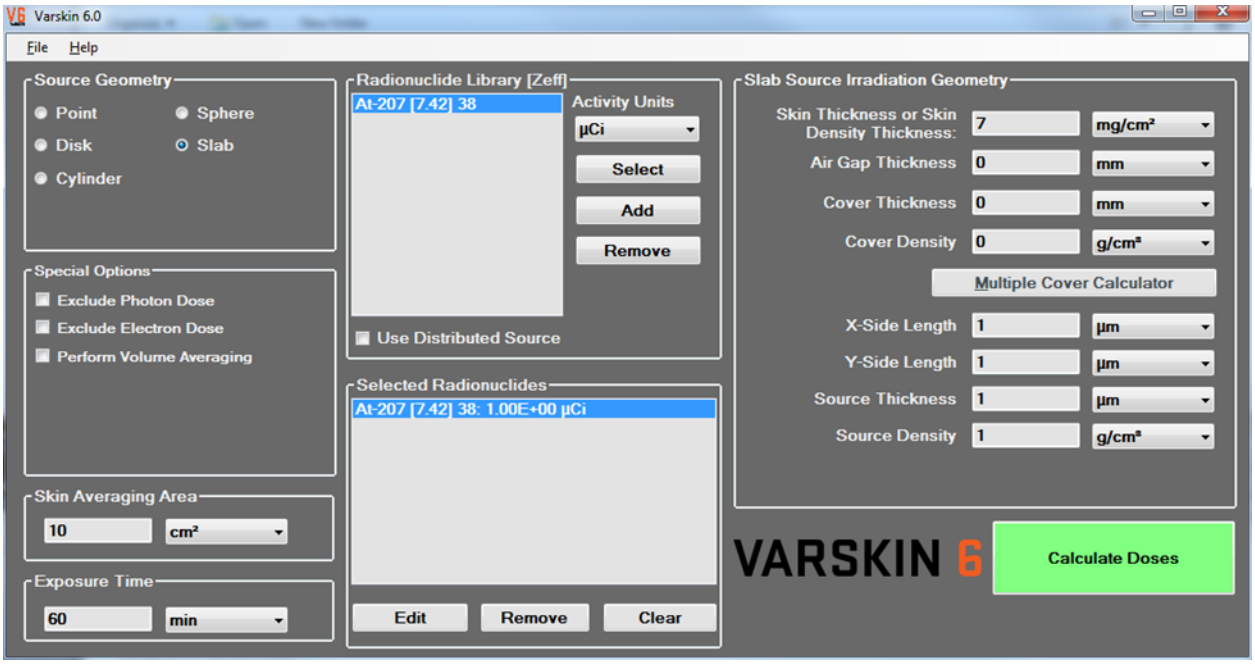

Figure 2-5 Slab Source Geometry Parameters (middle right)

In the disk geometry package, the user has the option of entering either the source diameter or the source area. This feature simplifies data entry for two-dimensional sources where the area and the total activity are known.

Table 2-1 Default Values and Units for Geometry Parameters

Parameter	Default Value
Skin Density Thickness	7 mg/cm^2
Air Gap Thickness	0 mm
Air Density (at standard temp & pressure, STP)	0.001293 g/cm^3
Cover Thickness	0 mm
Cover Density	0 g/cm^3
Source Area (Disk)	0.785 mm^2
Source Diameter (Disk)	1 mm
Source Diameter (Cylinder)	1 mm
Source Thickness (Cylinder)	1 mm
Source Diameter (Sphere)	1 mm
Source Thickness (Slab)	1 mm
Source X-Side Length (Slab)	1 mm
Source Y-Side Length (Slab)	1 mm
Source Density (Three-Dimensional Geometries)	1 g/cm^3

Source thickness and source density are equally important for calculating skin dose, especially for electron dosimetry. It is essential that these parameters are known accurately; otherwise, if necessary, their values should be underestimated so that conservative dose calculations will result. Modeling a lower source density and thickness decreases the effects of self-shielding, which in turn will generally increase shallow skin dose. If source dimensions are unknown, the following guidelines will help in choosing appropriate values:

- Diameter (disk and cylinder) and side lengths (slab): For sources of the same activity, the dose calculation for most radionuclides is relatively insensitive to these lengths for dimensions less than about 2 mm (for undetermined reasons, experience has shown that any source diameter less than about 0.2 nm will cause the code to freeze). Overestimating source dimensions will generally result in an overestimation of dose, unless the source size is larger than the averaging area.
- Thickness (disk and slab) and sphere diameter: The electron dose calculation is very sensitive to these dimensions, especially at low energies. Minimizing the value of this dimension will provide an overestimate of electron dose. For photons, these dimensions are not as critical for the dose calculation.
- Source density (volumetric geometries): For electron dosimetry, users should choose a source density that is consistent with the material containing the source. For hot particle contaminations, a typical density of stellite (cobalt/chromium alloy) is 8.3 g/cm^3, and a density of 14 g/cm^3 and effective Z of 25.8 is typical for fuel. For photon dose estimates,

the source is assumed to be air, with negligible consequence, except for large, dense sources and very low-energy photons.

Users can model the presence of a cover material and/or an air gap. The schematic drawing below (Figure 2-6) depicts the cylindrical source geometry to illustrate the cover/air-gap model. The required input to describe the cover is material thickness and its corresponding density. Both parameters are needed to account for the $1/r^2$ dependence of the Berger point kernel (geometric attenuation) and for the energy loss due to attenuation or residual energy absorption (material attenuation). For the air-gap model, only the thickness of the air gap is required for input.

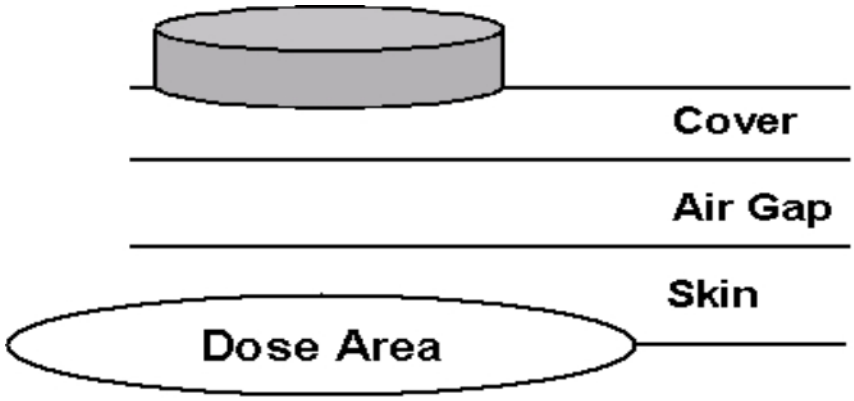

Figure 2-6 Schematic Showing the Cover Material and Air Gap Models

The physical characteristics of the air gap and cover material can significantly affect the calculated skin dose. While the air gap has little consequence for material attenuation, its effect on geometric attenuation can be significant for electron dosimetry. The air gap in photon dosimetry has the effect of disrupting charged particle equilibrium (CPE) and can appreciably influence dose at very shallow depths in tissue. Cover materials influence both the geometric and material attenuation. Table 2-2 gives some suggested thickness and density values.

VARSKIN 6 allows multiple cover materials to be modeled as a composite cover when the user clicks on the “Multiple Cover Calculator” button (Figure 2-1). The multiple-cover calculator allows the user to combine up to five covers (Figure 2-7). The user must enter a value for two of the following three parameters for each layer (while ensuring that the third parameter is blank): cover thickness, cover density, and cover density-thickness. The user can choose the units for density and thickness, but the value of density-thickness must be entered in mg/cm^2. The calculator determines the third parameter, combines the different layers, and calculates an effective thickness and density of the composite cover. The appropriate input boxes in the Source Geometry window are then populated with the composite cover density (mg/cm^3) and thickness (mm). If the user enters all three parameters, VARSKIN 6 will indicate an error and ask the user to enter only two of the three parameters for a given layer. The printout from a dose calculation will include the data for each cover layer, as well as the composite cover data.

Table 2-2 Suggested Values for Cover Thickness and Density

Material	Thickness (mm)	Density (g/cm^3)
Lab Coat (Plastic)	0.2	0.36
Lab Coat (Cloth)	0.4	0.9
Cotton Glove Liner	0.3	0.3
Surgeon Glove	0.05	0.9
Outer Glove (Thick)	0.45	1.1
Ribbed Outer Glove	0.55	0.9
Plastic Bootie	0.2	0.6
Rubber Shoe Cover	1.2	1
Coveralls	0.7	0.4

To include more than five covers in the composite cover calculation, the user should calculate the composite cover thickness and density for the first five covers and then run the calculator again entering the first composite cover thickness and density as one of the layers. Accordingly, if a composite cover is entered as one of the covers, the layers composing the composite cover will not be individually displayed in the printout.

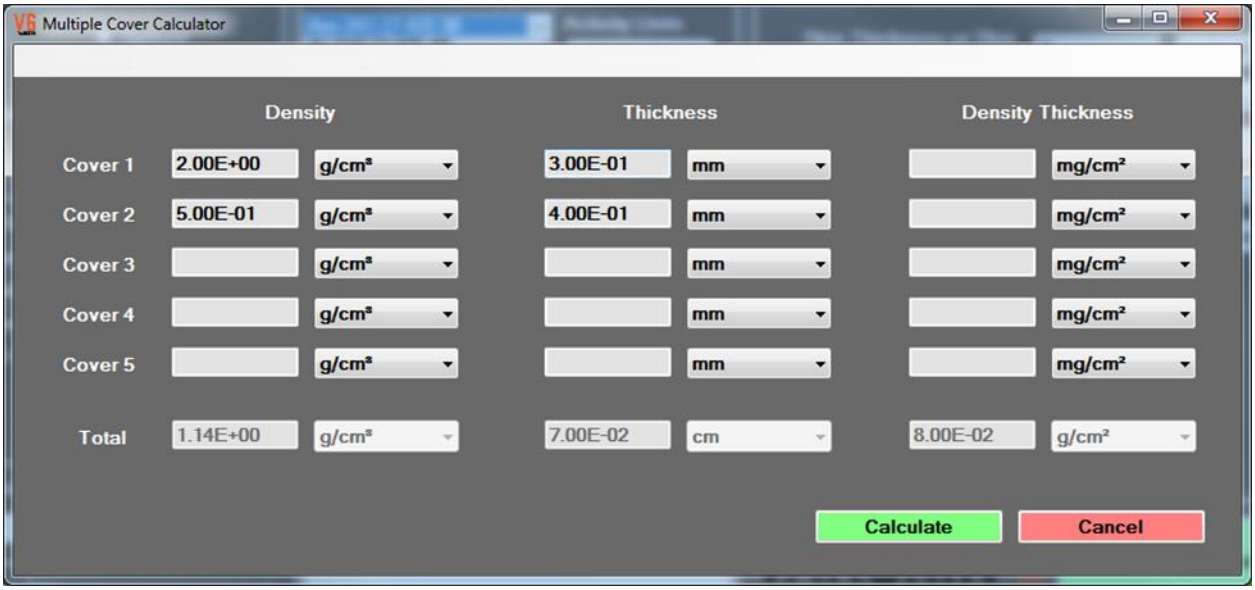

Figure 2-7 Multiple Cover Calculator Window

For example, suppose each of the items in Table 2-2 (same density and thickness) were somehow part of a composite cover. The cover calculator could be used on the first five items resulting in a combined thickness of 1.40 mm and a density of 0.759 g/cm^3. The final four items in Table 2-2 result in a combined thickness of 2.65 mm and a density of 0.791 g/cm^3. If we then combine those two thicknesses and densities in the calculator, we obtain a final composite result of 4.05 mm thickness and 0.78 g/cm^3 density.

2.2 Special Options

In the "Special Options" box (middle left of Figure 2-1), VARSKIN 6 will display at most three options, including: (1) Exclude Photon Dose; (2) Exclude Electron Dose; (3) Perform Volume Averaging; and (4) Offset Particle Model. Options 1, 2 and 3 are displayed for every source geometry, whereas option 4 is only displayed when the point source geometry is selected.

The default for options 1 and 2 (boxes unchecked) are to calculate both photon and electron dose. The user can, however, select either of these boxes, but not both, to exclude the calculation of dose from photons or electrons. A calculated dose of zero will be displayed in the dose field as zero ("0.00E+00"), whereas the appropriate field will be blank if the user elects to exclude one or the other dose calculations.

The third special option allows the calculation of dose to be averaged over a user-defined volume of tissue described by a cylinder of specific diameter and thickness. The use of the volume-averaging dose calculation can be important, for example, in predicting the dose averaged between 10 and 15 mg/cm^2, as recommended by the International Commission on Radiological Protection (1991), for evaluating the dermal effects of skin dose.

If volume averaging is chosen, the user is prompted (after selecting the "Calculate Doses" button) to enter the skin density thicknesses within which to bound the dose calculation (shallow and deeper tissue depths defining the cylindrical averaging volume). In this instance, skin density thickness must be entered in units of mg/cm^2. A range of suggested values for the shallow and deep tissue depths is provided based on the physical range of electrons associated with the selected radionuclide. Suggested values are from a skin density thickness of 0 mg/cm^2 to the maximum penetration depth of the electrons being modeled; however, any non-negative value of density thickness can be entered. The user is cautioned, however, to be certain of the depths requested; some depths may result in negative values for beta dose. If the user elects to exclude the calculation of electron dose, the shallow and deep depths will default to 0 mg/cm^2 and 1000 mg/cm^2. The VARSKIN model calculates the dose over the averaging area at 10 discrete layers between the shallow and deep tissue depths (Figure 2-8). Thus, the volume-averaged dose model requires 10-fold more execution time than that for a single depth.

The offset particle model, which allows dose to be calculated for a particle that is not centered over the dose area of interest, is useful for calculating dose from multiple hot particles. The offset particle model is off unless selected by the user. When the "Offset Particle Model" box is checked, the user is prompted to enter the offset distance. The offset distance is the lateral distance between the point source and the center of the skin averaging area. The value of the offset is the only additional input value that is required for the model. The dose result window will display the offset value, if this option has been selected. The offset particle model is for photon dosimetry only and is described in more detail in Section 3.

2.2.1 Calculating Dose

Once the desired geometric parameters and options have been selected, the user initiates the calculation by clicking the “Calculate Doses” button (Figure 2-1). A progress bar will appear below the VARSKIN 6 logo, which will scroll repeatedly depending on the complexity of the calculations. The number of radionuclides to be analyzed and the various options that have been selected will impact the calculation time.

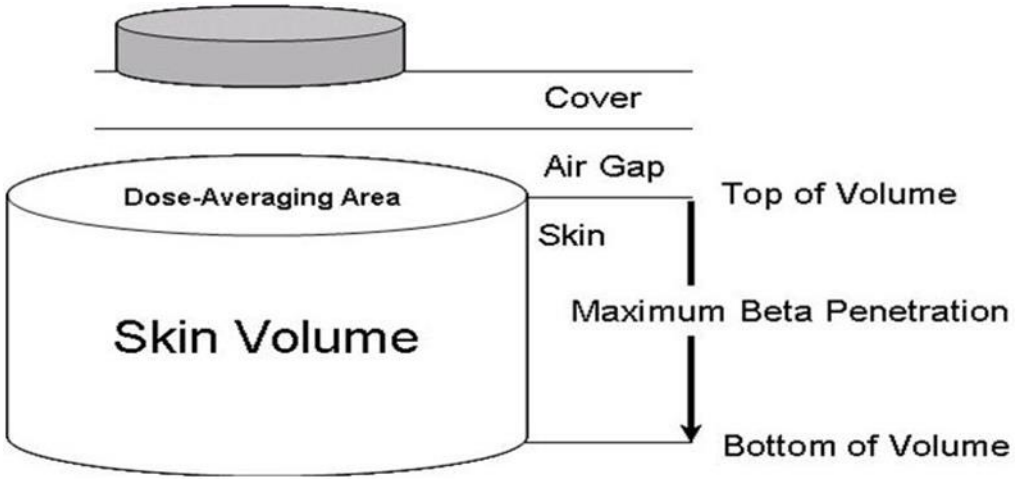

Figure 2-8 Schematic Diagram of the Volume-Averaged Dose Model Geometry

VARSKIN 6 calculates dose using compiled FORTRAN programs entitled *VarCalc.exe* and *GamCalc.exe*. When the user clicks the “Calculate Doses” button, the GUI writes the input data in a file called *output.dat*. *VarCalc.exe* and *GamCalc.exe* read *output.dat*, perform the calculations, and then write results to a file entitled *results.dat*. The GUI reads *results.dat* and displays those results in the output window. Note that *output.dat* and *results.dat* are internal files and are not intended to be accessed or edited by the user.

2.2.2 Output Window

The Results window for a non-volume-averaged calculation (Figure 2-9) is displayed when the dose calculation is complete. The window is separated into three distinct sections: results for individual radionuclides (upper left quadrant), combined results for all radionuclides (upper right quadrant), and source input data (lower half).

In the individual results section of the initial display, only the results for the first radionuclide are shown. The results from other radionuclides are viewed by highlighting the radionuclide of interest in the list box (upper left). This will display only the contribution to the dose from the selected radionuclide. The combined results section continues to display the total dose for all radionuclides. The data in this section cannot be edited and will not change unless a new calculation is made. This section of the output window also contains unit selection bubbles, which allow the user to select dose results in English or International (SI) units.

The lower half of the results window contains a mirror of the input data entered in the Main Input window. The format of this section will change depending on the geometry chosen for the calculation. This area of the output also contains buttons that allow the user to perform certain functions. Selecting the “Print Results” button prompts the user for a title and then creates an

.html file containing the data in the output window. Additionally, the user may save the input data to the calculation by closing the output window and selecting “Save” from the “File” dropdown list of the Main Input window.

A slightly different results window will appear for volume-averaged dose calculations (Figure 2-10). Since the dose could be averaged over different averaging volumes for different radionuclides, VARSKIN does not provide a section for combined results of a volume-averaged dose calculation. Instead, only the individual results from the highlighted radionuclide is displayed at any one time. The upper left section of the volume-averaged results window displays values of the shallow and deep skin depths, as well as the total volume over which the dose was averaged for the chosen radionuclide. Other radionuclides can be chosen individually by highlighting them in the radionuclide list box. As with the other results window, this output screen contains unit-selection bubbles allowing the user to select volume-averaged dose results in English or SI (Systeme Internationale) units. Again, a summary of the input parameters is displayed on the lower half of the screen and the print option (to an .html file) is available.

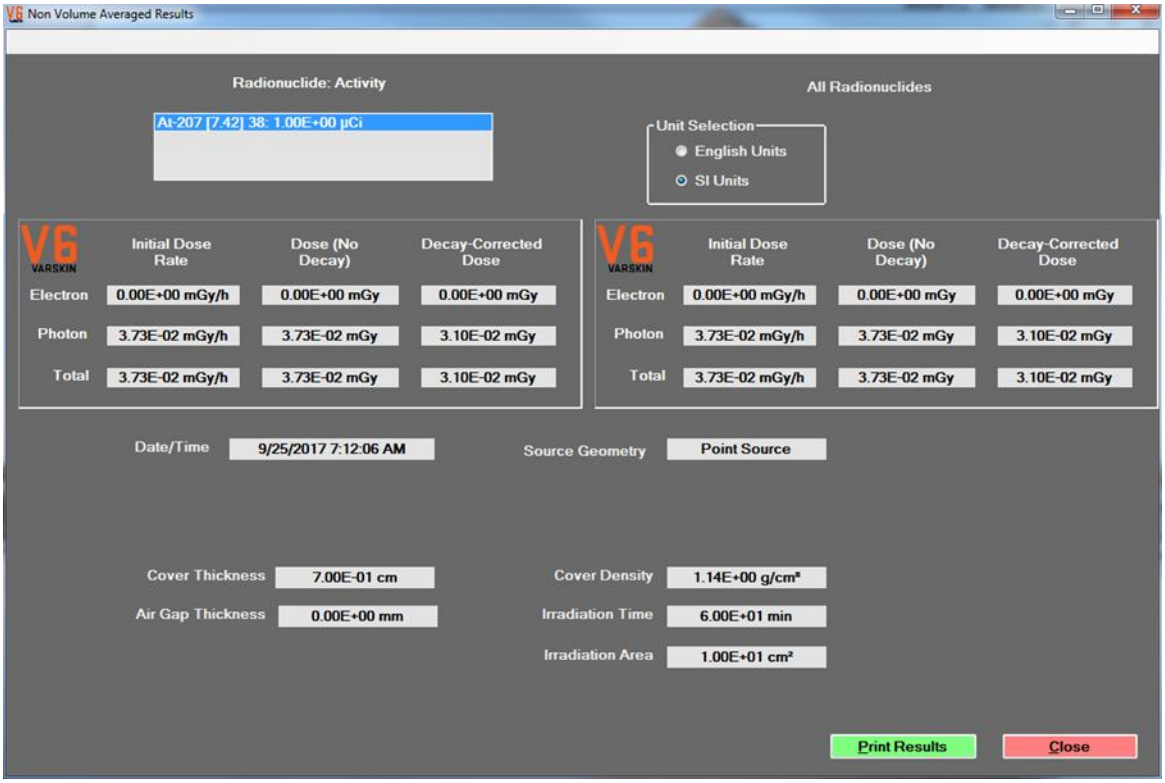

Figure 2-9 Results Window for a Typical Calculation

Calculations of dose and dose rate are carried out in the FORTRAN executable files and sent to the GUI for display. Decay-corrected and no decay doses are calculated in the GUI. An error was found in VARSKIN 5.2 that resulted in extremely high doses being calculated by the GUI for short-lived nuclides. The solution was to limit dose integration (from dose-rate) to no more than 20 half-lives; this solved the calculation problem.

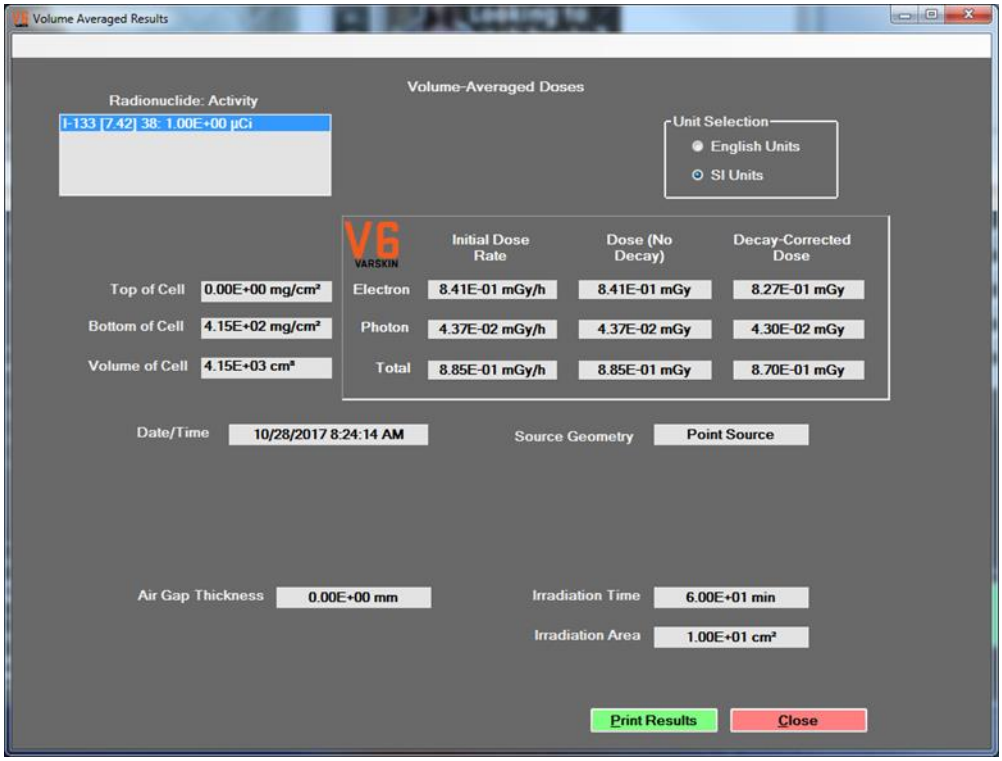

Figure 2-10 Results Window for a Volume-Averaged Calculation

2.3 Exiting VARSKIN

The VARSKIN code is exited from the main window (Figure 2-1), either by clicking the "X" in the upper right corner or by selecting "Exit" from the File dropdown menu. Before exiting, the user is asked if the current input file is to be saved. When the "Yes" button is clicked, the user is asked to create a file name in which the input data will be saved so that the calculation can be recreated. Clicking the "No" button will cause the program to end without saving the current data. Clicking the "Cancel" button will return the user to the Main Input window.

Data from a saved file are stored with a *.vs6* extension. When a saved file is recalled (by selecting "Open" from the File dropdown menu), VARSKIN 6 reads the *.vs6* to obtain the data for the calculation. These are internal files, should not be edited by the user.

3 DESCRIPTION OF DOSIMETRY MODELS

VARSKIN 6 uses updated electron (Mangini 2012; Hamby et al. 2014) and photon (Hamby et al. 2009) skin dosimetry models, which this chapter describes in detail. In addition, improvements to models throughout the VARSKIN series are incorporated and described herein.

3.1 Beta Dosimetry

As with VARSKIN 6, dosimetry codes based on the dose-point kernel (DPK) method rely on the numerical integration of a point kernel over the source volume and dose region of interest. While this is computationally much faster than a Monte Carlo simulation, accuracy is often sacrificed with the point kernel simplification. In one way or another, all DPKs relate the dose at a given point to a radiation source at some other point in a homogeneous medium. The medium for which the DPK is defined is typically water, as this allows for direct comparison with tissue. If the medium is not water, various scaling techniques (discussed later in this section) can be used to quantify energy loss along the charged-particle track and to simulate the scatter of particle energy.

3.1.1 Dose-Point Kernels

Doses in VARSKIN 6 are calculated through numerical integration methods where dose-point kernels are integrated over the entire source volume and dose averaging area. The point kernel is given by:

$$\dot{D}_\beta(r)\left[\frac{Gy}{\sec}\right] = \frac{1.6x10^{-10}\left[\frac{J\ \mathrm{g}}{MeV\ \mathrm{kg}}\right]\cdot A\left[\frac{dis}{\sec}\right]\cdot Y\left[\frac{\beta}{dis}\right]\cdot \overline{E_\beta}\left[\frac{MeV}{\beta}\right]\cdot F_\beta(\xi)}{4\pi r^2\cdot \rho\left[\frac{\mathrm{g}}{cm^3}\right]\cdot X_{90}[cm]} \qquad [3.1]$$

where $F_\beta(\xi)$ represents a scaled absorbed dose distribution (Berger 1971; Mangini 2012). The parameter ξ represents the density scaled distance (includes distances in the source cover, clothing, and air) from the source point to the dose point, written as a ratio normalized to the X_{90} distance. The distance r is the physical distance between the source point and the dose point.

The development of Monte Carlo electron transport codes over the years has brought with it the tabulation of increasingly accurate electron dose-point kernels. The main advantage of Monte Carlo-based energy deposition kernels is the ability to account for energy-loss straggling and provide more accurate results for $r > 0.9X_{90}$ (see Figs. 3-1 and 3-2). VARSKIN 6 calculates $F_\beta(\xi)$ using the Monte Carlo-based energy deposition kernels ($I(r)$) described below, thereby replacing Spencer's (1955, 1959) moment-based energy dissipation distributions used in the VARSKIN software through V4.0.

The Monte Carlo transport code, EGSnrc (Ljungberg 2012), was used to determine the radial energy distributions (or DPKs) and X_{90} values at electron energies of 0.01 MeV ≤ E ≤ 8 MeV (32 total energies). An isotropic mono-energetic point-source was positioned at the center of concentric spherical shells of the respective media. For all simulations, the shell thickness was 5% of the continuous slowing down approximation (CSDA) electron range, as taken from the ESTAR software of the National Institute of Standards and Technology (NIST). The last shell was at a radius 150% of the CSDA range to ensure complete absorption of the electron energy

(excluding radiative-losses). The maximum energy of 8 MeV covers all beta-particle endpoint energies published in ICRP Publication 107 (2008). The minimum energy of 0.01 MeV is based on the 0.001 MeV lower limit of electron cross-section data available in the Electron Gamma Shower (EGS) software. Additionally, the ESTAR CSDA range of a 0.01 MeV electron is only 0.252 mg cm^{-2}.

The EGS software was updated by the National Research Council (NRC) of Canada to create EGSnrc. The EGSnrc simulations were performed using the EDKnrc user code. The EDKnrc code can be used to calculate Energy Deposition Kernels (EDK) for photons or electrons (mono-energetic or poly-energetic) forced to interact at the center of a spherical geometry (Rogers 2011). The code can output energy deposition kernels in user defined spherical shells. The number of particle histories was set to one million and transport parameters were set to default settings except that: (1) PEGS data sets used with AE=AP=1 keV; (2) ECUT=PCUT=1 keV; (3) Rayleigh scattering is turned on; and (4) bremsstrahlung cross sections are set to NIST.

PEGSs data sets are the material cross section data used by EGSnrc. The parameters of AE and AP determine the lowest energy for which the cross-section values are defined. Generally, when AE and AP are lowered (minimum of 1 keV), the accuracy of the calculation increases; however, the computation time increases as well (Kawrakow and Rogers 2000). Electrons with energies below AE will not be transported and their energy is assumed to deposit locally. The same is true for photons (AP). The parameters ECUT and PCUT are related to AE and AP in that when an electron/photon energy falls below ECUT/PCUT, its energy is assumed to deposit locally. It is not possible to set ECUT and PCUT below AE and AP, respectively. These two parameters represent the Δ value in restricted stopping powers.

Turning on the Rayleigh scattering parameter allows for the simulation of coherent scattering. Raleigh scattering for bremsstrahlung photons may become important below ~1 MeV for high-Z materials and below 100-200 keV in low-Z materials. The updated NIST database for nuclear bremsstrahlung is strongly recommended for electron energies below 1-2 MeV with negligible improvements over default Bethe-Heitles cross sections above ~ 50 MeV. Sampling from the NIST database is faster at low energies but slower at high energies (Kawrakow and Rogers 2000).

Once the energy deposition kernels were determined at CSDA range increments, the X_{90} values for each energy were determined and the kernels re-tabulated with respect to ξ. These kernels were then read into *SadCalc.exe* for use in the SADD (scaled absorbed dose distribution) subroutine and SPENS function. As stated previously, the main advantage of Monte Carlo-based energy deposition kernels over moment-based kernels is the ability to account for energy-loss straggling, thereby improving dose estimations with depth. This is easily seen by plotting $F(\xi,E_0)$ values determined using both moment-based (VARSKIN 4 and earlier) and Monte Carlo-based (VARSKIN 5 and later) methods (Figure 3-1 and 3-2).

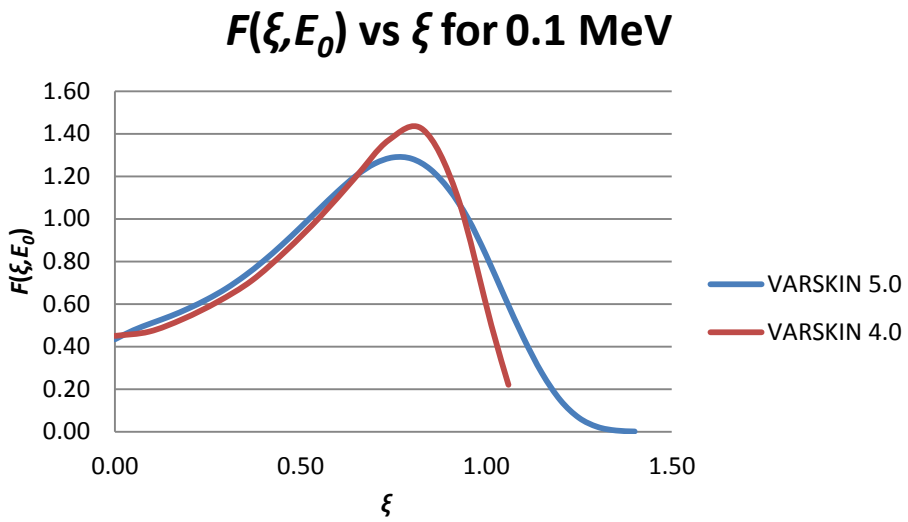

Figure 3-1 Scaled Absorbed Dose Distributions for 0.1 Mev Electrons

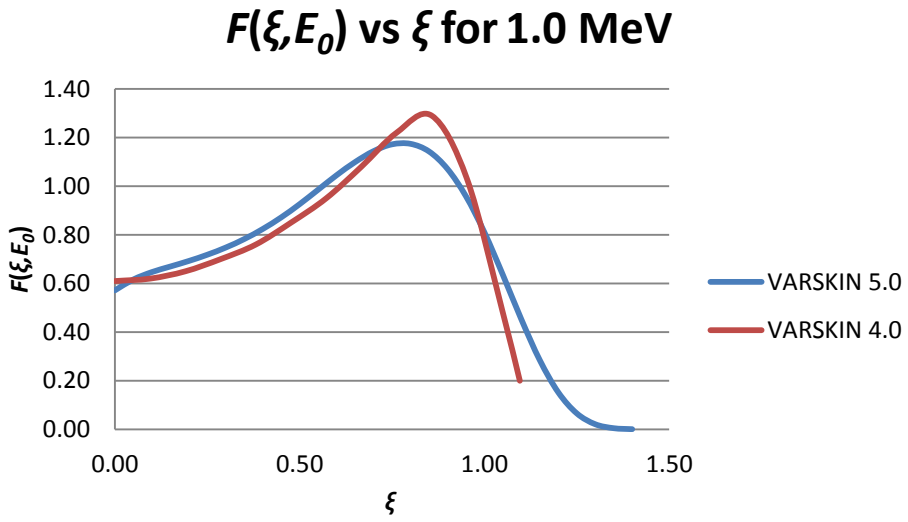

Figure 3-2 Scaled Absorbed Dose Distributions for 1.0 Mev Electrons

3.1.2 Numerical Integration of Dose-Point Kernels

DPK codes rely on an accurate and fast numerical integration method to calculate dose from a volumetric source to a given dose area. A typical integration process divides the source into very small sub-volumes (source points). The dose averaging area is divided into points at which the dose rate is to be calculated (dose points). The dose points (60 are used in VARSKIN 6) are positioned along the radius of a dose-averaging disk at a specified dose depth (Figure 3-3). Since the source geometry (cylindrical is used for this discussion) is symmetric about the dose-averaging area, dose points represent concentric isodose circles that describe the radial dose profile at a given depth in skin.

For each of the sixty dose points, a numerical integration is performed over the area of the cylindrical source at a given height in the source represented by eight elevations (z), eight radii (r'), and eight angular locations (θ). The dose rate at a dose point on an isodose circle of radius d' is evaluated using

$$\dot{D}(d') = S_v \int_0^{2\pi} \int_0^R \int_0^Z r' \; B(z, r', \theta) \; dz \; dr' \; d\theta \qquad [3.2]$$

where $B(z,r',\theta)$ is the dose per disintegration (rad nt^{-1}) from a source point with source-coordinates (cylindrical) of z, r', and θ; R and Z are the source radius and height; and S_v is the volumetric source strength (nt cm^{-3}). This procedure is repeated for each dose point beginning at the center of the irradiation area and extending to its edge. The dose rate averaged over an area at depth in the tissue is then calculated using

$$\bar{D} = \frac{2\pi \int_0^R \dot{D}(d') \; d' \, dd'}{\pi R^2} \qquad [3.3]$$

where R is the radius of the dose averaging area.

The integration starts by choosing one of the eight elevation points (▲) in the source (Figure 3-3). At one of these elevations, one of eight concentric circles (radial source-points ●) is chosen. One of these circles is then subdivided into eight source-points at 45-degree angles from each other (angular source-points ★). Finally, the dose rate is calculated at each dose point from each of these eight source-points at a given elevation and radius. The contribution to the dose from the first four points is compared to the contribution of the last four points in a given circle. If the relative difference between the two contributions is less than 0.01 percent, then convergence of the integral is achieved, and the procedure is repeated at the next radial position. If the relative difference between the two contributions is greater than the relative error, each of the two contributions is further subdivided into eight additional source-points, and the above procedure is repeated for each of the two sets of eight points. This process, known as the Newton-Cotes eight-panel quadrature routine, provides a fast and accurate method of numerically integrating complex functions such as dose-point kernels (Durham 1992, 2006; Hamby 2011).

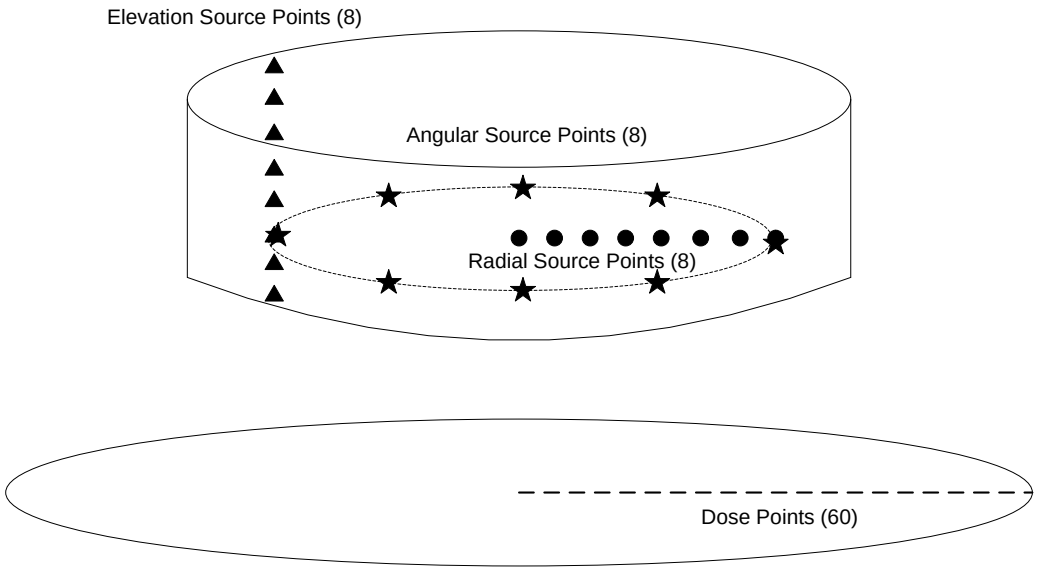

Figure 3-3 Schematic of the Eight-Panel Quadrature Routine (redrawn from Durham 2006)

3.1.3 Homogenous Dose-Point Kernels

The Monte Carlo transport code, EGSnrc (Ljungberg 2012), was used to determine the radial energy distributions (or DPKs) and X_{90} values for $7.42 < Z \leq 94$ (Figure 3-5, Table 3-1) at electron energies of 0.01 MeV ≤ E ≤ 8 MeV (30 total values). An isotropic mono-energetic point-source was positioned at the center of concentric spherical shells of the respective media (Figure 3-4). For all simulations, the shell thickness was 5% of the CSDA electron range, as taken from the ESTAR software provided by NIST. The last shell was at a radius 150% of the CSDA range to ensure complete absorption of the electron energy (excluding radiative-losses). The maximum energy of 8 MeV covers all beta-particle endpoint energies published in ICRP Publication 107 (2008). The minimum energy of 10 keV was chosen considering the 1 keV lower limit of electron cross-section data available in EGSnrc. Additionally, the CSDA range of a 10 keV electron is nominally 2.5 microns in water.

Monte Carlo simulation with the MCNP (Monte Carlo N-Particle) software can be useful to determine energy deposition kernels when the Integrated TIGER Series (ITS) software energy indexing algorithm is used and when special care is taken for high-resolution measurements (LANL 2003). EGSnrc on the other hand, was not only shown to be step-size independent, but it is significantly faster at transporting electrons than MCNP. For example, MCNP requires 103 minutes of central processing unit (CPU) time to measure energy deposition kernels for 1 MeV electrons in water (10^6 particle histories), whereas EGSnrc requires 9 minutes for the same simulation. This difference becomes even larger as electron energy and material Z increases. For these reasons, EGSnrc is used as the Monte Carlo code of choice for all simulations pertaining to the scaling and scattering models.

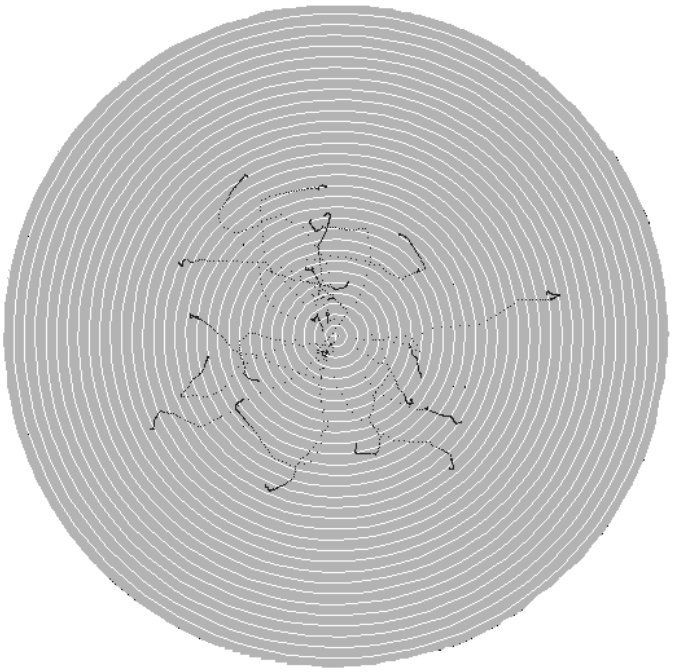

Figure 3-4 Schematic of EGSnrc Geometry for Determining Point-Source

Each shell thickness is 5% of the CSDA electron range. Total spherical radius is 150% of CSDA electron range. Simulated electron tracks are represented by the dark dotted lines.

Table 3-1 List of Source Materials Used to Develop the Scaling Model

Element	*Z*	Density (g cm^{-3})	Element	*Z*	Density (g cm^{-3})
Aluminum	13	2.70	Barium	56	3.59
Titanium	22	4.54	Neodymium	60	7.01
Iron	26	7.87	Gadolinium	64	7.90
Gallium	31	5.91	Ytterbium	70	6.90
Rubidium	37	1.63	Tantalum	73	16.65
Zirconium	40	6.51	Platinum	78	21.45
Ruthenium	44	12.37	Lead	82	11.35
Silver	47	10.50	Actinium	89	10.07
Tin	50	7.31	Plutonium	94	19.84

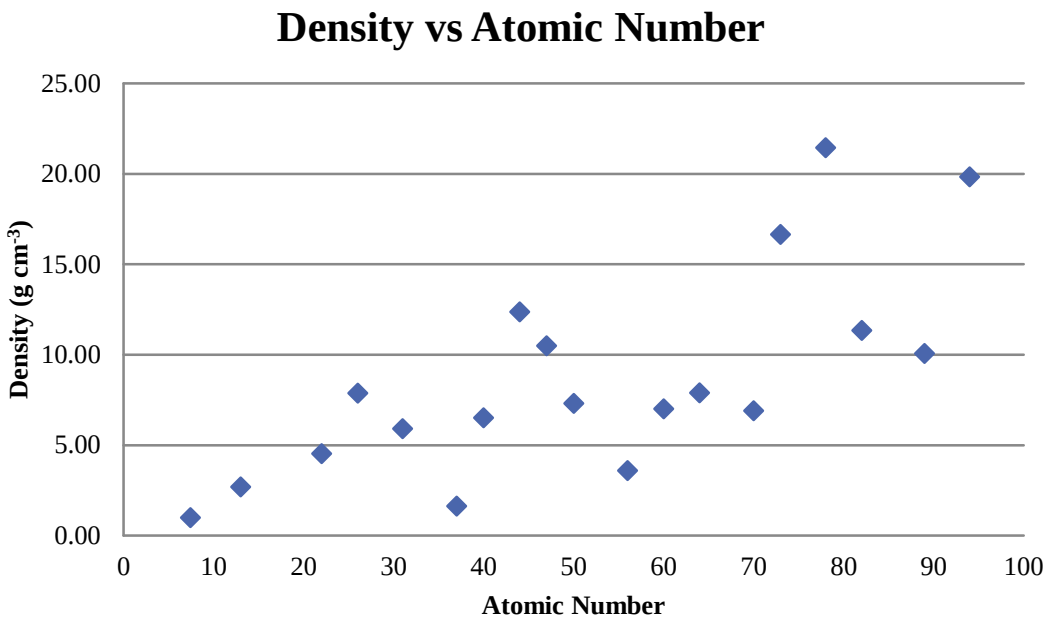

Figure 3-5 Plot Demonstrating the Wide Range of Densities and Atomic Numbers

All materials were solid in nature (except water).

EGSnrc simulations were performed using the EDKnrc user code. This code can be used to calculate EDKs for photons or electrons (mono-energetic or poly-energetic) forced to interact at the center of a spherical geometry (Rogers 2011). The code can output energy deposition kernels in user defined spherical shells.

3.1.4 Non-Homogenous Dose-Point Kernels

Non-homogeneous point-source DPKs also were determined for $7.42 < Z \leq 94$ at $0.01 \text{ MeV} \leq E \leq 8 \text{ MeV}$ using EGSnrc Monte Carlo simulations using identical transport parameters. The intent of calculating non-homogeneous DPKs is to determine how energy is deposited in spherical shells of water after a mono-energetic electron has been emitted from the center of a sphere composed of some medium other than water.

3.1.5 Beta-Particle Dose-Point Kernels

The end goal of the scaling model is the determination of non-homogeneous DPKs from homogeneous DPKs for beta-emitting radionuclides. By determining the depth and energy-scaling parameters for all energies between 0.01 and 8 MeV, it is possible to determine the non-homogeneous beta DPK for any known beta energy spectrum. This is accomplished by integrating over the beta energy spectrum for each source *Z*/thickness using

$$\Phi_{\beta}(R,Z,\rho) = \frac{1}{E_{av}} \int_{0}^{E_{\max}} ESP(R,E,Z,\rho) E\ N(E) \Phi(r,E) dE \qquad [3.4]$$

where r is the spherical shell radius, E_{max} is the endpoint energy of the beta spectrum, $N(E)dE$ is the fraction of electrons emitted per MeV per disintegration that have energies between E and $E+dE$, and

$$E_{av} = \int_0^{E_{max}} E\ N(E)dE \qquad [3.5]$$

For example, if the nuclide and source material in question are ^{60}Co and iron, the scaling parameters are used to create an n x m array of DPKs for ^{60}Co with source radii ranging from 0 to $\boldsymbol{a}\cdot X_{90}$ of iron and the water radii ranging from 0 to $\boldsymbol{b}\cdot X_{90}$ of water. The parameter $\boldsymbol{a}$ is based on complete electron energy absorption in the source material and $\boldsymbol{b}$ is based on complete electron energy absorption in water when the source thickness is zero.

Non-homogeneous beta-particle DPKs were determined by incorporating scaling equations into *SadCalc.exe*. The *SadCalc.exe* routine utilizes ICRP Publication 107 (2008) beta-emission spectra to calculate homogeneous water DPKs for each electron present in a given dose calculation. Linear interpolation was used to accommodate all source media with $7.42 \leq Z_{eff} \leq 94$.

Non-homogeneous DPKs were calculated for a wide range of electron energies (Table 3-2) and source materials (Table 3-3). Stainless steel and uranium oxide were chosen as they represent common hot particle materials, and tungsten alloy was chosen to demonstrate the model's ability to handle high-density media.

Table 3-2 List of Nuclides Used in Scaling and Scattering Models

Nuclide	$\bar{E}$ (MeV)	X_{90} (cm)
^{60}Co	0.0958	0.033
^{90}Sr	0.196	0.083
^{210}Bi	0.307	0.212
^{135}I	0.375	0.239
^{89}Sr	0.583	0.321
^{32}P	0.695	0.363
^{56}Mn	0.832	0.634
^{90}Y	0.934	0.533
^{144}Pr	1.217	0.696

Table 3-3 Source Materials Used for Non-Homogeneous Electron DPK Testing

Alloy	Z_{eff}	Density (g cm^{-3})
Stainless Steel (SS_302)	25.81	8.06
Tungsten Alloy (Mallory2000)	72.79	18.00
Uranium Oxide	87.88	10.96

3.1.6 Backscatter Model

A volumetric backscatter model is used in VARSKIN 6 to predict the dose perturbations from both source and atmospheric backscattering. The model is applicable for electron-emitting radionuclides in a spherical, cylindrical and slab source geometry, and for source materials with $7.42 < Z_{eff} \leq 94$. Being based on the DPK concept, VARSKIN 6 relies on the numerical integration of a point kernel over the source volume and the dose region of interest. The medium for which the DPK is defined is typically water, thus allowing for direct comparison with tissue. While the electron scattering contribution has been studied extensively for medical physics applications, it has been limited to point-source assumptions in the past yet has been expanded to volumetric sources for use in VARSKIN 6. In addition to internal source scatter, electron scattering must also be considered in the medium surrounding the source (i.e., atmospheric scattering).

Inherent to the development of electron DPKs is the assumption of an infinite homogeneous medium (water/water interface). The isotropic nature of DPK's assumes that electrons emitted away from the dose point can scatter back toward the dose point in an infinite homogeneous water medium and possibly contribute to dose at the point of interest. While scaling methods account for the non-homogeneous media that transmit the electrons, an additional adjustment is required to correct for the lack of scatter since an atmospheric medium is above the skin rather than a modeled water medium (i.e., an air/water interface). In the situation of a source resting on the skin, the air above the source (air/water interface) results in less backscatter than would have been modeled in developing the DPKs. This scenario is of particular importance for hot particle skin dosimetry.

In developing the electron dosimetry model for VARSKIN 5 (Mangini 2012), point-source planar dose profiles were determined using EGSnrc Monte Carlo simulations for the scattering media of water, air, and source materials with $7.42 < Z_{eff} \leq 94$ at electron energies of $0.01 \text{ MeV} \leq E \leq 8$ MeV. The planar dose volumes were 1 mg cm^{-2} thick, with a maximum normal depth of 1000 mg cm^{-2}. The dose averaging areas were 1 cm^2 and 10 cm^2, consistent with the monitoring areas recommended by ICRP Publication 103 (2007) and NCRP (National Council on Radiation Protection & Measurement) Statement No. 9 (2001), respectively. The scattering medium was assumed infinite (>> electron range) in both thickness and lateral extent.

In general, a backscatter factor is found by taking the ratio of the planar dose when the scattering material is present (non-homogeneous case) to that when water is present (homogeneous case). Air scattering corrections often are reported inversely such that they are greater than or equal to one (Cross 1991b, 1992c). Regardless, these backscatter factors will be dependent on electron energy, the effective atomic number (Z) of the backscattering medium, normal depth, and dose averaging area. When applied to an electron-emitting nuclide, the backscatter factor for a given dose averaging area takes the form of

$$B_\beta(Z,z) = \frac{\int_0^{E_{\max}} D_{A,S}(Z,z,E)N(E)dE}{\int_0^{E_{\max}} D_W(z,E)N(E)dE} \quad [3.6]$$

where z is the normal depth, D_W is the dose in the water/water geometry, $D_{A,S}$ is either the dose in the air/water geometry or the dose in the source/water geometry, and $N(E)dE$ is the fraction

of electrons emitted per MeV per disintegration that have energies between *E* and *E+dE.* Surface functions were used to determine mono-energetic electron planar dose profile curve fits for use in Eq. [3.6]. Once planar dose profile curve fits were determined, they were implemented into *SadCalc.exe*. The ICRP 107 electron-emission spectra were then used to calculate the electron backscatter factor of Eq. [3.6]. Linear interpolation was used for all $7.42 < Z \leq 94$.

It is important to remember that it is not possible to determine the absolute volumetric backscatter factor using the same procedures as point-sources. This is due to the largely different energy-degradation properties of air and water and their impact on the respective dose calculations. Therefore, a number of assumptions and estimations were made.

The method is based on a selective integration process over the entire source volume. Rather than applying an overall correction factor to final dose calculations, scattering corrections are applied at each step of the numerical integration of dose. If desired, the 'volumetric' correction factor could then be determined by taking the ratio of overall dose with the applied point-source scattering corrections to the overall dose without. Selection criteria are used to determine the proper type and amount of scattering correction for which to account. Scattering corrections are broken down into three components: source/water interface corrections (for the top and bottom of the source), air/water interface corrections (for both the top and the sides of the source), and air/source interface corrections (for the sides of the source).

During the numerical integration process for an 'infinitely large' source (dimensions > electron range), only source points positioned directly at the source/water interface (i.e., source/skin interface) will require the full application of the source/water scattering data (Figure 3-6). Source points positioned above this interface (Figure 3-7) require a more advance treatment. In this case, there is expected to be an increase in the energy absorption (i.e., dose) from downward scattering taking place in the upper portion of the source, as well as a decrease in dose from upward scattering in the lower portion of the source. If the contribution from downward scattering is greater than the contribution from upward scattering, the dose will be increased for that source-point kernel. Likewise, when the upward contribution is greater, the dose will be decreased. It can be seen from this argument that when the source point is at the top of the source, the application of both air/water and source/water correction results in an effective air/source correction.

Scattering contributions from both upward and downward scattering are determined using Eq. [3.7]. The scattering material thicknesses for the top and bottom of the source are given by the normal distances from the source-point to the upper- and lower-most points of the source, respectively. The source backscatter correction factor (BSCF) is then determined by multiplying net scattering effectiveness by the electron source/water scattering correction for point-sources;

$$Source\ BSCF_{top/bottom} = SW(SE_{top} - SE_{bottom}) \qquad [3.7]$$

where *SW* is the electron source/water scattering correction for point-sources, SE_{top} is the scattering effectiveness for the top portion of the source, and SE_{bottom} is the scattering effectiveness for the bottom portion of the source. The 'skin depth' at which the scattering factor is determined takes into account the normal density thickness of both the source and tissue through which the electron must traverse.

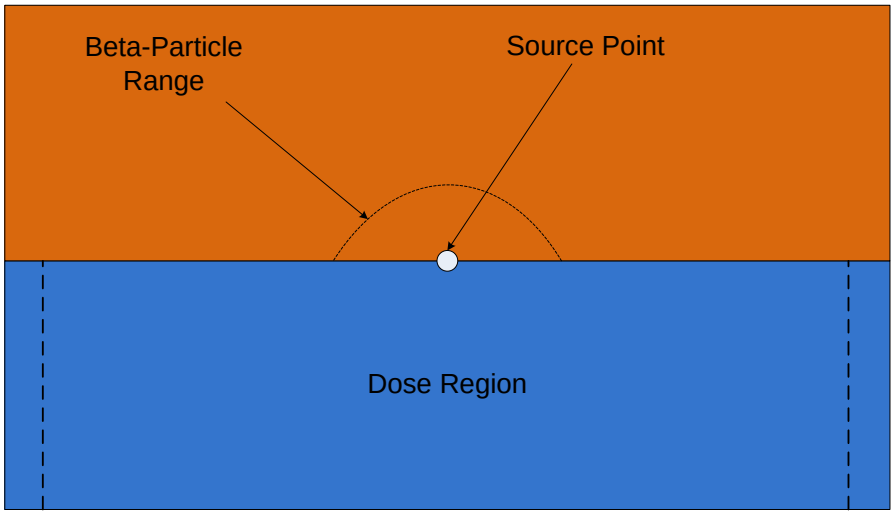

Figure 3-6 Schematic Demonstrating Conditions for Full Source-Water Scattering

The dimensions of the source (orange) are greater than the range of the electron.

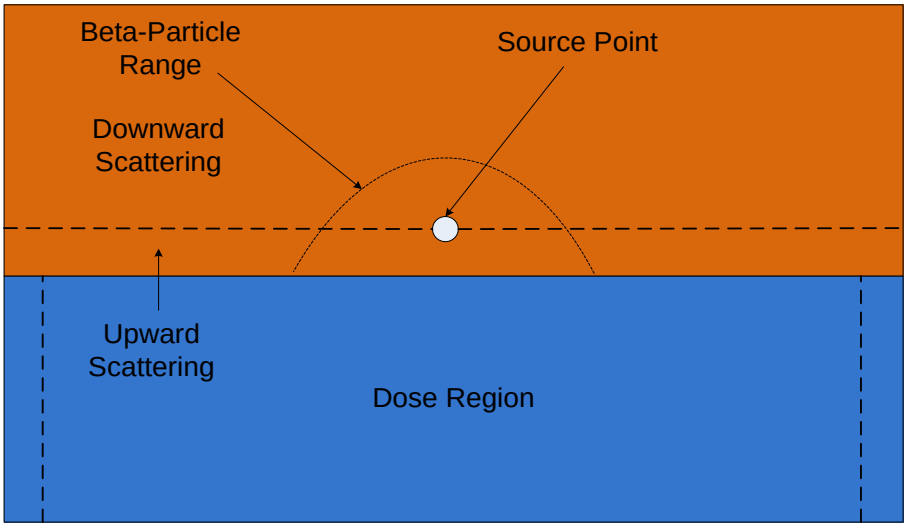

Figure 3-7 Schematic Demonstrating Conditions for Partial Source Scattering Conditions

The lower portion of the source causes upward scattering away from the dose region and the upper portion of the source causes downward scattering towards the dose region.

The point-source factors were developed with the assumption that the source medium is infinite in both height and lateral extent. As such, application to source points near or on the side of the source jeopardizes the accuracy of the results. However, approximations can be made to estimate source/scatter corrections for the sides of the source.

When the dimensions of the source are larger than the range of the electron, source points toward the center and the top-center of the source have minimal impact on dose. Therefore, source-points on both sides and the bottom of the source become more important. It is

estimated that scattering contributions from the sides of the source will reach a maximum when the scattering media thickness is 1.0 X/X_{90} and greater. Linear interpolation is used for X/X_{90} values less than 1.0.

Unlike source scattering for the top and bottom of the source, during the numerical integration process, the direction of the electron needs to be considered when correcting for side scatter. Side scattering is accounted for when the electron's path is directed away from the source and travels through air prior to reaching the dose region. The assumption is that an electron emitted in the 180 degree opposite direction would be permitted to backscatter off the source's side and still contribute to dose.

The amount of source material directly above the source point (considered the 'lateral' dimension in this case) will also have an impact on the scattering effectiveness. If the source point is located on the top corner of the source, the probability of a backscattering event toward the dose region is greatly decreased. On the other hand, if the source point is at the bottom corner of the source, the probability of backscattering event toward the dose region is much greater. It is estimated, therefore, that the normal distance to the upper most point of the source must be greater than 0.5 X/X_{90} (or ½ of the 'height' requirement) to have 100% scattering effectiveness from the top portion of the source. Therefore, the net scattering correction is given by

$$Source\ BSCF_{side} = SA\frac{X_{top}}{0.5}(X_{op\_side} - X_{side}) \qquad [3.8]$$

where *SA* is the electron source/air scattering correction for point-sources (ratio of source/water to air/water correction factor), X_{side} is the normal distance to the side of the source through which the electron travels, X_{op_side} is the normal distance to the opposite side of the source, and X_{top} is the normal distance to the top of the source. All distances are relative to X_{90}. If X_{top} is greater than 0.5, the full scattering correction is applied by setting X_{top} equal to 0.5. Similarly, if X_{side} or X_{op_side} are greater than 1.0, they are set equal to 1.0.

As the energy of the electron decreases and the scattered path angle relative to the air/water interface increases, the probability of the scattered beta depositing energy in the dose area greatly decreases (Figure 3-8). Conversely, high-energy electrons are expected to have a contribution extending to the edge of the dose area when scattered electrons enter the dose region at high incident angles. It is assumed that the scattering correction from the top and bottom of the source does not accurately account for such contributions due to its inherent geometry. Without knowing the angle at which a particular electron scatters and likely enters the dose region at each stage of the integration process, it is very difficult to correctly apply this additional correction factor. Therefore, the angle of incident (Figure 3-9) is used to estimate the frequency at which large angle scattering events occur. The side-scattering correction is only applied when the incident angle is greater than 70 degrees and when the density corrected path length (includes source and air) to the edge of the dose region, or the maximum scattered electron path length, is less than the electron X_{90} distance. The latter limitation prevents the side-scatter correction from being applied to low-energy electrons, where this form of scatter is believed unlikely (as explained above).

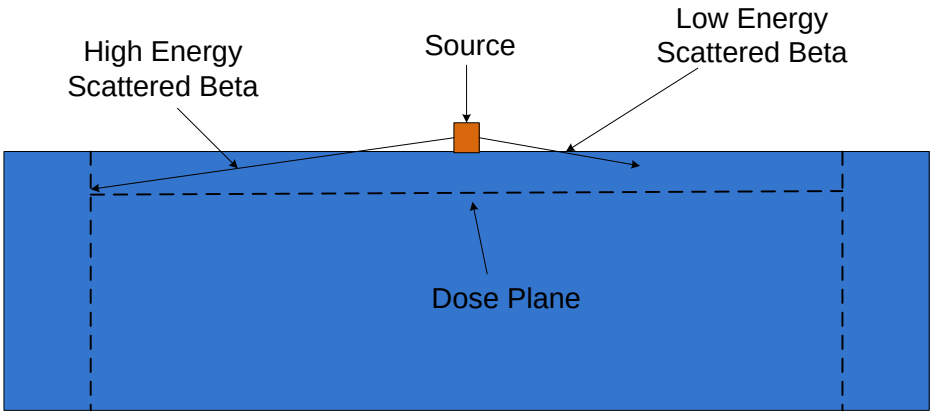

Figure 3-8 Schematic Illustrating Electron Energy Limitations of Side-Scatter Corrections

Both scattering paths assume the same incident angle.

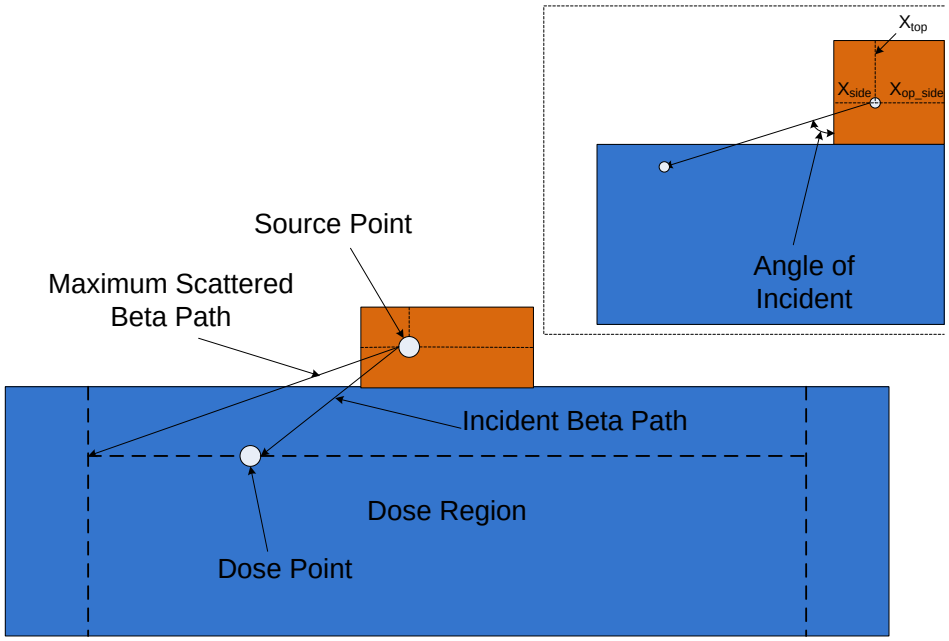

Figure 3-9 Schematic Illustrating Parameters Used for Side Scattering

As with scattering from the top/bottom of the source, the 'skin depth' at which the scattering factor is determined takes into account the normal density thickness of both the source and tissue through which the electron must traverse.

The application of scattering correction factors is more difficult with an air/water interface than with a source/water interface. In order to estimate the scattering effectiveness when source material is present between the air/water interface, simple linear interpolation is used. The two extreme cases are when there is no source material between the air and water boundaries (Figure 3-10) and when the path length from the top or sides of the source is equal to or greater than the electron range. The scattering effectiveness would be 100% and 0%, respectively. The

assumption is that if a backscattered electron can escape the source, there is a chance that a dose-contributing scatter event may still occur if water were surrounding the source. This is seen as a conservative estimate as an electron that travels 1.8 X/X_{90} (range estimate, Durham 2006) out of the top of a source will theoretically not be able to backscatter and contribute to skin dose at any depth.

The overall air BSCF is found using a weighted average. The BSCFs are calculated for all surfaces for which the electron can escape and reach air. Scattering contributions from the top of the source receive a 50% weight and the remaining 50% is evenly divided among the sides of the source. For cylinders and spheres, the shortest distance to the outer surface and the 180 degree opposite distance represent the two side distances (Figure 3-11). For slabs, four sides are used: the normal distances to the *x*-coordinate sides and the normal distances to the *y*-coordinate sides. The scattering reductions (for cylinders and spheres) are therefore given by

$$Air\ BSCF_{top} = AW\ 0.5\frac{1.8 - X_{top}}{1.8} \qquad [3.9]$$

$$Air\ BSCF_{side} = AW\ 0.25\frac{1.8 - X_{side}}{1.8} \qquad [3.10]$$

and

$$Air\ BSCF_{op\_side} = AW\ 0.25\frac{1.8 - X_{op\_side}}{1.8} \qquad [3.11]$$

where *AW* is electron air/water scattering correction for point-sources, X_{top}, X_{side}, and X_{op_side} are the distances to the top and sides of the source relative to X_{90}.

Unlike the source scattering corrections, no depth adjustments need to be made for materials traversed by the electron prior to entering the dose region. This is because corrections are made for scattering events occurring outside the source. The distance to the air/water interface is considered negligible in terms of electron energy degradation (assumed to be completely air). The overall air scattering correction is found by summing the three components above.

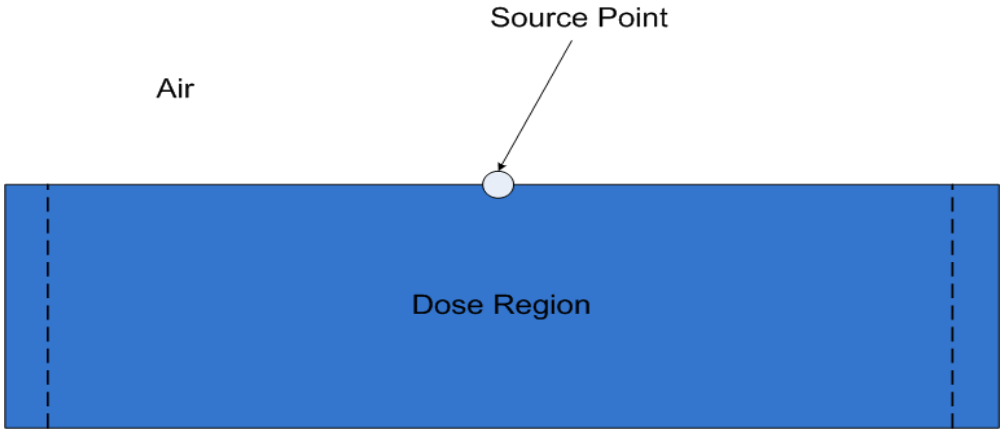

Figure 3-10 Schematic Demonstrating Conditions for Full Air-Water Scattering Conditions

All profiles were fit with a 28-parameter Chebyshev Series (LnX-Y, Order 6). While this is a complex fit equation, it allowed for all curves to be fit with the same functional form with a high goodness of fit (R^2 > 0.999). As an example, a second-order Chebyshev is given by,

$$Z = a + bT_1(x') + cT_1(y') + dT_2(x') + eT_1(y') + fT_2(y') \qquad [3.12]$$

where,

$$x' = \ln(x) = \ln(Normal\ Depth\ (cm)) \quad \text{scaled -1 to +1,}$$

$$y' = y = \ln(E\ (MeV)) \quad \text{scaled -1 to +1,}$$

$$T_n(x') = \cos(n * a * \cos(x')),$$

and Z is the square root of the dose rate per particle (Gy Bq^{-1} s^{-1}).

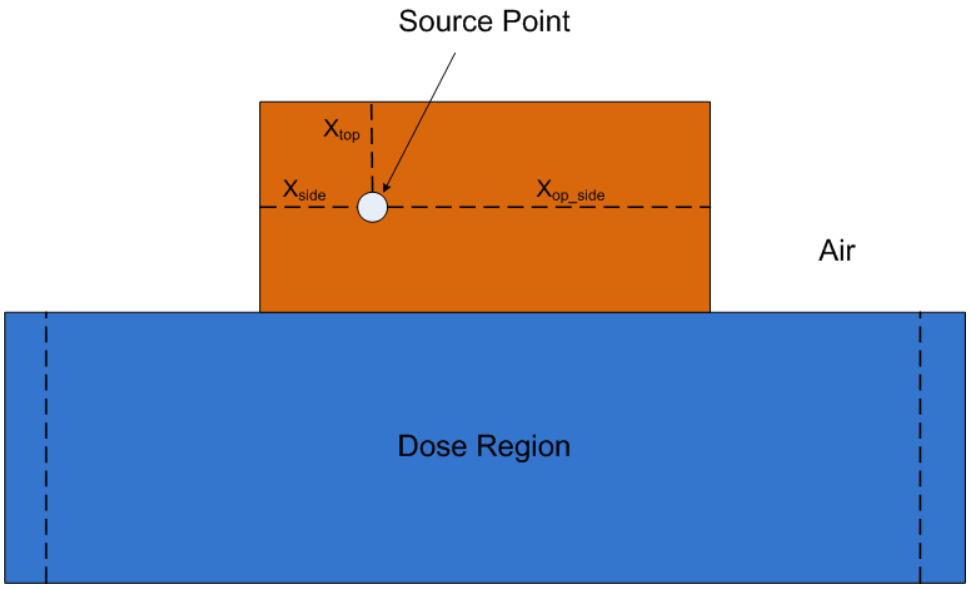

Figure 3-11 Schematic Demonstrating Conditions for Air-Water Scattering Correction

When the distance to the top and sides of the source are less than 1.8*X_{90}, a partial air-scattering correction is applied.

3.1.7 Scaling Models

The DPK scaling model consists of two parameters: a depth scaling parameter (*DSP*) and an energy scaling parameter (*ESP*). Mangini (2016) provides more detail.

3.1.7.1 Depth Scaling

The depth-scaling model begins with determining the range of the electron in both the homogeneous and non-homogeneous geometries. Given the difficulty of determining an absolute electron range, due to energy straggling and a torturous path, the spherical radius at which 99.0% energy deposition occurred was chosen as a range estimate. The difference in ranges between the homogeneous and non-homogeneous data is therefore attributed to the absorption sphere in the non-homogeneous case. For a given absorption radius, the resulting difference in ranges is called the depth-scaling parameter,

$$DSP(R, E_0, \rho, Z) = X_{99\_H} - X_{99\_NH} \quad [3.13]$$

where X_{99_H} is the homogeneous electron range, X_{99_NH} is the non-homogeneous electron range, ρ and Z are density and effective atomic number, respectively, of the absorption material.

As an example, consider an iron spherical source (r = 0.022 cm, Z = 26, ρ=7.874 g cm^{-3}) and an electron energy of 1 MeV. The radius of the iron source was chosen to be 0.5X_{90} to allow for sufficient electron self-absorption. Due to the presence of the 0.022 cm of iron, the electron range in the non-homogeneous shells is 0.120 cm less than the homogeneous range (Figure 3-12). Therefore, for a 1 MeV electron traversing 0.022 cm of iron, the depth-scaling parameter will be 0.120 cm. Shifting the homogeneous DPK data to the left (i.e., degraded electron energy

by self-absorption and therefore less skin penetration) by this amount will equate the ranges and provide the necessary depth adjustment (Figure 3-13).

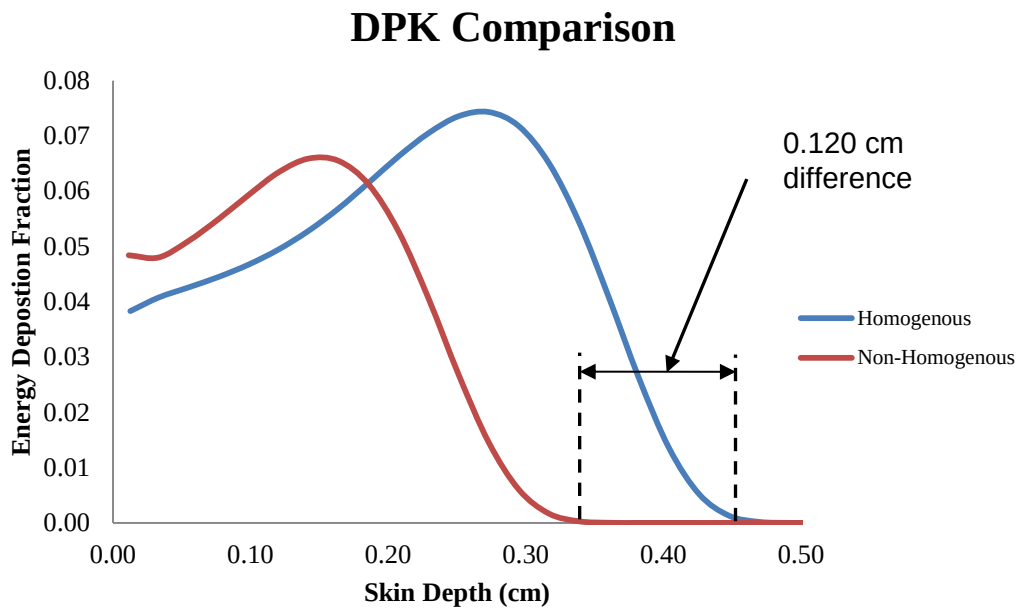

Figure 3-12 Comparison of 1 Mev Electron DPKs

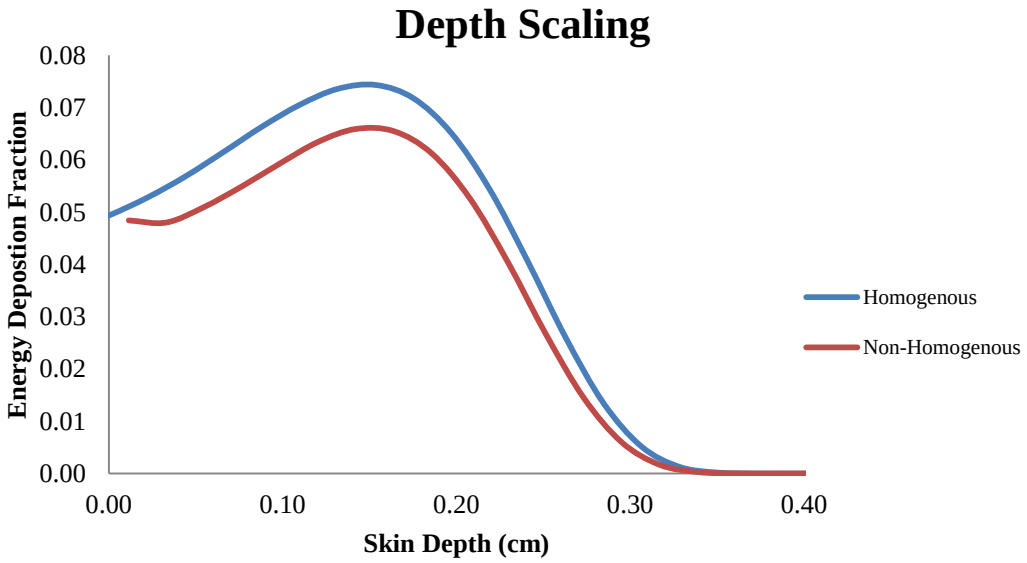

Figure 3-13 Example of Depth Scaling on the Homogeneous DPK Curve

The depth-scaling parameter was determined to be 0.120 cm.

When plotted together in three dimensions, the variability of depth scaling with respect to *Z* is difficult to discern, as they all follow the same curvature with little separation (Figure 3-14). The

variation in *DSP*s at small radii is greatest, with essentially no variability at large radii. Each curve is linear with a slope near unity. This is expected since density thickness is often used to estimate "water equivalent" path length for electrons in non-aqueous media (Cho 2004). The small *Z* dependence, coupled with 18 curve fits, allows for accurate interpolation for any 7.42 < $Z \leq 94$.

All curve fits for the *DSP*s took the form:

$$LN(DSP\ (cm)) = \frac{(a + bx + cx^2 + dx^3 + ey)}{(1 + fx + gx^2 + hx^3 + iy)} \quad [3.14]$$

where *x* is *LN*(*E* (*MeV*)) and y is $LN(X_x{*}\rho_x\ (g\ cm^{-2}))$. The terms X_x and ρ_x refer to the radius and density of the absorption sphere. The form of Eq. [3.14] was chosen because it was the equation that had the largest R^2 value (≥0.9999) and was able to fit all 18 plots. The fit parameters for each function demonstrated a slight *Z* dependence.

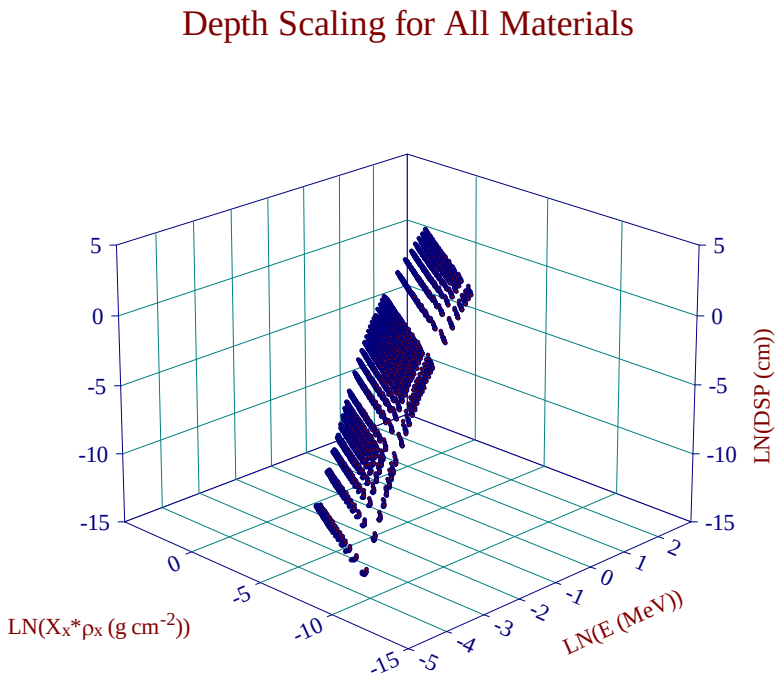

Figure 3-14 3D Plot of Depth-Scaling Data

3.1.7.2 Energy Scaling

The ESP is a direct result of energy conservation at distances within the electron's maximum range, or X_{99} (neglecting radiative loses beyond this distance). Once the homogeneous curve is shifted according to the depth-scaling parameter (Figure 3-13), the total energy deposition is found for each case. This is performed by summing the homogeneous DPKs for radii between the depth-scaling parameter and the X_{99} distance,

$$4\pi\rho \int_{DSP}^{X_{99}} r^2 \Phi(r, E_0) dr = E_{total} \qquad [3.15]$$

Similarly, the total energy deposition in the non-homogeneous case is found by summing DPKs from 0 to X_{99}. The law of energy conservation requires the two to be equal. Therefore, the energy-scaling parameter is found by taking the ratio of the non-homogeneous total to the homogeneous total, as:

$$ESP(R, E_0, \rho, Z) = \frac{4\pi\rho \int_{0}^{X_{99}} r^2 \Phi_{NH}(r, E_0) dr}{4\pi\rho \int_{DSP}^{X_{99}} r^2 \Phi_{H}(r, E_0) dr} \qquad [3.16]$$

Applying the resulting ratio to the homogeneous DPK equates the total energy depositions in the two geometries. For the iron source example, an energy-scaling parameter of 0.887 is computed. Thus, energy conservation is achieved by multiplying the homogeneous curve by the energy-scaling parameter of 0.887 (Fig. 3-15).

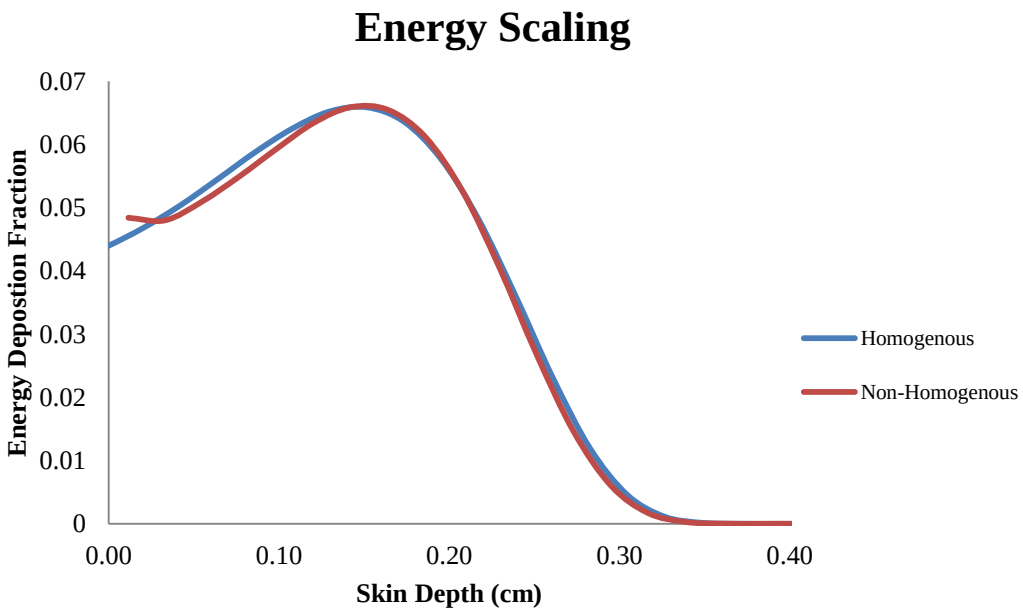

Figure 3-15 Example of Energy Scaling on the Homogeneous DPK Curve Presented in Figure 3-13

The energy-scaling parameter was determined to be 0.887.

As with the case of depth scaling, the natural logarithm of energy was used to decrease variability over the range of energies examined. The variability associated with the absorption-sphere radius was minimized by expressing it as a ratio of density thickness to the X_{90} distance in water, $X_x * \rho_x / X_{90w}$. The natural logarithm of the depth-scaling parameter multiplied by the initial electron energy, $LN(ESP * E_0)$, was chosen as the dependent variable. While the quantity

of $ESP*E_0$ has no physical meaning, using it as the dependent variable produced better-fitting surface plots than simply using *ESP.* Since E_0 is a known quantity, solving for *ESP* is simple.

The variability of the *ESP* curves (Fig. 3-16) with respect to *Z* is more pronounced than the *DSP* curves (Fig. 3-14). The variation of *ESP*s becomes quite large as the absorption-sphere radius increases. As *Z* approaches that of water (Z_{eff} of 7.42), the *ESP* approaches 1.0, as expected. As *Z* increases, the amount of energy reduction following depth scaling increases. Once again, this is expected given the lower profile of high-*Z* non-homogeneous DPK curves for the same absorption-sphere radius (with respect to X/X_{90}). Despite this increased variability, interpolation within surface plots is not seen as an issue.

All curve fits for the *ESP*s took the form:

$$LN(E*ESP\ (MeV)) = \frac{(a+bx+cx^2+dx^3+ey+\ fy^2)}{(1+gx+hx^2+iy+\ jy^2)} \qquad [3.17]$$

where *x* is *LN*(*E* (*MeV*)) and *y* is $X_x*\rho_x / X_{90w}$. The terms X_x and ρ_x refer to the radius and density of the absorption sphere. The above equation was chosen because it was the equation that had the largest R^2 value (≥0.999) and was able to fit all 18 plots. As with the *DSP*s, fit parameters demonstrated a slight *Z* dependence.

Integration of scaling parameters over a particular electron energy spectrum provides the non-homogeneous DPK for a given source thickness. Comparisons with EGSnrc non-homogeneous DPKs demonstrated excellent agreement over a range of electron energies and high-*Z* source materials by producing nearly identical DPKs for all absorption-sphere radii. In addition, when compared to Cross' (1967, 1968, 1982, 1992a) scaling model and density scaling, the ability to account for spectral hardening is clearly shown. This is in large part due to the scaling model's ability to accurately calculate non-homogeneous DPKs at each mono-energetic electron energy with a given emission spectrum.

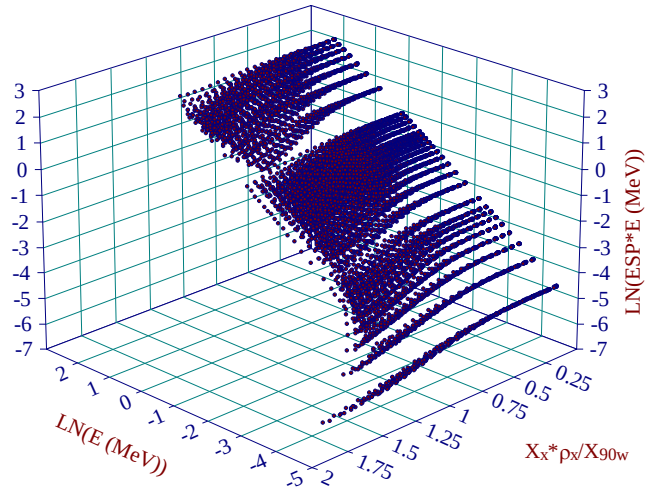

Figure 3-16 3D Plot of Energy-Scaling Data

3.2 Photon Dosimetry

The new photon dosimetry model, first implemented in VARSKIN 4 (Hamby et al. 2011), is an improvement to the basic photon model used in the VARSKIN 3 version. The model uses a point-kernel method that considers the buildup of CPE, transient CPE, photon attenuation, and off-axis scatter. The photon dose model has many of the basic assumptions carried in the beta dosimetry model, namely that the source can be a point, disk, cylinder, sphere, or slab and that dose is calculated to an averaging disk immediately beneath the skin surface at a depth specified by the user. Photon dose is calculated for a specific skin averaging area, also specified by the user.

A major problem associated with deterministic photon dosimetry is that of determining the amount of charged-particle buildup and electron scatter within shallow depths. Federal law (Title 10 of the *Code of Federal Regulations* (10 CFR) Section 20.1201(b)) states that a dose averaging area of 10 cm^2 is appropriate for skin dosimetry (specifically at the shallow-dose equivalent depth of 0.007 cm in tissue (i.e., 7 mg/cm^2 in unit density material)). Throughout this section, the word “depth” is meant to indicate the distance from the skin surface to some point directly beneath a point source, normal to the skin surface.

To begin the explanation of the dose model, we assume the simple instance of a volume of tissue exposed to a uniform fluence, Φ_0, of uncollided photons of energy, E, from a point source in a homogeneous medium. When we ignore attenuation and assume that CPE is established, the dose to any and every point in that volume of tissue is,

$$D(E) = \Phi_0 \cdot E \cdot \left(\frac{\mu_{en}}{\rho}\right)_{tissue} \quad [3.18]$$

where $\left(\frac{\mu_{en}}{\rho}\right)_{tissue}$ is the energy-dependent mass energy absorption coefficient for tissue. With this calculation of dose, we essentially assume that the tissue volume is infinitely thin and that interactions occur in two dimensions, normal to a beam of incident photons. The uncollided fluence originating from a point source can be determined by,

$$\Phi_0 = \frac{S}{4\pi d^2} \qquad [3.19]$$

where *S* has units of photons emitted per nuclear transition (i.e., yield), and *d* is the distance between the source and dose locations, in an infinitely large homogeneous volume. Thus, a point-kernel tissue dose per transition at distance, *d*, from a point source can be calculated for radionuclides emitting *i* photons of energy *E* and yield *y*, such that,

$$Dose\left[\frac{\mathrm{Gy}}{\mathrm{nt}}\right] = \frac{k\left[\frac{\mathrm{J\cdot g}}{\mathrm{MeV\cdot kg}}\right]}{4\pi d^2[\mathrm{cm}^2]} \cdot \sum_i \left[y_i \left[\frac{\mathrm{photon}}{\mathrm{nt}}\right] \cdot E_i \left[\frac{\mathrm{MeV}}{\mathrm{photon}}\right] \cdot \left(\frac{\mu_{en}}{\rho}\right)_{i,tissue} \left[\frac{\mathrm{cm}^2}{\mathrm{g}}\right] \right] \qquad [3.20]$$

where $k = 1.602x10^{-10}\left[\frac{\mathrm{J\cdot g}}{\mathrm{MeV\cdot kg}}\right]$.

If the point source is assumed to rest on the skin surface (with a density interface), and a profile of dose with depth in tissue is of interest, Eq. [3.20] must be modified to account for the attenuation of photons in tissue, the electronic buildup, and electron scatter at shallow depths leading to CPE. First, given that attenuation is occurring as photons travel through tissue, photon fluence is decreasing by an attenuation factor ($e^{-\mu d}$) where μ is the energy-dependent linear attenuation coefficient for tissue (coefficients are taken from International Commission on Radiation Units and Measurements (ICRU) Report 44, 1989). Since tissue typically is assumed to be of unit density (1 g/cm^3), the value of μ (in units of cm^{-1}) is numerically identical to the value of μ/ρ (in units of cm^2/g).

To simplify software coding, analytical expressions are used in VARSKIN 6 (as opposed to using "look-up tables") for a number of dosimetry parameters. An empirical relationship to estimate μ/ρ for tissue as a function of incident photon energy (in MeV) was developed and is given below. For energies less than or equal to 0.020 MeV,

$$\frac{\mu}{\rho}(E) = \frac{1}{0.0000145 + 3810E^{2.5} + 134400E^3} \qquad [3.21]$$

and for energies from 0.020 to 3 MeV,

$$\frac{\mu}{\rho}(E) = e^{\left[-3.22 - 0.11(lnE)^2 + 0.5566\sqrt{E} - 0.7713lnE + \left(0.000721/E^2\right)\right]} \qquad [3.22]$$

Figure 3-17 shows a comparison between the ICRU 44 (1989) values of μ/ρ for soft tissue and the functions of Eqs. [3.21] and [3.22].

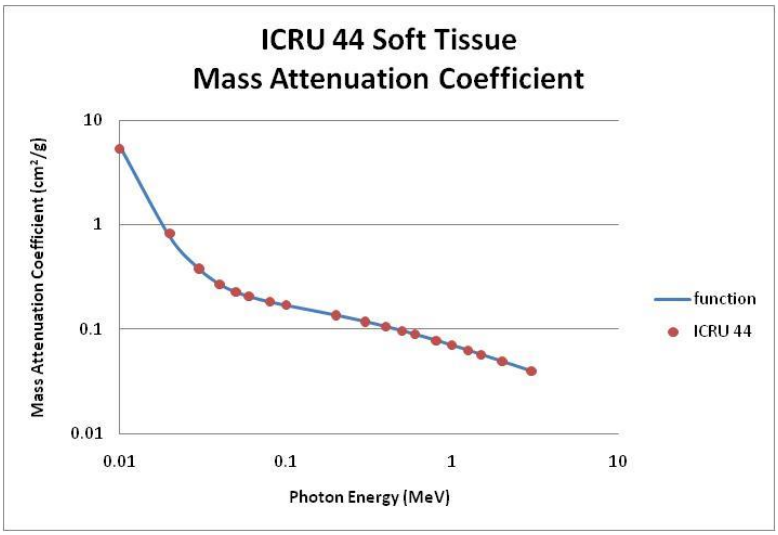

Figure 3-17 ICRU 44 Soft Tissue Mass Attenuation Coefficients

The function shown in Eq. [3.23] was also developed to approximate the energy-dependent value of μ_{en}/ρ for tissue. That function,

$$\frac{\mu_{en}}{\rho}(E) = \frac{a+clnE+e(lnE)^2+g(lnE)^3+i(lnE)^4}{1+blnE+d(lnE)^2+f(lnE)^3+h(lnE)^4+j(lnE)^5} \quad [3.23]$$

has a different set of coefficients for energies less than or equal to 0.030 MeV and energies from 0.030 to 3 MeV. Table 3-4 provides the coefficients and Figure 3-18 gives the fit of Eq. [3.23] to the ICRU 44 (1989) data.

In consideration of CPE, Attix (1986) states that the condition exists if, in an infinitely small volume, "…each charged particle of a given type and energy leaving [the volume] is replaced by an identical particle of the same energy entering." For dose at shallow depths to be accurate, we must determine the degree (fraction) to which CPE, as a function of depth, has been achieved. The VARSKIN 6 estimation of the CPE fraction is based on Monte Carlo simulations and the difference between kinetic energy released in matter (KERMA) and energy absorbed (dose) as a function of depth.

Since energy transfer (i.e., KERMA) from photons and energy absorption (i.e., dose) from the resulting charged particles does not occur in the same location (Johns and Cunningham, 1983), there is a "buildup region" in which dose is zero at the skin surface and then increases until a depth is reached at which dose and KERMA are essentially equal. The depth at which equilibrium occurs is approximately equal to the range of the most energetic electron created by the incident photons (Johns and Cunningham, 1983). We determined an energy-dependent factor accounting for CPE buildup (f_{cpe}) by Monte Carlo simulation (using MCNP5); this factor is the ratio of dose, *D*, to KERMA, *K*, for a particular incident photon energy at a given tissue depth, such that,

$$f_{cpe}(E,d) = {}^{D}/_{K} \quad [3.24]$$

Table 3-4 Coefficients for Eq. [3.23]

Coefficient	E ≤ 30 keV	E > 30 keV
a	0.02971	0.03072
b	0.7453	0.4972
c	0.01519	0.009879
d	0.2236	0.1825
e	0.0009557	-0.0002386
f	0.03370	0.07303
g	-0.0001513	0.0006930
h	0.002545	0.01520
i	0.00006018	0.0003239
j	0.00007744	0.001084

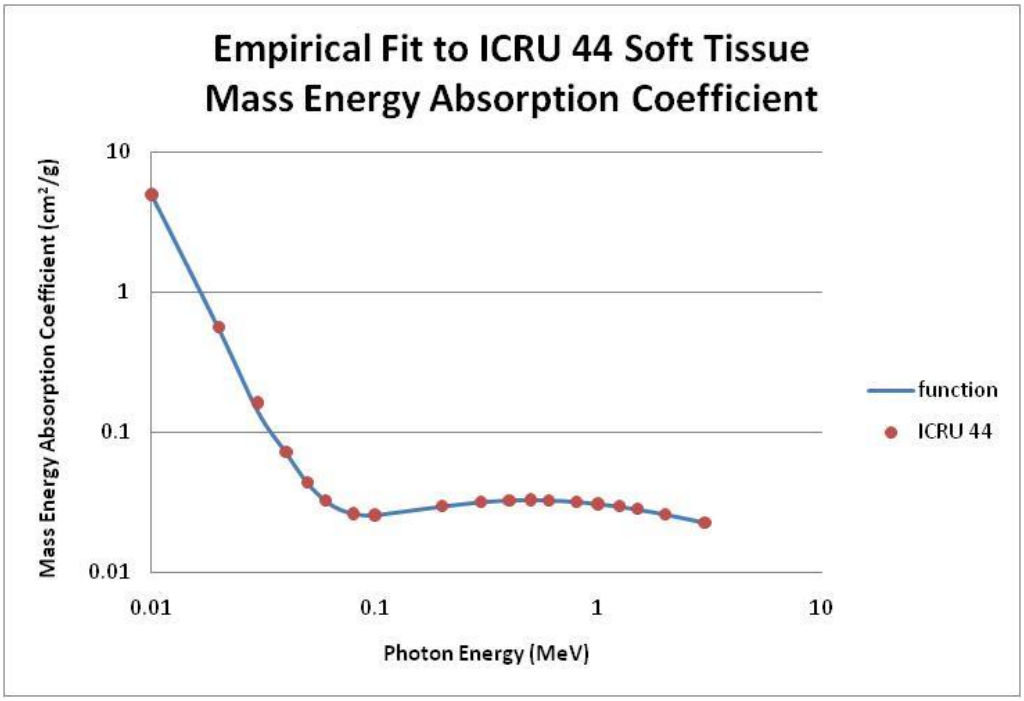

Figure 3-18 ICRU 44 Soft Tissue Mass Energy Absorption Coefficients

When considering CPE and attenuation, a relationship is achieved with depth in a medium in which dose is proportional to KERMA (Attix, 1986); this relationship is referred to as transient charged particle equilibrium (TCPE). Dose reaches a maximum "at the depth where the rising slope due to buildup of charged particles is balanced by the descending slope due to attenuation" (Attix, 1986), and then dose continues to decrease with depth because of subsequent attenuation of photons. At the point where TCPE occurs, dose is essentially equal to KERMA for low-energy photons and the value of f_{cpe} is equal to unity (1). As photon energy increases over about 1 MeV, this assumption of dose and KERMA equality begins to fail, but not so significantly that it affects dose estimations at depth appreciably. Based on experience with the Monte Carlo simulation of shallow and deep depths, the model used in VARSKIN 6 limits the value of f_{cpe} to 1.05 (i.e., it allows dose to exceed KERMA by no more than 5 percent at depth).

A function for f_{cpe} that is dependent on initial photon energy is given as,

$$f_{cpe}(x) = \frac{1}{a+bln(x)+{}^{c}/_{\sqrt{x}}} \quad [3.25]$$

where x (in cm) is a function of energy and is equal to the point kernel distance between source point and dose point, and the coefficients a, b, and c are functions of energy (in keV) as described below:

$$a = 19.78 + 0.1492\,ElnE - 0.008390\,E^{1.5} + 0.00003624\,E^{2} + 3.343\,\sqrt{E}lnE - {}^{10.72\,E}/_{lnE} \quad [3.26]$$

$$b = 1.217x10^{-12}E^{4} - 5.673x10^{-9}E^{3} + 7.942x10^{-6}E^{2} - 0.002028E + 0.3296 \quad [3.27]$$

$$c = 9.694x10^{-13}E^{4} - 4.861x10^{-9}E^{3} + 7.765x10^{-6}E^{2} - 0.001856E + 0.1467 \quad [3.28]$$

The f_{cpe} factor is used for all materials; any buildup for photon dosimetry in air or thin covers is expected to be insignificant as compared to tissue.

3.2.1 Off-Axis Scatter Correction

Estimates of f_{cpe} were determined assuming that the line created between the source and dose points was normal to the surface. For a given distance, however, the fractional CPE for point kernel calculations, in which the dose point is located off axis and near the edge of the averaging disk, will vary because of the escape of energetic particles near the air-tissue interface. This loss of energy occurs for more energetic particles, generally from photons of energy greater than a few hundred keV. We have accounted for this off-axis scatter of energy out of tissue, slowing the buildup of equilibrium, by including an off-axis scatter factor, F_{oa}. The factor, taking on values between 0 and 1, is necessary only for point-kernel calculations in which the angle between the central axis at the surface and the dose point is greater than 70 degrees from normal, and for photon energies greater than 300 keV; otherwise, F_{oa} is set equal to unity (1). The off-axis scatter factor is calculated from empirical data obtained through Monte Carlo simulation. The factor is represented by,

$$F_{oa} = (-1.57 + 0.000334\,\theta^{2.5} - 0.0000325\,\theta^{3})(0.93 + 0.1R) \quad [3.29]$$

where R is the radius (cm) of the dose-averaging disk and θ is the off-axis scatter angle (in degrees). Figure 3-19 gives a plot of off-axis correction as a function of scatter angle and the area of the dose-averaging disk. The considerable dip in the function for a 0.1-cm^2 averaging area is an artifact of Eq. [3.29] and is not phenomenologically significant.

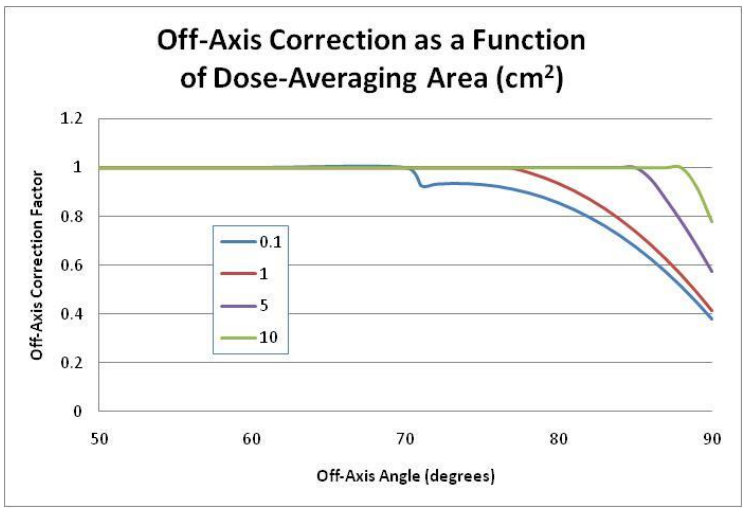

Figure 3-19 Off-Axis Correction Factor as a Function of Off-Axis Angle and Dose-Averaging Area

Fully accounting for charged particle buildup and attenuation, Eq. [3.20] now becomes:

$$Dose\left[\frac{Gy}{nt}\right] = \frac{k}{4\pi d^2} \cdot \sum_i \left[y_i \cdot E_i \cdot \left(\frac{\mu_{en}}{\rho}\right)_{i,tissue} \cdot \left(f_{cpe}\right)_i \cdot \left(F_{oa}\right)_i \cdot e^{-\mu_i d} \right] \quad [3.30]$$

3.2.2 Integration Methods

As stated above, Federal law currently requires the determination of shallow dose to skin averaged over an area of 10 cm^2 at a depth in tissue of 7 mg/cm^2. To determine average photon dose at depth from a source at the surface, we must integrate Eq. [3.30] over the averaging area. Integrating the exponential, however, results in a solution with imaginary components. Therefore, a stepwise numerical integration of Eq. [3.30] is necessary, essentially providing an average of the point-kernel dose over combinations of photon emission locations within the volume of the radioactive source and dose point locations within an infinitely thin disk of tissue at depth, *h*, from the surface.

Studies were conducted to determine which numerical integration method achieved convergence most rapidly (i.e., dividing the dose-averaging disk into the fewest number of segments) for photon dosimetry. The studies investigated three segmenting methods (see Fig. 3-20): (1) segments determined by equal radii of the dose-averaging disk, (2) segments determined by equal off-axis angles, and (3) segments determined by equal annular area.

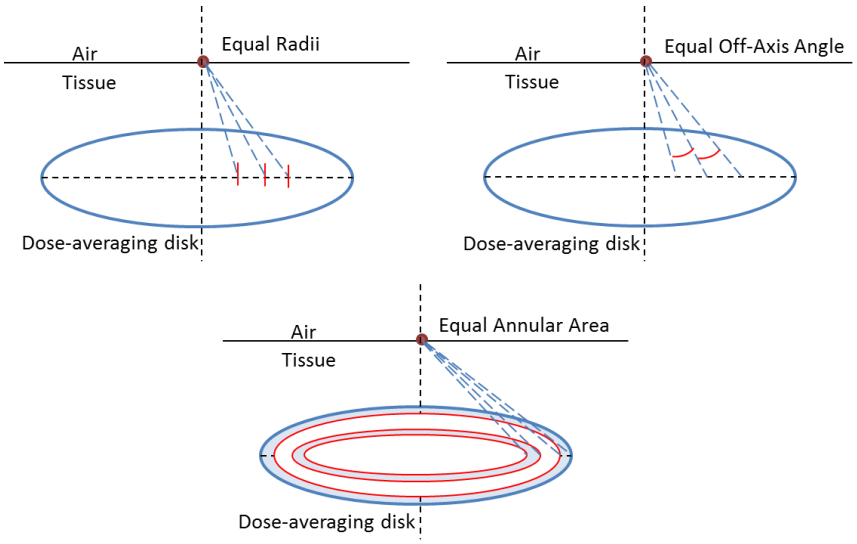

Figure 3-20 Depiction of Methods for Determining Integration Segments of the Dose-Averaging Disk

These studies indicated that segments divided according to equal lengths (radii) along the radius of the averaging disk converged with the fewest number of iterations, with segments divided by equal annular area requiring the most iterations. Figure 3-21 shows that convergence was achieved within about 300 iterations for equal lengths along the radius of a 10-cm^2 averaging disk; the VARSKIN 6 numerical integration, therefore, utilizes 300 segments along the radius/diameter. Convergence was achieved with fewer segments when analyzing a smaller averaging disk.

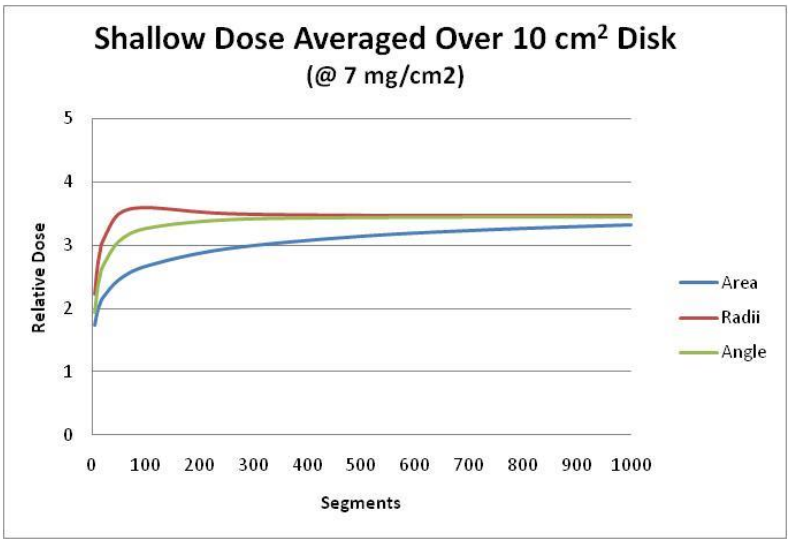

Figure 3-21 Relative Dose as a Function of the Number of Segments in a Numerical Integration

Therefore, given a point source on the skin, the first task in the integration process is to divide the dose-averaging disk into *N* small segments (annuli), *j*, of uniform incremental radii. If an averaging area, *A*, of radius, *R*, is at some depth, *h*, beneath the surface of skin, a method

based on the convergence study is used in which values of radii, R_j, of the averaging disk are selected such that a radial increment, Δr, is defined,

$$\Delta r = \frac{R}{N} \quad [3.31]$$

and

$$R_j = \sum_{j=0}^{N}(j \cdot \Delta r) \quad [3.32]$$

If point-kernel dose calculations are conducted where dose is estimated to the midpoint of the annulus, each dose must be weighted by w_j, the ratio of the annular area to the total area of the disk. Given that $R_0 = 0$ and $R_N = R$, the values of w_j are determined by,

$$w_j = \frac{R_j^2 - R_{j-1}^2}{R^2} \quad [3.33]$$

where *j* takes on values from 1 to *N*. We also define r_j, which represents the average of the two radii describing the annulus in each calculation, such that,

$$r_j = \frac{R_j - R_{j-1}}{2} \quad [3.34]$$

Once all weighting factors are determined, then the dose per nuclear transition for a given point source radionuclide with *i* emissions, averaged over an infinitely thin disk of radius *R*, at normal depth in tissue *h* and radius r_j, is calculated by,

$$\dot{D}(h,R)\left[\frac{\mathrm{Gy}}{\mathrm{nt}}\right] = \frac{k}{4\pi} \cdot \sum_{j=1}^{N} \frac{w_j}{d_j^2}\left[\sum_i \left[y_i \cdot E_i \cdot \left(\frac{\mu_{en}}{\rho}\right)_i \cdot \left(f_{cpe}\right)_{i,j} \cdot \left(F_{oa}\right)_{i,j} \cdot e^{-\mu_i d_j}\right]\right] \quad [3.35]$$

where $d_j = \sqrt{\left(h^2 + r_j^2\right)}$.

3.2.3 Attenuation Coefficients for Cover Materials

For the selection of attenuation coefficients in photon dose calculations, the cover materials are "forced" to be either latex or cotton. This determination is made by the density entry, i.e., if the density is less than or equal to 1.25 g/cm^3, then latex is assumed, but if greater, cotton is assumed. These are the two most likely materials used for cover. For photons, cover attenuation is relatively minor and this assumption should be insignificant for the dose calculation.

We use an empirical function of energy for attenuation coefficients for cotton and latex, namely:

$$\mu = e^{\left(a + b\sqrt{E} \cdot \ln(E) + c\sqrt{E}\right)} \quad [3.36]$$

where a = -1.0132, b = 0.31505, and c = -1.6086 for cotton, and a = -1.0286, b = 0.32189, and c = -1.6217 for latex. And, coefficients for air were determined from,

$$\mu_{air} = \left(\left(a + \frac{b}{\sqrt{E}}\right) + \left(c \cdot \frac{\ln(E)}{E}\right) + \left(\frac{d}{E}\right) + \left(\frac{e}{E^{1.5}}\right) + \left(f \cdot \frac{\ln(E)}{E^2}\right) + \left(\frac{g}{E^2}\right)\right) * 0.001168 \quad [3.37]$$

where a = 0.027413, b = -0.12826, c = 0.11227, d = 0.060526, e = 0.12508, f = -0.0030978, and g = -0.021571. Both of these functions track very well with data from ICRP 44.

3.2.4 Offset Particle Model

The offset particle model allows calculation of skin dose averaged over areas that are not directly beneath the contaminant. This model was developed to determine dose to a single averaging area resulting from multiple hot particles. The offset particle model is available only for photons and the point-source geometry. It requires only one input variable, the distance of the offset. For multiple hot-particle irradiations, the dose from each hot particle is calculated separately, with the user running VARSKIN once for each source. The offset particle model does not calculate the maximum dose to skin from several particles (Section 6.2 outlines the iterative process for determining the maximum dose to the dose-averaging area); rather, the user must manually add doses from each of the sources to a common dose-averaging disk at depth.

3.2.5 Off-Axis Calculation of Dose

The model described thus far is constructed under the assumption that the source of photons is a point, located directly above and on axis with the averaging disk, and that there is symmetry in dose calculations along a radius of the dose-averaging disk (Fig. 3-22).

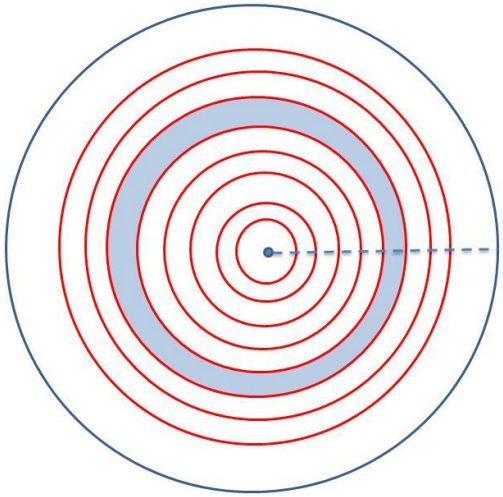

Figure 3-22 Dose-Averaging Disk with the Source Point Located on Axis

To extend the model to handle point-kernel calculations for volumetric sources, or for multiple point sources, we must consider the case where the point source is off axis yet still over the dose-averaging disk (Figs. 3-23 and 3-24) and the case where the point source is completely removed from the dose-averaging disk (Figs. 3-25 and 3-26). The implication is simply a geometric determination of the distance between source and dose points in each point-kernel calculation and an area-weighted factor for the symmetric dose location on the averaging disk.

In the first case, where the point source is off axis yet still over the dose area, there is symmetry along a diameter of the dose-averaging disk. The average of the point-kernel doses will be determined by a weighting of dose calculated along the diameter. The calculation begins by projecting the dose point to the averaging disk, normal to the skin surface (see Figure 3-23).

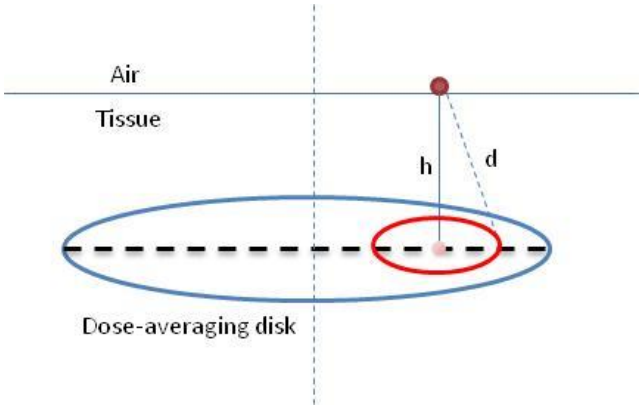

Figure 3-23 Dose-Averaging Disk Located at Depth h Beneath an Offset Point Source

The averaging disk then is divided, as described above, into a series of concentric annuli, about the projected dose point, until the radius of the annuli reaches the nearest edge of the averaging disk (Fig. 3-24). At this point, the weighting model transitions to a series of arcs passing through the averaging disk; these arcs are created by differential radii of two intersecting circles (Fig. 3-25). The model creates a total of 300 annuli and arcs. Point kernel dose is calculated along the diameter in each of the 300 segments defined by the differential annuli and arcs and then weighted based on the fractional area of each segment.

The weight, or fractional area, of each annulus to the total is straightforward, in that,

$$w_i = \frac{\pi\left(r_i^2 - r_{i+1}^2\right)}{\pi R^2} = \frac{r_i^2 - r_{i+1}^2}{R^2} \qquad [3.38]$$

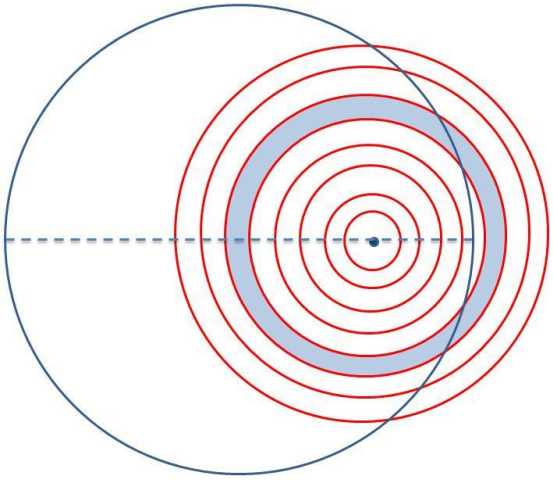

Figure 3-24 Dose-Averaging Disk with the Source Point Located off Axis, on Disk

The weight of each arc is determined by a method considering intersecting circles. In the case of Figure 3-25, the area of the "lens" created by the two intersecting circles is given by:

$$A_i = r^2 cos^{-1}\left(\frac{d^2 + r^2 - R^2}{2dr}\right) + R^2 cos^{-1}\left(\frac{d^2 + R^2 - r^2}{2dR}\right)$$

$$-\frac{1}{2}\sqrt{(-d+r+R)(d+r-R)(d-r+R)(d+r+R)} \qquad [3.39]$$

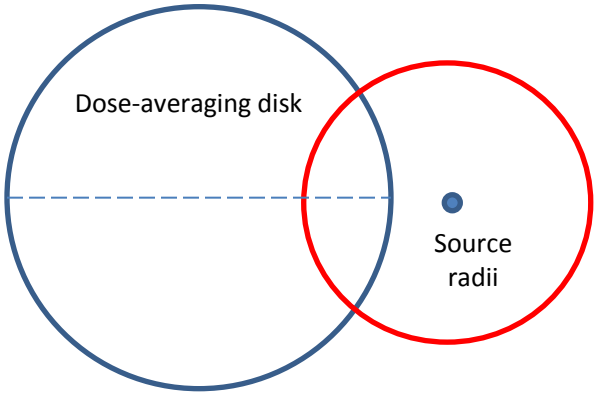

Figure 3-25 Relationship Between the Source-Averaging Disk and One of the Radii

The area of the arc formed (Fig. 3-25) by two concentric circles (two radii from the point source) that overlap another circle (the averaging disk) is the difference in the area calculations of Eq. [3.38]. The arc weight is then the ratio of the arc area to the total area of the averaging disk. In the case where the source projection does not fall on the dose-averaging disk (Fig. 3-26), the weighting scheme is based solely on arcs.

The numerical integration is conducted from the point source to each of 300 locations along the diameter of the averaging disk (or along the radius if the source point is directly on axis with the disk). Then, for volumetric sources, point source locations are chosen in equal symmetric increments at fifteen point locations in each of the three dimensions within the source volume, relative to the averaging-disk diameter. For each volumetric source dose estimate, 1,000 calculations of dose from each of 15 x 15 x 15 source point locations are executed (1 million dose calculations).

The VARSKIN 6 photon dosimetry model accounts for attenuation in cover materials and in air. As with the electron dosimetry model, up to five layers above the skin are allowed, with the air layer only acceptable just above the skin surface. For photon calculations, the material layers are restricted to cotton and/or latex (by way of attenuation coefficient), and the source material is assumed to have the same characteristics as air. This latter assumption is not significant for very small volumetric sources and for photon energies above about 50 keV. For example, if we examine the ratio of air attenuation to lead, tin, copper, aluminum, and water attenuation, the greatest difference is obviously at low photon energies with higher-Z materials (i.e., instances of higher interaction probability).

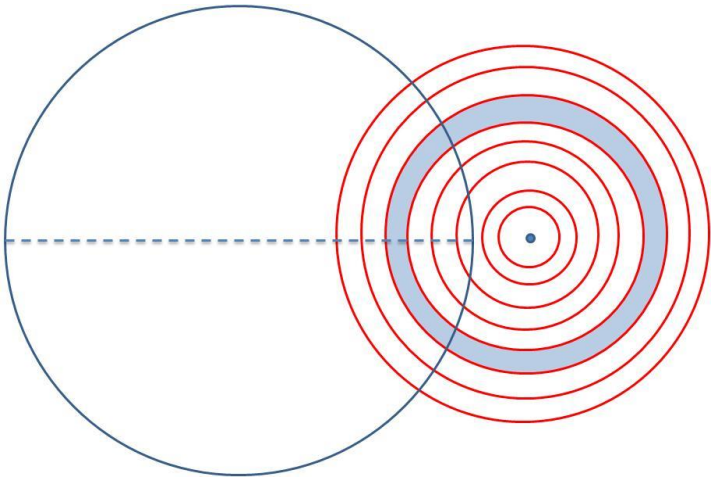

Figure 3-26 Dose-Averaging Disk from Above with Source Point Located off Axis, off Disk

The data indicate that, for volumetric sources with a maximum linear dimension less than about 100 microns, the assumption that the source material is similar to air is of no consequence whatsoever for photon energies above 10 keV. As the source particle dimensions increase in size, an assumption of air for the source material can be quite significant for very low photon energies (< 40 keV). The significance, however, is one of conservatism in that more low-energy photons than actual will be modeled as striking the skin surface when source dimensions are large. Our analysis also shows that, in terms of attenuation, the assumption of air and water (tissue) being similar over very short distances (< 5 mm) is a good assumption.

3.3 Cover Layer and Air Gap Models

VARSKIN 6 has the ability to model cover materials and air gaps. The models use the concept of effective path length to determine the electron energy lost in either a cover material or air before it enters the skin. The path length is not the true path traversed by the electron; rather, it is merely a mathematical convenience introduced to provide a measure of the energy lost in each layer. To minimize unintended applications of VARSKIN, the air gap is limited to a maximum of 20 cm.

Figure 3-27 illustrates the method used to determine path length within the source and within the cover material. For the pictured cylindrical source, the known values in the figure are the source radius (R_{max}), the horizontal distance from the centerline to the source point (S_{RAD}), the source thickness (S_{THICK}), the cover thickness (C_{THICK}), the skin depth (S_{DEP}), the source and cover densities (Δ_s and Δ_c, respectively), the angular distance from the center of the dose area to the dose point (P_s), and the distance from the skin to the plane of the source point (D_{RAD}).

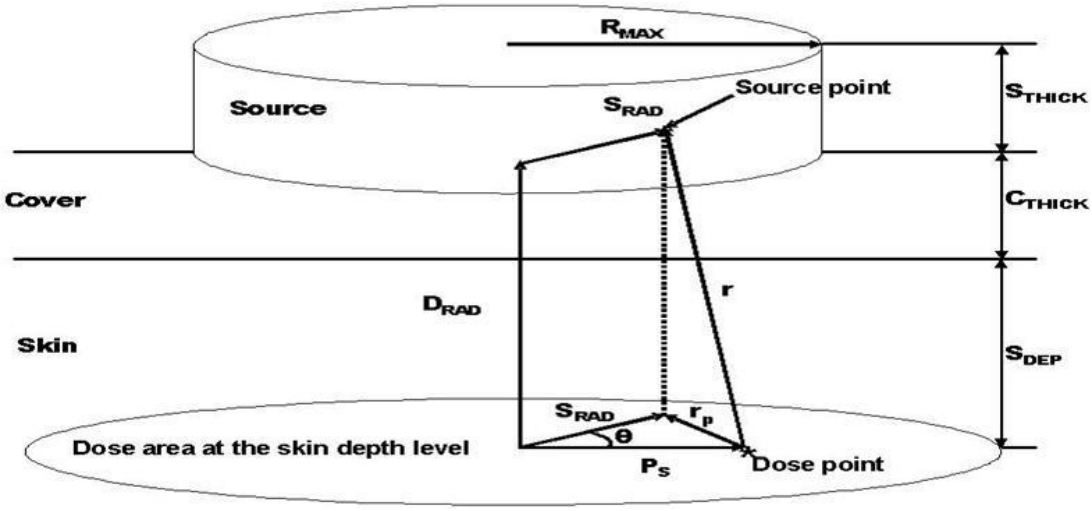

Figure 3-27 Schematic of a Generic Dose Calculation for Cylindrical Geometry

The quadrature routines are coded to choose values for S_{RAD}, the distance from the centerline to the P_s source point; θ, the angle between S_{RAD} and P_s; and D_{RAD}, the height of the dose point. The first quantity to be calculated is r, the physical distance from a source point to a dose point. To do this, the square of the projected distance, r_p^2, is calculated using the law of cosines:

$$r_p^2 = P_s^2 + S_{rad}^2 - 2P_s S_{rad} cos\theta \quad [3.40]$$

The quantity r is used in the denominator of the expression in Eq. [3.1] and represents the geometric attenuation between the dose point and the source point. This quantity is further analyzed to calculate the modified path length used to evaluate the scaled absorbed dose distribution.

By the law of similar triangles, the ratio to r of each of the actual distances along r through the source, the cover material, and the tissue is the same as the ratios of the thickness of the cover material to D_{RAD}, the thickness of tissue layer to D_{RAD}, and the remaining distance along r to D_{RAD} respectively, provided that the line connecting the dose point and the source point exits through the part of the source that is in contact with the cover material. Thus, the distance traveled through the cover material is written as the following:

$$r_c = C_{thick} \cdot \left({}^{r}/_{D_{rad}}\right) \quad [3.41]$$

The distance traveled through the skin is given by:

$$r_t = S_{dep} \cdot \left({}^{r}/_{D_{rad}}\right) \quad [3.42]$$

And, the distance traveled through the source is given by:

$$r_s = \left(D_{rad} - C_{thick} - S_{dep}\right) \cdot \left({}^{r}/_{D_{rad}}\right) \quad [3.43]$$

For electron dosimetry, the modified path length r_1 is then found using the following equation:

$$r_1 = \frac{(r_s\rho_s + r_c\rho_c + r_t\rho_t)}{\rho_t} \quad [3.44]$$

where the variables ρ_s, ρ_c and ρ_t represent the density of the source, the cover material, and tissue, respectively. The density of tissue is assumed to be equal to that of water (1 g cm^{-3}).

For small-diameter sources, the path between the dose point and the source point may pass through the side of the source (e.g., the path may exit the source and pass through air before passing into skin). Thus, the quantity in Eq. [3.44] must be further analyzed to determine the path length within the source and the path length outside the source but above the level of the cover material. The actual path length within the source is multiplied by the source density, and the path length outside the source and above the cover material is multiplied by the density of the material outside the source, assumed to be air.

In spherical geometry, the physical distance from source point to dose point is given by:

$$r_p^2 = P_s^2 + S_{rad}^2 sin^2\phi - 2P_s S_{rad} sin\phi cos\theta \quad [3.45]$$

In slab geometry, the physical distance is given by:

$$r = \sqrt{[(X_{source} - X_{dose})^2 + (Y_{source} - Y_{dose})^2 + (Z_{source} - Z_{dose})^2]} \quad [3.46]$$

Recent investigations [Anspach and Hamby 2017; McDaniel and Hamby 2017; Dubeau et al. 2018] have shown that the cover and air-gap models for electron dosimetry are too conservative, i.e., energy degradation of electrons appears to be too great as the travel through material prior to entering the skin. The user is cautioned not to rely on VARSKIN for source geometries involving cover materials greater than a few centimeters.

3.4 Volume Averaged Dose Model

The volume-averaged dose model (shown schematically in Fig. 2-8) allows the calculation of dose averaged over a given tissue volume. This model works with both photons and electrons yet is really only meaningful for electron dose calculations. Any two planes of irradiated skin can be assigned to bound the skin volume. For sources in contact with the skin, the maximum penetration depth for electrons is equal to the X_{99} distance. Doses averaged over the dose-averaging area are calculated at 10 skin depths between two limits set by the user, and a cubic spline (a third-order piecewise polynomial curve fit) is fit to this depth-dose distribution. When the user specifies the skin depths corresponding to the volume of interest, VARSKIN 6 integrates the depth dose function over the region of interest to obtain the volume-averaged dose.

4 VALIDATION AND VERIFICATION

To validate the new photon and electron dosimetry models incorporated into VARSKIN 6 and previous versions, results were compared to the general-purpose radiation transport codes, MCNP5 and EGSnrc. The two software packages are Monte Carlo transport codes that simulate interaction and transport of particles in material (Los Alamos National Laboratory, 2003; Ljungberg et al. 2012). We also compared VARSKIN 5.3 with results from various methodologies in the literature [Anspach and Hamby 2017]. Since the unveiling in the late 1980's (Traub et al. 1987), VARSKIN results have been examined for comparison sake with many different authors. In the sections that follow, we continue to provide inter-comparisons with former versions of VARSKIN so that the user can see how dose estimates have changed over the years. In addition, the reader will see comparisons with Monte Carlo simulation, as well as comparisons with the literature.

4.1 Inter-Code Comparisons

The VARSKIN 6 photon and electron dosimetry models have gone through extensive enhancements over the past several years. Comparisons of dose calculated using VARSKIN 3.1, 4, 5.3, and 6.0 for point sources are given below (using ICRP 38 data for historical consistency) to demonstrate how the four versions differ in dose estimation for the few scenarios considered.

4.1.1 Point Source Directly on Skin

Calculations were made using several versions of VARSKIN for the case of a ^{60}Co point source placed directly on the skin (i.e., no material and no air gap between the source and skin). For a 37-kBq hot particle and a 1-hour exposure time, the electron and photon dose averaged over 1 cm^2 at a depth of 7 mg/cm^2 was calculated. Table 4-1 shows the results of this calculation. Changes to electron dosimetry indicate a reduction of about 10% at this shallow depth, due primarily to changes in the calculation of specific absorbed dose distribution. Photon dose estimates changed dramatically because of the inclusion of charged particle buildup and photon attenuation.

Table 4-1 Comparison of Shallow Dose Estimates for Point Sources

Nuclide	V3.1 β Dose (mGy)	V4 β Dose (mGy)	V5.3 β Dose (mGy)	V6.0 β Dose (mGy)	V3.1 γ Dose (mGy)	V4 γ Dose (mGy)	V5.3 γ Dose (mGy)	V6.0 γ Dose (mGy)
Co-60	37.6	37.6	34.5	34.5	3.29	0.79	0.79	0.79

4.1.2 Point Source on Cover Material

Dose calculations at 7 mg/cm^2 were also performed for ^{60}Co, ^{137}Cs/^{137m}Ba, and ^{90}Sr/^{90}Y with three different cover material configurations. In each case, a 37-kBq point source and an exposure time of 1 hour were assumed with no gap between the layers of cover material. Doses were calculated for a 1-cm^2 averaging disk. Table 4-2 shows the results of these calculations. Changes to electron dosimetry are shown to either increase or decrease, due to model enhancements that affect particle track lengths, energy loss, backscatter characteristics, conversion electron consideration, etc. Photon dose at shallow depths for the scenario

considered decreases by about a factor of two after model enhancement, again, primarily due to the consideration of charged particle buildup and photon attenuation.

Table 4-2 Comparison of Shallow Dose Estimates for Various Cover Materials

Nuclide	Air Gap (cm)	Cover Material	V3.1 β Dose (mGy)	V4 β Dose (mGy)	V5.3 β Dose (mGy)	V6.0 β Dose (mGy)	V3.1 γ Dose (mGy)	V4 γ Dose (mGy)	V5.3 γ Dose (mGy)	V6.0 γ Dose (mGy)
Co-60	0.2	M_1	1.96	1.96	2.17	2.17	0.571	0.292	0.290	0.292
Cs-137D	0.2	M_1	14.0	14.0	13.7	13.5	0.199	0.0969	0.0959	0.0917
Sr-90D	0.2	M_1	32.6	32.6	29.1	28.2	0	0	0	0
Co-60	0.2	$2M_1$	0	0	0.0789	0.0789	0.558	0.258	0.257	0.258
Cs-137D	0.2	$2M_1$	4.75	4.75	6.50	6.44	0.181	0.0842	0.0834	0.0797
Sr-90D	0.2	$2M_1$	20.7	20.7	19.5	19.1	0	0	0	0
Co-60	1.0	M_1	0.813	0.813	0.813	0.813	0.0797	0.0429	0.0427	0.0429
Cs-137D	1.0	M_1	2.79	2.79	2.59	2.53	0.0277	0.0129	0.0128	0.0122
Sr-90D	1.0	M_1	5.37	5.37	4.74		0	0	0	0
Co-60	1.0	$2M_1$	0	0	0.0409	0.0409	0.0836	0.0404	0.0402	0.0404
Cs-137D	1.0	$2M_1$	1.40	1.40	1.53	1.49	0.0270	0.0121	0.0121	0.0115
Sr-90D	1.0	$2M_1$	3.95	3.95	3.66	3.51	0	0	0	0
Co-60	1.0	$M_1 + M_2$	0	0	0.00838	0.00838	0.0876	0.0400	0.0400	0.0400
Cs-137D	1.0	$M_1 + M_2$	0.770	0.770	1.03	1.01	0.0271	0.0120	0.0120	0.0114
Sr-90D	1.0	$M_1 + M_2$	3.26	3.26	3.11	3.00	0	0	0	0
Co-60	5.0	$M_1 + M_2$	0	0	0.00045	0.00045	0.0045	0.0020	0.0025	0.0025
Cs-137D	5.0	$M_1 + M_2$	0.0384	0.0384	0.0521	0.0513	0.0013	0.0006	0.0006	0.0006
Sr-90D	5.0	$M_1 + M_2$	0.167	0.167	0.158	0.153	0	0	0	0

Cs-137D includes the progeny ^{137m}Ba; Sr-90D includes the progeny ^{90}Y
M_1 — Cover material = thickness of 0.37 mm, density of 0.70 g/cm^3
$2M_1$ — Cover material = thickness of 0.74 mm, density of 0.70 g/cm^3
M_2 — Cover material = thickness of 0.40 mm, density of 1.1 g/cm^3

4.1.3 Infinite Plane Electron Source on the Skin

Calculations were performed for various nuclides using VARSKIN 4, 5.3, and 6.0 (the electron dosimetry model is unchanged between 3.1 and 4) to compare specifically the electron dose estimate for a large distributed disk source (simulating an infinite plane) on the skin for an exposure period of 1 hour (Table 4-3). The electron dose at a depth of 7 mg/cm^2 was calculated for a simulated contamination scenario with a concentration of 37 kBq/cm^2 on a circular source of 100 cm^2. A dose-averaging area of 1 cm^2 was assumed. Table 4-4 provides additional VARSKIN comparisons at various shallow depths in tissue for a source of ^{90}Y.

Table 4-3 Comparison of Electron Dose with Infinite Plane Source

Nuclide	V4	V5.3	V6.0
C-14	11.2	11.1	11.1
P-32	66.3	58.7	58.7
Co-60	37.7	34.5	34.5
I-131	52.4	48.4	48.4
Cs-137	51.2	47.8	47.8
Cs-137D	-	-	53.5
Sr-90	54.7	49.7	49.7
Y-90	68.3	59.7	59.7
Sr-90D	-	-	110

Cs-137D includes the progeny ^{137m}Ba; Sr-90D includes the progeny ^{90}Y; no dose estimates are given for V4 and V5.3 since those versions did not automatically include decay progeny.

Table 4-4 Dose vs. Depth for Distributed Disk Sources

Method	4 mg/cm^2	7 mg/cm^2	10 mg/cm^2	40 mg/cm^2
VARSKIN 4	79.0	68.3	61.4	40.7
VARSKIN 5.3	65.9	59.7	55.5	38.4
VARSKIN 6.0	65.9	59.7	55.5	38.4

4.2 Dosimetry V&V Using Monte Carlo Simulations

For the simulations, we used MCNP5 for photon comparisons and EGSnrc for electron comparisons. With each code, various source geometries were modeled close to the skin. The fundamental geometry, illustrated in Fig. 4-1, involves an infinite volume of air located above an infinite volume of tissue. Composition of these materials was taken from NIST standards for each material. Each of the sources was situated 1 micron above the skin and above the perpendicular bisect of the volume of tissue over which the dose is calculated.

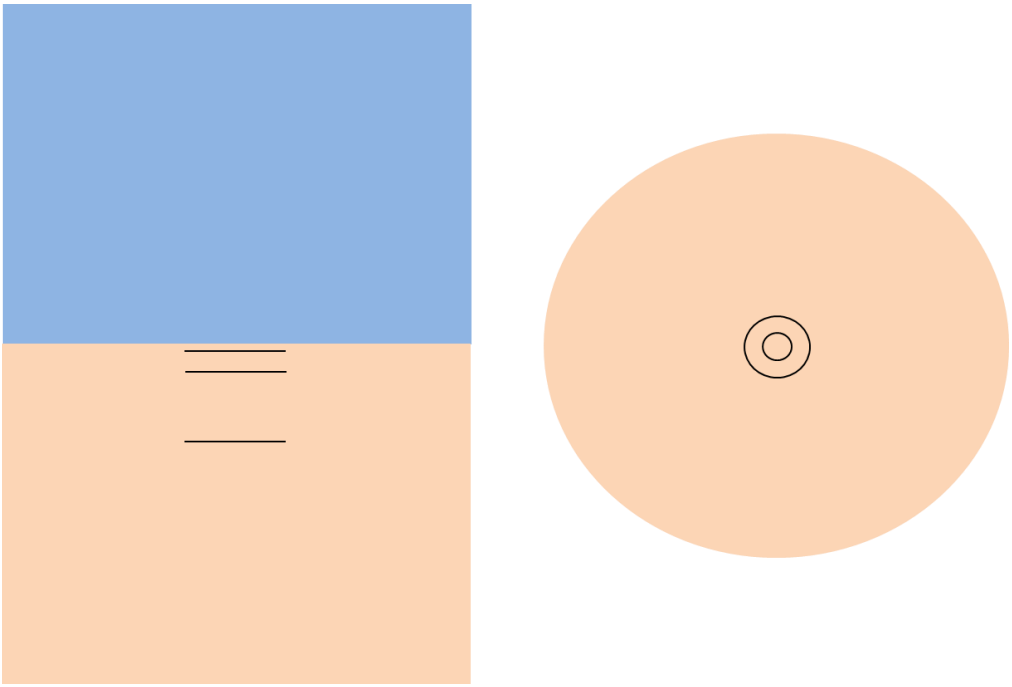

Figure 4-1 Horizontal (left) and Vertical (right) Cross-Sectional Views of the MCNP5 Geometry

As illustrated in Fig. 4-2, the dose per particle (photon or electron) was calculated for each of the sources at tissue depths of 7, 100, 300, and 1,000 mg/cm^2. The density thicknesses of 7, 300, and 1,000 mg/cm^2 correspond to the depth required by 10 CFR Part 20, “Standards for Protection against Radiation,” for calculation of dose to the skin, lens of the eye, and the deep dose, respectively. Although the value of 100 mg/cm^2 does not correspond to a regulatory-significant density thickness, results at that depth are provided as an indication of accuracy at an intermediate, yet shallow, depth.

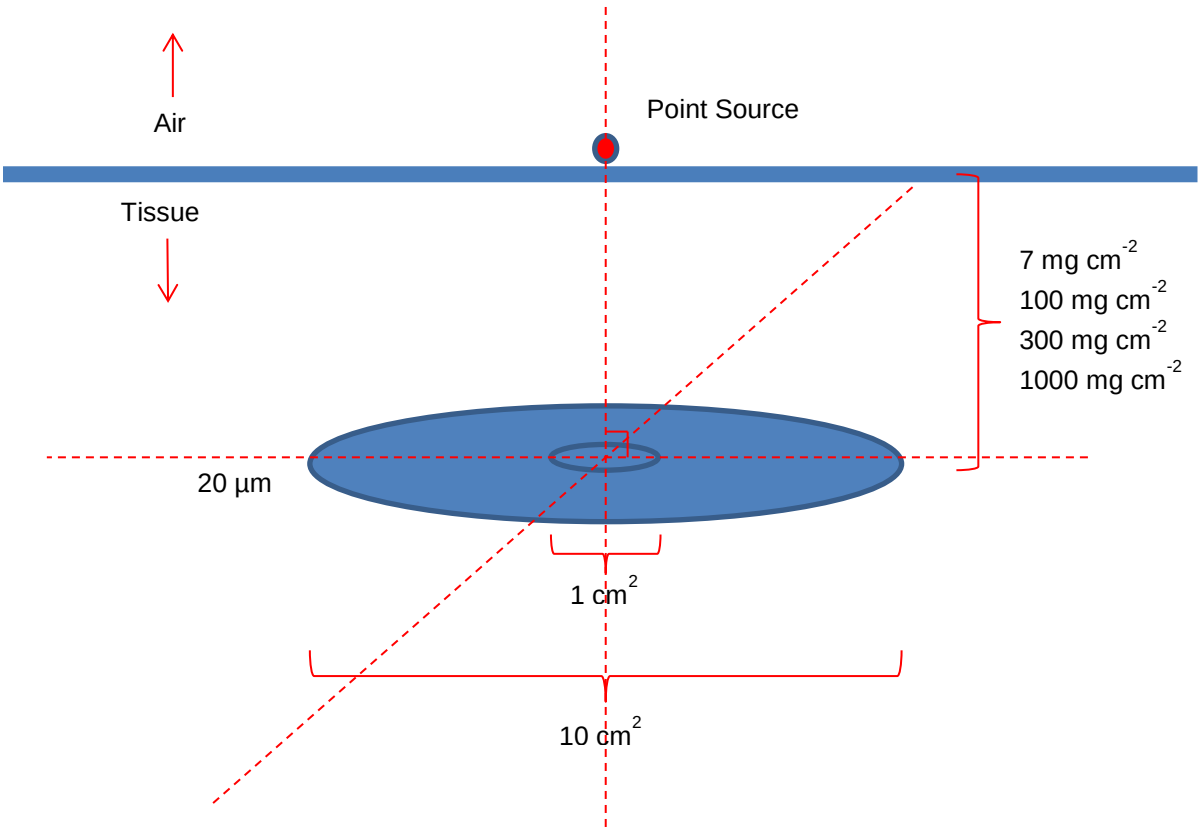

Figure 4-2 Point Source Geometry of Tissue Volumes

At each density thickness, the dose to two volumes of tissue, 0.002 cm^3 and 0.02 cm^3, was calculated. These dimensions correspond to cylindrical volumes within tissue, each having a thickness of 20 µm and a cross-sectional area of 1 cm^2 and 10 cm^2, respectively. The value of 20 µm was selected to create a volume large enough that uncertainties resulting from low numbers of particles interacting in the volume would not be an issue. Sherbini et al. [2008] showed that at thicknesses greater than 10 µm, any effects of dose averaging over increasingly smaller volumes are avoided.

Energy deposited in the volume of interest was calculated for dose estimation. The number of particle histories executed was sufficiently high to maintain statistical errors below 6%, with the majority producing an error of approximately 3%. Dose rate was calculated for a simulated source strength of 37 kBq, with a yield of 100 percent at a given energy ranging from 0.025 to 3 MeV. While this is not specific to any particular nuclide, it demonstrates the energy dependence of each methodology and shows which models are accurate predictors (as compared to MCNP5/EGSnrc) and which are not. Appendix A provides results for photon dosimetry comparisons, with Appendix B providing similar results, but for electron dosimetry. The appendices are arranged as follows.

For photon dosimetry, V&V focused on seven geometries, including: (1) point source; (2) 1 mm diameter 2D disk source; (3) 1 mm diameter by 1 mm height cylindrical source; (4) 1 mm cube slab source; (5) 1 mm diameter spherical source; (6) point source with an air gap and a cotton cover; and (7) point source that is 1 cm off axis. Dose estimates from VARSKIN 5 as a function of photon energy were compared with MCNP5 results at depths of 7, 100, 300, and 1000

mg/cm^2 for each of the geometries considered. VARSKIN 4 was shown to be a very good predictor at various tissue depths when the point- and disk-source geometries are modeled. VARSKIN 4, however, consistently overpredicts dose (compared to MCNP5) in the cylindrical, slab, and spherical geometries at energies greater than about 200 keV.

For electron dosimetry, results of the V&V exercise are provided in seven geometries: (1) point source; (2) 0.5 mm diameter 2D disk source; (3) 1 mm diameter 2D disk source; (4) 5 mm diameter 2D disk source; (5) 1 mm diameter by 1 mm height cylindrical source; (6) 1 mm diameter spherical source; and (7) 1 mm cube slab source. For each geometry, dose estimates from VARSKIN 5 as a function of electron energy were compared with EGSnrc and MCNP5 results at depths of 7, 100, 300, and 1000 mg/cm^2. Additionally, comparisons with four beta-emitting nuclides (^{28}Al, ^{42}K, ^{66}Cu, and ^{138}Cs) were conducted to show how the current VARSKIN electron dose predictions compare to previous estimates. VARSKIN 5 estimates of dose compare very well with EGSnrc and MCNP5, although MCNP5 estimates are slightly higher at deeper depths.

For additional evidence on the efficacy of VARSKIN, the user is directed to two publications in which VARSKIN 5.3 results are compared with historic literature on electron skin dosimetry [Anspach and Hamby 2017; Dubeau et al. 2018].

5 VARSKIN 6 LIMITATIONS

VARSKIN 6 calculates skin dose to an infinitely thin disk at depth in tissue for comparison to the NRC shallow dose limit of 0.5 gray (Gy) for both point and distributed sources (NRC, 2006). VARSKIN 6 can calculate the dose to averaging areas from a minimum of 0.01 cm^2 to a maximum of 100 cm^2. Users are cautioned that VARSKIN is designed to calculate the dose to skin from skin contamination. Using VARSKIN to perform calculations that are beyond the intended application of the code may result in erroneous dose estimates. This section discusses the known limitations of VARSKIN 6 and establishes the limits over which the code has been tested.

VARSKIN 6 offers the option of dose calculations based on the decay date of ICRP 38 or ICRP 107. ICRP 38 offers 838 radionuclides in the master library, while ICRP 107 offers more than 1200.

Dose calculations involving air gaps greater than 20 cm have not been tested and are, therefore, not allowed. It is likely that erroneous results may be obtained for large air gaps because the code does not account for multiple scattering events in air. These events may result in the dose being delivered to an area greater than that determined using VARSKIN 6 and can lead to inaccurate results. VARSKIN 6 is limited such that calculations for air gaps greater than 20 cm are not possible and a warning message is displayed.

VARSKIN 6 has not been tested extensively for dose-averaging areas other than 1 and 10 cm^2. However, because of the nature of the calculations performed by VARSKIN, there is no reason to believe that doses to areas less than or greater than 10 cm^2 will result in errors. A quick and limited study of dose results as a function of averaging disk area shows that the code appears to be stable and linear in this regard from 0.01 to 100 cm^2.

5.1 Electron Dosimetry

The VARSKIN V&V results indicated differences between VARSKIN 5 and EGSnrc for beta dosimetry on scenarios involving volumetric sources and intermediate electron energies (APPENDIX B). The V&V results for low-energy electrons at shallow depths are similar to the results seen at all depths where the electron is reaching its maximum range (even for the point-sources to a certain degree). These larger deviations are apparent at the tail end of the beta-dose profiles, as well (Mangini, 2012). Either way, it is clear from these results that the accuracy of VARSKIN 6 decreases as the electron reaches its maximum depth. In dose calculations for a distribution of electrons, this effect is still present since, approaching the deeper depths, the deposited energy is occurring at the tail end of the electron range.

VARSKIN 6 has been shown to be reliable for particulate sources that have dimensions less than eight times the X_{99} distance of the radionuclide in tissue. The X_{99} distance is essentially 99 percent of the range of beta particles in tissue emitted by nuclides in the source term. When the physical size of the source approaches this value, VARSKIN 6 may give unreliable results. A user who wants to model sources larger than this limit may wish to begin with smaller sources and increase the source size gradually to ensure that spurious results are not being generated. Modeling a source of this size is generally not necessary, however, as most of the source does not contribute to beta skin dose because of self-shielding. If the source dimensions selected are too large, VARSKIN 6 prompts the user with a warning of the potential for inaccurate results.

The X_{99} distance is included on the printout of a calculation to assist the user in determining the appropriateness of input source dimensions.

Also of note, VARSKIN 6 calculates shallow skin dose with the assumption that air is behind the source, i.e., an air/water (simulating tissue) interface at the skin surface. Users are reminded to use caution when comparing VARSKIN results to other calculations of skin dose that may have been executed with water behind the source (i.e., water/water interface). The backscatter correction factor used in VARSKIN 6 accounts for this interface difference.

5.1.1 DPK's and Scaling Model

DPK's have always underestimated dose at depths approaching the range of the electron. Monte Carlo is the standard and DPK models begin to fail when energy and range straggling becomes more and more important at greater depths. The effects of straggling are dominant at that part of the electron path. We suspect that the scaling model is not a contributor to the discrepancies noted. In fact, the accuracy of the scaling model is highest towards the end of the electron path. The interface between the source material and water is where the model has its largest deviations. This is likely not the cause, as dose at deeper depths will be dominated by electrons traversing very little of the source material (i.e., 0.25 X/X90); the model is extremely accurate in this case.

5.1.2 Scattering Model

In developing the scattering model, the Monte Carlo (EGSnrc) data used for the model all had a standard error less than 5%. Simulations with a greater error were eliminated with a dose contribution of zero. However, once the curve fits in *SadCalc.exe* were developed for the dose profiles, the error in the predicted dose values from the curve fits became extremely unreliable at very low dose values and the deeper depths. In examining the raw data used to create the scattering model and dose profiles, it became apparent that the dose values reached an asymptote of about $1x10^{-12}$ (Gy per electron). At these dose values the standard error of the Monte Carlo simulations begins to exceed 5%. VARSKIN 6 was modified to set all dose contributions to zero if the calculation resulted in something less than $1x10^{-12}$ Gy/electron. This patch is justified since the model begins to fail at such low doses (and the standard error from Monte Carlo calculations is very high). When averaging over a beta spectrum, these contributions to the BSCF and dose are negligible. Setting dose to zero at these depths is executed for both the source scattering profile and the water scattering profile, thereby setting the BSCF equal to one (1). Nonetheless, for doses just greater than $1x10^{-12}$ Gy/electron, the VARSKIN 6 model will be rather inaccurate for dose calculations at depths near the end of the electron range.

5.2 Photon Dosimetry

The photon dosimetry model assumes that all volume sources are composed of air. This assumption results in greater accuracy when modeling larger, less dense sources (e.g., a gas cloud). However, when modeling volumetric sources of greater density, VARSKIN 6 is optimized for small dimensions (less than about a millimeter). This optimization is the result of a tradeoff between attenuation and charge particle buildup within the source itself. The user should exercise care when modeling large-volume sources (i.e., if the source is large enough to impact self-absorption of photons).

5.3 Creation of SADD and Backscatter Data for Progeny Inclusion

When adding a nuclide to the user library (using “ADD”), the SADD routine compiles two SADD files, one for each of electron and photon dosimetry (.rad and .photon, respectively). These files contain decay data necessary for the dose calculation. The .rad file contains average beta energy, half-life, maximum (X90) beta range, yield, electron emission distributions, backscatter factors, etc. Likewise, the .photon file contains a list of photon energies (and yield) emitted during decay.

When the user elects to include progeny (“D”) in the parent-nuclide dose calculation, the SADD calculations are a bit more involved. For photons, the .photon file simply includes a longer list of photon energies/yields. For electrons, however, a single SADD file is created for all beta/electron emissions from the parent and all of its progeny. This single SADD file contains all the same data, but now based on a combination of beta/electron emissions from all nuclides in the decay chain. Combining the SADD file in this way simply results in a composite emitted electron probability distribution for the chain nuclides. This being the case, dose calculations for parent/progeny electrons may be different from the same dose calculated by summing individual nuclides (rather than relying on the automatic progeny inclusions). These deviations are shown to be the result of the difference in backscatter factors calculated individually, or for the combined decay data (because a singular backscatter factor is applied based on average electron energy rather than on the probability distribution). One example in which this is most prominent is the difference between the sum of ^{90}Sr and its progeny ^{90}Y, versus the combined ^{90}Sr/^{90}Y calculation by selecting “D”. The difference is generally less than 1% and no more than about 3%, varying by nuclide.

The most revealing evidence is a plot of backscatter factors as a function of skin depth for ^{90}Sr, ^{90}Y, and ^{90}Sr/^{90}Y combined (Fig. 5-1). It is evident that the backscatter factors for the combined case are totally driven by the presence of ^{90}Y. This is expected given the higher energy of the ^{90}Y beta and the method in which the backscatter factors are integrated over the beta spectra in the SADD routine (see Section 3.1.6). However, when the source geometry deviates from that of a point source, the combined backscatter factor is unable to properly account for the change in overall dose contribution for the two radionuclides. For example, Fig 5-1 shows the combined backscatter factor being dominated by ^{90}Y. However, in the presence of a volume source or an air gap, the path length that a beta traverses prior to entering the dose area will change compared to that of a simple point source geometry. If the change in geometry has the effect of decreasing the overall path length in tissue, the increase in dose would be more significant for the lower energy ^{90}Sr beta at shallow skin depths of interest. The change in dose relative to the higher energy ^{90}Y beta will be properly accounted for in the SADD values found in the .rad file. However, the impact will be lost on the combined backscatter factor and the ^{90}Y-driven correction factor will be slightly off when applied to the added ^{90}Sr dose component. Again, however, this discrepancy is at most 3% different and is seen as insignificant in the shallow skin dose calculation.

In the two examples that follow, we calculate the shallow skin dose for a millimeter-dimensioned cylindrical source. In the first case (Table 5-1) we examine ^{90}Sr, ^{90}Y, and the combined ^{90}Sr/^{90}Y; and in the second case (Table 5-2) we examine ^{133}I, ^{133}Xe, ^{133m}Xe, the combined ^{133}I with its progeny. As can be seen in the tables, the discrepancy with ^{90}Sr/^{90}Y is 3% and there is only a rounding difference (in photon dose) for ^{133}I and its progeny. This scenario is worked out in Example 4 of Appendix C.

Table 5-1 Dose from Individual and Combined Parent/Progeny for Sr/Y-90

Nuclide Selection	Branching Ratio	Relative electron dose	Relative photon dose
Sr-90		2.12	-
Y-90	1.000	2.74	-
SUM		4.86	-
Sr-90D*		4.71	-
Difference		3%	

*includes dose from Y-90 as calculated in VARSKIN 6.0 with progeny inclusion

Table 5-2 Dose from Individual and Combined Parent/Progeny for I/Xe-133

Nuclide Selection	Branching Ratio	Relative Electron Dose	Relative Photon Dose
I-133		2.77	0.0295
Xe-133	0.971	0.794	0.0270
Xe-133m	0.029	2.33	0.0123
Xe-133	1.000	0.794	0.0107
SUM		3.63	0.0405
I-133D*		3.63	0.0402
Difference		0%	0.9%

*includes dose from Xe-133 and Xe-133m as calculated in VARSKIN 6.0 with progeny inclusion

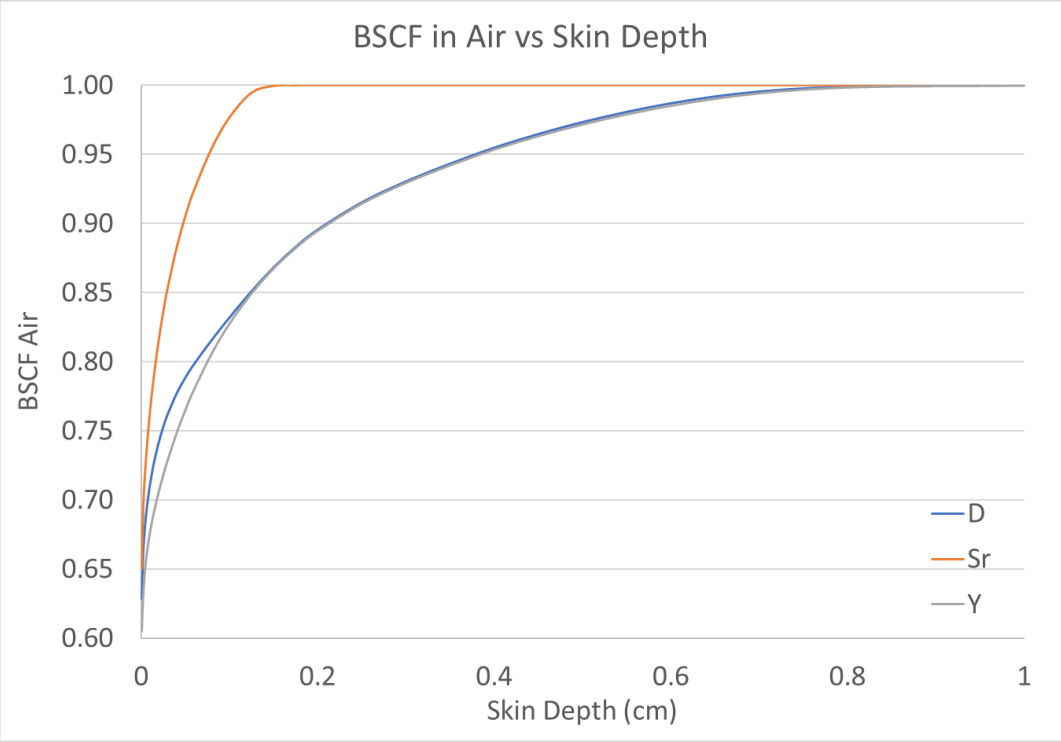

Figure 5-1 Backscatter Factors in Air as a Function of Depth in Tissue

6 SPECIAL TOPICS

VARSKIN 6 is designed to be very flexible while maintaining a high level of accuracy. However, the code can be misused, particularly when modeling infinitely large sources (i.e., sources with physical dimensions greater than the X_{99} distance for the source radionuclides). This section describes this possible misuse of VARSKIN and how it can be avoided. This section also describes a method to determine the maximum photon dose to an area from multiple hot particles.

6.1 Infinite Sources

When modeling infinite or semi-infinite sources (e.g., an enveloping cloud) with VARSKIN 6, the tendency is to choose very large dimensions for the source. This approach will result in the calculation of a grossly inaccurate dose or a zero dose because the integration routine becomes unstable. The correct method is to determine the maximum penetration distance (i.e., the X_{99} distance) and set the source dimensions as described below.

The X_{99} distance can be found by running a simple calculation for the radionuclide of interest and looking at the printout for the value. The maximum source radius (r_{max}) and the side lengths are then determined using the equation,

$$r_{max} = r_{dos} + \left({}^{X_{99}}/_{\rho_{min}}\right)\rho_w \qquad [6.1.1]$$

where r_{dos} is the radius of the dose-averaging area (in cm), is the density of water, and is the smallest density of the covering material, source, air (if an air gap is included), or tissue. Using the density of the least dense material will ensure that the dose-averaging area includes contributions from the entire source. If an air gap is included, using the VARSKIN 6 default value for the density of air (0.001293 g/cm^3) is appropriate. If no cover material is specified, using tissue density (1 g/cm^3) is the best choice.

When modeling infinite sources, the use of the cylinder source geometry is recommended. When using the cylinder source geometry, the source thickness, Δt_{max}, should be determined using the equation,

$$\Delta t_{max} = \frac{X_{99}\rho_w}{\rho_s} \qquad [6.1.2]$$

where ρ_s is the source density. Source area in this case can be maximized at a value of 100 cm^2 to simulate the infinite lateral dimension.

6.2 Maximum Dose from Multiple Contamination Sources

Determining the maximum dose to the dose-averaging area for multiple contaminations requires multiple calculations. These calculations require elements that are not available in VARSKIN 6 but can be accomplished manually, as described below.

Before attempting to run the offset particle model, the user should determine the size of the irradiation area directly beneath each of the contaminated areas. Note that the size of sources does not need to be the same for each particle. By comparing these areas for each source, it may be possible to eliminate one or more of the contaminated areas because there are no

associated overlapping fields. However, for contaminated areas with overlapping fields, plot the doses and their relative positions leaving plenty of room between the sources for results from additional calculations.

Next, perform VARSKIN 6 calculations using the offset particle model for photons with locations midway between any two contaminated areas. For more than two sources that are not in a straight line, choose a central location, and calculate the dose at this point using the offset particle model. Thus, for three contaminated areas in a triangular formation, perform four calculations. Choose the value of the offset as one-half of the distance between any two sources, with one additional dose calculation performed in the center of the triangle.

After performing these calculations, the user must use discretion to determine the most probable area of highest dose based on the distribution of dose on the graph paper. After determining this area, the user can perform a final calculation for each particle by using the offset particle model. The user should not anticipate an accuracy greater than 20 percent.

6.3 Manipulation of Files for Extended Utility

The knowledgeable user can modify VARSKIN 6 in a couple of ways for added utility: first, to model a mono-energetic electron, and second, to model a water/water interface at the skin surface. In the first case, the user should modify the ICRP 38 data (the ICRP38.DAT file in the **dat** folder) for one of the nuclides (this should also work using ICRP 107 data file). We have found that ^{7}Be is one of the easiest to modify. Figure 1 shows the first few lines of ICRP38.DAT for the original data (left) and modified data (right).

```
H-3    12.35y              1      H-3    12.35y              1
5 1.00000E+02 5.68276E-03        5 1.00000E+02 5.68276E-03
Be-7    53.3d              4      Be-7    53.3d              4
1 1.03400E+01 4.77605E-01        1 0.00000E+00 0.00000E-00
6 8.04306E-06 4.77550E-01        6 1.00000E+00 0.75000E-00
6 1.18019E-07 4.77605E-01        6 0.00000E+00 0.00000E-00
2 1.63500E-02 5.47500E-05        2 0.00000E+00 0.00000E-00
Be-10  1.6E6y              1     Be-10  1.6E6y              1
5 1.00000E+02 2.52256E-01        5 1.00000E+02 2.52256E-01
C-11   20.38m              4     C-11   20.38m              4
4 9.97600E+01 3.85535E-01        4 9.97600E+01 3.85535E-01
3 1.99520E+02 5.11000E-01        3 1.99520E+02 5.11000E-01
2 1.61920E-04 1.83300E-04        2 1.61920E-04 1.83300E-04
2 8.09600E-05 1.83300E-04        2 8.09600E-05 1.83300E-04
```

Figure 6-1 Input Example for the ICRP38.DAT File

On examination of the original data (left), we see that ^{7}Be has a half-life of 53.3 days and four major emissions per decay. The first in the list is a gamma ray (code 1) with a yield of 10.34% and an energy of 0.477605 MeV. The second and third lines show emission of conversion electrons (code 6) with very low yields and roughly the same energies as the photon. The final emission is a low-energy X-ray (code 2) with a yield of 1.635%. We cannot simply remove three of the data lines and indicate that ^{7}Be has only one emission; if we did, indices throughout the VARSKIN data files would be in disarray. Therefore, we will set yields and energies to zero (data on the right) except for one entry. The modified entry shows the emission of an electron with 100% yield and an energy of 0.75 MeV. This will simulate the emission of a mono-energetic electron; no other alterations are necessary.

The second modification allows the user to change the VARSKIN 6 simulation (normally an air/water interface at the skin surface) to model a water/water interface. We accomplish this by modifying the .rad file (in the **dat** folder) for the nuclide of choice. The final 160 lines of data written to that file (by *SadCalc.exe*) are backscatter factors for use in the half-space scenario (air/water interface). Manually setting each of these factors to “1” removes consideration of half-space such that VARSKIN 6 will model a homogeneous water medium (a water/water interface).

Incidentally, the emission codes in the .DAT decay data files are as follows:

(1) gamma ray;
(2) X ray;
(3) annihilation photon;
(4) positron;
(5) electron (beta);
(6) conversion electron;
(7) Auger electron;

And ICRP107.DAT includes these, as well (but they are never accessed):

(8) alpha;
(9) recoil nucleus;
(10) fission fragment; and
(11) neutron

7 REFERENCES

Anspach, L.J.; Hamby, D.M. Performance of the VARSKIN 5 (v5.3) Electron Dosimetry Model. *Radiation Protection Dosimetry*. DOI:10.1093/rpd/ncx302; December 2017.

Attix, F.H. Introduction to Radiological Physics and Radiation Dosimetry. New York, NY: John Wiley & Sons. 1986.

Berger, M.J. "Distribution of Absorbed Dose around Point Sources of Electrons and Beta Particles in Water and Other Media." Medical Internal Radiation Dose Committee, Pamphlet No. 7. *Journal of Nuclear Medicine*. Vol. 12, Supplement No. 5. pp. 5–22. 1971.

Berger, M.J. "Improved Point Kernals for Electron and Beta-Ray Dosimetry". NBSIR 73-107. Center for Radiation Research. National Bureau of Standards. Washington, DC; February 1973.

Berger, M.J., J.S. Coursey, M.A. Zucker, and J. Chang. "Stopping-Power & Range Tables for Electrons, Protons, and Helium Ions." ESTAR, PSTAR, and ASTAR databases. National Institute of Standards and Technology. Washington, DC. Last accessed December 2017.

https://www.nist.gov/pml/stopping-power-range-tables-electrons-protons-and-helium-ions

Chung, M.; Foderaro, A.H.; Jester, W.A.; Levine, S.H. Microcomputer Monte Carlo electron transport codes for beta skin dose calculations. IEEE Transactions on Nuclear Science. 18(3); June 1991a.

Chung, M.; Levine, S.H.; Jester, W.A. Monte Carlo calculation and silicon detector measurement of the hot particle dose. *Health Physics*. 61(6):843-848; 1991b.

Covens, P.; Berus, D.; Caveliers, V.; Struelens, L.; Vanhavere, F.; Verellen, D. Skin dose rate conversion factors after contamination with radiopharmaceuticals: influence of contamination area, epidermal thickness and percutaneous absorption. *Journal of Radiological Protection*. 33:381-393; 2013.

Cross, W.G., N.O. Freedman, and P.Y. Wong. "Tables of Beta-Ray Dose Distributions in Water." AECL 10521, CA9200298. Chalk River, Ontario, Canada: Chalk River Laboratories, Dosimetric Research Branch. 1992.

Delacroix, D. "Beta Particle and Electron Absorbed Dose Calculations for Skin Surface Contaminations" (in French). DCES/SPR/SRI/86–656. Paris, France: Commissariat à l'Energie Atomique. 1986.

Dubeau, J., Hakmana Witharana, S.S., Sun, J., Heinmiller, B.E., Chase, W.J. A Comparison of Beta Skin Doses Calculated with VARSKIN 5.3 and MCNP5. *Radiation Protection Dosimetry*. DOI:10.1093/rpd/ncy108; July 2018.

Durham, J.S. "VARSKIN 3: A Computer Code for Assessing Skin Dose from Skin Contamination." NUREG/CR-6918. Washington, DC: U.S. Nuclear Regulatory Commission. 2006.

Durham, J.S. "VARSKIN Mod 2 and SADDE Mod 2: Computer Codes for Assessing Skin Dose from Skin Contamination." NUREG/CR-5873, PNL-7913. Washington, DC: NRC. 1992.

Durham, J.S., and M.W. Lantz. “Determination of Gamma Dose Rates and Charged Particle Equilibrium from Hot Particles.” *Radiation Protection Management*. 8(3): 35–41; 1991.

Faw, R.E. Absorbed dose to skin from radionuclide sources on the body surface. *Health Physics*. 63(4):443-448; 1992.

Halbleib, J.A.; Melhorn, T.A. ITS: Integrated TIGER series of coupled electron/photon Monte Carlo transport codes. Report No. SAND 84-0573. Sandia National Laboratories. Albuquerque, NM; 1984.

Hamby, D.M., Mangini, C.D., Caffrey, J.A., Tang, M. “VARSKIN 5: A Computer Code for Skin Contamination Dosimetry.” NUREG/CR-6918, Rev 2. Washington, DC: U.S. Nuclear Regulatory Commission. 2014.

Hamby, D.M., Lodwick, C.J., Palmer, T.S., Reese, S.R., Higley, K.A. “VARSKIN 4: A Computer Code for Skin Contamination Dosimetry.” NUREG/CR-6918, Rev 1. Washington, DC: U.S. Nuclear Regulatory Commission. 2011.

International Commission on Radiation Units and Measurements. “Tissue Substitutes in Radiation Dosimetry and Measurement.” ICRU Report 44. Bethesda, MD: International Commission on Radiation Units and Measurements. 1989.

International Commission on Radiological Protection. “The Biological Basis for Dose Limitation in the Skin.” Publication 59. Oxford, England: Pergamon Press. 1991.

International Commission on Radiological Protection. “Radionuclide Transformations.” Publication 38. Oxford, England: Pergamon Press. 1983.

International Commission on Radiation Protection. “Nuclear Decay Data for Dosimetric Calculations.” Publication 107. Ann. ICRP 38 (3). 2008

Johns, H.E., and J.R. Cunningham. The Physics of Radiology. 4th Edition. Springfield, IL: Charles C. Thomas. 1983.

Kawrakow, I., & Rogers, D. W. The EGSnrc code system: Monte Carlo simulation of electron and photon transport. *Technical Report* PIRS-701. Ottawa, Canada: National Research Council of Canada. 2000.

Kocher, D.C., and K.F. Eckerman. “Electron Dose-Rate Conversion Factors for External Exposure of the Skin from Uniformly Deposited Activity on the Body Surface.” *Health Physics*. 53: 135–141; 1987.

Lantz, M.W., and M.W. Lambert. “Charged Particle Equilibrium Corrections for the Gamma Component of Hot Particle Skin Doses.” *Radiation Protection Management*. 7(5): 38–48; 1990.

Ljungberg, M., S.E. Strand, and M.A. King. Monte Carlo Calculations in Nuclear Medicine, Second Edition. CRC Press. Chapter 10:175–195; 2012.

Los Alamos National Laboratory, X-5 Monte Carlo Team. “MCNP—A General Monte Carlo N-Particle Transport Code, Version 5. LA-CP-03-0245. Los Alamos, NM: LANL. 2003.

Mangini, C.D., and D.M. Hamby. “Scaling Parameters for Hot-Particle Beta Dosimetry”. Radiation Protection Dosimetry. 172(4): 356-366; 2016.

Mangini, C.D. “Beta-particle backscatter factors and energy-absorption scaling factors for use with dose-point kernels.” Doctoral Dissertation. Oregon State University. December 2012.

McDaniel, N.S.; Hamby, D.M. The Efficacy of VARSKIN 5.3 for Eye Dosimetry. VARSKIN Technical Session. Annual Domestic RAMP User’s Meeting. Bethesda, MD; October 2017.

NIST website, http://physics.nist.gov/PhysRefData/Star/Text/ESTAR.html). Last accessed December 2017.

Piechowski, J. “Dosimetry and Therapy of Skin Contaminations” (in French). CEA–R–5441. Paris, France: Commissariat à l’Energie Atomique. 1988.

Radiation Safety Information Computational Center. “MCNP4c2, Coupled Neutron, Electron Gamma 3-D Time-Dependent Monte Carlo Transport Calculations.” CCC–701. Oak Ridge, TN: RSICC. 2001.

Radiation Safety Information Computational Center. “NUCDECAY: Nuclear Decay Data for Radiation Dosimetry Calculations for ICRP and MIRD.” CCC–701. Oak Ridge, TN: RSICC. 1995.

Reece, W.D., S.D. Miller, and J.S. Durham. “SADDE (Scaled Absorbed Dose Distribution Evaluator), A Code to Generate Input for VARSKIN.” NUREG/CR–5276. Washington, DC: NRC. 1989.

Rogers, D. W. O. Fifty years of Monte Carlo simulations for medical physics. *Physics in Medicine and Biology.* 51: R287-R301; 2006.

Rohloff, F. A Monte Carlo program for the transport of beta particles through layers of different materials. Proceedings of the International Beta Dosimetry Symposium. Feb 15-18, 1983. Washington, DC. NUREG/CP-0050. pg 25; 1984.

Rohloff, F. and M. Heinzelmann. “Calculation of Dose Rates for Skin Contamination by Beta Radiation.” *Radiation Protection Dosimetry*. 14: 279–287; 1986.

Sherbini, S., J. DeCicco, A.T. Gray, and R. Struckmeyer. “Verification of the VARSKIN Beta Skin Dose Calculation Computer Code,” *Health Physics.* 94: 527–538; 2008.

Shultis, J.K. and Faw, R.E. Radiation Shielding. American Nuclear Society. ISBN 0-89448-456-7. La Grange Park, IL. 2000.

Spencer, L. V. Theory of electron Penetration. *Physical Review.* 98: 1597-1615; 1955.

Spencer, L. V. Energy Dissipation by Fast Electrons. *National Bureau of Standards Monograph 1*; 1959.

Taylor, D.C.; Hussein, E.M.A.; Yuen, P.S. Skin dose from radionuclide contamination on clothing. *Health Physics*. 72(6):835-841; 1997.

Traub, R.J., W.D. Reece, R.I. Scherpelz, and L.A. Sigalla. “Dose Calculation for Contamination of the Skin Using the Computer Code VARSKIN.” NUREG/CR–4418. Washington, DC: NRC. 1987.

U.S. Nuclear Regulatory Commission. News Release No. 02-039. April 2, 2002. https://www.nrc.gov/docs/ML0209/ML020990362.pdf Last accessed December 2017.

APPENDIX A
SUPPORTING FIGURES FROM SECTION 4

A.1 GEOMETRY 1: POINT SOURCE

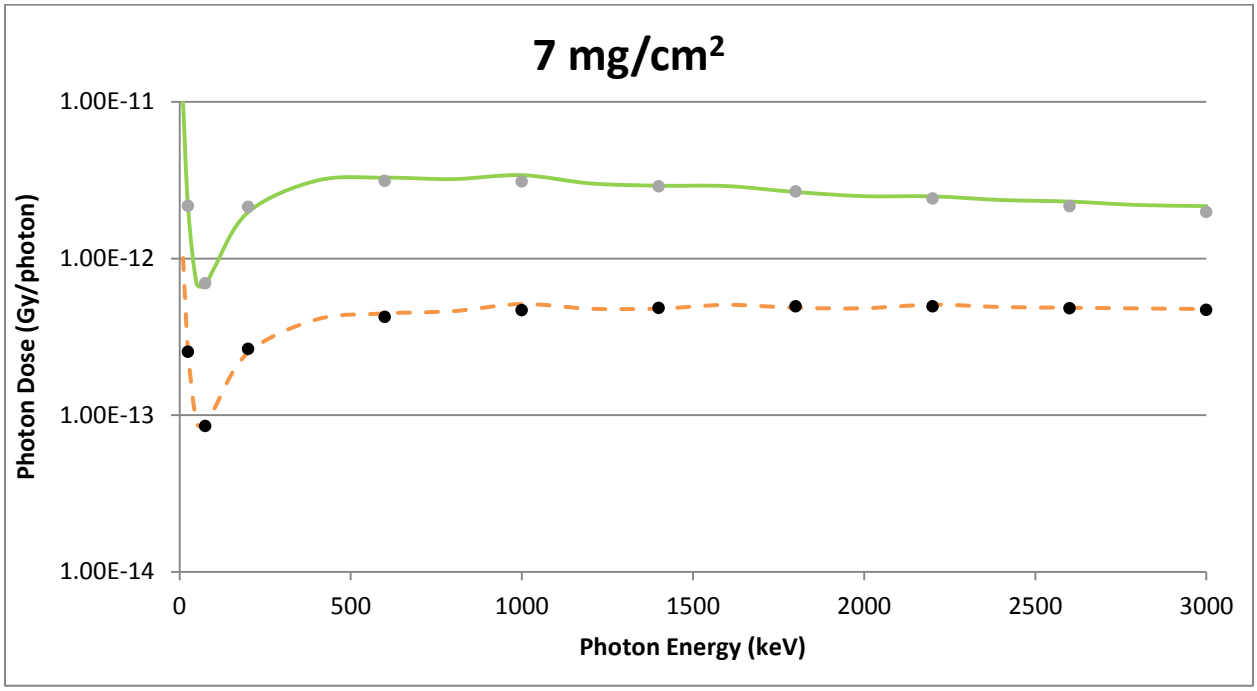

Figure A-1 **A Point Source Geometry Comparison of VARSKIN 5 (Circles) and MCNP5 (lines) Predicted Dose Per Initial Photon as a Function of Photon Energy in Tissue at a Density Thickness of 7 mg/cm^2 and a Tissue Volume Cylinder of Area 1 cm^2 (solid line) and 10 cm^2**

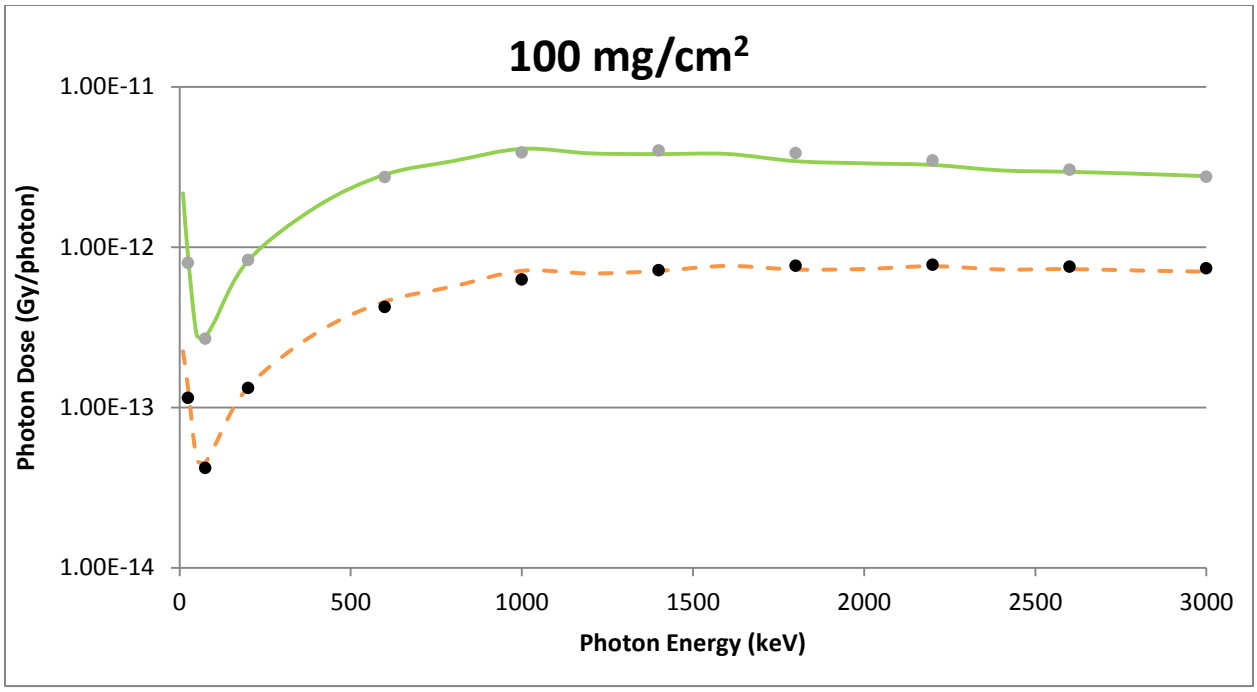

Figure A-2 **A Point Source Geometry Comparison of VARSKIN 5 (circles) and MCNP5 (lines) Predicted Dose Per Initial Photon as a Function of Photon Energy in Tissue at a Density Thickness of 100 mg/cm^2 and a Tissue Volume Cylinder of Area 1 cm^2 (solid line) and 10 cm^2 (dashed line), With a Thickness of 20 mm**

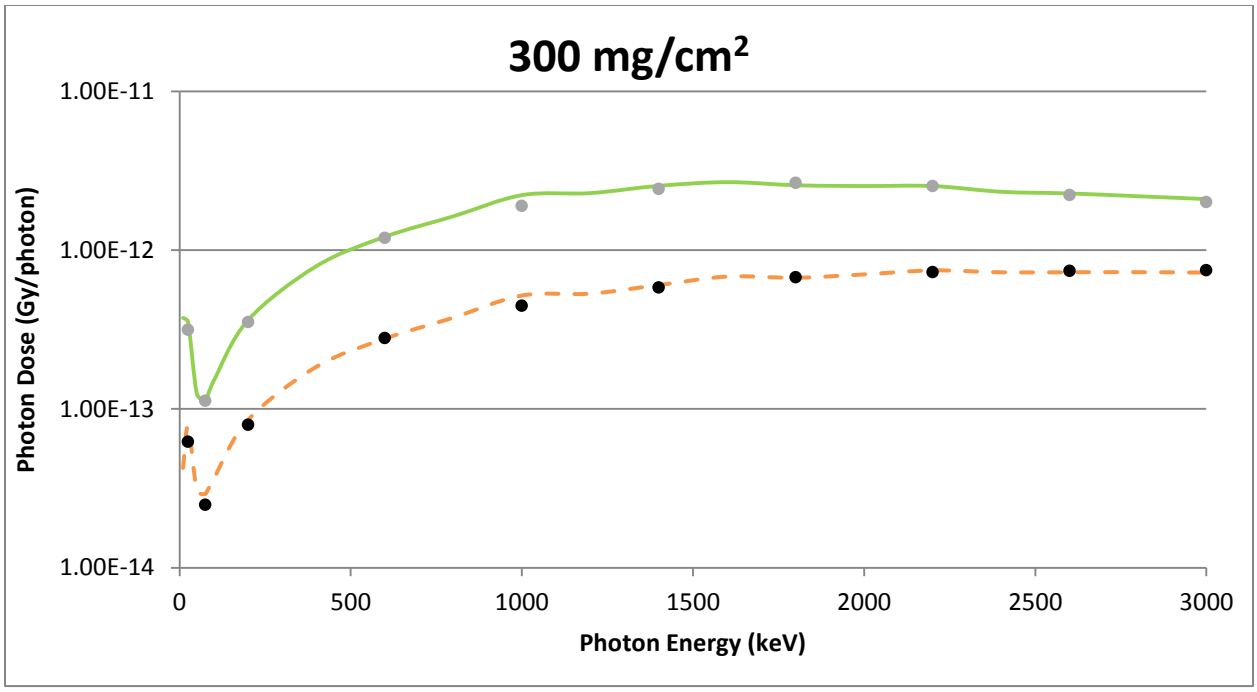

Figure A-3 **A Point Source Geometry Comparison of VARSKIN 5 (circles) and MCNP5 (lines) Predicted Dose Per Initial Photon as a Function of Photon Energy in Tissue at a Density Thickness of 300 mg/cm^2 and a Tissue Volume Cylinder of Area 1 cm^2 (solid line) and 10 cm^2 (dashed line), With a Thickness of 20 mm**

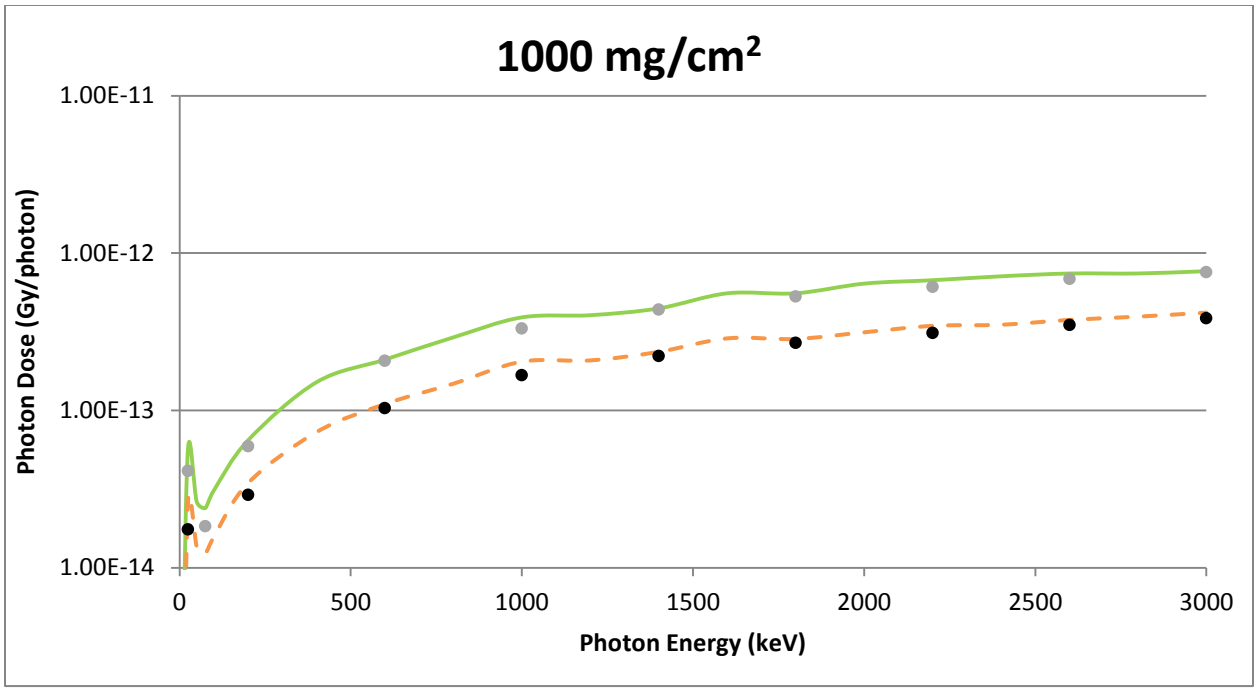

Figure A-4 **A Point Source Geometry Comparison of VARSKIN 5 (circles) and MCNP5 (lines) Predicted Dose Per Initial Photon as a Function of Photon Energy in Tissue at a Density Thickness of 1000 mg/cm^2 and a Tissue Volume Cylinder of Area 1 cm^2 (solid line) and 10 cm^2 (dashed line), With a Thickness of 20 mm**

A.2 GEOMETRY 2: DISK SOURCE

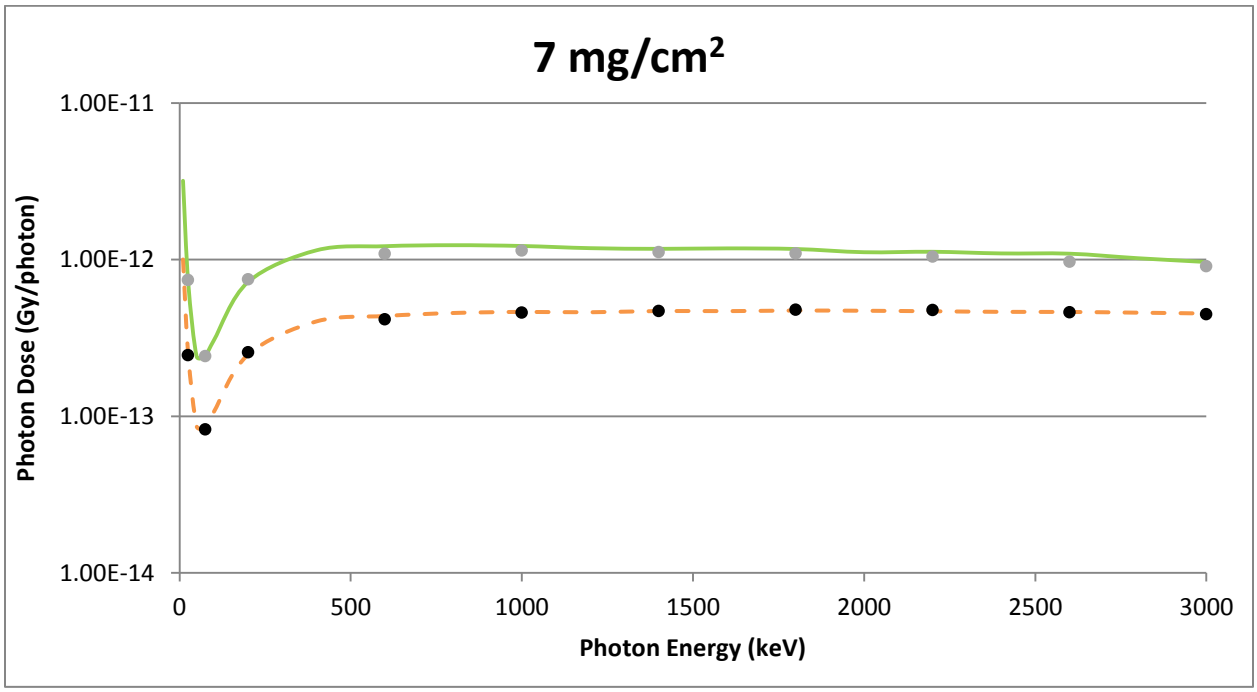

Figure A-5 **A Disk Source Geometry Comparison of VARSKIN 5 (circles) and MCNP5 (lines) Predicted Dose Per Initial Photon as a Function of Photon Energy in Tissue at a Density Thickness of 7 mg/cm² and a Tissue Volume Cylinder of Area 1 cm² (solid line) and 10 cm² (dashed line), With a Thickness of 20 mm**

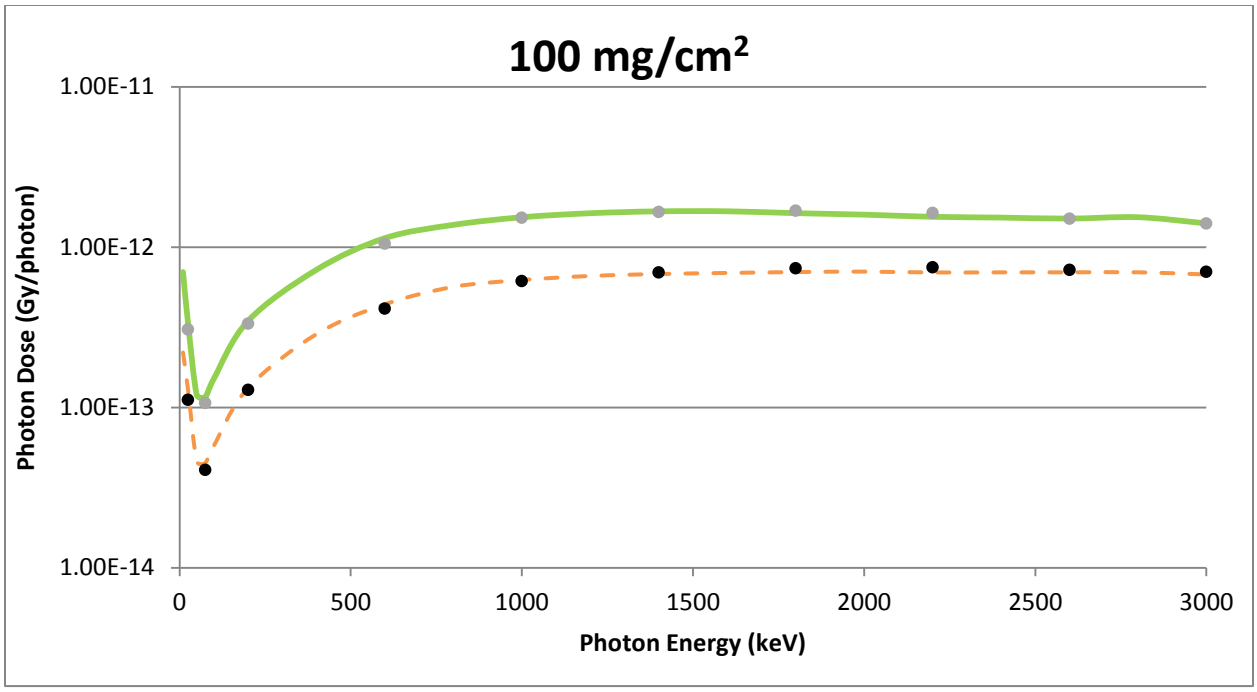

Figure A-6 **A Disk Source Geometry Comparison of VARSKIN 5 (circles) and MCNP5 (Lines) Predicted Dose Per Initial Photon as a Function of Photon Energy in Tissue at a Density Thickness of 100 mg/cm^2 and a Tissue Volume Cylinder of Area 1 cm^2 (solid line) and 10 cm^2 (dashed line), With a Thickness of 20 mm**

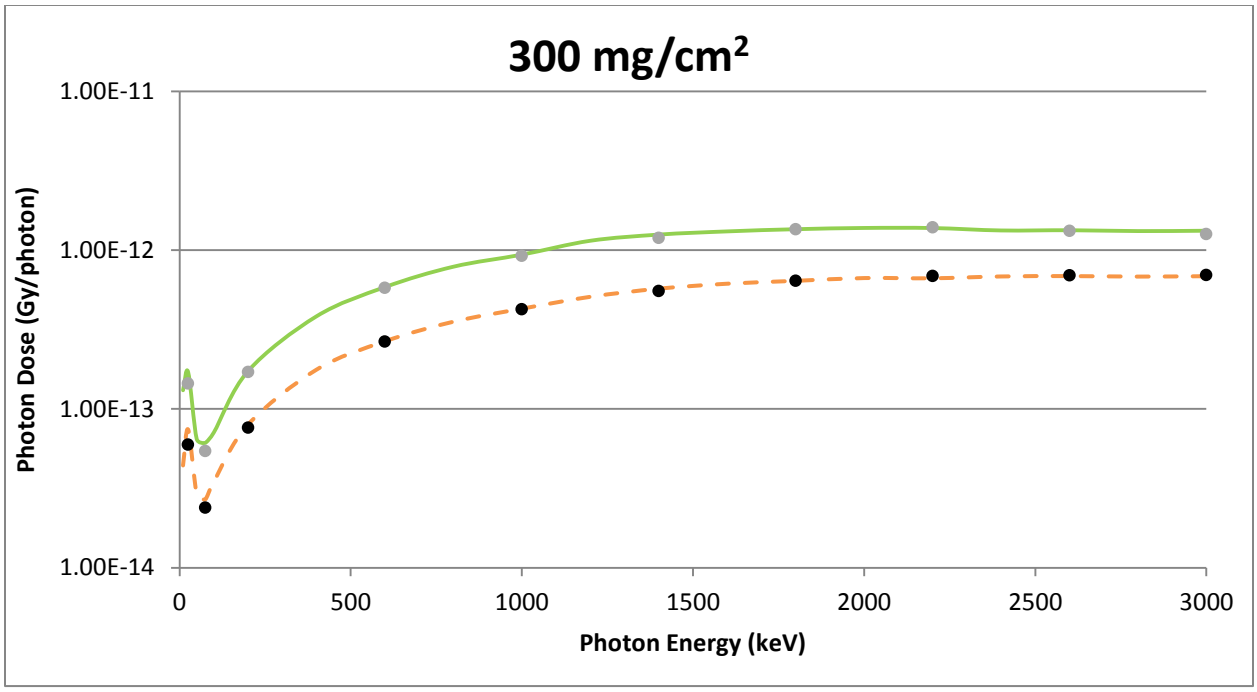

Figure A-7 **A Disk Source Geometry Comparison of VARSKIN 5 (circles) and MCNP5 (lines) Predicted Dose Per Initial Photon as a Function of Photon Energy in Tissue at a Density Thickness of 300 mg/cm^2 and a Tissue Volume Cylinder of Area 1 cm^2 (solid line) and 10 cm^2 (dashed line), With a Thickness of 20 mm**

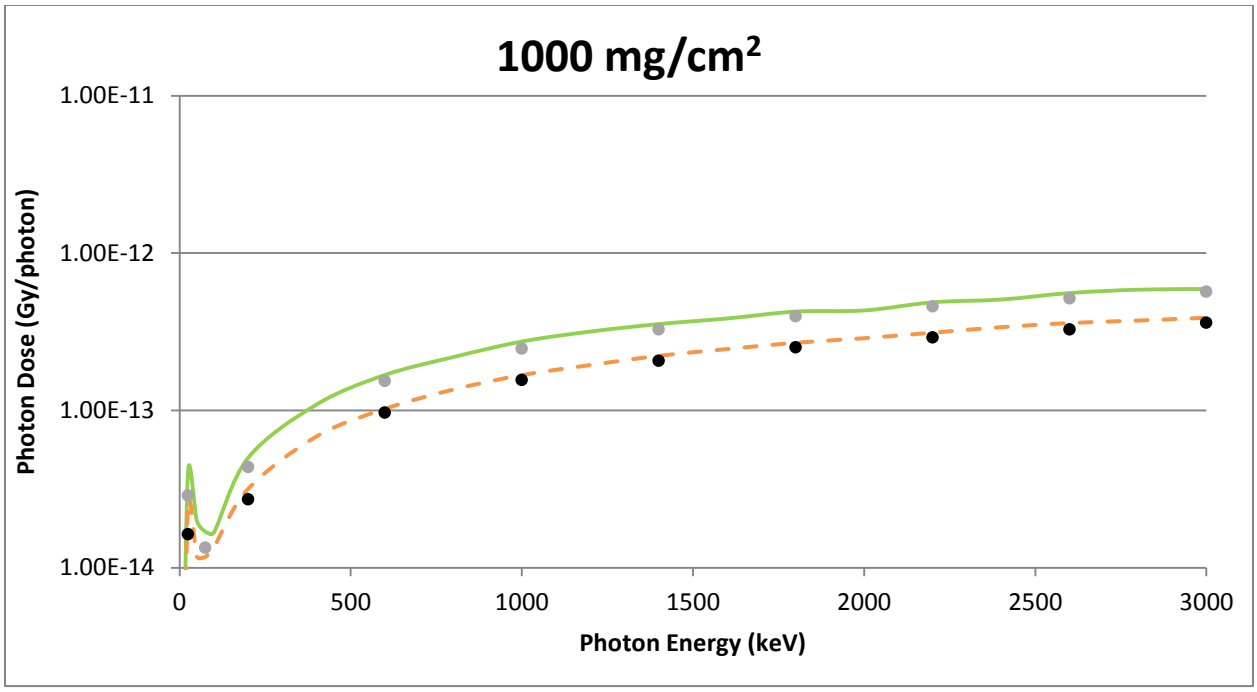

Figure A-8 **A Disk Source Geometry Comparison of VARSKIN 5 (circles) and MCNP5 (lines) Predicted Dose Per Initial Photon as a Function of Photon Energy in Tissue at a Density Thickness of 1000 mg/cm^2 and a Tissue Volume Cylinder of Area 1 cm^2 (solid line) and 10 cm^2 (dashed line), With a Thickness of 20 mm**

A.3 GEOMETRY 3: CYLINDRICAL SOURCE

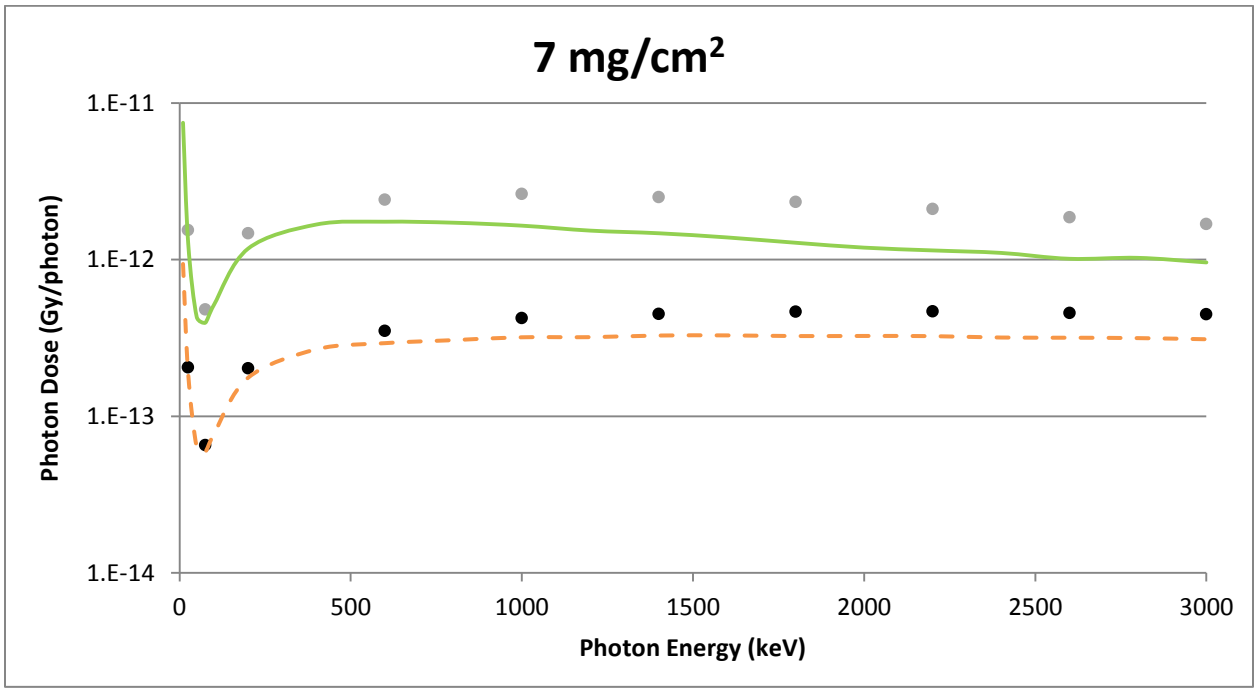

Figure A-9 **A Cylindrical Source Geometry Comparison of VARSKIN 5 (circles) and MCNP5 (lines) Predicted Dose Per Initial Photon as a Function of Photon Energy in Tissue at a Density Thickness of 7 mg/cm² and a Tissue Volume Cylinder of Area 1 cm² (solid line) and 10 cm² (dashed line), With a Thickness of 20 mm**

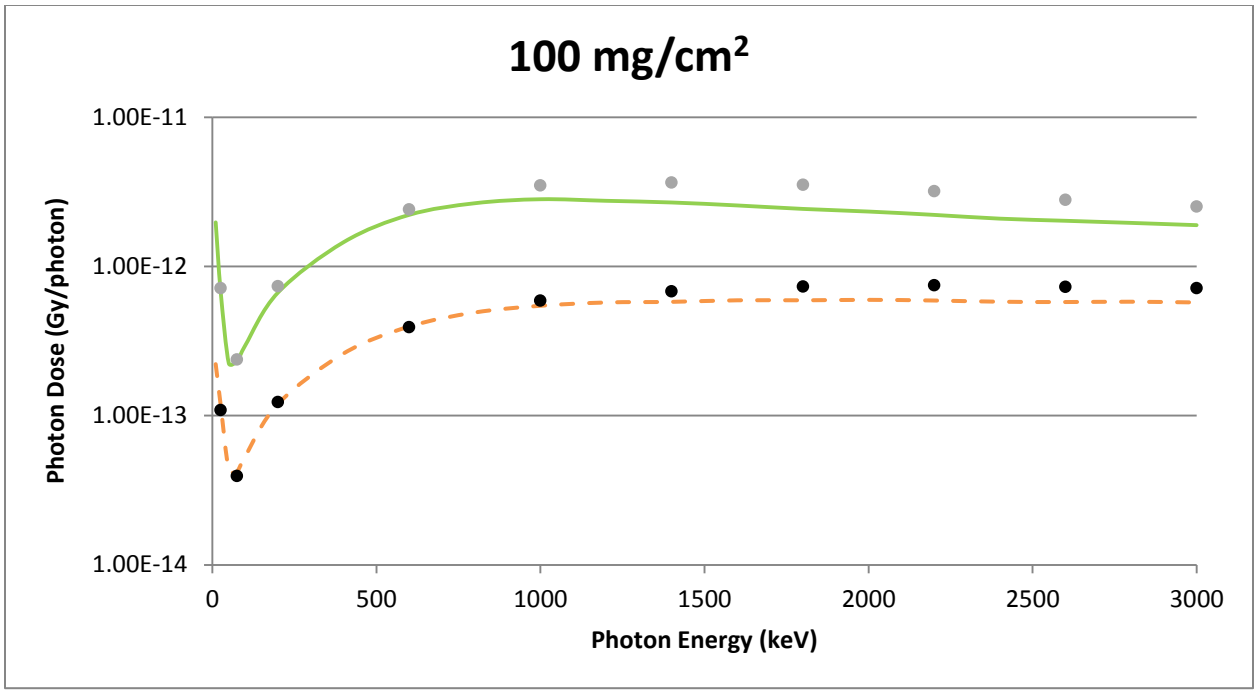

Figure A-10 **A Cylindrical Source Geometry Comparison of VARSKIN 5 (circles) and MCNP5 (lines) Predicted Dose Per Initial Photon as a Function of Photon Energy in Tissue at a Density Thickness of 100 mg/cm^2 and a Tissue Volume Cylinder of Area 1 cm^2 (solid line) and 10 cm^2 (dashed line), With a Thickness of 20 mm**

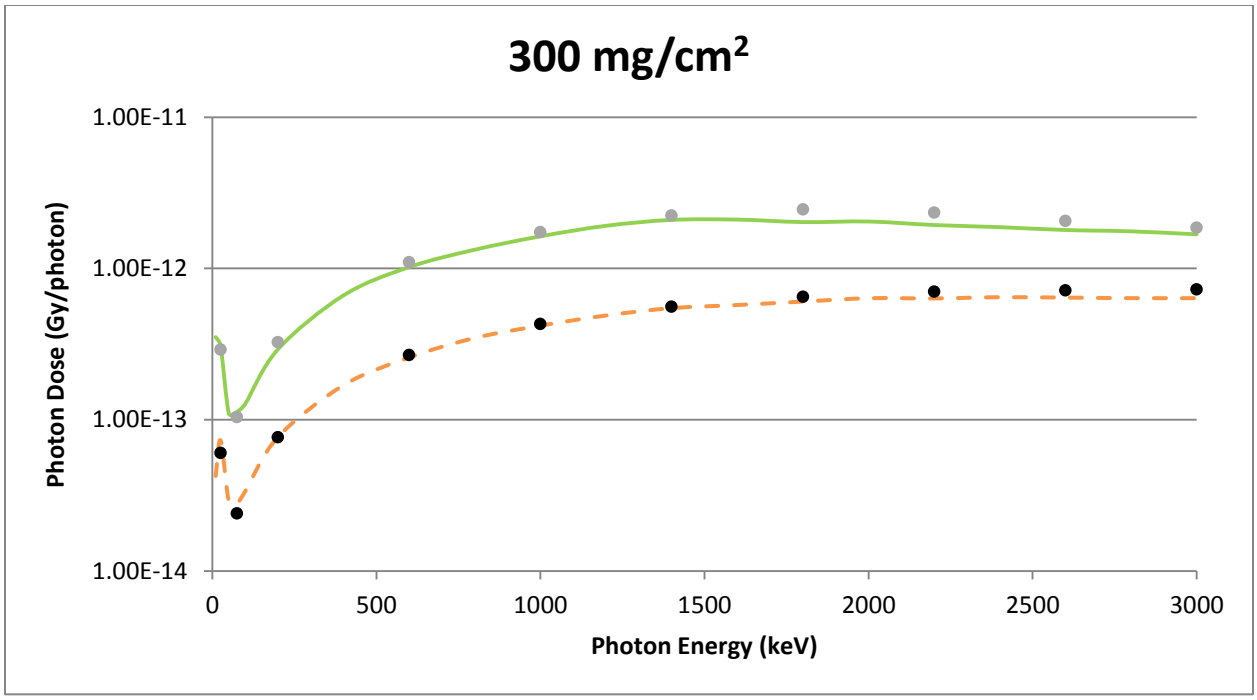

Figure A-11 **A Cylindrical Source Geometry Comparison of VARSKIN 5 (circles) and MCNP5 (lines) Predicted Dose Per Initial Photon as a Function of Photon Energy in Tissue at a Density Thickness of 300 mg/cm^2 and a Tissue Volume Cylinder of Area 1 cm^2 (solid line) and 10 cm^2 (dashed line), With a Thickness of 20 mm**

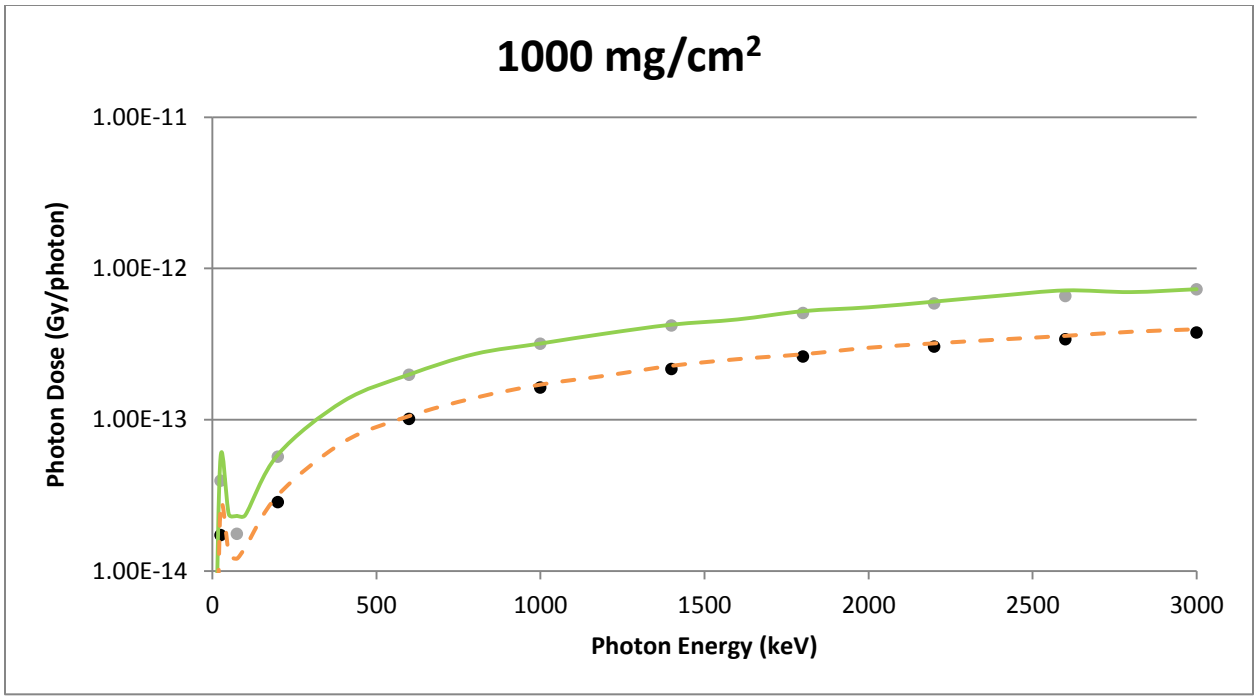

Figure A-12 **A Cylindrical Source Geometry Comparison of VARSKIN 5 (circles) and MCNP5 (lines) Predicted Dose Per Initial Photon as a Function of Photon Energy In Tissue at a Density Thickness of 1000 mg/cm² and a Tissue Volume Cylinder of Area 1 cm² (solid line) and 10 cm² (dashed line), With a Thickness of 20 mm**

A.4 GEOMETRY 4: SLAB SOURCE

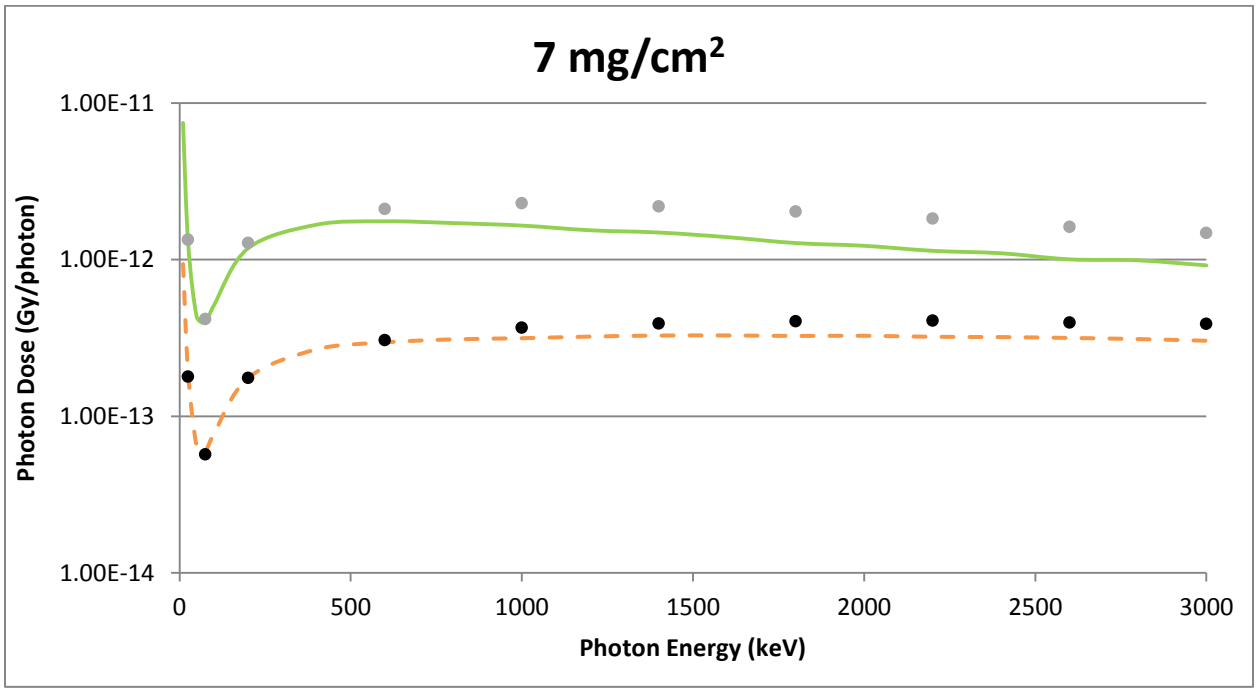

Figure A-13 **A Slab Source Geometry Comparison of VARSKIN 5 (circles) and MCNP5 (lines) Predicted Dose Per Initial Photon as a Function of Photon Energy in Tissue at a Density Thickness of 7 mg/cm² and a Tissue Volume Cylinder of Area 1 cm² (solid line) and 10 cm² (dashed line), With a Thickness of 20 mm**

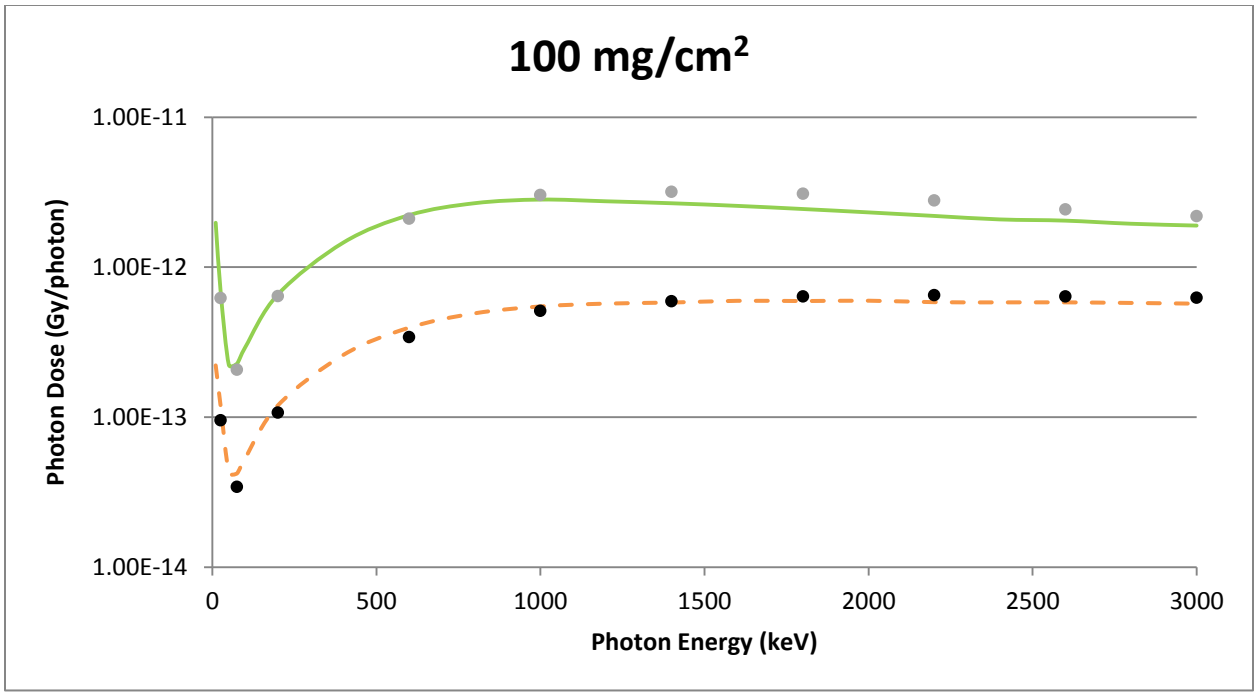

Figure A-14 **A Slab Source Geometry Comparison of VARSKIN 5 (circles) and MCNP5 (lines) Predicted Dose Per Initial Photon as a Function of Photon Energy in Tissue at a Density Thickness of 100 mg/cm^2 and a Tissue Volume Cylinder of Area 1 cm^2 (solid line) and 10 cm^2 (dashed line), With a Thickness of 20 mm**

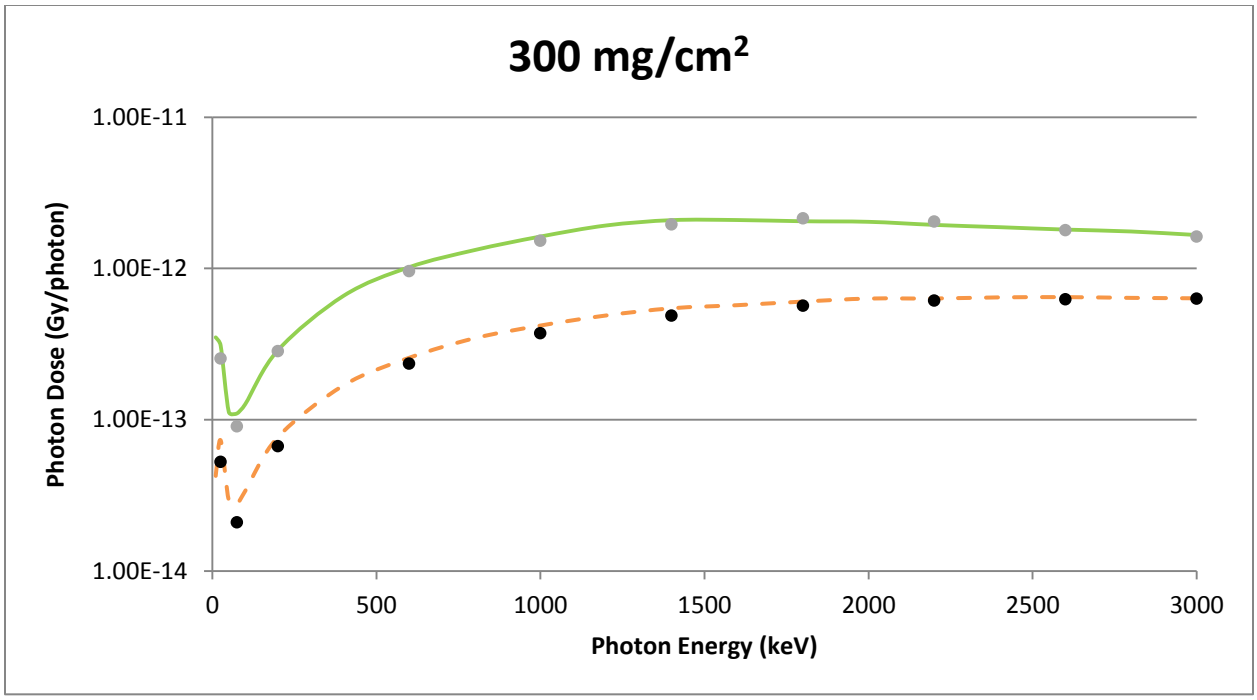

Figure A-15 **A Slab Source Geometry Comparison of VARSKIN 5 (circles) and MCNP5 (lines) Predicted Dose Per Initial Photon as a Function of Photon Energy in Tissue at a Density Thickness of 300 mg/cm² and a Tissue Volume Cylinder of Area 1 cm² (solid line) and 10 cm² (dashed line), With a Thickness of 20 mm**

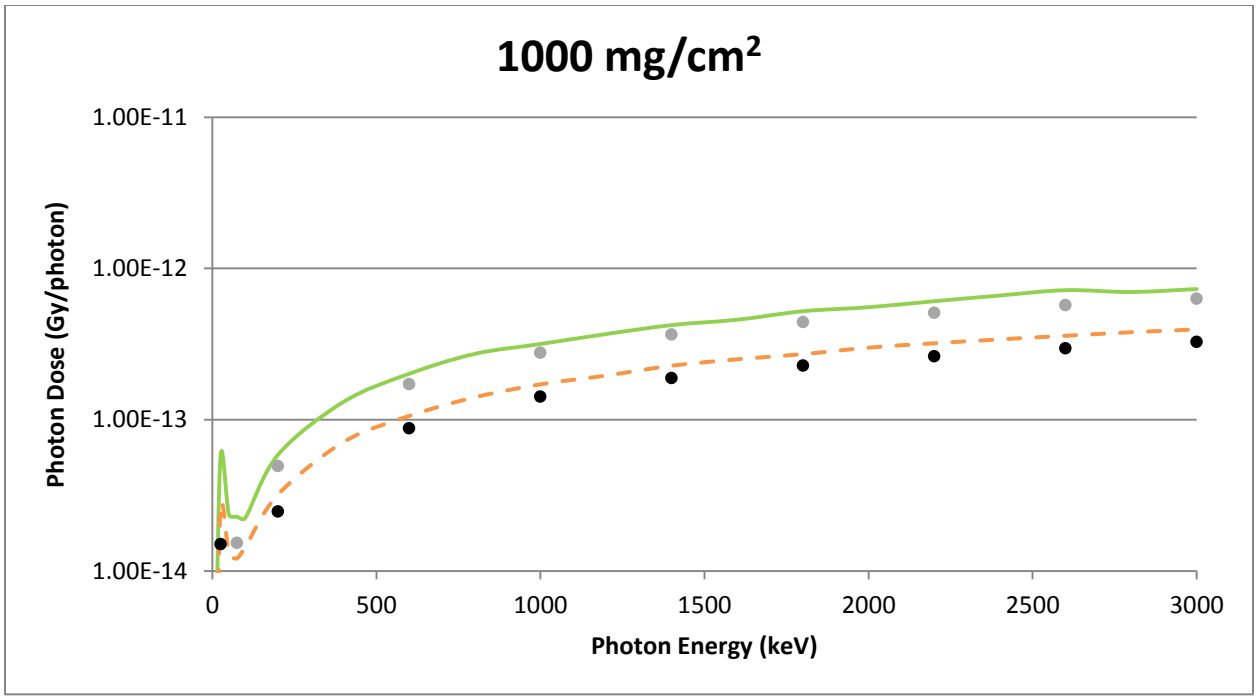

Figure A-16 **A Slab Source Geometry Comparison of VARSKIN 5 (circles) and MCNP5 (lines) Predicted Dose Per Initial Photon as a Function of Photon Energy in Tissue at a Density Thickness of 1000 mg/cm² and a Tissue Volume Cylinder of Area 1 cm² (solid line) and 10 cm² (dashed line), With a Thickness of 20 mm**

A.5 GEOMETRY 5: SPHERICAL SOURCE

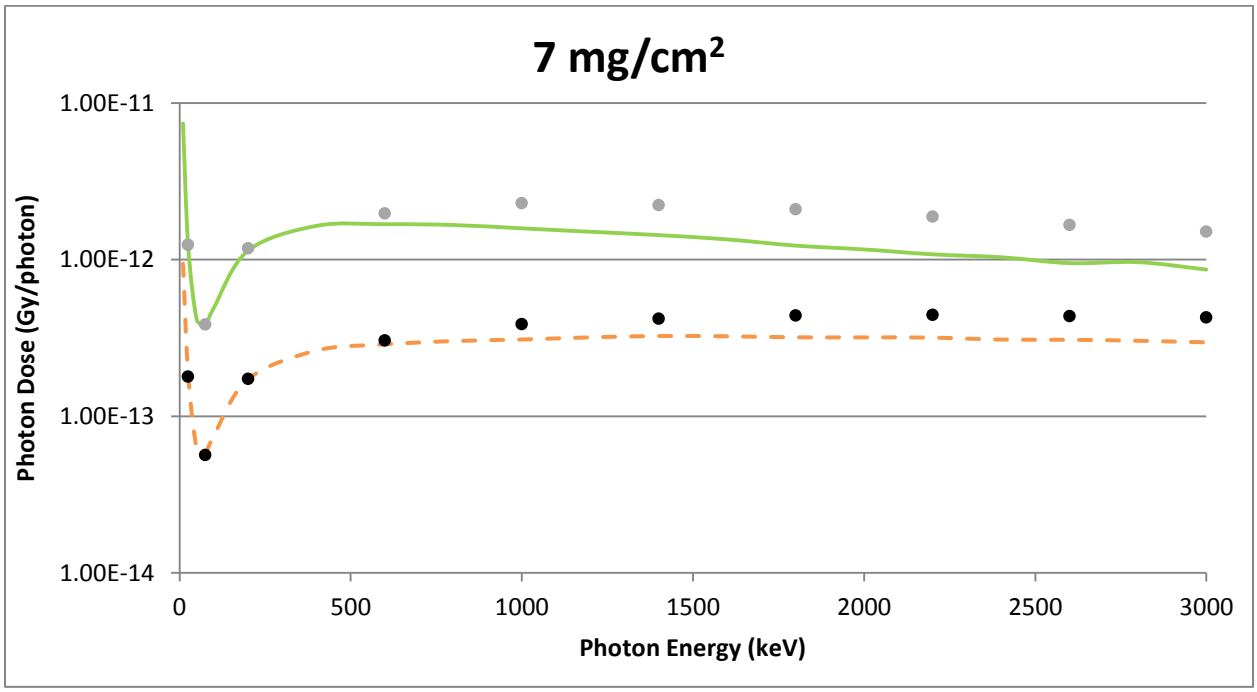

Figure A-17 **A Spherical Source Geometry Comparison of VARSKIN 5 (circles) and MCNP5 (Lines) Predicted Dose Per Initial Photon as a Function of Photon Energy in Tissue at a Density Thickness of 7 mg/cm² and a Tissue Volume Cylinder of Area 1 cm² (solid line) and 10 cm² (dashed line), With a Thickness of 20 mm**

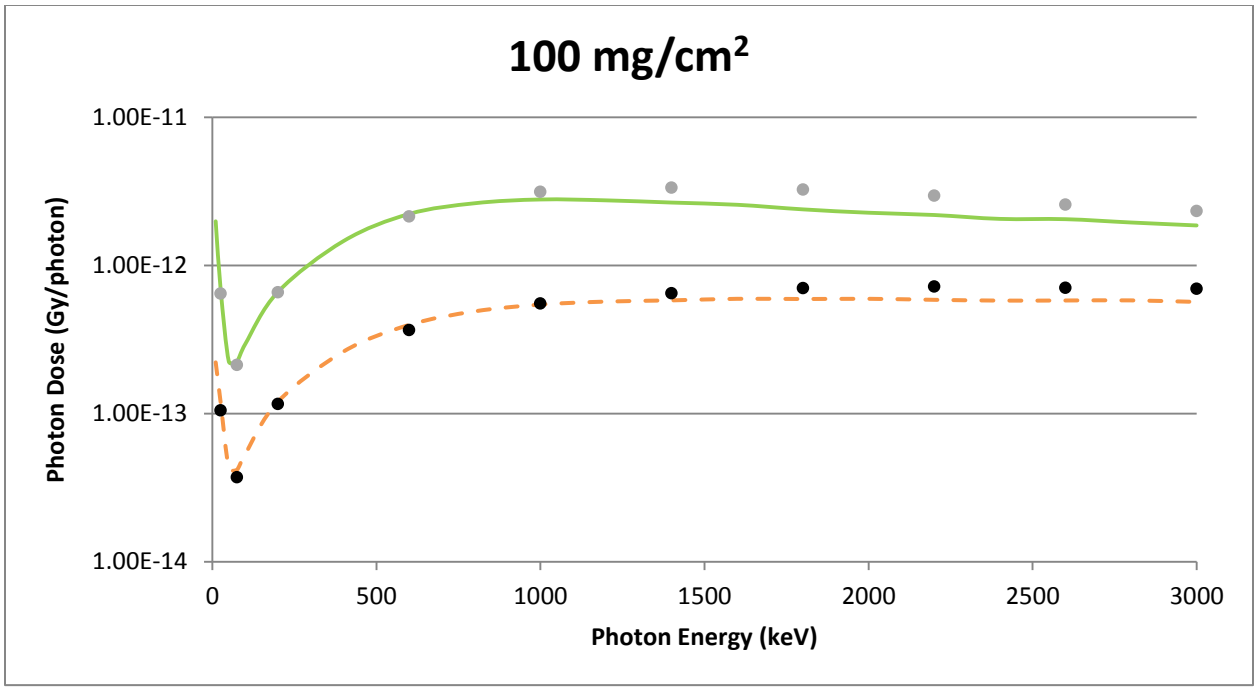

Figure A-18 **A Spherical Source Geometry Comparison of VARSKIN 5 (circles) and MCNP5 (lines) Predicted Dose Per Initial Photon as a Function of Photon Energy in Tissue at a Density Thickness of 100 mg/cm² and a Tissue Volume Cylinder of Area 1 cm² (solid line) and 10 cm² (dashed line), With a thickness of 20 mm**

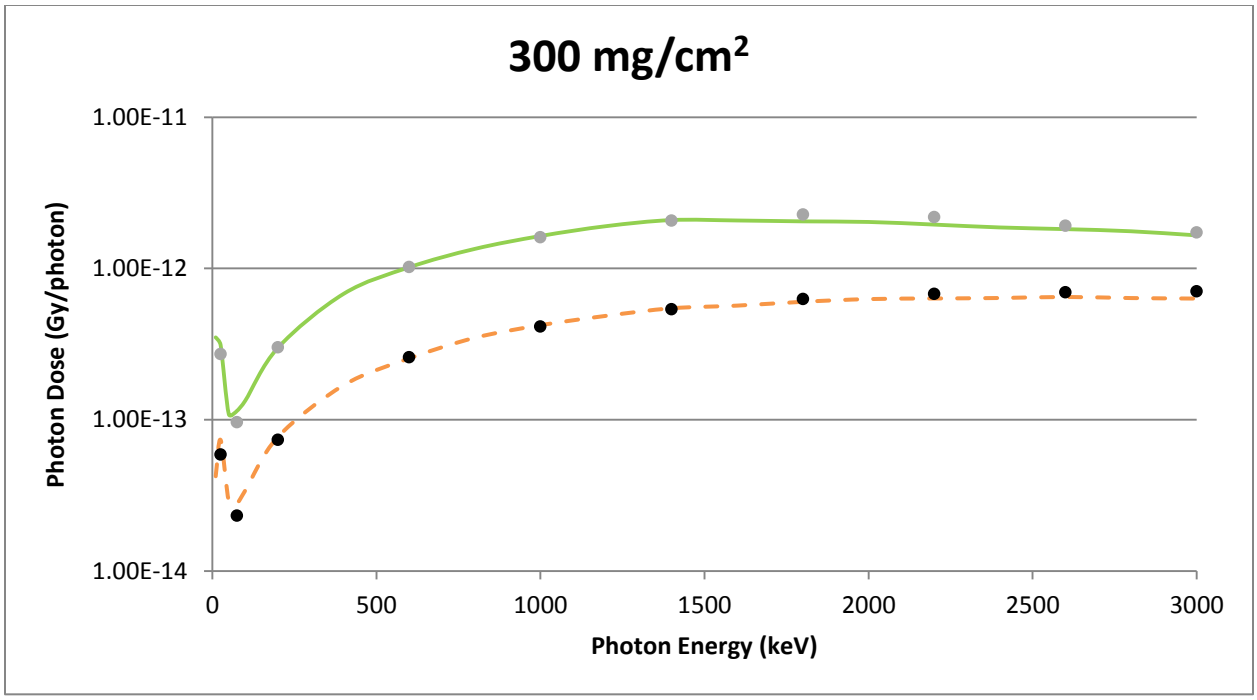

Figure A-19 **A Spherical Source Geometry Comparison of VARSKIN 5 (circles) and MCNP5 (lines) Predicted Dose Per Initial Photon as a Function of Photon Energy in Tissue at a Density Thickness of 300 mg/cm² and a Tissue Volume Cylinder of Area 1 cm² (solid line) and 10 cm² (dashed line), With a Thickness of 20 mm**

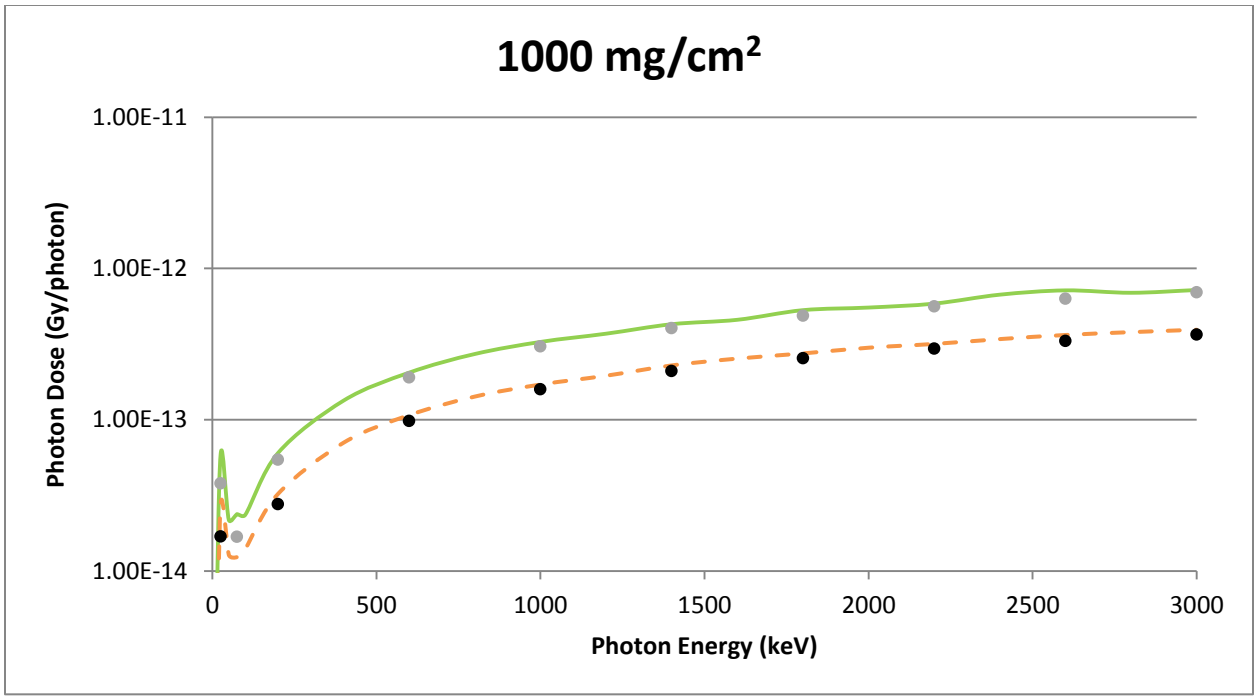

Figure A-20 **A Spherical Source Geometry Comparison of VARSKIN 5 (circles) and MCNP5 (lines) Predicted Dose Per Initial Photon as a Function of Photon Energy in Tissue at a Density Thickness of 1000 mg/cm² and a Tissue Volume Cylinder of Area 1 cm² (solid line) and 10 cm² (dashed line), With a Thickness of 20 mm**

A.6 GEOMETRY 6: POINT SOURCE (with Air Gap And Cotton Cover)

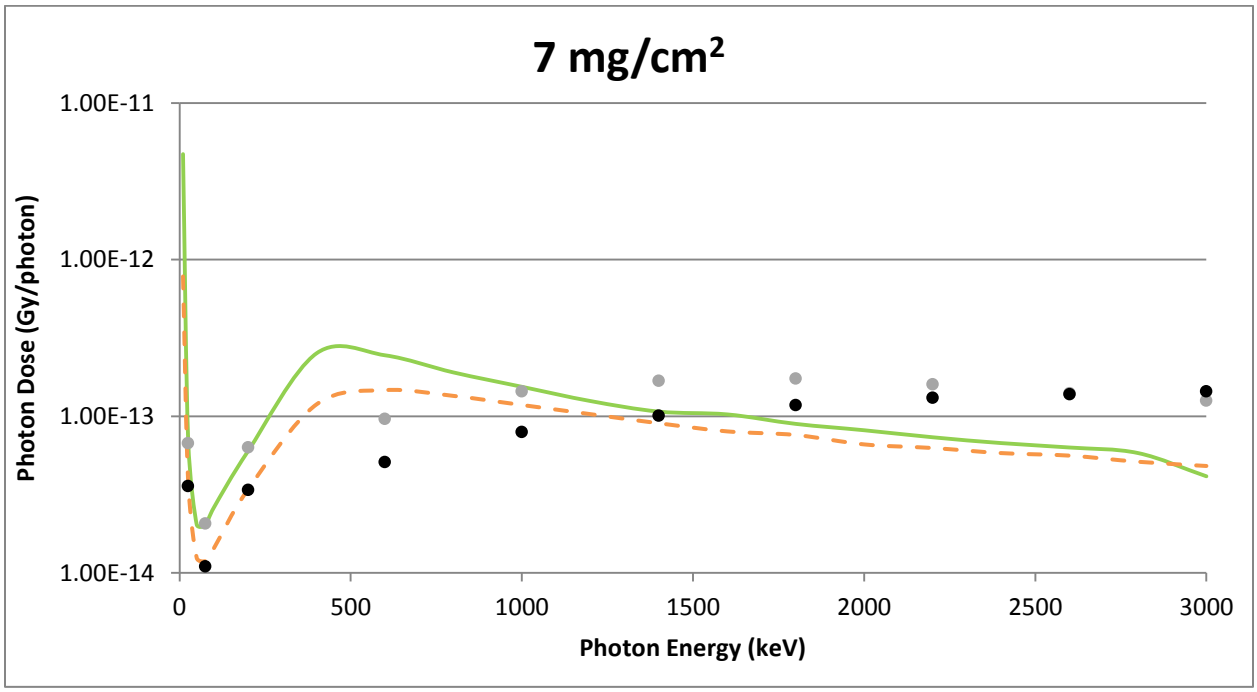

Figure A-21 **A Point Source Geometry With a Cotton Cover and a 1 cm Air Gap Comparison of VARSKIN 5 (circles) and MCNP5 (lines) Predicted Dose Per Initial Photon as a Function of Photon Energy in Tissue at a Density Thickness of 7 mg/cm^2 and a Tissue Volume Cylinder of Area 1 cm^2 (solid line) and 10 cm^2 (dashed line); Thickness of 20 mm**

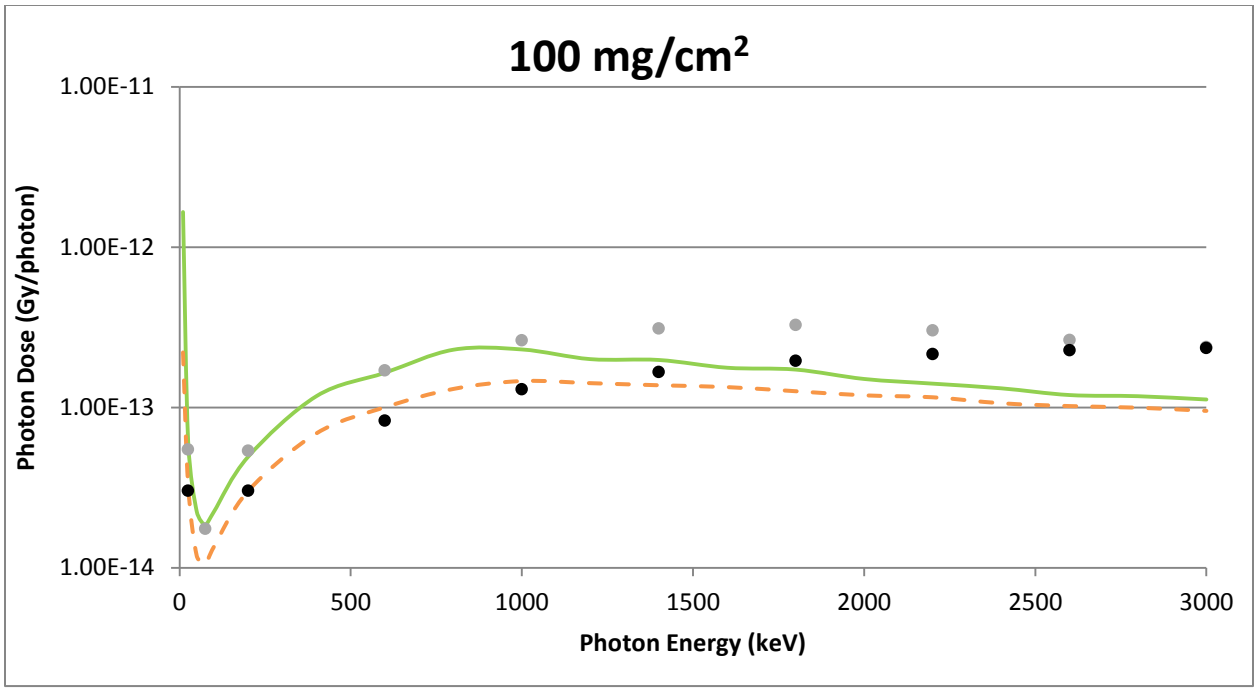

Figure A-22 **A Point Source Geometry With a Cotton Cover and a 1 cm Air Gap Comparison of VARSKIN 5 (circles) and MCNP5 (lines) Predicted Dose Per Initial Photon as a Function of Photon Energy in Tissue at a Density Thickness of 100 mg/cm^2 and a Tissue Volume Cylinder of Area 1 cm^2 (solid line) and 10 cm^2 (dashed line); Thickness of 20 mm**

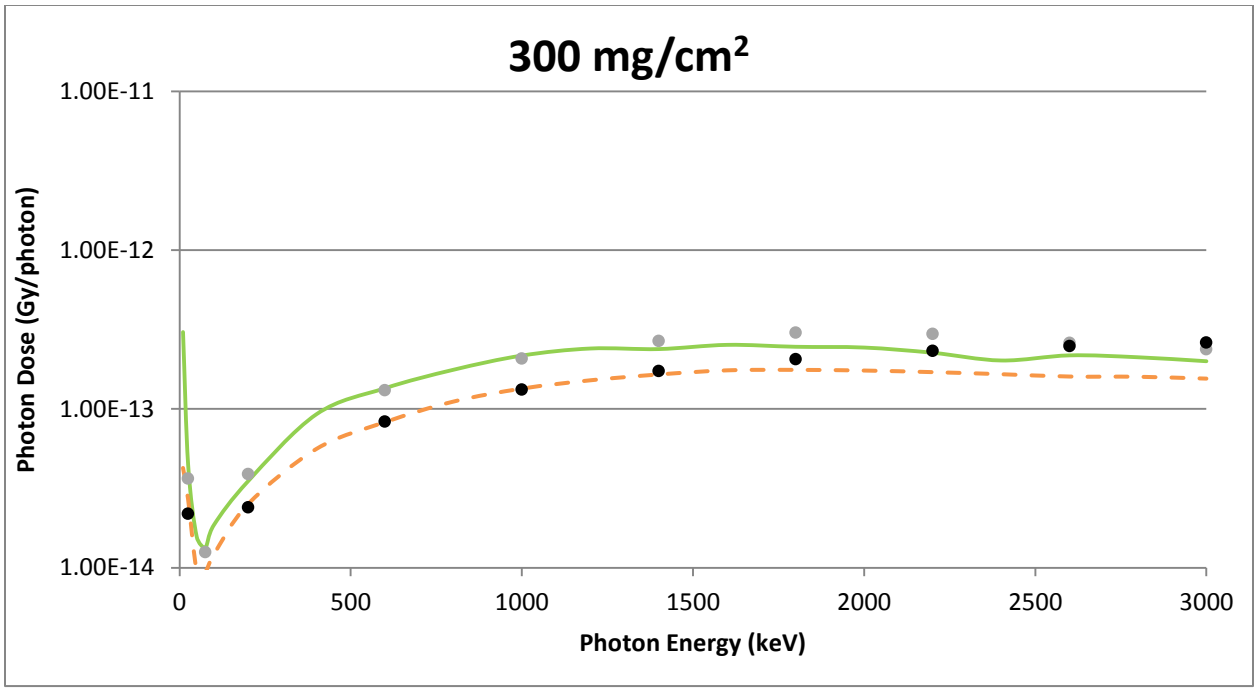

Figure A-23 **A Point Source Geometry With a Cotton Cover and a 1 cm Air Gap Comparison of VARSKIN 5 (circles) and MCNP5 (lines) Predicted Dose Per Initial Photon as a Function of Photon Energy in Tissue at a Density Thickness of 300 mg/cm^2 and a Tissue Volume Cylinder of Area 1 cm^2 (solid line) and 10 cm^2 (dashed line); Thickness of 20 mm**

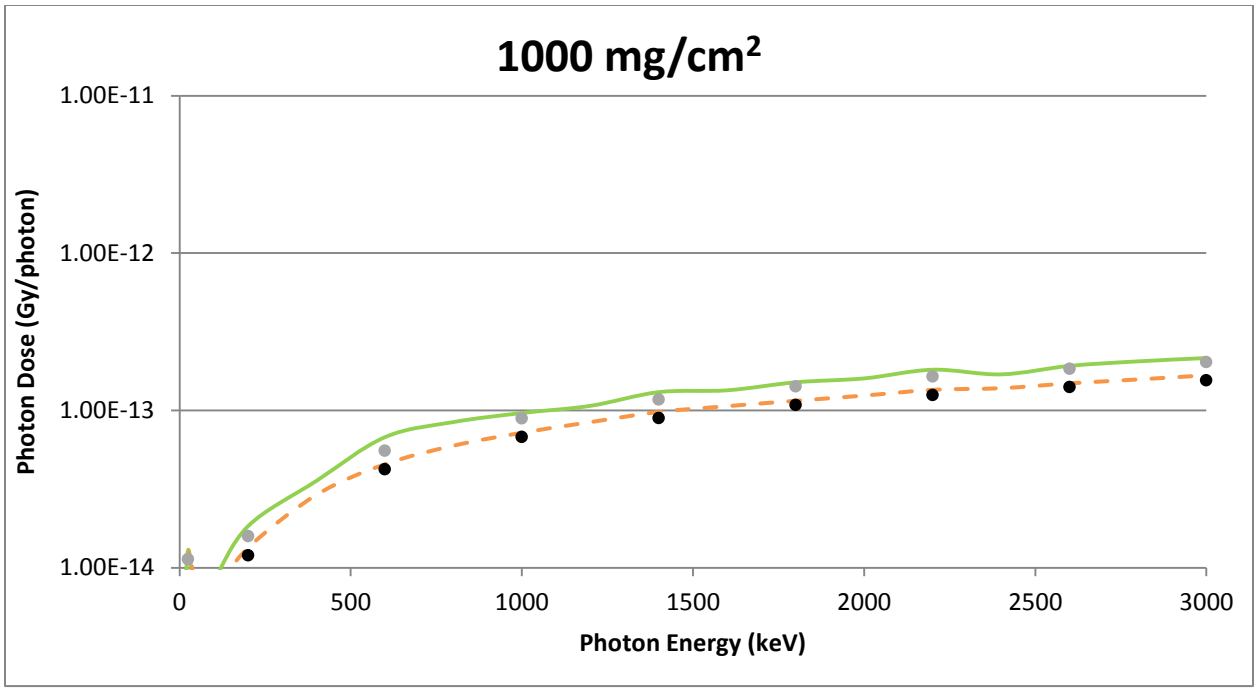

Figure A-24 **A Point Source Geometry With a Cotton Cover and a 1 cm Air Gap Comparison of VARSKIN 5 (circles) and MCNP5 (lines) Predicted Dose Per Initial Photon as a Function of Photon Energy in Tissue at a Density Thickness of 1000 mg/cm^2 and a Tissue Volume Cylinder of Area 1 cm^2 (solid line) and 10 cm^2 (dashed line); Thickness of 20 mm**

A.7 GEOMETRY 7: POINT SOURCE (1 cm off axis)

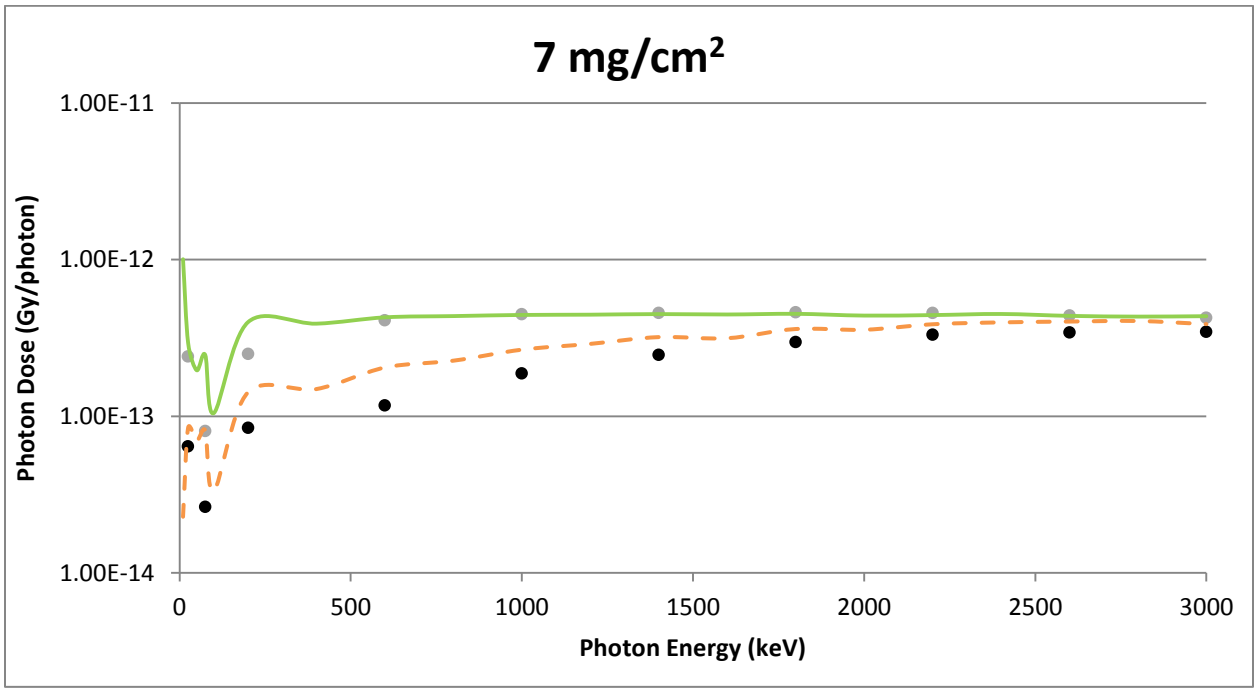

Figure A-25 **A Point Source Geometry 1 cm Off-Axis Comparison of VARSKIN 5 (circles) and MCNP5 (lines) Predicted Dose Per Initial Photon as a Function of Photon Energy in Tissue at a Density Thickness of 7 mg/cm² and a Tissue Volume Cylinder of Area 1 cm² (solid line) and 10 cm² (dashed line), With a Thickness of 20 mm**

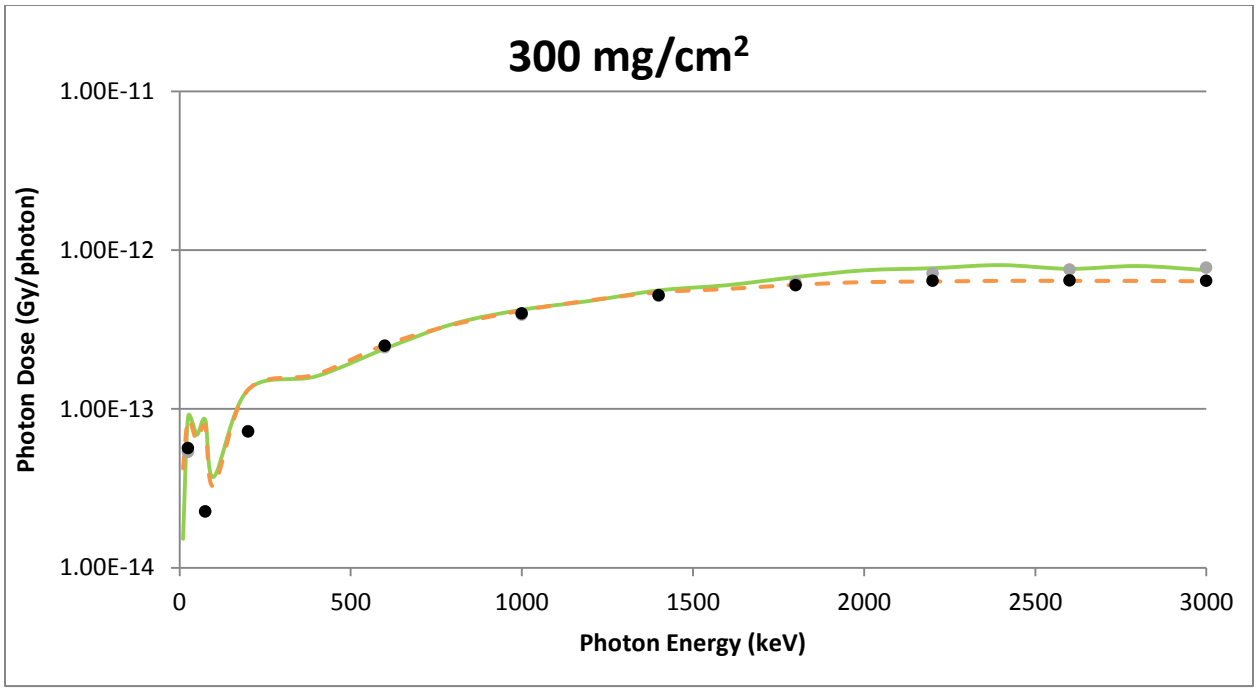

Figure A-26 **A Point Source Geometry 1 cm Off-Axis Comparison of VARSKIN 5 (circles) and MCNP5 (lines) Predicted Dose Per Initial Photon as a Function of Photon Energy in Tissue at a Density Thickness of 300 mg/cm^2 and a Tissue Volume Cylinder of Area 1 cm^2 (solid line) and 10 cm^2 (dashed line), With a Thickness of 20 mm**

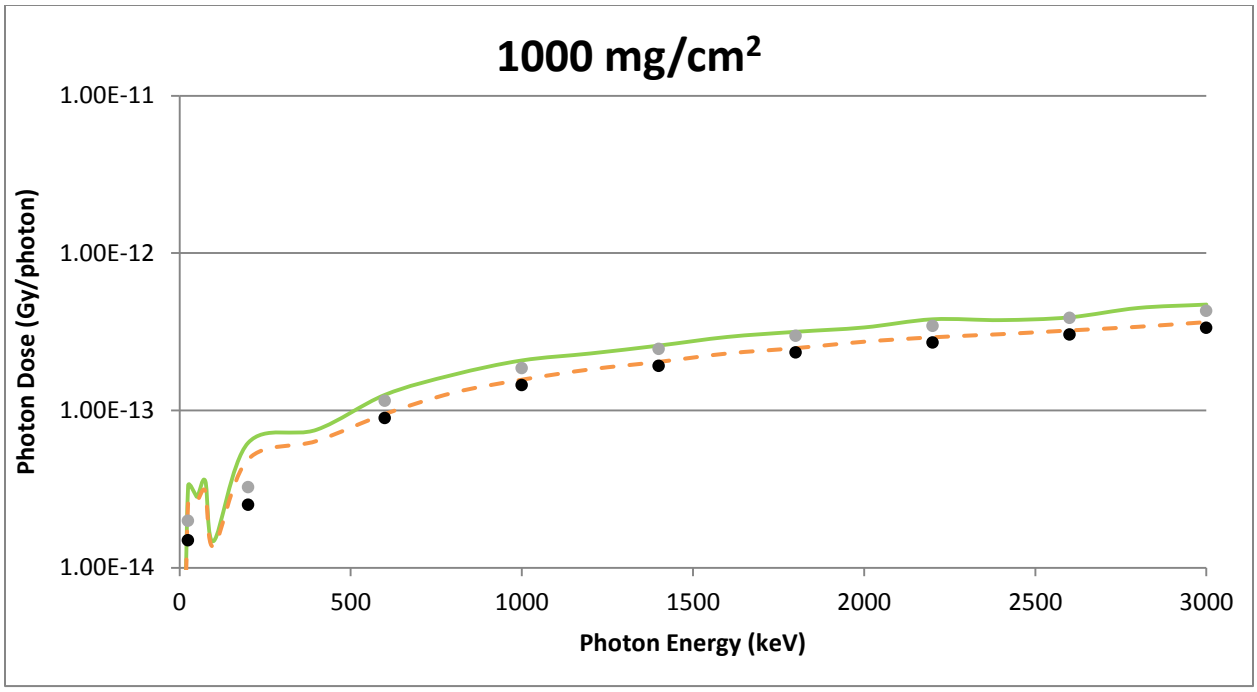

Figure A-27 **A Point Source Geometry 1 cm Off-Axis Comparison of VARSKIN 5 (circles) and MCNP5 (lines) Predicted Dose Per Initial Photon as a Function of Photon Energy in Tissue at a Density Thickness of 1000 mg/cm^2 and a Tissue Volume Cylinder of Area 1 cm^2 (solid line) and 10 cm^2 (dashed line), With a Thickness of 20 mm**

APPENDIX B
SUPPORTING FIGURES FROM SECTION 5

B.1 GEOMETRY 1: POINT SOURCE

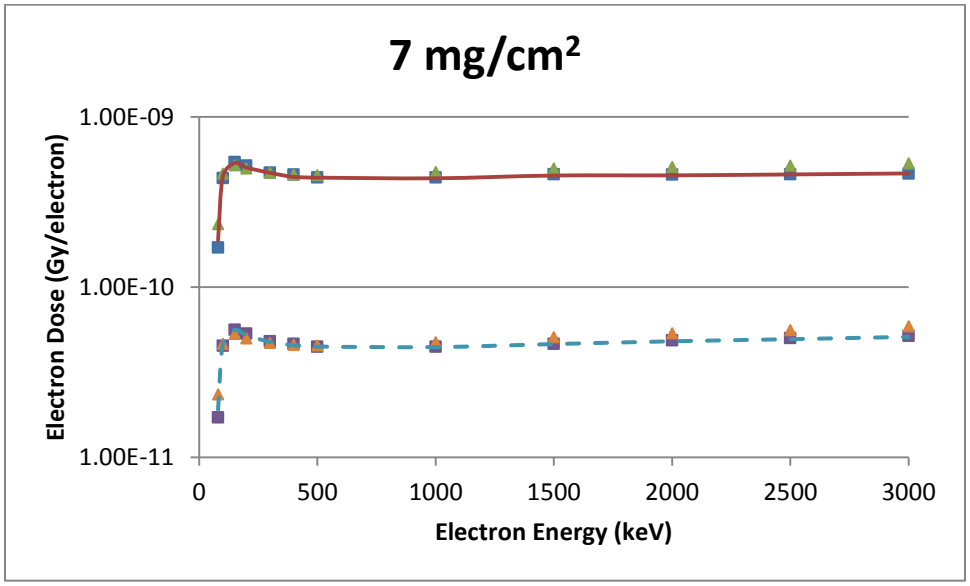

Figure B-1 **A Point Source Geometry Comparison of VARSKIN 5 (boxes), MCNP5 (triangles) and EGSnrc (lines) Predicted Dose Per Initial Electron as a Function of Electron Energy in Tissue at a Density Thickness of 7 mg/cm^2 and a 20 mm Thick Tissue Volume Cylinder of Area 1 cm^2 (solid line) and 10 cm^2 (dashed line)**

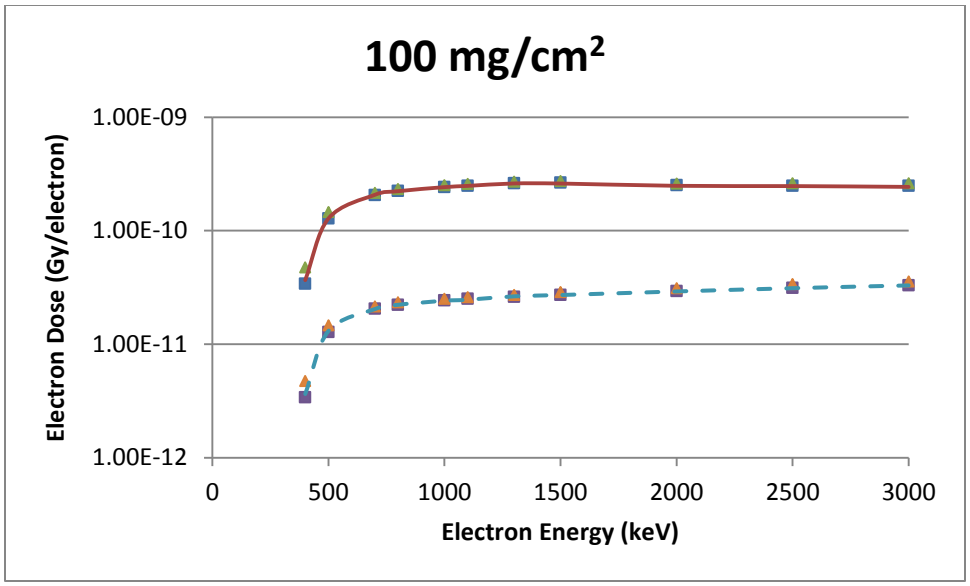

Figure B-2 **A Point Source Geometry Comparison of VARSKIN 5 (boxes), MCNP5 (triangles) and EGSnrc (lines) Predicted Dose Per Initial Electron as a Function of Electron Energy in Tissue at a Density Thickness of 100 mg/cm^2 and a 20 mm Thick Tissue Volume Cylinder of Area 1 cm^2 (solid line) and 10 cm^2 (dashed line)**

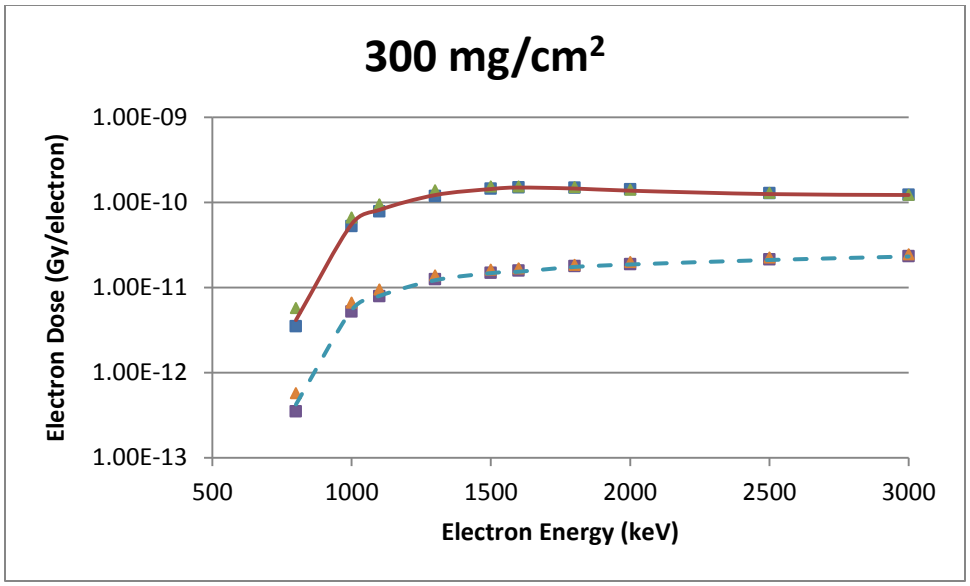

Figure B-3 **A Point Source Geometry Comparison of VARSKIN 5 (boxes), MCNP5 (triangles) and EGSnrc (lines) Predicted Dose Per Initial Electron as a Function of Electron Energy in Tissue at a Density Thickness of 300 mg/cm^2 and a 20 mm Thick Tissue Volume Cylinder of Area 1 cm^2 (solid line) and 10 cm^2 (dashed line)**

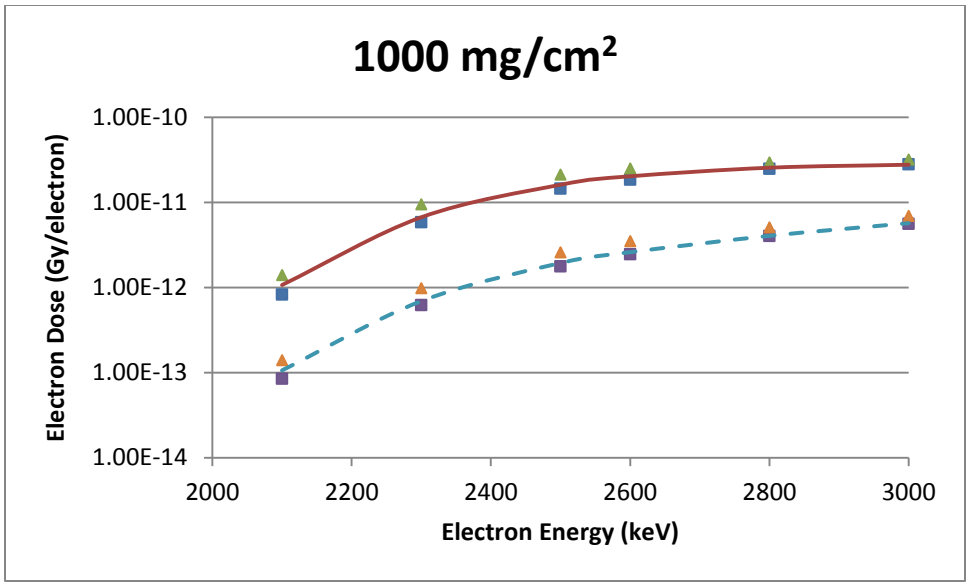

Figure B-4 **A Point Source Geometry Comparison of VARSKIN 5 (boxes), MCNP5 (triangles) and EGSnrc (lines) Predicted Dose Per Initial Electron as a Function of Electron Energy in Tissue at a Density Thickness of 1000 mg/cm^2 and a 20 mm Thick Tissue Volume Cylinder of Area 1 cm^2 (solid line) and 10 cm^2 (dashed line)**

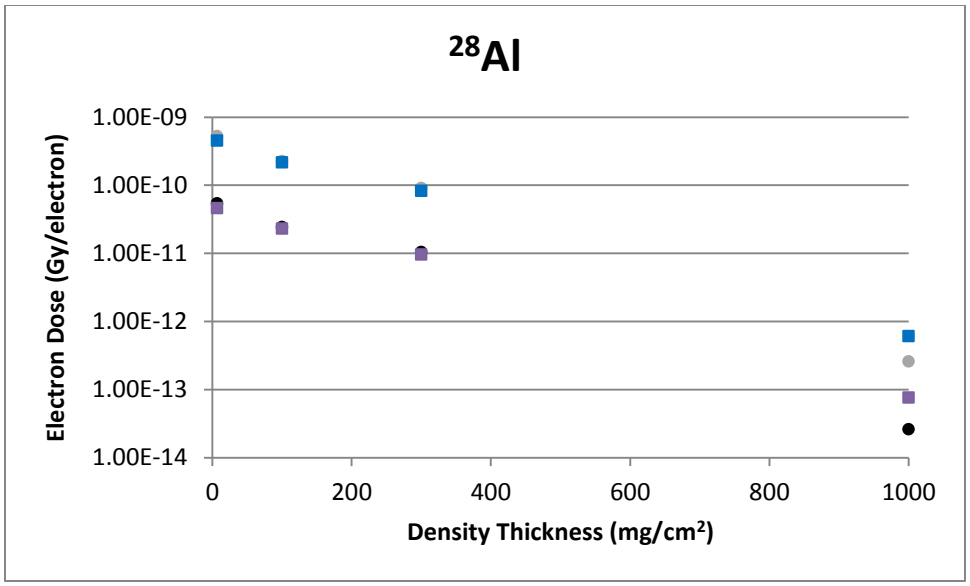

Figure B-5 **A Point Source Geometry Comparison of VARSKIN 5 (boxes) and VARSKIN 4 (circles) Predicted Dose Per Initial Beta From ^{28}Al as a Function of Density Thickness in Tissue and a Tissue Volume Cylinder of Area 1 cm^2 (upper) and 10 cm^2 (lower), With a Thickness of 20 mm**

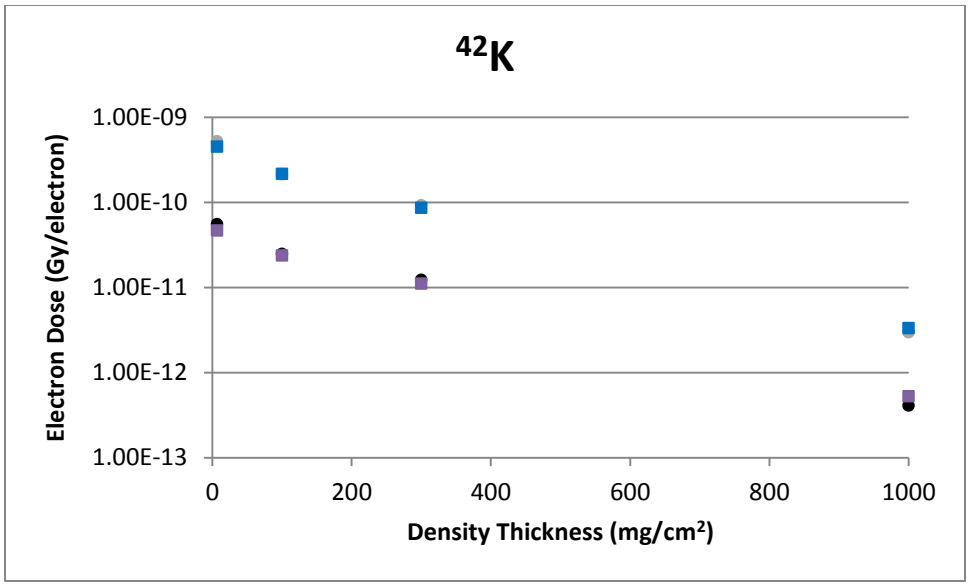

Figure B-6 **A Point Source Geometry Comparison of VARSKIN 5 (boxes) and VARSKIN 4 (circles) Predicted Dose Per Initial Beta From 42K as a Function of Density Thickness in Tissue and a Tissue Volume Cylinder of Area 1 cm^2 (upper) and 10 cm^2 (lower), With a Thickness of 20 mm**

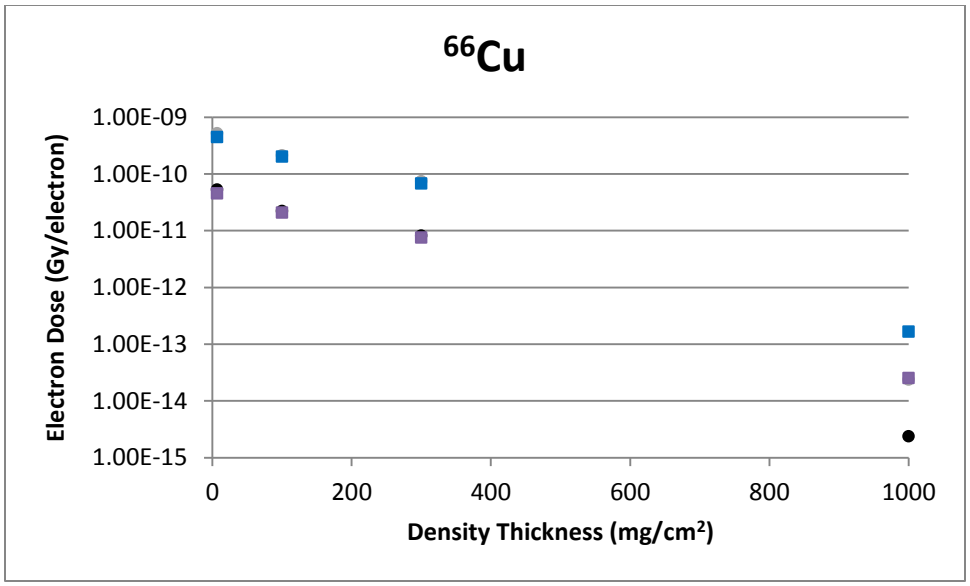

Figure B-7 **A Point Source Geometry Comparison of VARSKIN 5 (boxes) and VARSKIN 4 (circles) Predicted Dose Per Initial Beta From ^{66}Cu as a Function of Density Thickness in Tissue and a Tissue Volume Cylinder of Area 1 cm^2 (upper) and 10 cm^2 (lower), With a Thickness of 20 mm**

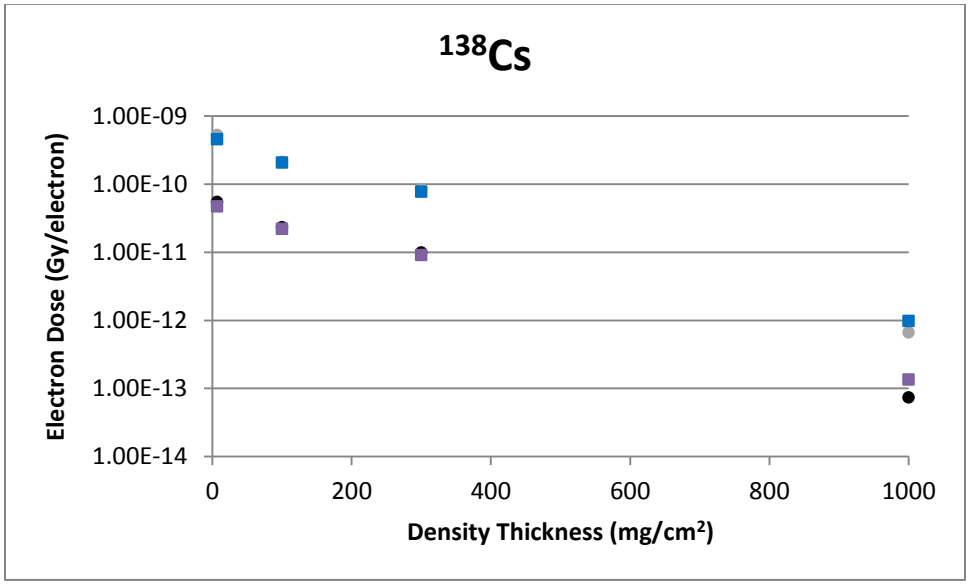

Figure B-8 **A Point Source Geometry Comparison of VARSKIN 5 (boxes) and VARSKIN 4 (circles) Predicted Dose Per Initial Beta From ^{138}Cs as a Function of Density Thickness in Tissue and a Tissue Volume Cylinder of Area 1 cm^2 (upper) and 10 cm^2 (lower), With a Thickness of 20 mm**

B.2 GEOMETRY 2: DISK SOURCE (0.5 mm dia)

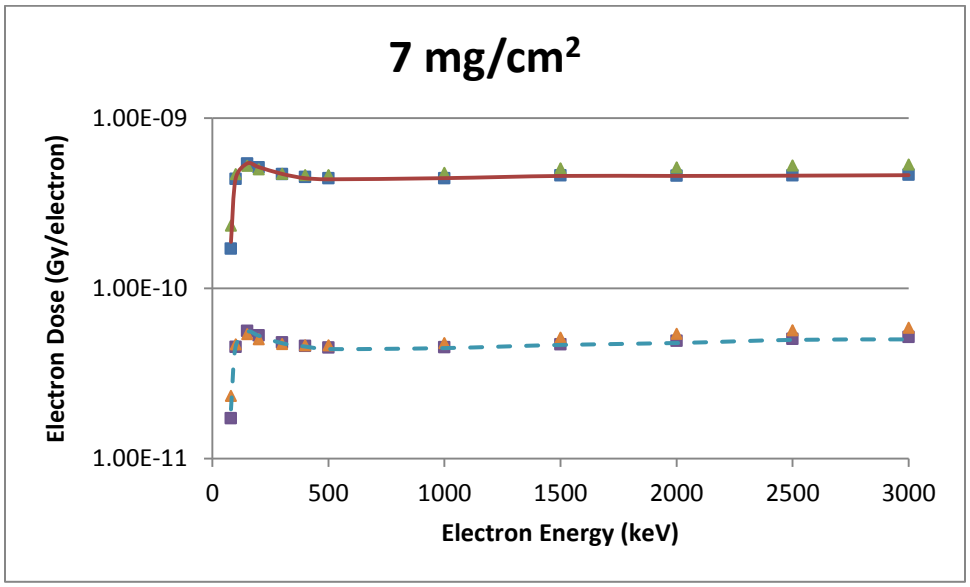

Figure B-9 **A 0.5 mm Diameter Disk Source Geometry Comparison of VARSKIN 5 (boxes), MCNP5 (triangles) And EGSnrc (lines) Predicted Dose Per Initial Electron as a Function of Electron Energy in Tissue at a Density Thickness of 7 mg/cm^2 and a Tissue Volume Cylinder of Area 1 cm^2 (solid line) and 10 cm^2 (dashed line), With a Thickness of 20 mm**

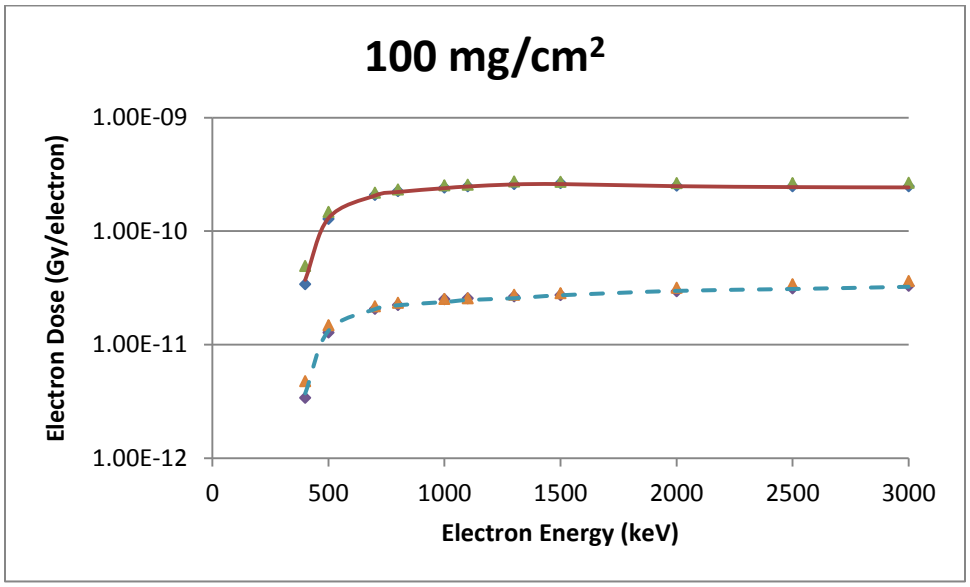

Figure B-10 **A 0.5 mm Diameter Disk Source Geometry Comparison of VARSKIN 5 (boxes), MCNP5 (triangles) and EGSnrc (lines) Predicted Dose Per Initial Electron as a Function of Electron Energy in Tissue at a Density Thickness of 100 mg/cm^2 and a Tissue Volume Cylinder of Area 1 cm^2 (solid line) and 10 cm^2 (dashed line), With a Thickness of 20 mm**

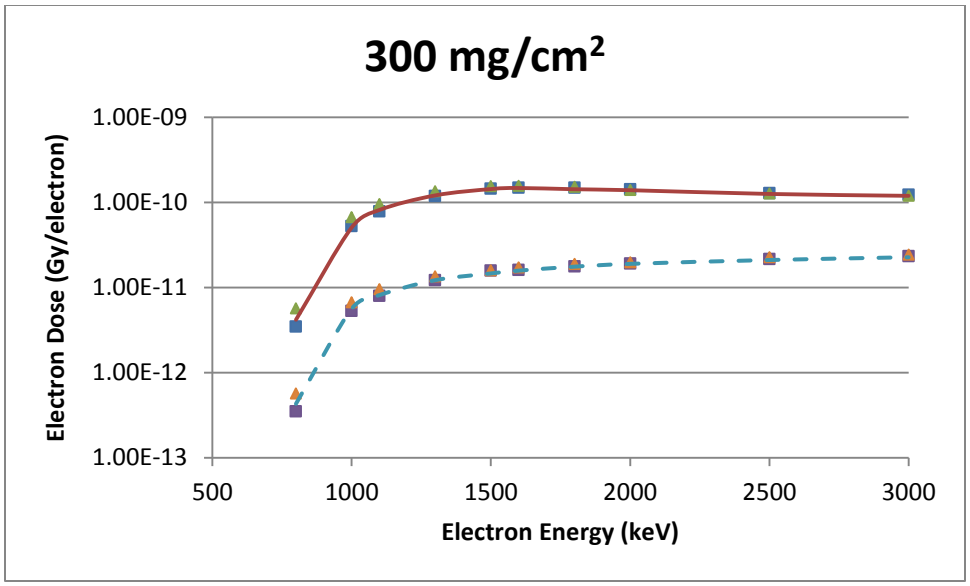

Figure B-11 **A 0.5 mm Diameter Disk Source Geometry Comparison of VARSKIN 5 (boxes), MCNP5 (triangles) and EGSnrc (lines) Predicted Dose Per Initial Electron as a Function of Electron Energy in Tissue at a Density Thickness of 300 mg/cm^2 and a Tissue Volume Cylinder of Area 1 cm^2 (solid line) and 10 cm^2 (dashed line), With a Thickness of 20 mm**

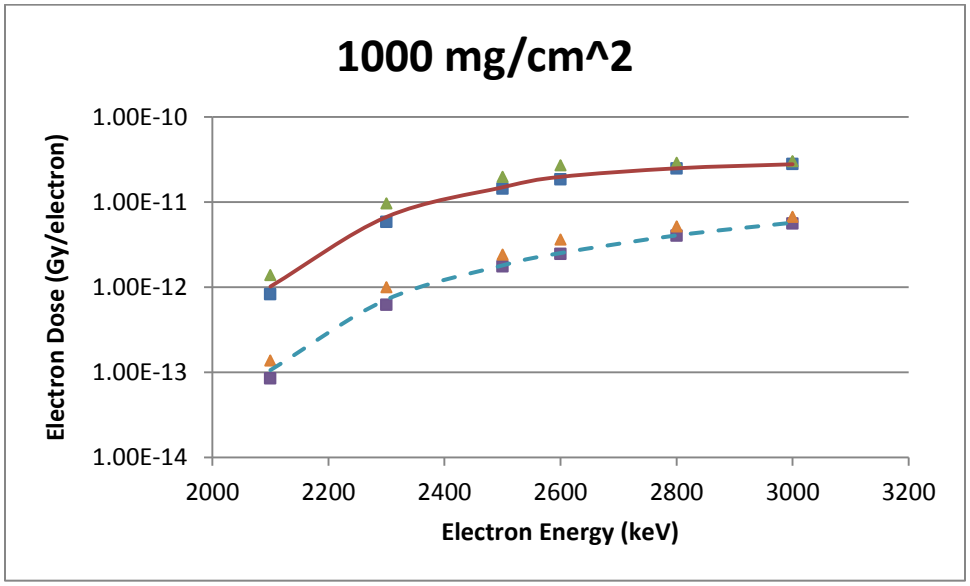

Figure B-12 **A 0.5 mm Diameter Disk Source Geometry Comparison of VARSKIN 5 (boxes), MCNP5 (triangles) and EGSnrc (lines) Predicted Dose Per Initial Electron as a Function of Electron Energy in Tissue at a Density Thickness of 1000 mg/cm^2 and a Tissue Volume Cylinder of Area 1 cm^2 (solid line) and 10 cm^2 (dashed line), With a Thickness of 20 mm**

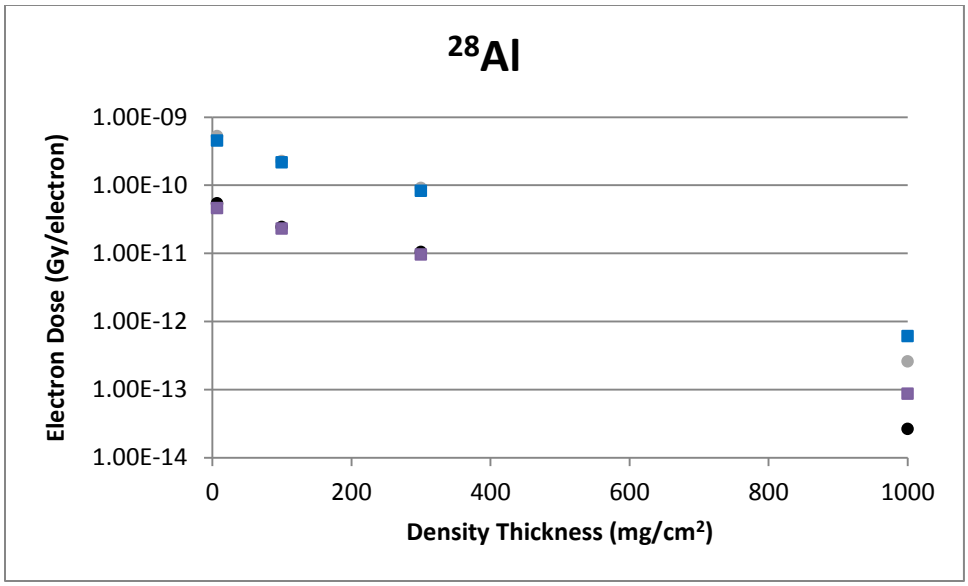

Figure B-13 **A 0.5 mm Diameter Disk Geometry Comparison of VARSKIN 5 (boxes) and VARSKIN 4 (circles) Predicted Dose Per Initial Beta From ^{28}Al as a Function of Density Thickness in Tissue and a Tissue Volume Cylinder of Area 1 cm^2 (upper) and 10 cm^2 (lower), With a Thickness of 20 mm**

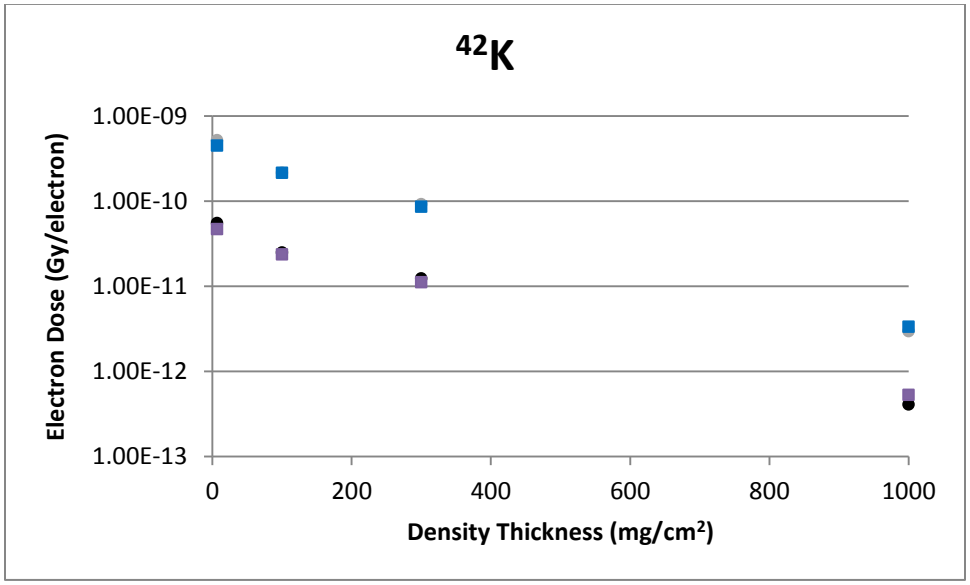

Figure B-14 **A 0.5 mm Diameter Disk Geometry Comparison of VARSKIN 5 (boxes) and VARSKIN 4 (circles) Predicted Dose Per Initial Beta From 42K as a Function of Density Thickness in Tissue and a Tissue Volume Cylinder of Area 1 cm^2 (upper) and 10 cm^2 (lower), With a Thickness of 20 mm**

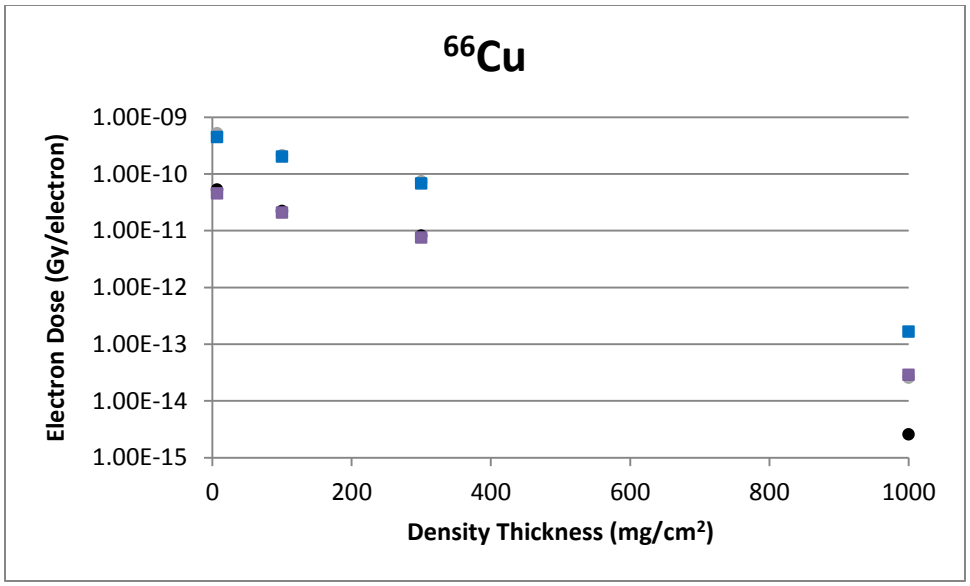

Figure B-15 **A 0.5 mm Diameter Disk Geometry Comparison of VARSKIN 5 (boxes) and VARSKIN 4 (circles) Predicted Dose Per Initial Beta From ^{66}Cu as a Function of Density Thickness in Tissue and a Tissue Volume Cylinder of Area 1 cm^2 (upper) and 10 cm^2 (lower), With a Thickness of 20 mm**

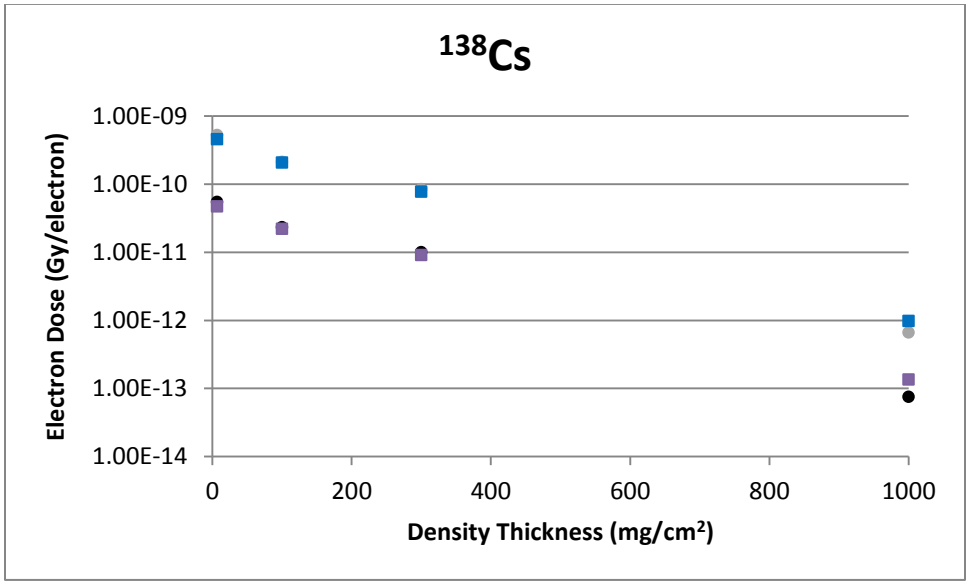

Figure B-16 **A 0.5 mm Diameter Disk Geometry Comparison of VARSKIN 5 (boxes) and VARSKIN 4 (circles) Predicted Dose Per Initial Beta From ^{138}Cs as a Function of Density Thickness in Tissue and a Tissue Volume Cylinder of Area 1 cm^2 (upper) and 10 cm^2 (lower), With a Thickness of 20 mm**

B.3 GEOMETRY 3: DISK SOURCE (1 mm dia)

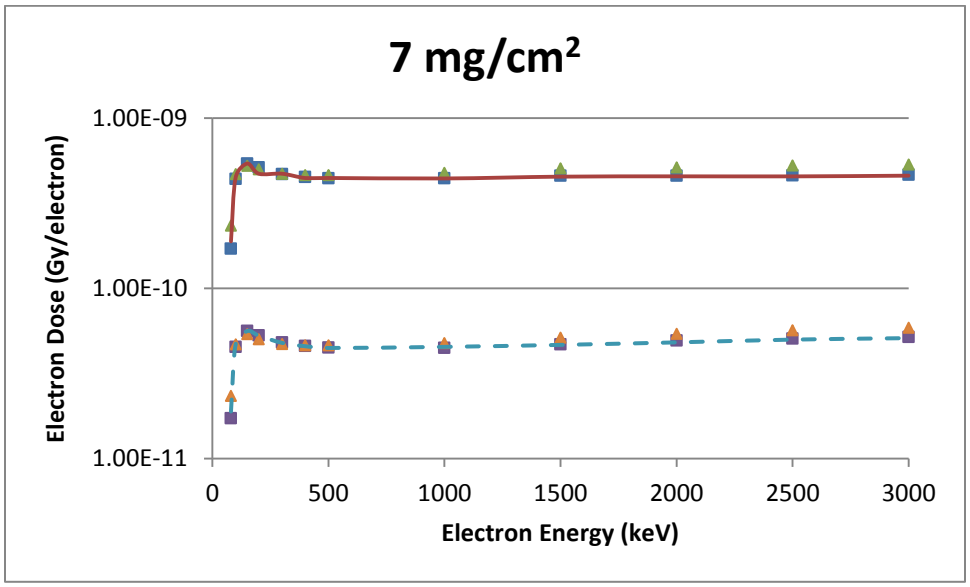

Figure B-17 **A 1 mm Diameter Disk Source Geometry Comparison of VARSKIN 5 (boxes), MCNP5 (triangles) and EGSnrc (lines) Predicted Dose Per Initial Electron as a Function of Electron Energy in Tissue at a Density Thickness of 7 mg/cm² and a Tissue Volume Cylinder of Area 1 cm² (solid line) and 10 cm² (dashed line), With a Thickness of 20 mm**

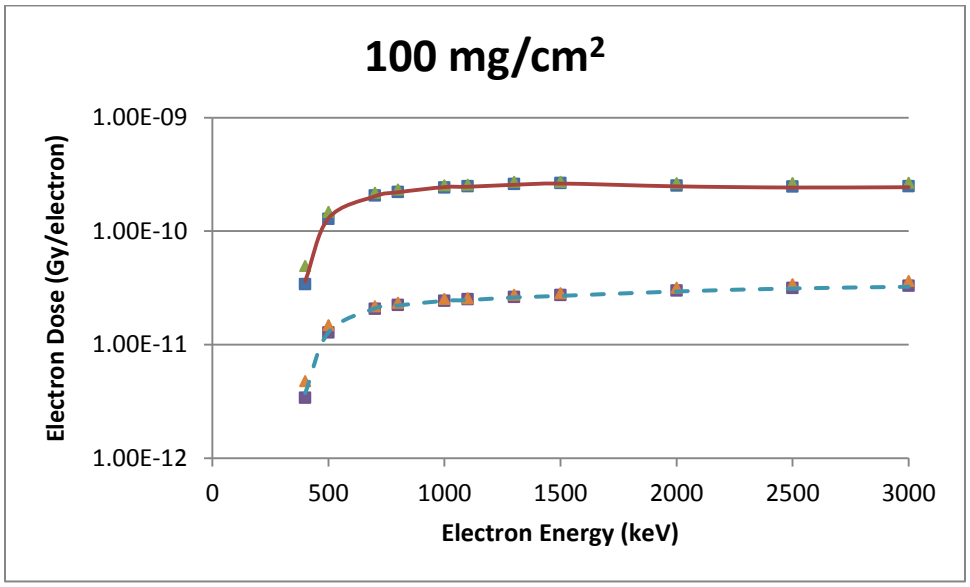

Figure B-18 **A 1 mm Diameter Disk Source Geometry Comparison of VARSKIN 5 (boxes), MCNP5 (triangles) and EGSnrc (lines) Predicted Dose Per Initial Electron as a Function of Electron Energy in Tissue at a Density Thickness of 100 mg/cm² and a Tissue Volume Cylinder of Area 1 cm² (solid line) and 10 cm² (dashed line), With a Thickness of 20 mm**

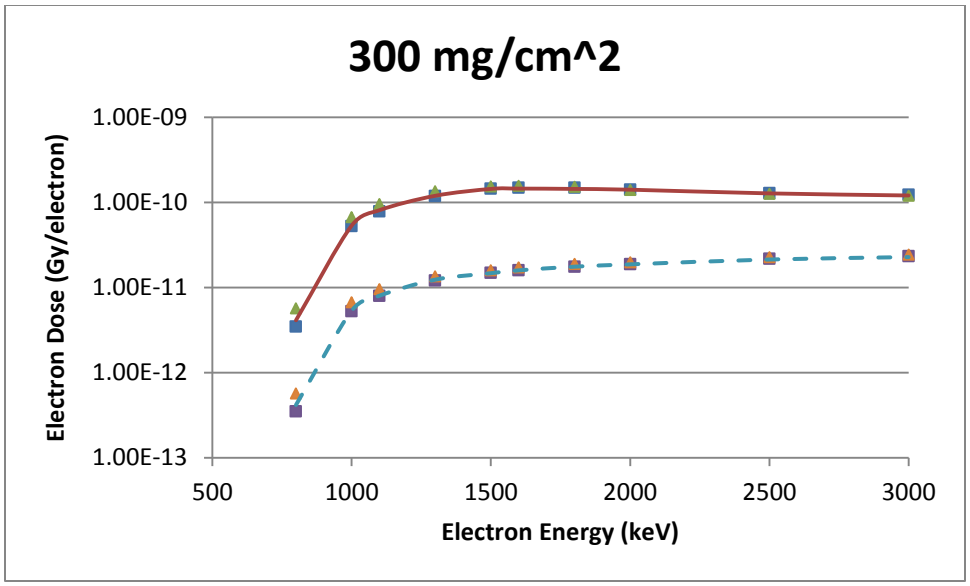

Figure B-19 **A 1 mm Diameter Disk Source Geometry Comparison of VARSKIN 5 (boxes), MCNP5 (triangles) and EGSnrc (lines) Predicted Dose Per Initial Electron as a Function of Electron Energy in Tissue at a Density Thickness of 300 mg/cm^2 and a Tissue Volume Cylinder of Area 1 cm^2 (solid line) and 10 cm^2 (dashed line), With a Thickness of 20 mm**

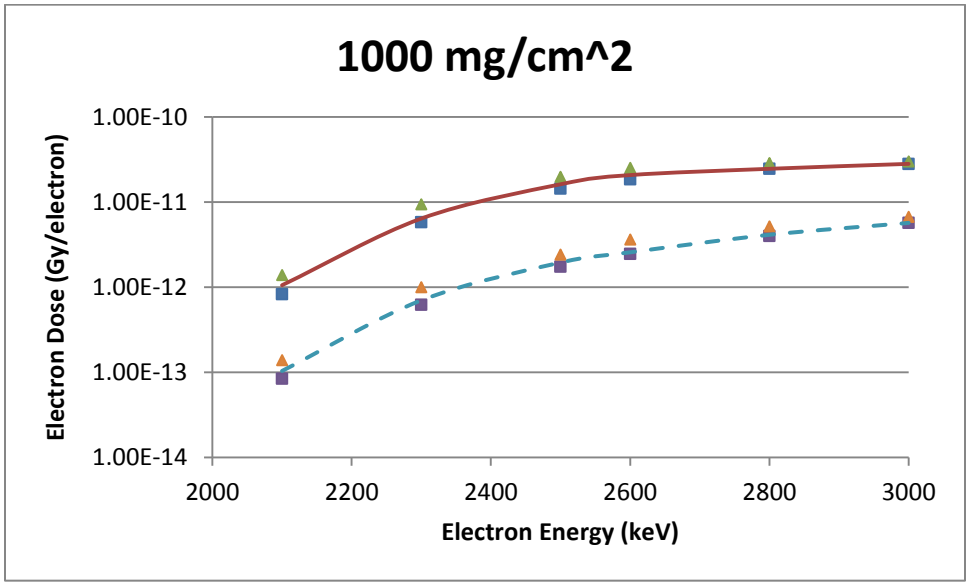

Figure B-20 **A 1 mm Diameter Disk Source Geometry Comparison of VARSKIN 5 (boxes), MCNP5 (triangles) and EGSnrc (lines) Predicted Dose Per Initial Electron as a Function of Electron Energy in Tissue at a Density Thickness of 1000 mg/cm^2 and a Tissue Volume Cylinder of Area 1 cm^2 (solid line) and 10 cm^2 (dashed line), With a Thickness of 20 mm**

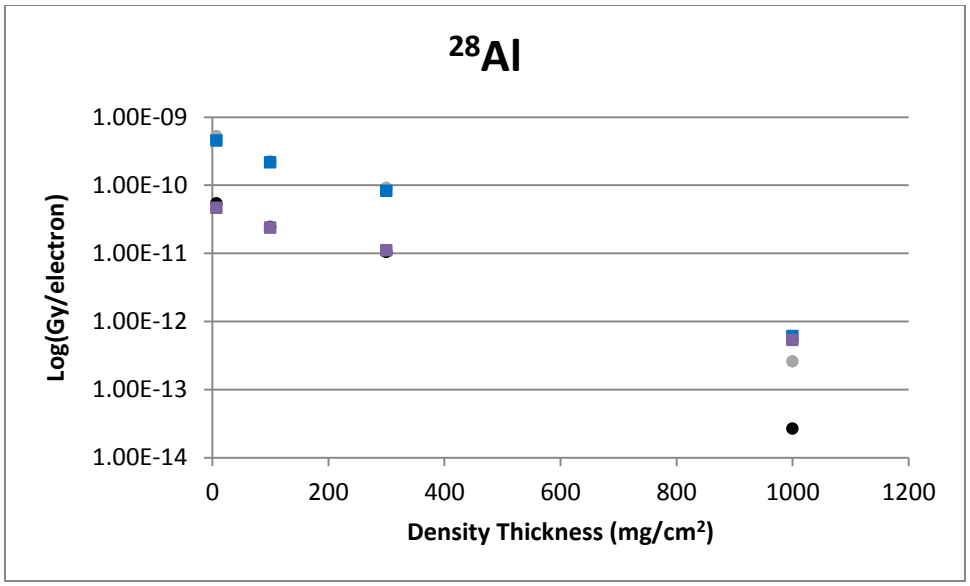

Figure B-21 **A 1 mm Diameter Disk Geometry Comparison of VARSKIN 5 (boxes) and VARSKIN 4 (circles) Predicted Dose Per Initial Beta From ^{28}Al as a Function of Density Thickness in Tissue and a Tissue Volume Cylinder of Area 1 cm^2 (upper) and 10 cm^2 (lower), With a Thickness of 20 mm**

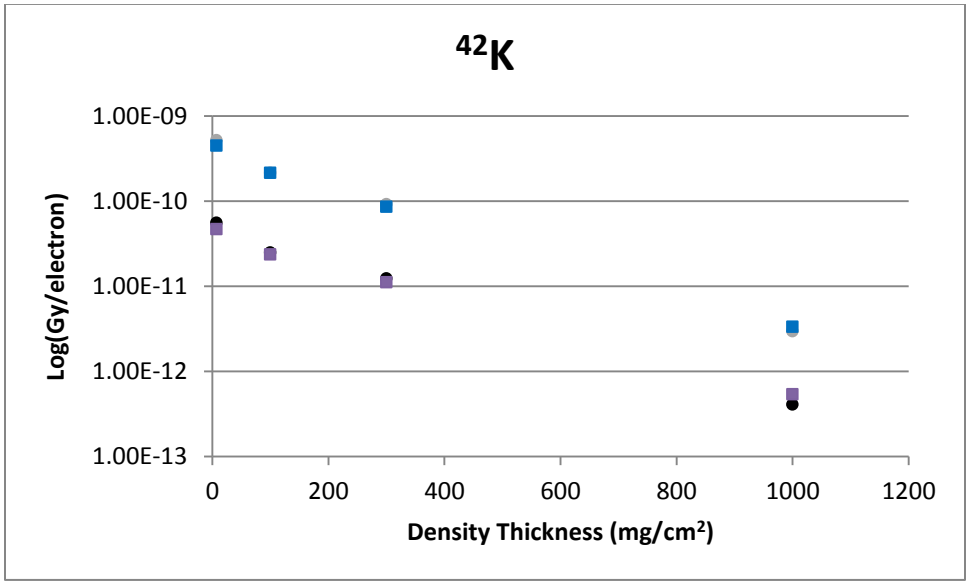

Figure B-22 **A 1 mm Diameter Disk Geometry Comparison of VARSKIN 5 (boxes) and VARSKIN 4 (circles) Predicted Dose Per Initial Beta From 42K as a Function of Density Thickness in Tissue and a Tissue Volume Cylinder of Area 1 cm^2 (upper) and 10 cm^2 (lower), With a Thickness of 20 mm**

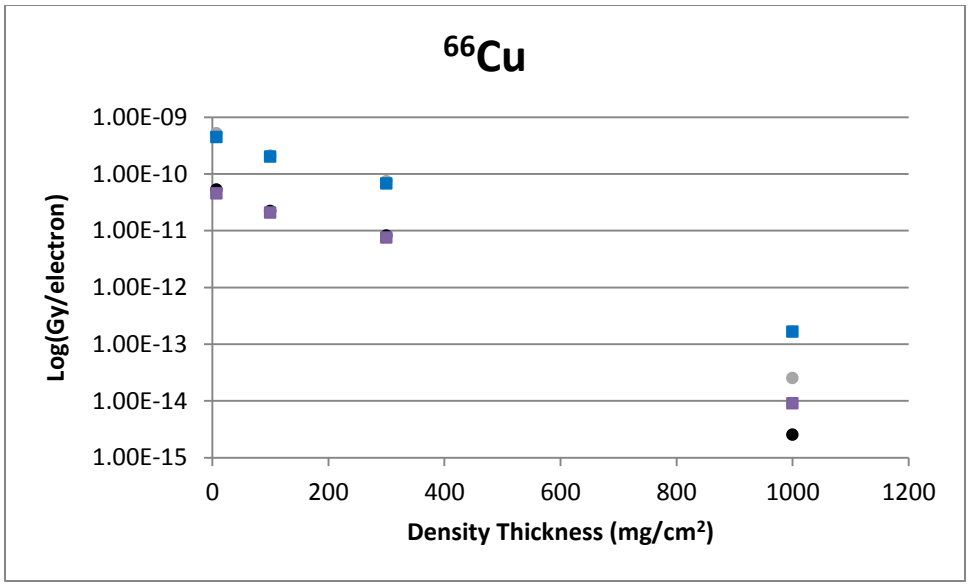

Figure B-23 **A 1 mm Diameter Disk Geometry Comparison of VARSKIN 5 (boxes) and VARSKIN 4 (circles) Predicted Dose Per Initial Beta From ^{66}Cu as a Function of Density Thickness in Tissue and a Tissue Volume Cylinder of Area 1 cm^2 (upper) and 10 cm^2 (lower), With a Thickness of 20 mm**

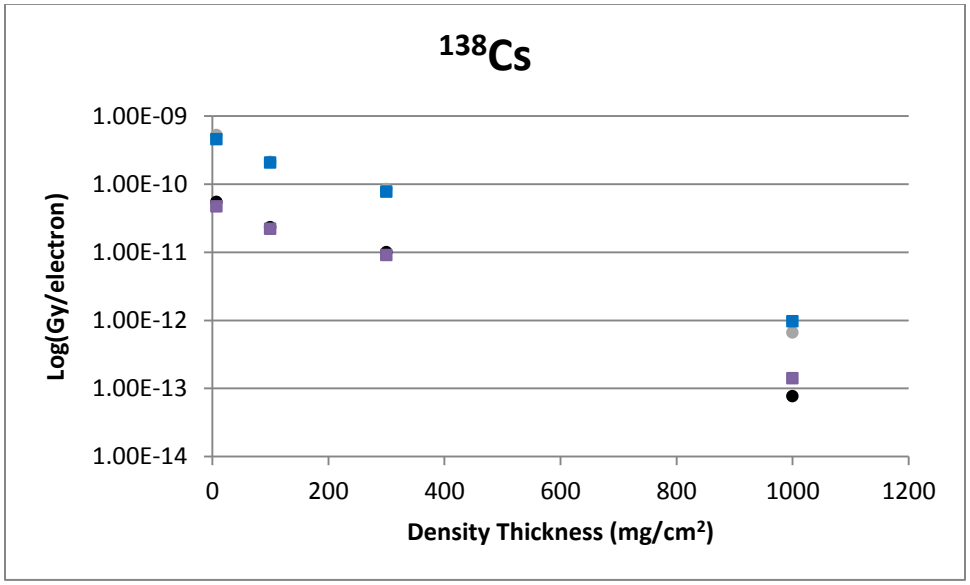

Figure B-24 **A 1 mm Diameter Disk Geometry Comparison of VARSKIN 5 (boxes) and VARSKIN 4 (circles) Predicted Dose Per Initial Beta From ^{138}Cs as a Function of Density Thickness in Tissue and a Tissue Volume Cylinder of Area 1 cm^2 (upper) and 10 cm^2 (lower), With a Thickness of 20 mm**

B.4 GEOMETRY 4: DISK SOURCE (5 mm dia)

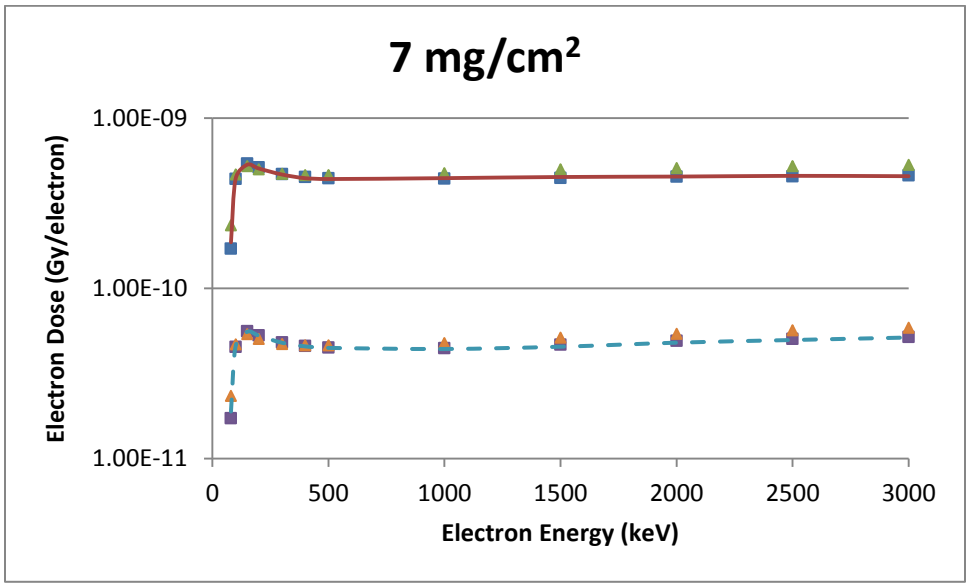

Figure B-25 **A 5 mm Diameter Disk Source Geometry Comparison of VARSKIN 5 (boxes), MCNP5 (triangles) And EGSnrc (lines) Predicted Dose Per Initial Electron as a Function of Electron Energy in Tissue at a Density Thickness of 7 mg/cm² and a Tissue Volume Cylinder of Area 1 cm² (solid line) and 10 cm² (dashed line), With a Thickness of 20 mm**

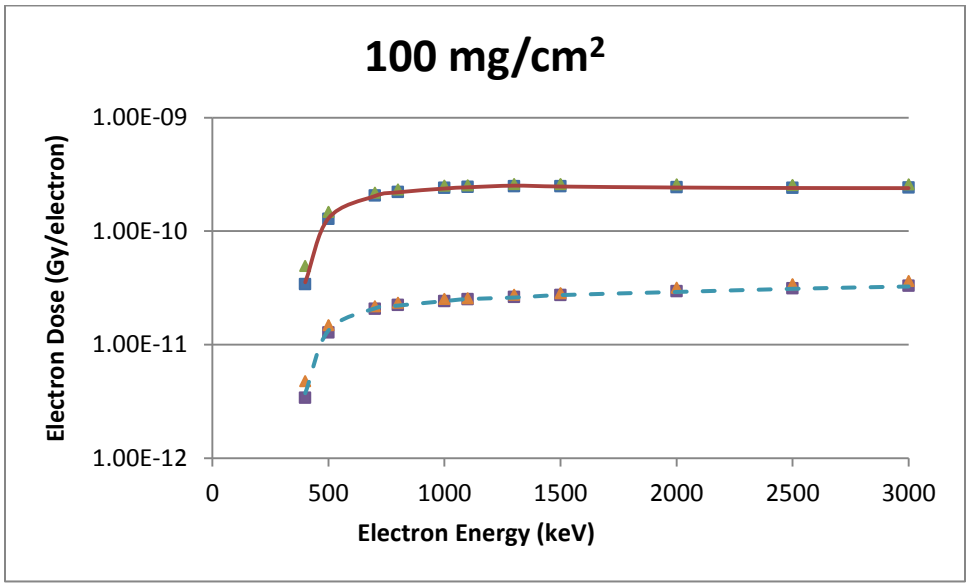

Figure B-26 **A 5 mm Diameter Disk Source Geometry Comparison of VARSKIN 5 (boxes), MCNP5 (triangles) and EGSnrc (lines) Predicted Dose Per Initial Electron as a Function of Electron Energy in Tissue at a Density Thickness of 100 mg/cm² and a Tissue Volume Cylinder of Area 1 cm² (solid line) and 10 cm² (dashed line), With a Thickness of 20 mm**

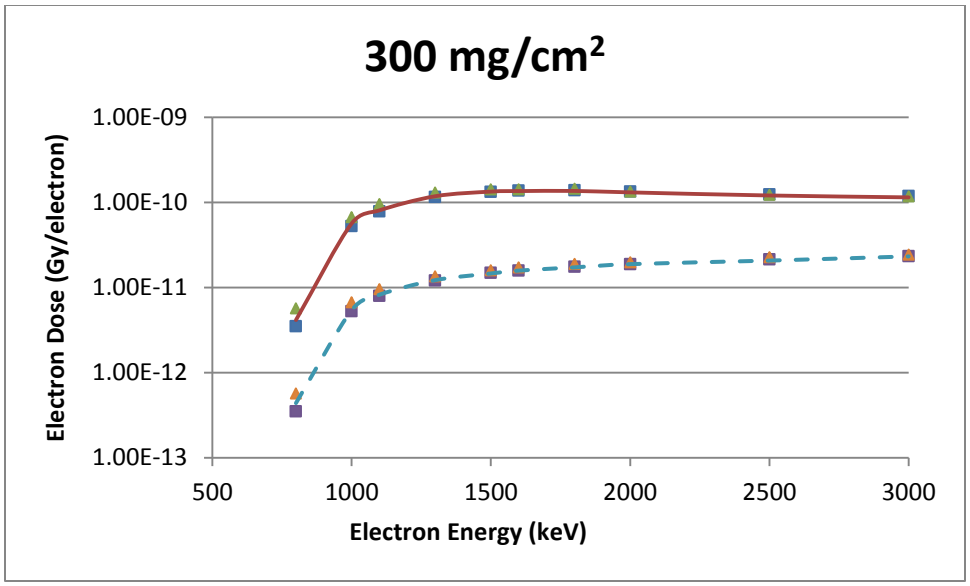

Figure B-27 **A 5 mm Diameter Disk Source Geometry Comparison of VARSKIN 5 (boxes), MCNP5 (triangles) and EGSnrc (lines) Predicted Dose Per Initial Electron as a Function of Electron Energy in Tissue at a Density Thickness of 300 mg/cm^2 and a Tissue Volume Cylinder of Area 1 cm^2 (solid line) and 10 cm^2 (dashed line), With a Thickness of 20 mm**

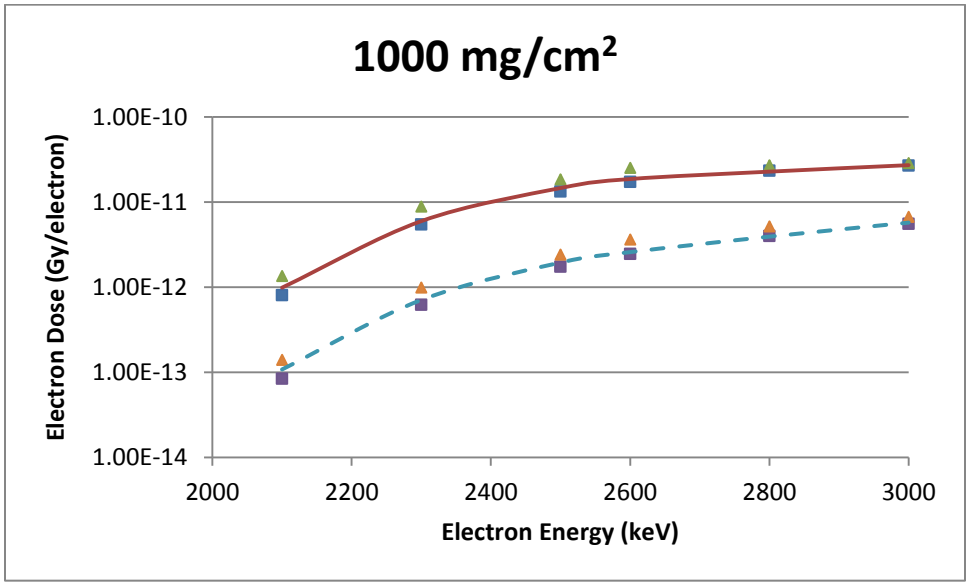

Figure B-28 **A 5 mm Diameter Disk Source Geometry Comparison of VARSKIN 5 (boxes), MCNP5 (triangles) and EGSnrc (lines) Predicted Dose Per Initial Electron as a Function of Electron Energy In Tissue at a Density Thickness of 1000 mg/cm^2 and a Tissue Volume Cylinder of Area 1 cm^2 (solid line) and 10 cm^2 (dashed line), With a Thickness of 20 mm**

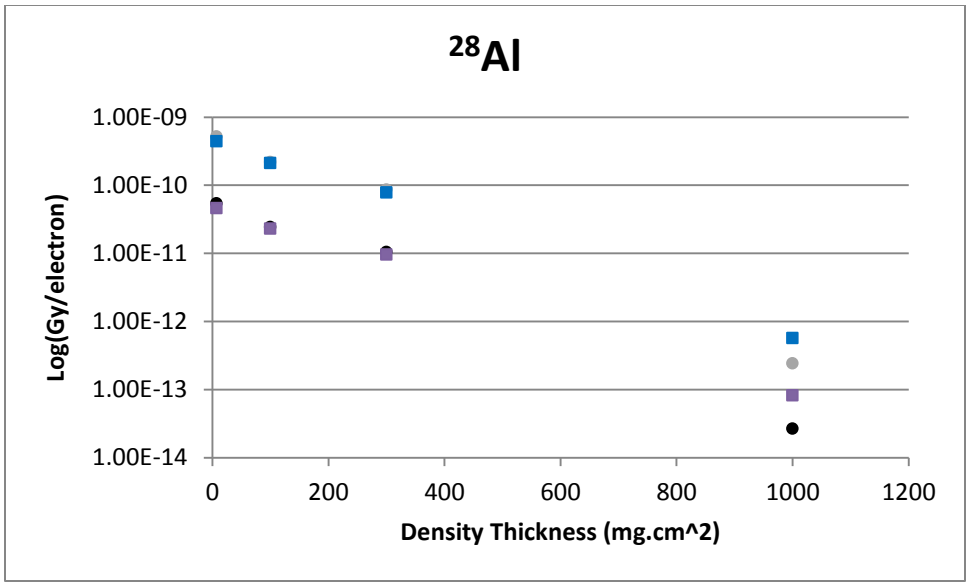

Figure B-29 **A 5 mm Diameter Disk Geometry Comparison of VARSKIN 5 (boxes) and VARSKIN 4 (circles) Predicted Dose Per Initial Beta From ^{28}Al as a Function of Density Thickness in Tissue and a Tissue Volume Cylinder of Area 1 cm^2 (upper) and 10 cm^2 (lower), With a Thickness of 20 mm**

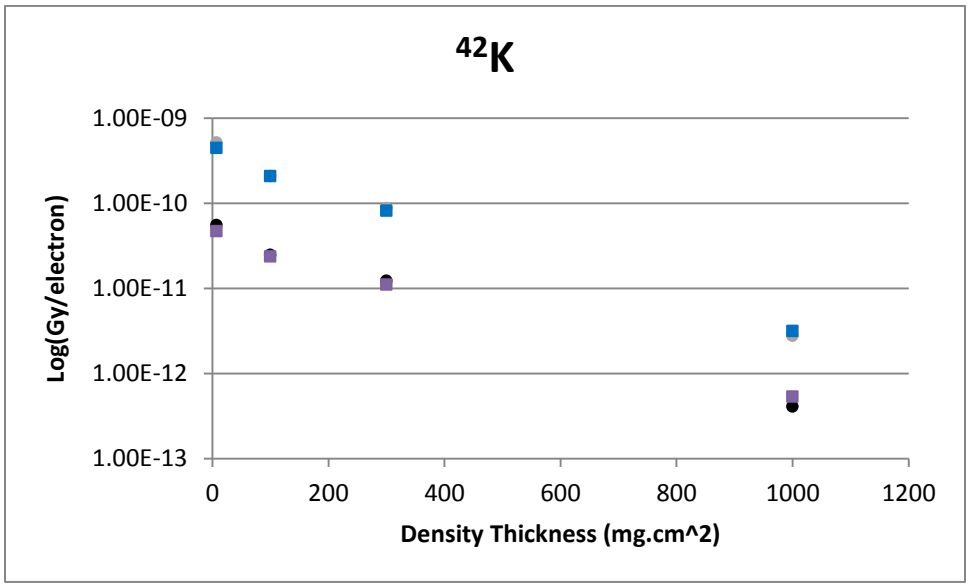

Figure B-30 **A 5 mm Diameter Disk Geometry Comparison of VARSKIN 5 (boxes) and VARSKIN 4 (circles) Predicted Dose Per Initial Beta From 42K as a Function of Density Thickness in Tissue and a Tissue Volume Cylinder of Area 1 cm^2 (upper) and 10 cm^2 (lower), With a Thickness of 20 mm**

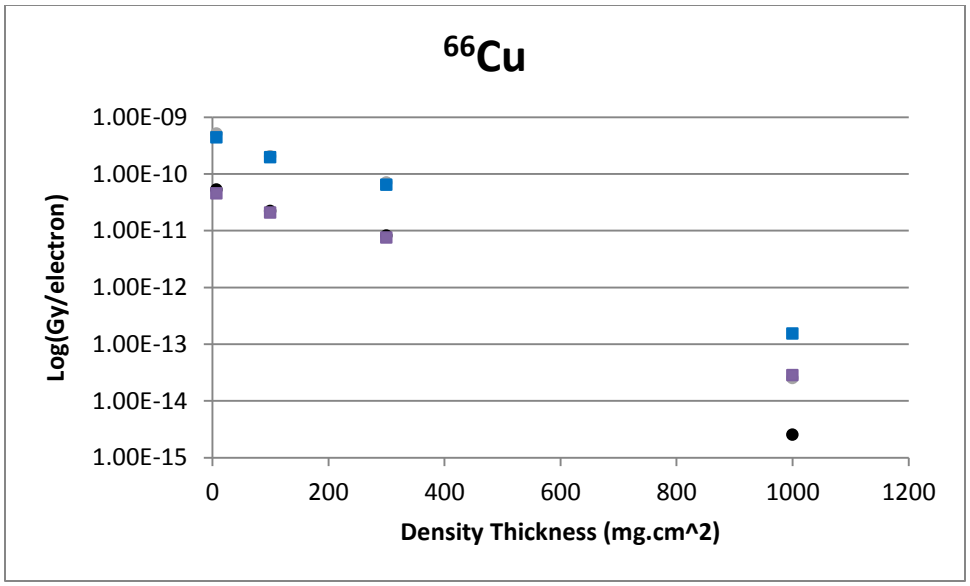

Figure B-31 **A 5 mm Diameter Disk Geometry Comparison of VARSKIN 5 (boxes) and VARSKIN 4 (circles) Predicted Dose Per Initial Beta From ^{66}Cu as a Function of Density Thickness in Tissue and a Tissue Volume Cylinder of Area 1 cm^2 (upper) and 10 cm^2 (lower), With a Thickness of 20 mm**

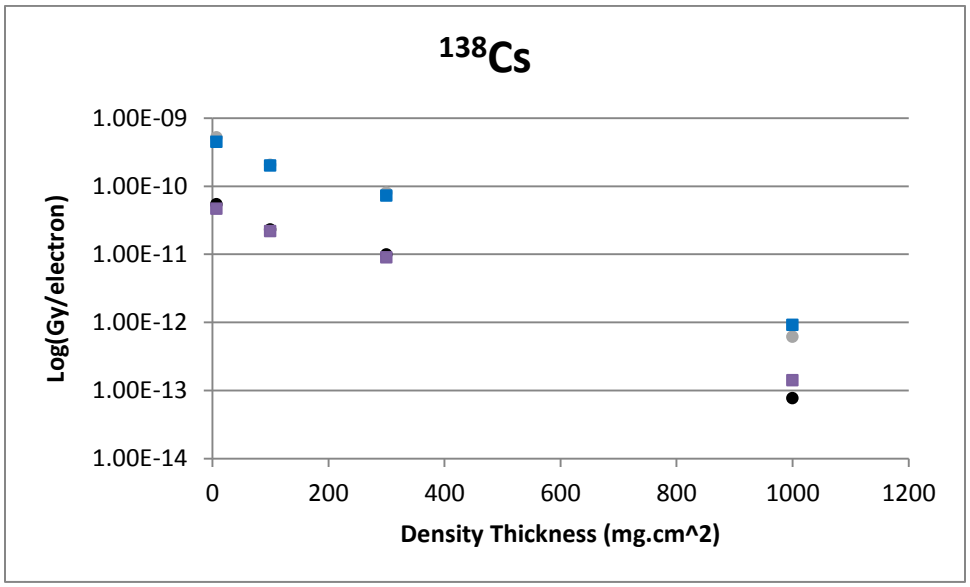

Figure B-32 **A 5 mm Diameter Disk Geometry Comparison of VARSKIN 5 (boxes) and VARSKIN 4 (circles) Predicted Dose Per Initial Beta From ^{138}Cs as a Function of Density Thickness In Tissue and a Tissue Volume Cylinder of Area 1 cm^2 (upper) and 10 cm^2 (lower), With a Thickness of 20 mm**

B.5 GEOMETRY 5: CYLINDRICAL SOURCE

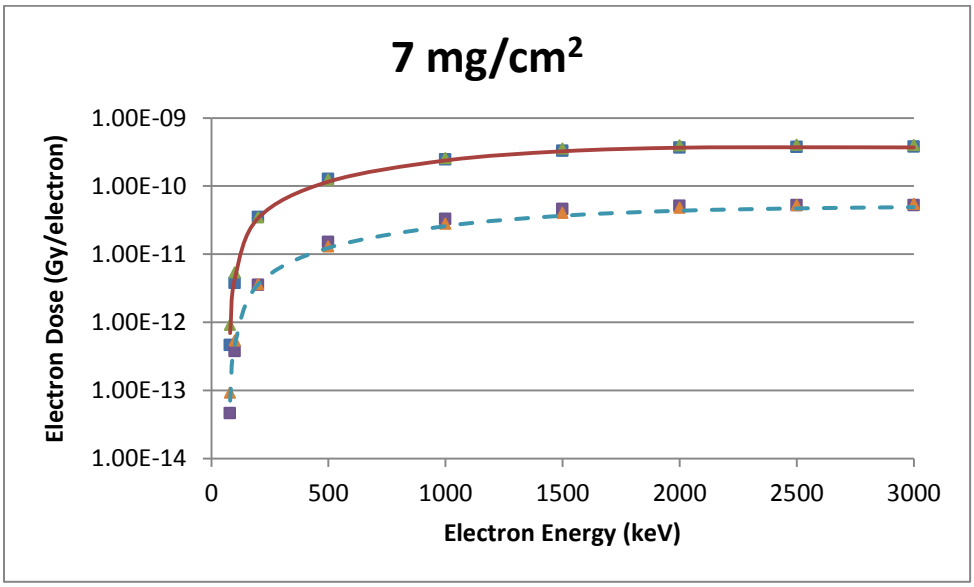

Figure B-33 **A Cylindrical Source Geometry Comparison of VARSKIN 5 (boxes), MCNP5 (triangles) and EGSnrc (lines) Predicted Dose Per Initial Electron as a Function of Electron Energy in Tissue at a Density Thickness of 7 mg/cm² and a Tissue Volume Cylinder of Area 1 cm² (solid line) and 10 cm² (dashed line), With a Thickness of 20 mm**

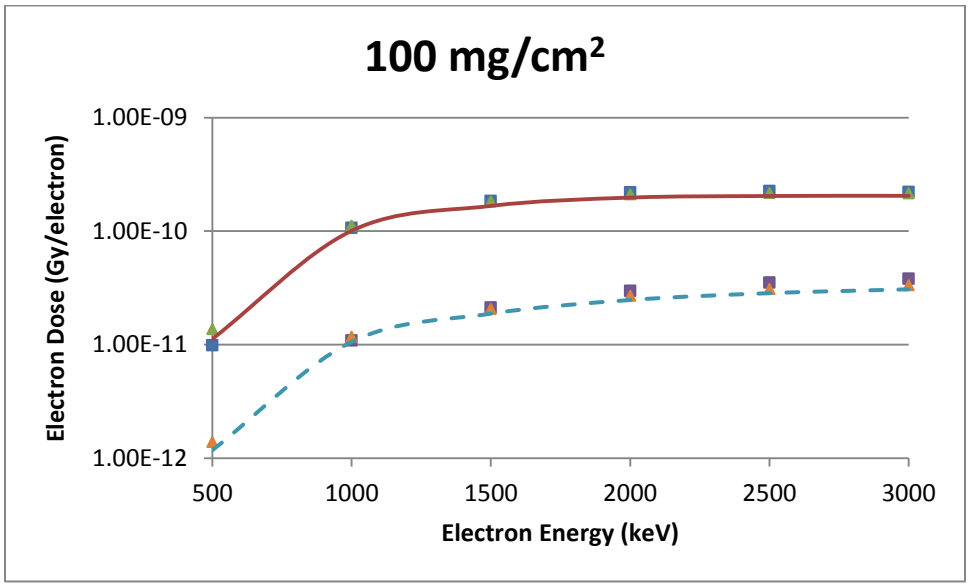

Figure B-34 **A Cylindrical Source Geometry Comparison of VARSKIN 5 (boxes), MCNP5 (triangles) and EGSnrc (lines) Predicted Dose Per Initial Electron as a Function of Electron Energy in Tissue at a Density Thickness of 100 mg/cm² and a Tissue Volume Cylinder of Area 1 cm² (solid line) and 10 cm² (dashed line), With a Thickness of 20 mm**

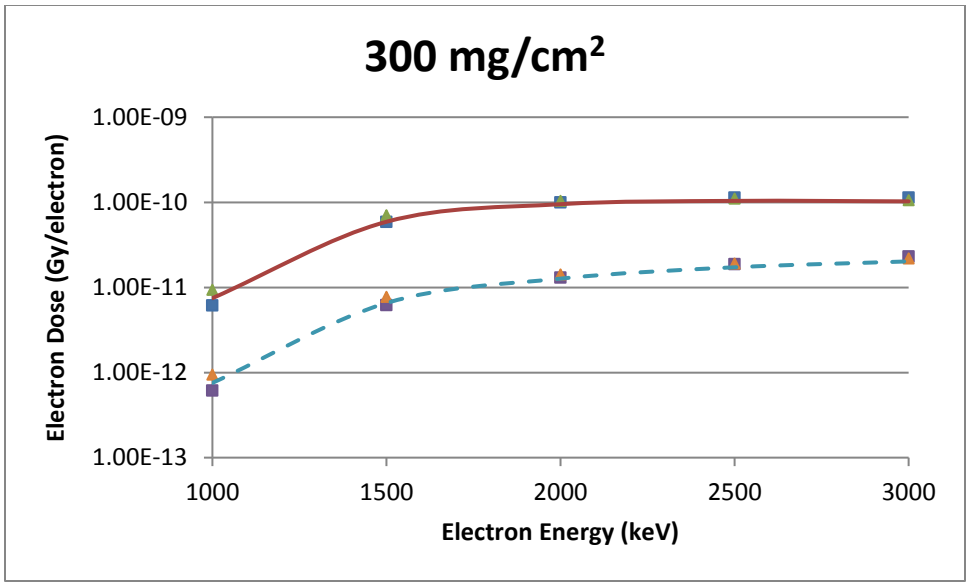

Figure B-35 **A Cylindrical Source Geometry Comparison of VARSKIN 5 (boxes), MCNP5 (triangles) and EGSnrc (lines) Predicted Dose Per Initial Electron as a Function of Electron Energy in Tissue at a Density Thickness of 300 mg/cm^2 and a Tissue Volume Cylinder of Area 1 cm^2 (solid line) and 10 cm^2 (dashed line), With a Thickness of 20 mm**

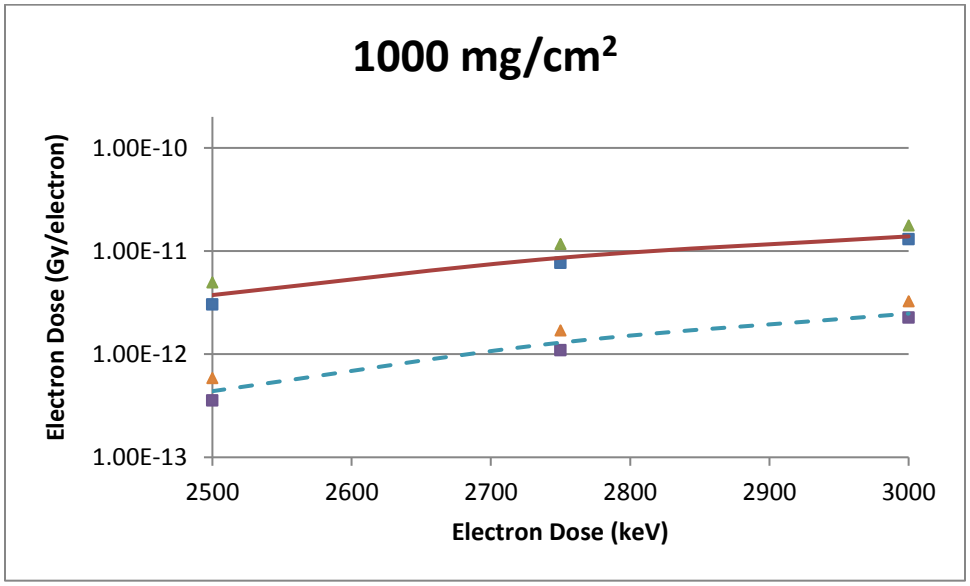

Figure B-36 **A Cylindrical Source Geometry Comparison of VARSKIN 5 (boxes), MCNP5 (triangles) and EGSnrc (lines) Predicted Dose Per Initial Electron as a Function of Electron Energy in Tissue at a Density Thickness of 1000 mg/cm^2 and a Tissue Volume Cylinder of Area 1 cm^2 (solid line) and 10 cm^2 (dashed line), With a Thickness of 20 mm**

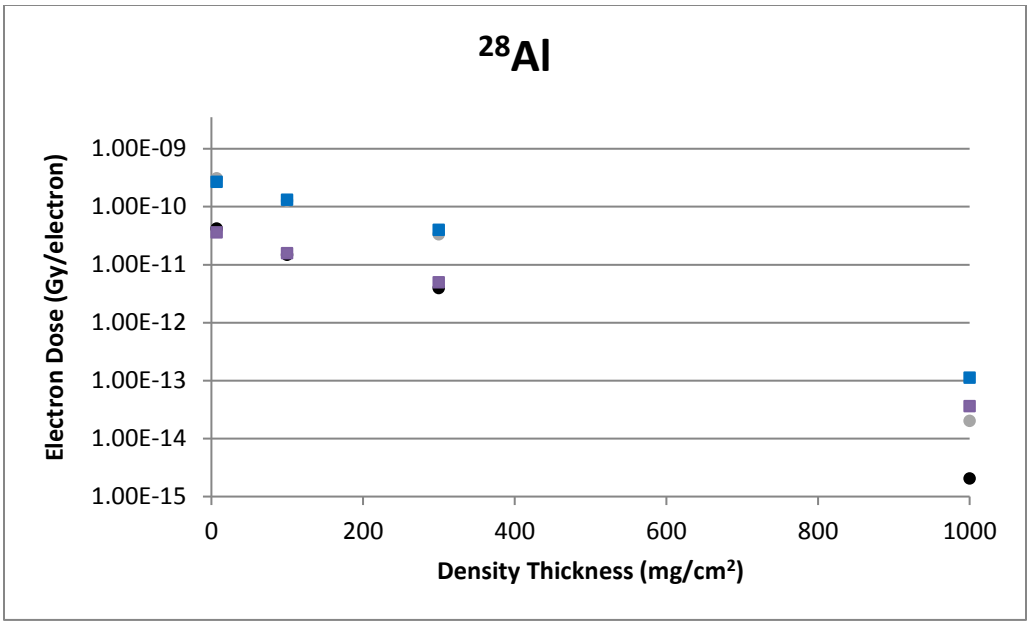

Figure B-37 **A Cylindrical Source Geometry Comparison of VARSKIN 5 (boxes) and VARSKIN 4 (circles) Predicted Dose Per Initial Beta From ^{28}Al as a Function of Density Thickness in Tissue and a Tissue Volume Cylinder of Area 1 cm^2 (upper) and 10 cm^2 (lower), With a Thickness of 20 mm**

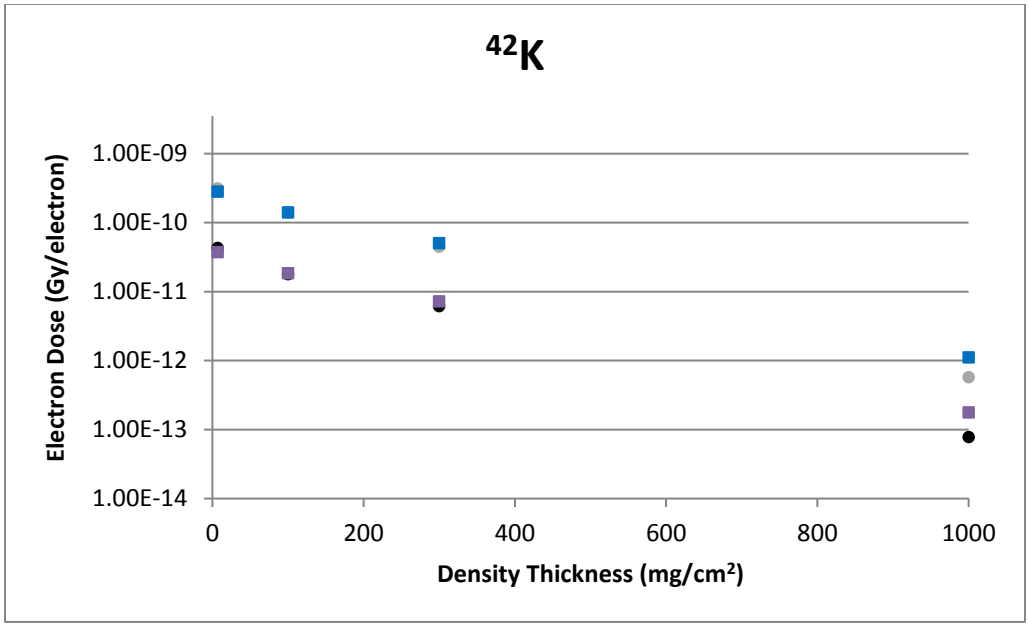

Figure B-38 **A Cylindrical Source Geometry Comparison of VARSKIN 5 (boxes) and VARSKIN 4 (circles) Predicted Dose Per Initial Beta From ^{42}K as a Function of Density Thickness in Tissue and a Tissue Volume Cylinder of Area 1 cm^2 (upper) and 10 cm^2 (lower), With a Thickness of 20 mm**

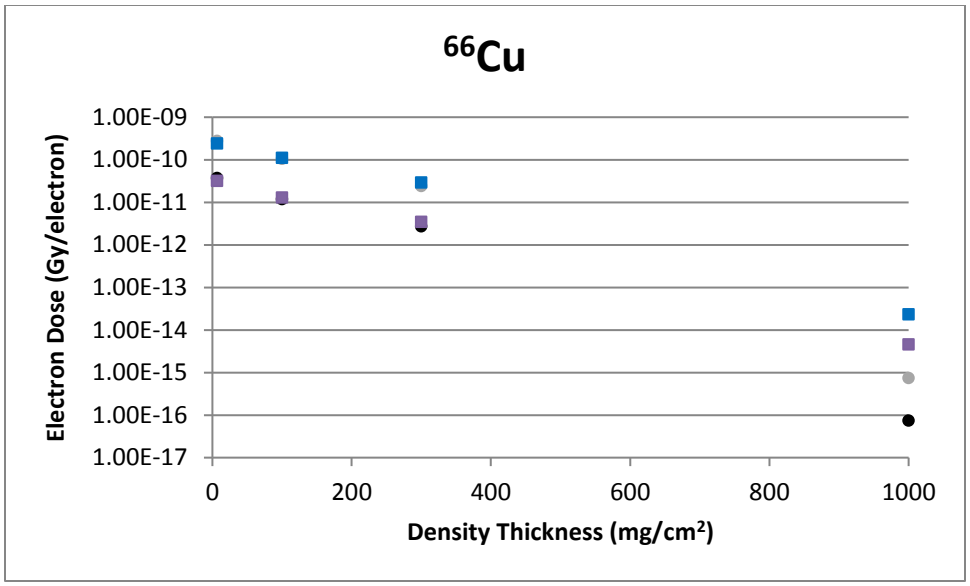

Figure B-39 **A Cylindrical Source Geometry Comparison of VARSKIN 5 (boxes) and VARSKIN 4 (circles) Predicted Dose Per Initial Beta From ^{66}Cu as a Function of Density Thickness in Tissue and a Tissue Volume Cylinder of Area 1 cm^2 (upper) and 10 cm^2 (lower), With a Thickness of 20 mm**

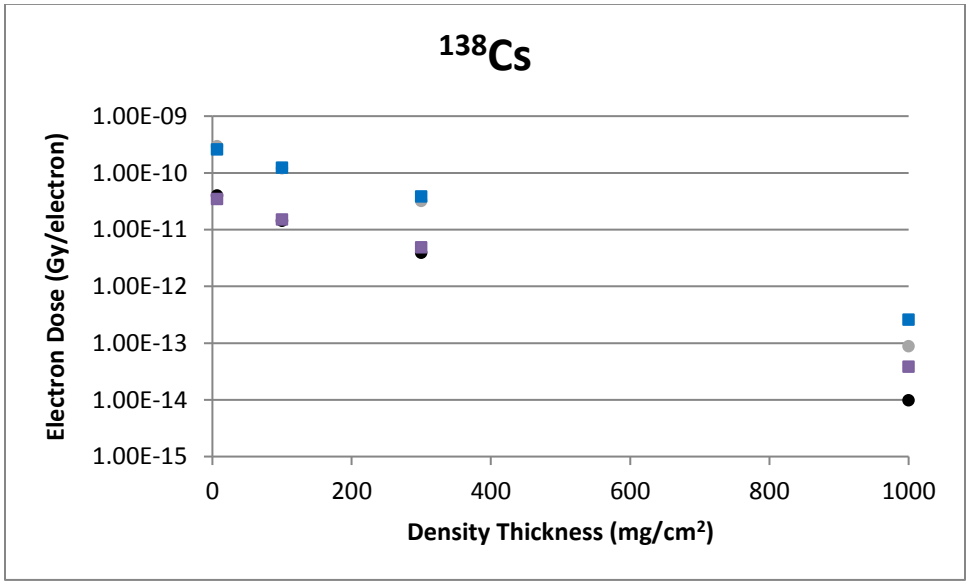

Figure B-40 **A Cylindrical Source Geometry Comparison of VARSKIN 5 (boxes) and VARSKIN 4 (circles) Predicted Dose Per Initial Beta From ^{138}Cs as a Function of Density Thickness in Tissue and a Tissue Volume Cylinder of Area 1 cm^2 (upper) and 10 cm^2 (lower), With a Thickness of 20 mm**

B.6 GEOMETRY 6: SPHERICAL SOURCE

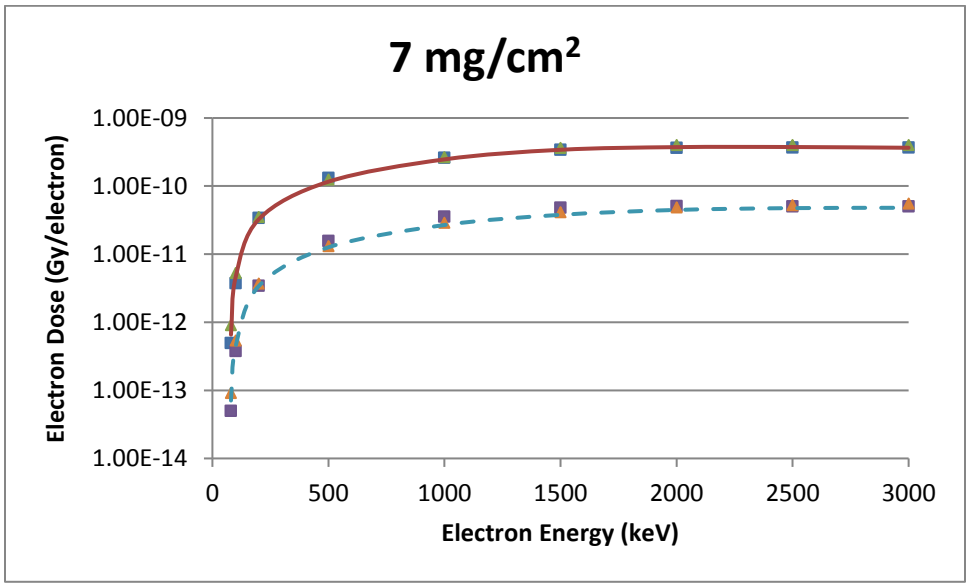

Figure B-41 **A Spherical Source Geometry Comparison of VARSKIN 5 (boxes), MCNP5 (triangles) and EGSnrc (lines) Predicted Dose Per Initial Electron as a Function of Electron Energy in Tissue at a Density Thickness of 7 mg/cm² and a Tissue Volume Cylinder of Area 1 cm² (solid line) and 10 cm² (dashed line), With a Thickness of 20 mm**

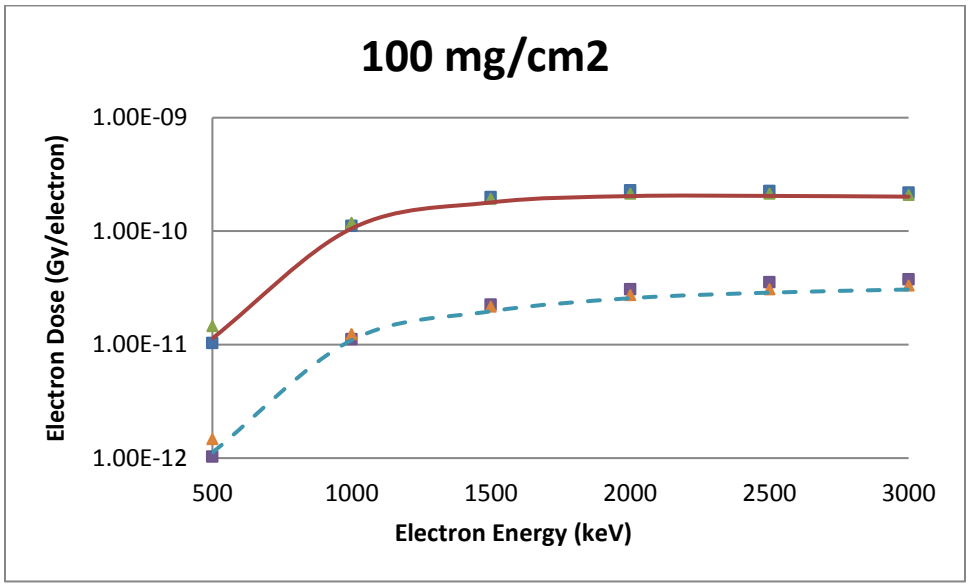

Figure B-42 **A Spherical Source Geometry Comparison of VARSKIN 5 (boxes), MCNP5 (triangles) and EGSnrc (lines) Predicted Dose Per Initial Electron as a Function of Electron Energy in Tissue at a Density Thickness of 100 mg/cm² and a Tissue Volume Cylinder of Area 1 cm² (solid line) and 10 cm² (dashed line), With a Thickness of 20 mm**

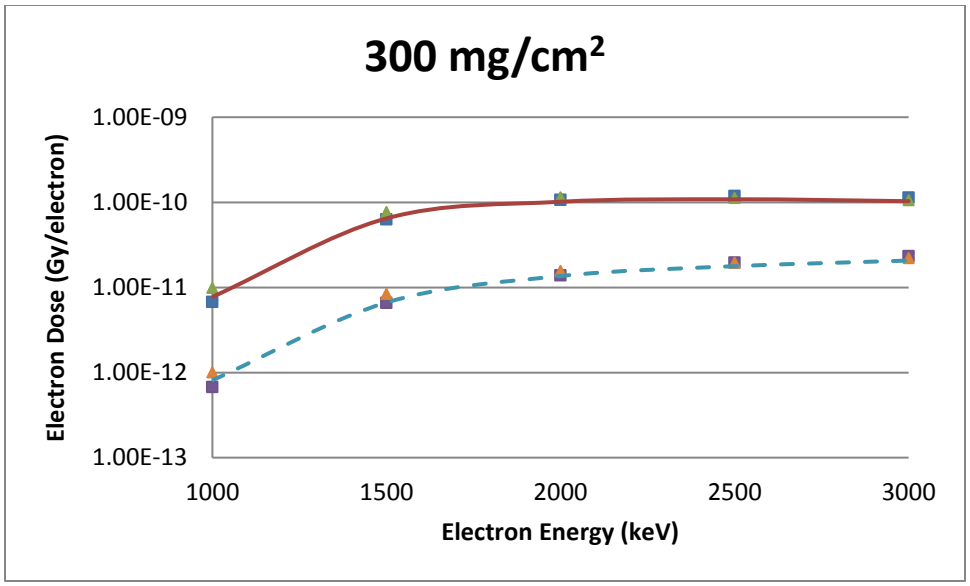

Figure B-43 **A Spherical Source Geometry Comparison of VARSKIN 5 (boxes), MCNP5 (triangles) and EGSnrc (lines) Predicted Dose Per Initial Electron as a Function of Electron Energy in Tissue at a Density Thickness of 300 mg/cm^2 and a Tissue Volume Cylinder of Area 1 cm^2 (solid line) and 10 cm^2 (dashed line), With a Thickness of 20 mm**

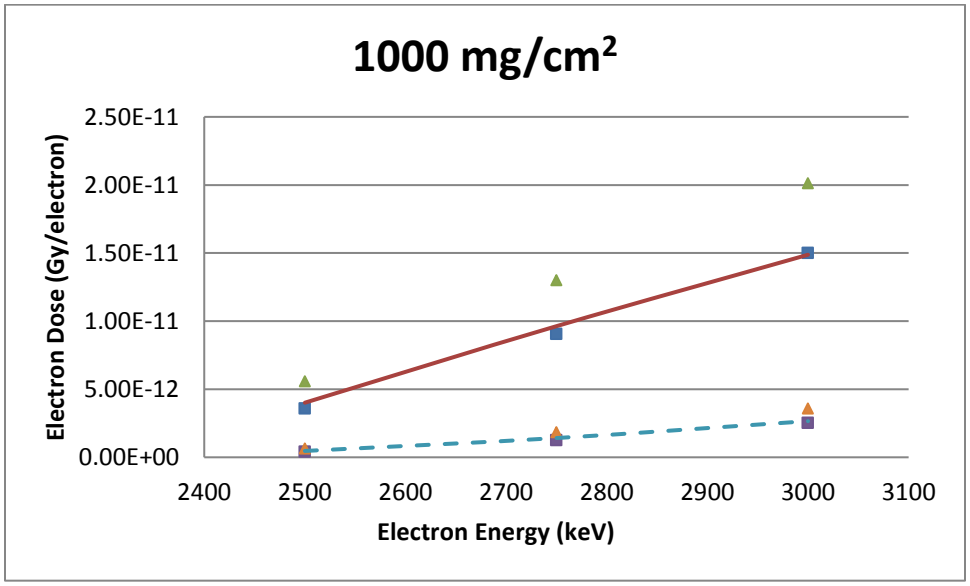

Figure B-44 **A Spherical Source Geometry Comparison of VARSKIN 5 (boxes), MCNP5 (triangles) and EGSnrc (lines) Predicted Dose Per Initial Electron as a Function of Electron Energy in Tissue at a Density Thickness of 1000 mg/cm^2 and a Tissue Volume Cylinder of Area 1 cm^2 (solid line) and 10 cm^2 (dashed line), With a Thickness of 20 mm**

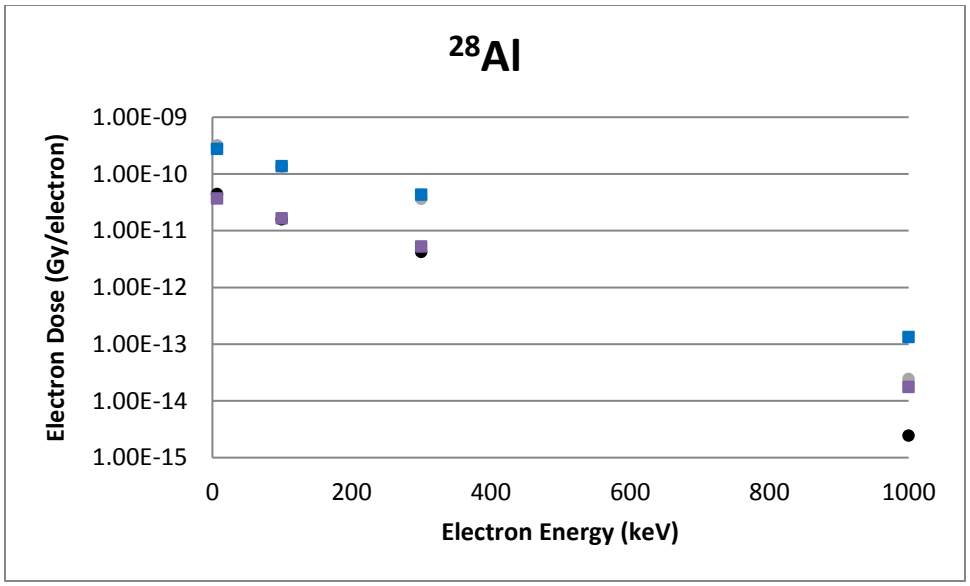

Figure B-45 **A Spherical Source Geometry Comparison of VARSKIN 5 (boxes) and VARSKIN 4 (circles) Predicted Dose Per Initial Beta From ^{28}Al as a Function of Density Thickness in Tissue and a Tissue Volume Cylinder of Area 1 cm^2 (upper) and 10 cm^2 (lower), With a Thickness of 20 mm**

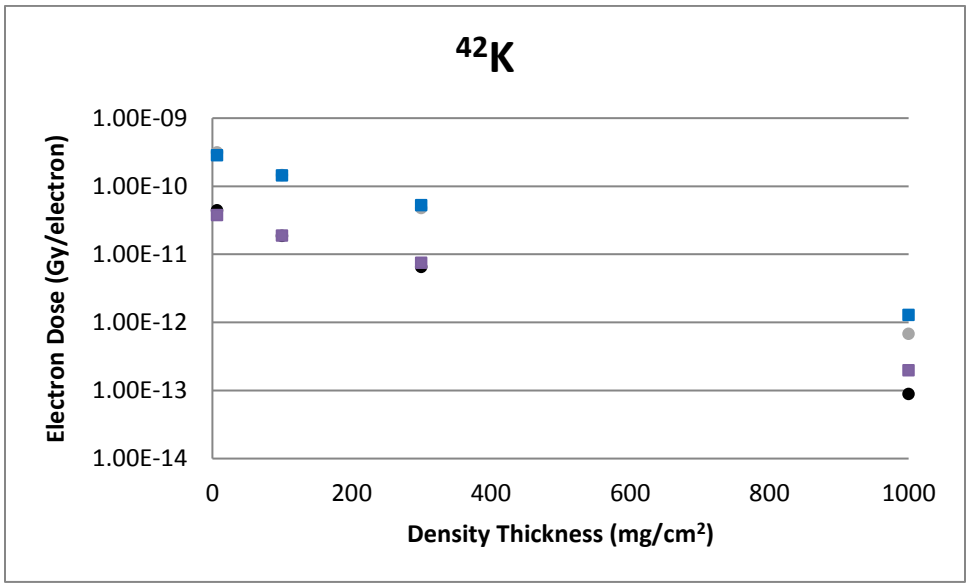

Figure B-46 **A Spherical Source Geometry Comparison of VARSKIN 5 (boxes) and VARSKIN 4 (circles) Predicted Dose Per Initial Beta From ^{42}K as a Function of Density Thickness in Tissue and a Tissue Volume Cylinder of Area 1 cm^2 (upper) and 10 cm^2 (lower), With a Thickness of 20 mm**

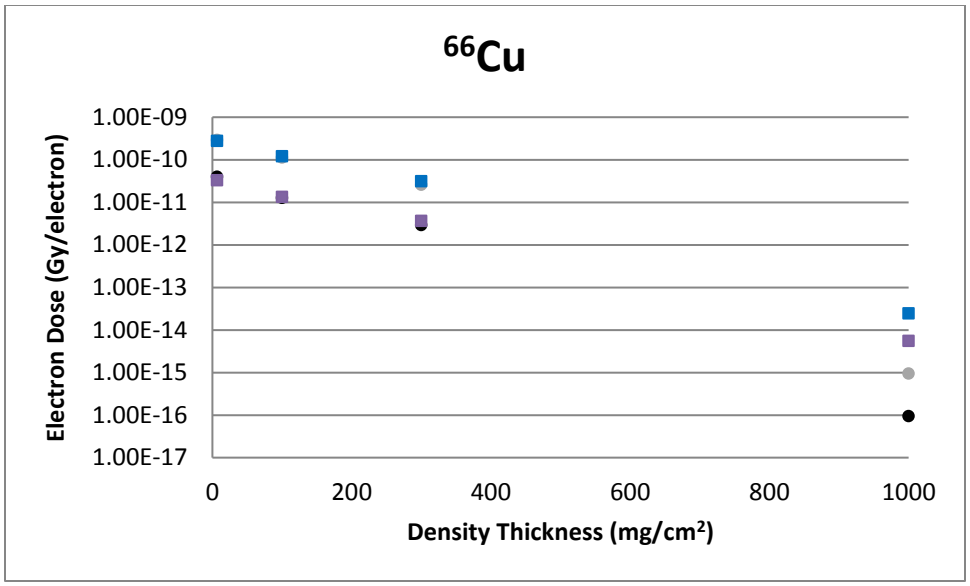

Figure B-47 **A Spherical Source Geometry Comparison of VARSKIN 5 (boxes) and VARSKIN 4 (circles) Predicted Dose Per Initial Beta From ^{66}Cu as a Function of Density Thickness in Tissue and a Tissue Volume Cylinder of Area 1 cm^2 (upper) and 10 cm^2 (lower), With a Thickness of 20 mm**

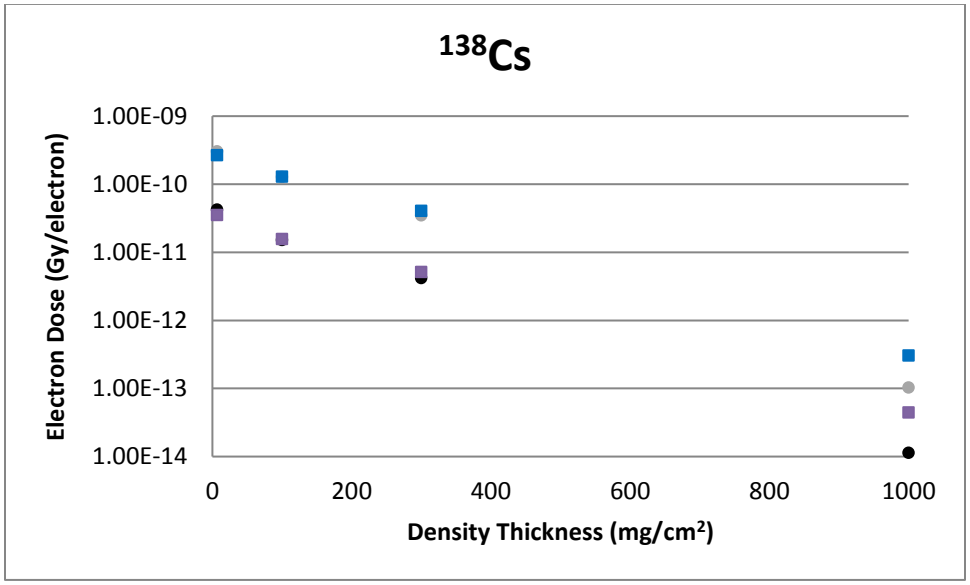

Figure B-48 **A Spherical Source Geometry Comparison of VARSKIN 5 (boxes) and VARSKIN 4 (circles) Predicted Dose Per Initial Beta From ^{138}Cs as a Function of Density Thickness in Tissue and a Tissue Volume Cylinder of Area 1 cm^2 (upper) and 10 cm^2 (lower), With a Thickness of 20 mm**

B.7 GEOMETRY 7: SLAB SOURCE

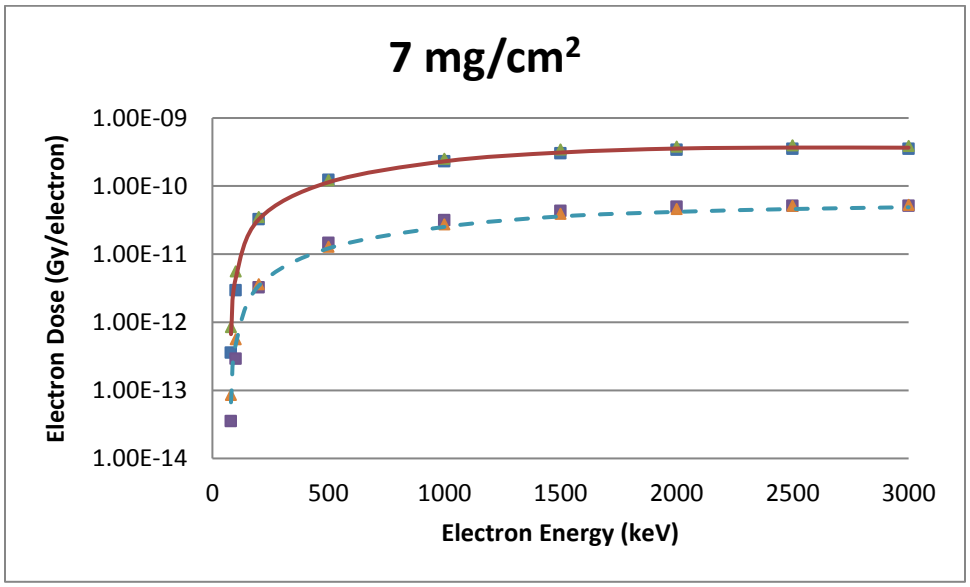

Figure B-49 **A Slab Source Geometry Comparison of VARSKIN 5 (boxes), MCNP5 (triangles) and EGSnrc (lines) Predicted Dose Per Initial Electron as a Function of Electron Energy in Tissue at a Density Thickness of 7 mg/cm² and a Tissue Volume Cylinder of Area 1 cm² (solid line) and 10 cm² (dashed line), With a Thickness of 20 mm**

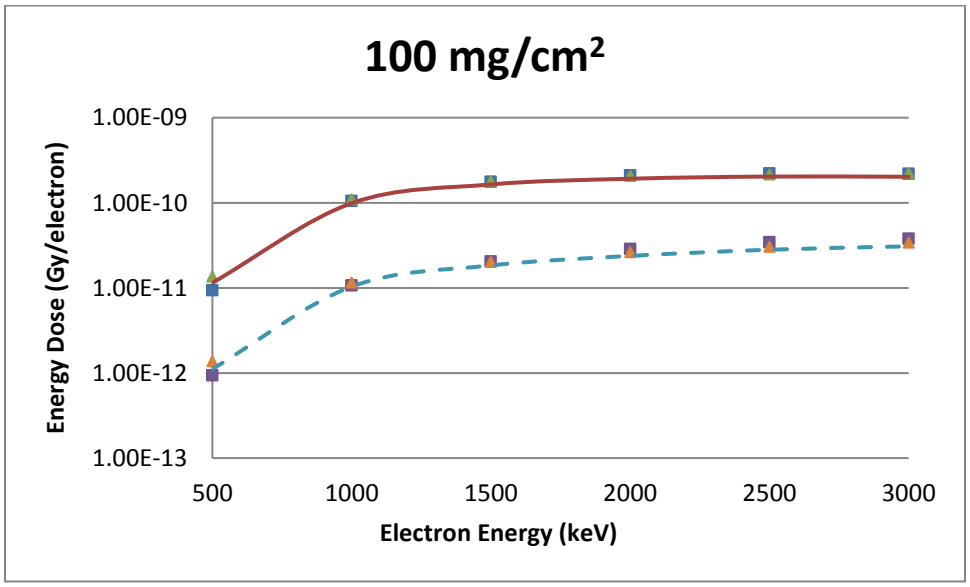

Figure B-50 **A Slab Source Geometry Comparison of VARSKIN 5 (boxes), MCNP5 (triangles) and EGSnrc (lines) Predicted Dose Per Initial Electron as a Function of Electron Energy in Tissue at a Density Thickness of 100 mg/cm² and a Tissue Volume Cylinder of Area 1 cm² (solid line) and 10 cm² (dashed line), With a Thickness of 20 mm**

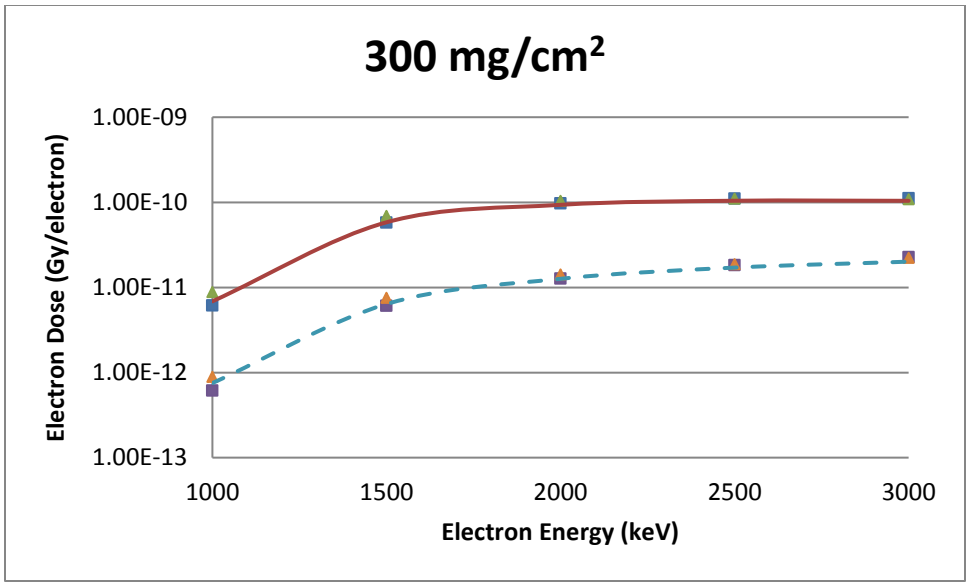

Figure B-51 **A Slab Source Geometry Comparison of VARSKIN 5 (boxes), MCNP5 (triangles) and EGSnrc (lines) Predicted Dose Per Initial Electron as a Function of Electron Energy in Tissue at a Density Thickness of 300 mg/cm^2 and a Tissue Volume Cylinder of Area 1 cm^2 (solid line) and 10 cm^2 (dashed line), With a Thickness of 20 mm**

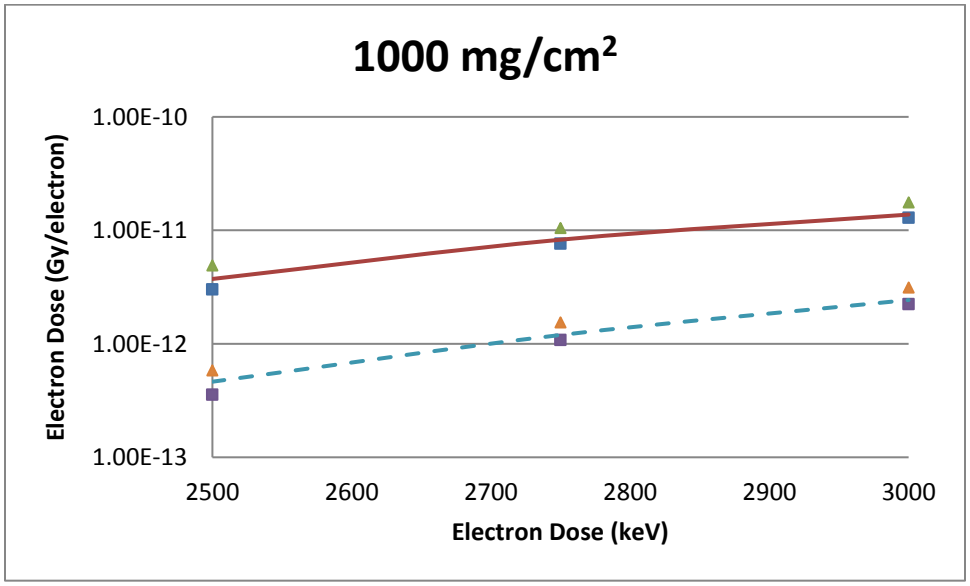

Figure B-52 **A Slab Source Geometry Comparison of VARSKIN 5 (boxes), MCNP5 (triangles) and EGSnrc (lines) Predicted Dose Per Initial Electron as a Function of Electron Energy in Tissue at a Density Thickness of 1000 mg/cm^2 and a Tissue Volume Cylinder of Area 1 cm^2 (solid line) and 10 cm^2 (dashed line), With a Thickness of 20 mm**

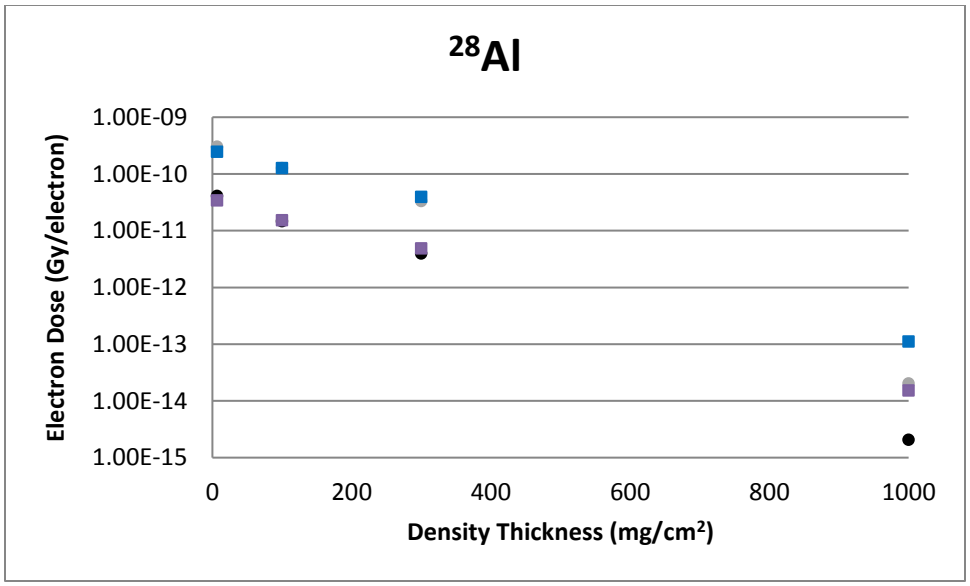

Figure B-53 **A Slab Source Geometry Comparison of VARSKIN 5 (boxes) and VARSKIN 4 (circles) Predicted Dose Per Initial Beta From ^{28}Al as a Function of Density Thickness in Tissue and a Tissue Volume Cylinder of Area 1 cm^2 (upper) and 10 cm^2 (lower), With a Thickness of 20 mm**

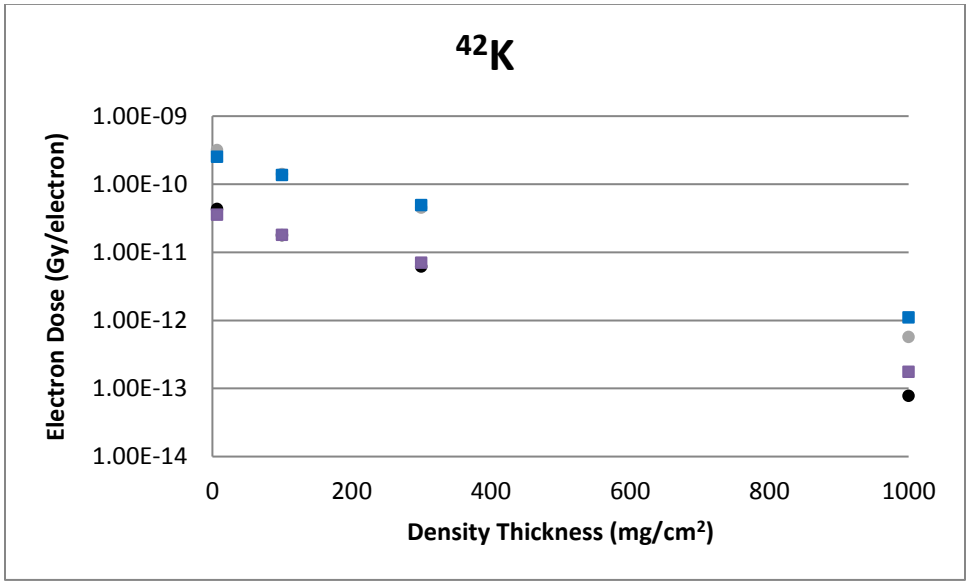

Figure B-54 **A Slab Source Geometry Comparison of VARSKIN 5 (boxes) and VARSKIN 4 (circles) Predicted Dose Per Initial Beta From ^{42}K as a Function of Density Thickness in Tissue and a Tissue Volume Cylinder of Area 1 cm^2 (upper) and 10 cm^2 (lower), With a Thickness of 20 mm**

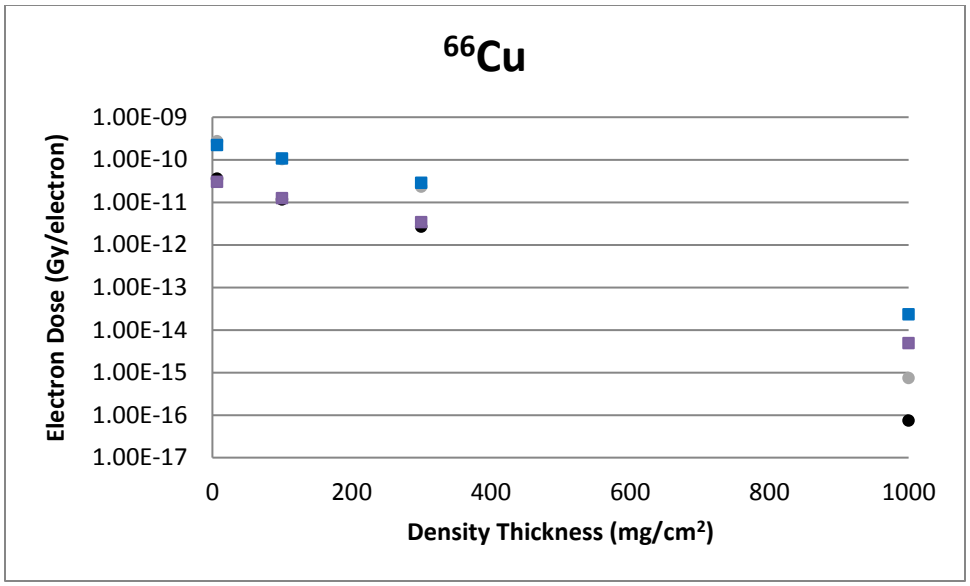

Figure B-55 **A Slab Source Geometry Comparison of VARSKIN 5 (boxes) and VARSKIN 4 (circles) Predicted Dose Per Initial Beta From ^{66}Cu as a Function of Density Thickness in Tissue and a Tissue Volume Cylinder of Area 1 cm^2 (upper) and 10 cm^2 (lower), With a Thickness of 20 mm**

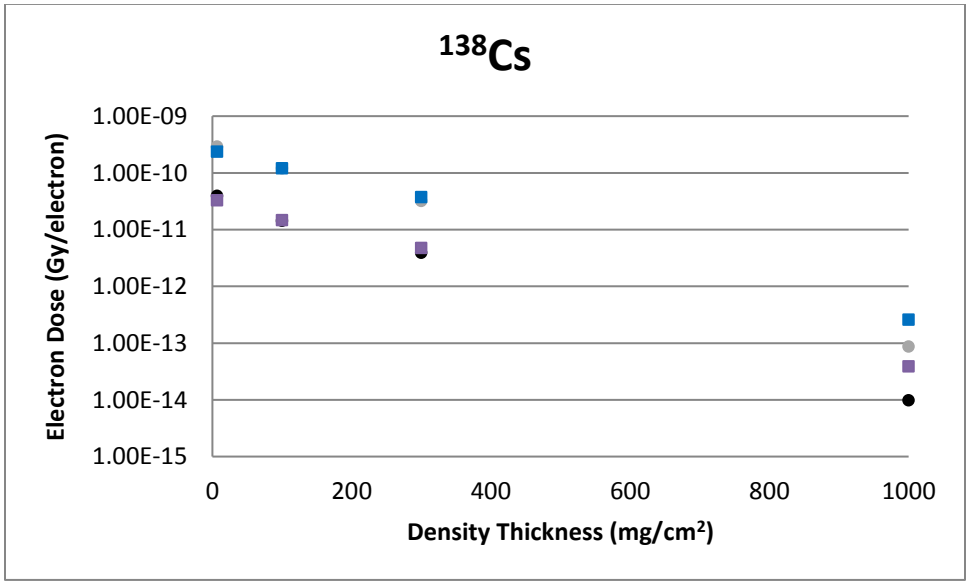

Figure B-56 **A Slab Source Geometry Comparison of VARSKIN 5 (boxes) and VARSKIN 4 (circles) Predicted Dose Per Initial Beta From ^{138}Cs as a Function of Density Thickness in Tissue and a Tissue Volume Cylinder of Area 1 cm^2 (upper) and 10 cm^2 (lower), With a Thickness of 20 mm**

APPENDIX C EXAMPLES AND SOLUTIONS USING VARSKIN 6

EXAMPLES AND SOLUTIONS USING THE VARSKIN 6 MODELS

This appendix describes three different practical applications of VARSKIN using an example/solution format. Each example describes a situation followed by a solution that involves the use of VARSKIN 6 to estimate skin dose at 7 mg/cm^2 and dose at a depth of 1000 mg/cm^2. The purpose of these examples is to lead a new user of VARSKIN through several calculations that highlight many of its features. Because VARSKIN is a flexible tool, there are always several ways to calculate the dose for a given example. The solutions presented here reflect the recommendations that are provided throughout the user's manual. With some experience, most VARSKIN users will not need to perform all of the steps described in the solution in an actual situation. It is suggested that the user complete all three examples in the order in which they are presented to develop familiarity with VARSKIN. The examples given below all utilize the ICRP 38 (no decay progeny) database.

It is important to note that, even though we use VARSKIN 6 to calculate dose at depths other than 7 mg/cm^2, these values do not ensure compliance with requirements of 10 CFR 20. The examples herein simply change the tissue depth from 7 mg/cm^2 to some different value without changing other pertinent parameters of the dose averaging calculation. We want to stress here that when, in the following scenarios, the depth is changed from 7 mg/cm^2 to 1000 mg/cm^2, for example, we are not attempting to calculate deep dose equivalent, but simply demonstrating the utility of the code for estimating energy absorption at various depths in tissue.

Example 1: Radiopharmaceutical Technician in Nuclear Medicine

At a research hospital, a doctor prescribes a 5-milliliter (mL) administration from a stock solution containing 370 kiloBequerels per milliliter (kBq/mL) of rhenium-186 (^{186}Re) for a clinical research study at 1 p.m. that day. Around 12:30 p.m., a lab technician loads the dose under the hood. Subsequently, a fellow employee bumps into her, and the needle slips out of its container. The entire 5 mL of the solution is spilled on the arm of her cloth lab coat in a circular shape with an area of approximately 50 square centimeters (cm^2). She is unaware of the accident and continues with her work until the end of the day. Around 5 p.m., a routine survey for contamination is performed, and the contamination is discovered.

Solution 1: Radiopharmaceutical Technician in Nuclear Medicine

The point source geometry is suggested as a starting point to estimate the magnitude of the dose and to collect some other useful information. Run VARSKIN 6 and check the user "Radionuclide Library." If ^{186}Re does not appear in the "Radionuclide Library" window, add ^{186}Re by selecting the "Add" button, selecting the ICRP 38 bubble with "OK", and double-clicking ^{186}Re in the Add Radionuclide to Library window (with an effective Z of equivalent-water, Z = 7.42). Enter the Exposure Time as 4.5 and change the time unit to hours using the drop-down menu or the down-arrow key. Because the point source geometry is being used, it is necessary to calculate the source strength by multiplying the concentration of the stock solution (370 kBq/mL) by the size of the administration (5 mL) to get a total source strength of 1.85 MBq. Be sure that the source strength units are set to MBq, then double-click the ^{186}Re library entry. When VARSKIN asks for the source strength, enter 1.85. The other defaults will establish a dose calculation at 7 mg/cm^2 and a dose-averaging disk of 10 cm^2. All other entries should retain their

default values. Click “Calculate Doses.” After the calculation is performed, the VARSKIN 6 Non-Volume Averaged Results window will appear.

The results window shows two groups of nine dose or dose-rate values (the group to the left is for nuclide-specific doses and the group to the right is total (over all nuclides) dose). Since only one nuclide has been selected, the two groups will display the same dose values. For each of electron, photon, and total, the initial dose rate, the dose with no decay, and the decay-corrected dose are displayed. As described earlier, the dose with no decay is provided so that the user can assume either that the source has a very long half-life or that the radionuclide is in secular equilibrium with its parent. Note that ^{186}Re has a relatively short half-life; therefore, the decay-corrected dose is the appropriate dose for the current calculation. Looking at either the VARSKIN results window or the results printout (by clicking the “Print Results” button) will show that the decay-corrected total dose is **1.31 Gray (Gy)** (**1.31 Gy** from electrons and **0.673 milliGy (mGy)** from photons), a total dose that exceeds regulatory limits. To calculate the dose at a 1 cm depth, for example, return to the main VARSKIN window (i.e., close the results window), change the value of the Skin Thickness or Skin Density Thickness to 1,000 milligrams per square centimeter (mg/cm^2), and click “Calculate Doses.” The VARSKIN results screen now displays a decay-corrected beta dose of **0** (zero) and a photon dose of **0.0712 mGy**.

The total shallow dose calculated using the point geometry was above regulatory limits. However, the situation described in this example will obviously be more accurately modeled using the disk or cylinder geometries. A more realistic, yet conservative approach would be to use the disk geometry and calculate the dose as if all of the contamination were directly on the skin. Return to the main VARSKIN window and choose “Disk” in the Source Geometry frame. Confirm the Exposure Time of 4.5 hours. Next, enter the Source Area as 50 cm^2 (do not forget to change the units from the default setting). Note that the Source Diameter is automatically calculated to be 7.98 cm (this value will be needed for the next model). Change the Skin Thickness or Skin Density Thickness back to the shallow depth of 7 mg/cm^2 and click “Calculate Doses.” The results screen shows a decay-corrected electron dose of **0.262 Gy** and a photon dose of **0.149 mGy**. While the total dose is still quite high, it is now below regulatory limits.

Even more realism can be introduced by using the cylinder model to simulate contamination that is uniformly distributed throughout the thickness of the lab coat. In this case, the lab coat is assumed to soak up the contamination instead of acting as a protective cover material. The data in Table 2-2 for a cloth lab coat give a thickness of 0.4 millimeters (mm) and a density of 0.9 g/cm^3. After returning to the main VARSKIN window, choose “Cylinder” in the Source Geometry frame. Confirm the exposure time of 4.5 hours. Paying close attention to each unit’s entry, confirm the Source Diameter as 7.98 cm (from the disk calculation), and establish a Source Thickness of 0.4 mm (the thickness of the lab coat) and a Source Density of 0.9 g/cm^3 (the density of the lab coat). Click “Calculate Doses”; after a longer calculational period (due to the geometric complexity), the VARSKIN results screen then will display **0.169 Gy** and **0.126 mGy** as the decay-corrected electron and photon doses, respectively.

It is interesting to see what the beta dose would be if the lab coat was impervious to the liquid contamination, and the contamination resided as an infinitely thin layer of contamination on the plastic. In this case, the plastic lab coat acts as a cover material instead of defining the size and density of the source. To perform this calculation, return to the main VARSKIN window and change the Source Geometry to a “Disk” source. Confirm the Exposure Time of 4.5 hours and the source area of 50 cm^2. Enter a Cover Thickness of 0.2 mm with a density of 0.36 g/cm^3. After the user clicks “Calculate Doses,” the VARSKIN results screen will display decay-corrected doses of **0.186 Gy** for electrons and **0.124 mGy** for photons. It can be concluded that,

based on the above calculations, a thicker, absorbent lab coat will give more protection than a thin, impervious material.

Example 2: Radiation Worker in Reactor Containment

A worker damages his outer glove while working inside containment during an outage at a nuclear reactor. His outer glove is removed, leaving only a surgeon's glove. The worker proceeds to the step-off pad, which takes about 15 minutes. During the exit survey, contamination is detected on the surgeon's glove, and the glove is removed and taken to the laboratory for analysis. The laboratory report concludes that the contamination is a stellite hot particle with the following characteristics:

- Radioactive contaminant: ^{60}Co
- Source strength: 92.5 MBq
- Particle thickness and density: 50 μm; 8.3 g/cm^3
- Particle size: 80 microns x 70 microns
- Stellite assumed atomic number (cobalt-chromium alloy): 25.5
- Glove thickness: 0.3 mm
- Glove density: 0.6 g/cm^3

Solution 2: Radiation Worker in Reactor Containment

First, we will use the point source geometry to estimate the magnitude of the dose and to collect some other useful information. Start or "Reset" (from the File drop-down menu) VARSKIN 6. If Co-60 does not appear in the Radionuclide Library frame, add Co-60 by selecting the "Add" key, selecting the ICRP 38 bubble with "OK", and double-clicking "Co-60" in the Add Radionuclide to Library window (with an effective Z of 25.5). Enter an Exposure Time of 15 minutes. Double-click "Co-60" in the Radionuclide Library and enter 92.5 MBq. Enter a Cover Thickness of 0.3 mm and a Cover Density of 0.6 g/cm^3. After you click "Calculate Doses," the VARSKIN results window will display an electron dose of **0.325 Gy**, a photon dose of **0.105 Gy,** and a total dose of **0.431 Gy**, a value approaching the regulatory limit. Thus, a more realistic calculation is desirable. In addition, there is a photon component to the dose, so a dose calculation at 1 cm is warranted.

Using the cylinder model will result in a more realistic calculation because the effects of self-shielding of the beta particles will be considered. As described in Section 2.1.2, the slab and cylinder models can be used for a particle that is known to be rectangular. Return to the main VARSKIN window and choose the "Cylinder" source geometry. Confirm 15 minutes as the Exposure Time, 0.3 mm as the Cover Thickness, and 0.6 g/cm^3 as the Cover Density. Enter 50 μm as the Source Thickness. The diameter of a disk source, with the same area as the rectangular source, is found by:

$$d = 2\sqrt{X \cdot Y/\pi} = 2\sqrt{80\ \mu m \cdot 70\ \mu m/\pi} = 84\ \mu m$$

Enter 84 μm for the Source Diameter and 8.3 g/cm^3 for the Source Density, and then click "Calculate Doses." After a short time, the VARSKIN results screen will display an electron dose of **0.131 Gy**, a photon dose of **0.106 Gy**, and a total dose of 0.237 Gy. Including the effects of self-shielding greatly reduced the electron dose and resulted in a dose that is now below regulatory limits. To investigate the dosimetric influence of tissue depth, calculate dose at 1 cm

by returning to the main window, and changing the Skin Thickness or Skin Density Thickness to 1,000 mg/cm^2. Click "Calculate Doses." The VARSKIN results screen will display a dose at 1 cm of **0.0324 Gy**, all from photons.

Example 3: Contaminated Metal in a University Laboratory Hood

During a radiation survey of a fume hood, a new Radiation Safety Officer (RSO) at a university discovers a contaminated aluminum plate inside the hood. Upon further investigation, it is found that the plate was used to hold beakers of solution containing carbon-14 (^{14}C) for use in radiobiology experiments. The RSO decides that the plate should be disposed of as low-level radioactive waste and that the activity of ^{14}C on the plate must be determined. The plate is 15.24 centimeters (cm) by 15.24 cm and is uniformly contaminated over the entire surface. The RSO uses a calibrated circular detector with an area of 50 cm^2 and a window thickness of 3 mg/cm^2 to measure a dose rate of 1.90 mGy/hr on contact and 0.60 mGy/hr at a distance of 2.54 cm. The RSO uses these dose-rate measurements and VARSKIN results to estimate the activity of ^{14}C on the plate. VARKSIN must be configured to mimic the measurements.

Solution 3: Contaminated Metal in a University Laboratory Hood

The solution to this example demonstrates a method in which VARSKIN 6 might be used for applications other than skin contamination events; users are cautioned not to relying too heavily on such calculations. In this situation, the Skin Averaging Area will be set to 50 cm^2 to correspond to the area of the probe, the Skin Density Thickness will be set to 3 mg/cm^2 to correspond to the thickness of the probe window, and the Source Area will be set to 232 cm^2 to correspond to the area of the contaminated plate. An initial source strength of 1 MBq/cm^2 will be used for the calculation, and the results then scaled to the measurements obtained by the RSO. Both of the measurements can be modeled because the air gap in Example 3 is smaller than 5 cm.

For this solution, first "Reset" VARSKIN 6 and choose the "Disk" geometry. If the Radionuclide Library does not contain ^{14}C, add it by clicking "Add", selecting the ICRP 38 bubble with "OK", and double-clicking "C-14" in the Add Radionuclide to Library screen (with an effective Z of 7.42). From the main VARSKIN window, click the "Use Distributed Source" checkbox. Notice that the default unit for activity has changed; set that to "MBq/cm^2". Double-click "C-14" and set the source strength to 1 MBq/cm^2. Set the Skin Averaging Area to 50 cm^2, the Skin Thickness or Skin Density Thickness to 3 mg/cm^2, and the Source Area to 232 cm^2. For this example, dose rate is of interest, so the irradiation time can remain at the default value of 60 minutes. Click "Calculate Doses"; the VARSKIN results window will appear, displaying an initial electron dose rate of **1,210 mGy/hr**, with no photon dose. The activity concentration on the plate then can be found using,

$$\frac{[A_{act}]}{[A_{cal}]} = \frac{\dot{D}_{meas}}{\dot{D}_{cal}}$$

Therefore, the activity concentration on the plate is given by:

$$\frac{\left(1\ {}^{MBq}/_{cm^2}\right)\left(1.90\ {}^{mGy}/_{hr}\right)}{1{,}210\ {}^{mGy}/_{hr}} = 0.00157\ {}^{MBq}/_{cm^2}$$

Multiplying the activity concentration by the area of the plate (232 cm^2) results in a total activity of 0.364 MBq.

The measurement at a distance of 2.54 cm can be used to verify this result. Close the results window and return to the main window; enter an Air Gap Thickness of 2.54 cm and change the activity to 0.364 MBq. After you click "Calculating Doses," the VARSKIN results window will display an initial electron dose rate of **0.602 mGy/hr**, compared to the measurement of 0.60 mGy/hr with the calibrated detector.

Example 4: Use of Decay Databases and Automatic Progeny Selection

This example is not specific to a particular contamination scenario but is provided here to demonstrate the internal calculations of VARSKIN 6 as it automatically includes decay progeny in the calculation of skin dose, and to give the user an appreciation of the possible differences between the two ICRP decay databases. The simulation itself is quite simply modeled as an infinite plane source of ^{144}Ce on the skin surface. The shallow skin dose is calculated at a depth of 7 mg/cm^2, normalized to an activity of 1 Bq for a 1 sec exposure, resulting in a dose prediction per decay of ^{144}Ce. The calculation is executed using ICRP 38 data in the first case, and then using ICRP 107 data in the second case. The photon and electron data are provided explicitly so that the user can better understand the origin of differences in the dose predictions.

Cerium-144 (^{144}Ce) decays by β^- emission (see **Fig. C-1**), with a half-life of about 285 days, through several energetic routes to praseodymium-144 (^{144}Pr). One of the ^{144}Ce decay routes stops at the metastable state ^{144m}Pr (~1% yield), with a half-life of about 7 minutes. Praseodymium-144 then decays again by β^- decay, with a half-life of about 17 minutes, to neodymium-144 (^{144}Nd). They're not all shown in the figure, but a large number of gamma-ray photons, conversion electrons, characteristic X rays, and Auger electrons are also emitted during these decay processes. The emission data, as extracted by VARSKIN 6, are provided in **Tables C-1 and C-2** (divided by **(a)** photons and **(b)** electrons) according to both ICRP 38 and ICRP 107, respectively. It is evident from the data that we can expect differences in the dose calculations using the two datasets.

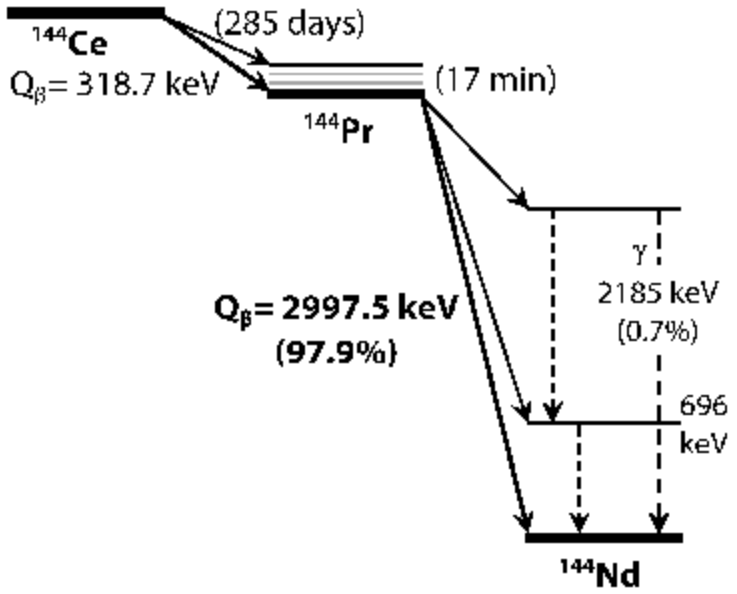

Figure C-1 The Decay Scheme of ^{144}Ce to Stable ^{144}Nd

Table C-1a ICRP 38 Photon Emission Data for the Decay of 144Ce to Stable 144Nd

Nuclide	Branching Ratio	Photon Yield (%)	Photon Energy (MeV)	Nuclide	Photon Yield (%)	Photon Energy (MeV)
^{144}Ce		1.6416	0.0801199	^{144}Ce(D)	1.6416	0.0801199
		10.8	0.13353		10.8	0.13353
		5.40195	0.0360263		5.40195	0.0360263
		2.95756	0.0355502		2.95756	0.0355502
		1.06958	0.0407484		1.06958	0.0407484
^{144}Pr	0.9822	1.48	0.69649		1.45366	0.69649
^{144m}Pr	0.0178	15.7456	0.0360263		0.280272	0.0360263
		8.62071	0.0355502		0.153449	0.0355502
		3.11763	0.0407484		0.05549381	0.0407484
		1.25177	0.0417924		0.02228151	0.0417924
		1.60605	0.0406532		0.02858769	0.0406532
		4.53392	0.00503329		0.08070377	0.00503329
		1.63137	0.00548929		0.02903838	0.00548929
^{144}Pr	0.999	1.48	0.69649		0.02631766	0.69649

^{144}Ce(D) represents the combined “nuclide” in VARSKIN 6 having selected the option to include progeny.

Table C-2b ICRP 38 Electron Emission Data for the Decay of ^{144}Ce to Stable ^{144}Nd

Nuclide	Half-life (hours)	Electron Yield (%)	Electron Avg Energy (MeV)	Electron X90 (cm)
^{144}Ce	6823.2	1.57344	0.09230879	0.02774469
^{144}Pr	0.288	1.0006	1.2079	0.695699
^{144m}Pr	0.12	3.37682	0.617	0.004115152
^{144}Ce(D)	6823.2	1.57344	0.654206	0.682593

^{144}Ce(D) represents the combined "nuclide" in VARSKIN 6 having selected the option to include progeny.

Table C-3a ICRP 107 Photon Emission Data for the Decay of ^{144}Ce to Stable ^{144}Nd

Nuclide	Branching Ratio	Photon Yield (%)	Photon Energy (MeV)	Nuclide	Photon Yield (%)	Photon Energy (MeV)
^{144}Ce		1.36407	0.08012	^{144}Ce(D)	1.36407	0.08012
		11.09	0.133515		11.09	0.133515
		4.40559	0.0360557		4.40559	0.0360557
		2.41237	0.0355671		2.41237	0.0355671
^{144}Pr	0.99023	1.342	0.69651		1.32889	0.69651

^{144}Ce(D) represents the combined "nuclide" in VARSKIN 6 having selected the option to include progeny.

Table C-3b ICRP 107 Electron Emission Data for the Decay of ^{144}Ce to Stable ^{144}Nd

Nuclide	Half-life (hours)	Electron Yield (%)	Electron Avg Energy (MeV)	Electron X90 (cm)
^{144}Ce	6837.84	2.34621	0.09170876	0.0285164
^{144}Pr	0.288	1.00107	1.20882	0.696917
^{144m}Pr	0.12	10.231	0.296957	0.004116936
^{144}Ce(D)	6837.84	2.34621	0.654899	0.682717

^{144}Ce(D) represents the combined "nuclide" in VARSKIN 6 having selected the option to include progeny.

Solution 4: Use of Decay Databases and Automatic Progeny Selection

This example begins with the selection of scenario, along with the manual selection of parent and progeny nuclides using the ICRP 38 decay database. We follow up with the selection of automatic decay progeny inclusion and a comparison of shallow skin dose predictions.

For this solution, first "Reset" VARSKIN 6 and choose the "Disk" geometry. Select an Exposure Time of 1 second, Activity Units of "Bq", and set the Source Area to 100 cm^2 (this will approximate an infinite plane source for a dose averaging area of 10 cm^2). All other inputs should remain as they are, in the default state.

On examination of the decay scheme for ^{144}Ce, we see that its decay progeny includes ^{144}Pr and ^{144m}Pr. Therefore, if those nuclides must be in your Radionuclide Library. If the Radionuclide Library does not contain ^{144}Ce from the ICRP 38 library, add it by clicking "Add",

selecting the “ICRP 38” bubble, pressing “OK”, and then double-clicking “Ce-144” in the Add Radionuclide to Library screen (for simplicity, we’ll use the default effective Z of 7.42). Next, do the same for “Pr-144” and “Pr-144m”. Additionally, to add ^{144}Ce with its decay progeny, click “Add” and select the “ICRP 38D” bubble, press “OK” and then double-click “Ce-144”. Then, to include those nuclides in the dose calculation for this scenario, double-click “Ce-144” in your Radionuclide Library and enter an activity to 1 Bq (repeat for ^{144}Pr, ^{144m}Pr, and ^{144}Ce(D)).

Recheck the input window to see that all parameters contain the appropriate values, including the four nuclides listed in the Selected Radionuclides box, and then click “Calculate Doses” to generate the VARSKIN results. With the results (**Table C-3**), we will compare a manual calculation of the total dose (SUM in Table C-3) and compare that with the automatic calculation using the progeny option (^{144}Ce(D) in Table C-3). We calculate the SUM using,

$$D = D_{Ce} + (BR_{Pr}D_{Pr}) + (BR_{m}D_{m}) + (BR_{m}BR_{\mathrm{Pr}*}D_{Pr})$$

$$D = 2.40x10^{-9} + (0.9822 \cdot 4.58x10^{-9}) + (0.0178 \cdot 5.55x10^{-13}) + (0.0178 \cdot 0.999 \cdot 4.58x10^{-9})$$

$$D = 6.98x10^{-9}\ mGy/nt$$

Table C-3 Dose Results from VARSKIN 6 with Progeny Using the ICRP 38 Decay Database

Nuclide	Branching Ratio	Electron Dose (mGy/nt)	Photon Dose (mGy/nt)
^{144}Ce		2.40x10^{-9}	3.63x10^{-12}
^{144}Pr	0.9822	4.58x10^{-9}	7.78x10^{-13}
^{144m}Pr	0.0178	5.55x10^{-13}	1.42x10^{-11}
^{144}Pr*	0.999	4.58x10^{-9}	7.78x10^{-13}
SUM		**6.98x10^{-9}**	**4.66x10^{-12}**
^{144}Ce(D)		6.93x10^{-9}	4.66x10^{-12}
Difference		-0.7%	0%

^{144}Ce(D) represents the combined “nuclide” in VARSKIN 6 having selected the option to include progeny.

*this entry represents ^{144}Pr as the decay product of ^{144m}Pr.

The “discrepancy” (percent difference) in the dose calculations is shown to be within the tolerance of rounding (within 1%). To execute VARSKIN 6 with the ICRP 107 decay database, simply “Add” the proper nuclides in the same fashion as above, except this time selecting the “ICRP 107” and “ICRP 107D” bubbles, where appropriate. ICRP 107 does not provide branching for ^{144m}Pr, therefore, the metastable state of ^{144}Pr is not included in the calculation. Dose results for the ICRP 107 comparison are given in **Table C-4**. Electron and photon dose estimates with comparing manual to automatic progeny selection give results within rounding.

Table C-4 Dose results from VARSKIN 6 with progeny using the ICRP 107 decay database

Nuclide	Branching Ratio	Electron Dose (mGy/nt)	Photon Dose (mGy/nt)
^{144}Ce		2.44×10^{-9}	3.27×10^{-12}
^{144}Pr	0.99023	4.58×10^{-9}	7.05×10^{-13}
SUM		$\mathbf{6.98 \times 10^{-9}}$	$\mathbf{3.97 \times 10^{-12}}$
^{144}Ce(D)		6.93×10^{-9}	3.97×10^{-12}
Difference		-0.7%	0.0%

^{144}Ce(D) represents the combined “nuclide” in VARSKIN 6 having selected the option to include progeny.

NRC FORM 335
(12-2010)
NRCMD 3.7

U.S. NUCLEAR REGULATORY COMMISSION

BIBLIOGRAPHIC DATA SHEET

(See instructions on the reverse)

1. REPORT NUMBER
(Assigned by NRC, Add Vol., Supp., Rev., and Addendum Numbers, if any.)

NUREG/CR-6918, Rev. 3

2. TITLE AND SUBTITLE

VARSKIN 6

A Computer Code for Skin Contamination Dosimetry

3. DATE REPORT PUBLISHED

MONTH	YEAR
October	**2018**

4. FIN OR GRANT NUMBER

5. AUTHOR(S)

Vered Anzenberg Shaffer

6. TYPE OF REPORT

Technical

7. PERIOD COVERED (Inclusive Dates)

8. PERFORMING ORGANIZATION - NAME AND ADDRESS (If NRC, provide Division, Office or Region, U. S. Nuclear Regulatory Commission, and mailing address; if contractor, provide name and mailing address.)

Division of System Analysis
Office of Nuclear Regulatory Research
U.S. Nuclear Regulatory Commission
Washington, DC 20555-001

9. SPONSORING ORGANIZATION - NAME AND ADDRESS (If NRC, type "Same as above", if contractor, provide NRC Division, Office or Region, U. S. Nuclear Regulatory Commission, and mailing address.)

Division of System Analysis
Office of Nuclear Regulatory Research
U.S. Nuclear Regulatory Commission
Washington, DC 20555-001

10. SUPPLEMENTARY NOTES

11. ABSTRACT (200 words or less)

The original VARSKIN computer code, an algorithm to calculate skin dose from radioactive skin contamination, has been modified on several occasions. VARSKIN is a U.S. NRC computer code used by staff members and NRC licensees to calculate occupational dose to the skin resulting from exposure to radiation emitted from hot particles or other contamination on or near the skin. These assessments are required by 10 CFR 20.1201(c) in which the assigned shallow dose equivalent is to the part of the body receiving the highest exposure over a contiguous 10 cm^2 of skin at a tissue depth of 0.007 centimeters (7 mg/cm^2).

This user manual describes the updates to VARSKIN 6.0, in addition to aiding the user in installing VARSKIN 6.0.

12. KEY WORDS/DESCRIPTORS (List words or phrases that will assist researchers in locating the report.)

Dose, Internal Dosimetry, RAMP, Dosimetry Computer Codes

13. AVAILABILITY STATEMENT

unlimited

14. SECURITY CLASSIFICATION

(This Page)
unclassified

(This Report)
unclassified

15. NUMBER OF PAGES

16. PRICE

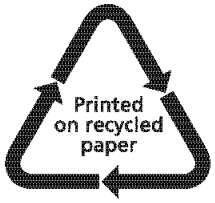

Federal Recycling Program

UNITED STATES
NUCLEAR REGULATORY COMMISSION
WASHINGTON, DC 20555-0001

OFFICIAL BUSINESS